Flavor Technology

Physical Chemistry, Modification, and Process

Chi-Tang Ho, EDITOR
Rutgers University

Chee-Teck Tan, EDITOR
International Flavors & Fragrances, Inc.

Chao-Hsiang Tong, EDITOR
Rutgers University

Flavor technology

This book is printed on acid-free, recycled paper.

Foreword

THE ACS SYMPOSIUM SERIES was first published in 1974 to provide a mechanism for publishing symposia quickly in book form. The purpose of this series is to publish comprehensive books developed from symposia, which are usually "snapshots in time" of the current research being done on a topic, plus some review material on the topic. For this reason, it is necessary that the papers be published as quickly as possible.

Before a symposium-based book is put under contract, the proposed table of contents is reviewed for appropriateness to the topic and for comprehensiveness of the collection. Some papers are excluded at this point, and others are added to round out the scope of the volume. In addition, a draft of each paper is peer-reviewed prior to final acceptance or rejection. This anonymous review process is supervised by the organizer(s) of the symposium, who become the editor(s) of the book. The authors then revise their papers according to the recommendations of both the reviewers and the editors, prepare camera-ready copy, and submit the final papers to the editors, who check that all necessary revisions have been made.

As a rule, only original research papers and original review papers are included in the volumes. Verbatim reproductions of previously published papers are not accepted.

Preface

FLAVOR IS ONE OF THE KEY ATTRIBUTES in determining food palatability. The chemistry of food aromas has been studied intensively for the past 50 years. Much research has been focused on the analytical, synthetic, and organic chemistry of flavors. Very little work has been devoted to applying physical chemistry in understanding the phenomenon of flavor formation in the preparation of flavor products.

The purpose of this book is to bring together aspects of aroma research covering reaction kinetics, modeling, physical phenomena associated with flavor emulsion and encapsulation, and the effect of processing and storage on flavor. The purpose of the symposium on which this book is based was to bring together researchers from academia and industry to present their latest findings and to stimulate fellow scientists to participate in dialogues on current developments in the physical chemistry of food flavors.

We are indebted to the contributing authors for their worthy contributions. Without their dedication, expertise, and hard work, timely publication of this book would not have been possible.

CHI-TANG HO
Department of Food Science
Cook College
Rutgers University
P.O. Box 231
New Brunswick, NJ 08903–0231

CHEE-TECK TAN
International Flavors & Fragrances, Inc.
1515 Highway 36
Union Beach, NJ 07735

CHAO-HSIANG TONG
Department of Food Science
Cook College
Rutgers University
P.O. Box 231
New Brunswick, NJ 08903–0231

July 13, 1995

Chapter 1

Physical Chemistry in Flavor Products Preparation

An Overview

Chee-Teck Tan

International Flavors & Fragrances, Inc., 1515 Highway 36, Union Beach, NJ 07735

Physical chemistry plays an important role in the variety of processes used in flavor production. Examples of these processes are extraction, isolation, separation, concentration, purification, etc. Many flavors are first produced in a concentrated form or in a physical form which cannot be readily used for food applications. Further processing is needed to convert them into more practical useful forms for more specific uses. Some flavors are volatile or sensitive to oxidation and they need protection or encapsulation to impart stability until final food applications. The common processes for these modifications are: compounding, spray drying, powder adsorption, spray chilling, emulsification, molecular inclusion, co-crystallization, coacervation and liposome formation, etc. The principles of physical chemistry are involved in all of these processes.

It is obvious that physical chemistry plays an important role in the processing of flavors. The application of physical chemistry principles to flavor processing is a vast subject and can be subdivided into many smaller subjects. For example, physical chemistry in flavor reactions; flavor generation; flavor analysis; flavor products preparations and flavor perception. This paper will discuss the physical chemistry principles involved in the preparation of several flavor products.

Studying and understanding the physical chemistry of flavors is complex because of the large number of chemicals that contribute to the flavor. The number of flavor components in one flavor could be as high as fifty or more. These components are extracted from natural products, generated from natural processes or chemical reactions, and then they are subjected to isolation, separation, purification, concentration, etc. Physical chemistry principles are involved in each of these steps.

Most flavors for use in food products are not a single flavor chemical. A flavor is usually created by compounding many flavor materials at the proper concentration of each component to produce the desired flavor characteristics and profile.

Many flavor materials when they are first produced through the steps mentioned above have one or more of the following characteristics:

- Highly concentrated
- Highly volatile
- Immiscible with water
- Prone to oxidation.

A flavor material in high concentration usually can not be used directly in food. Its concentration should be reduced to the acceptable level for food use. There are several ways to reduce the concentration level. The most common method is to dilute the liquid flavor with a proper solvent, or to dissolve a solid flavor in a solvent.

Almost all the flavors which are aromatic have different degrees of volatility. It is the volatility of the flavor which stimulates the olfactory receptors. Although they can be compounded into a flavor to provide the desired flavor characteristics they must be "fixed" to prevent losses due to volatilization.

The advantage of converting all flavor components into liquid form is that they can be easily mixed together and will achieve a homogeneous distribution of each individual component in the finished flavor if they are miscible in each other. Problems arise when the flavor components are in two different phases, such as oil and water phases. These two phases are not miscible. In order to make them into a homogeneous mixture, emulsification is needed.

In many of the flavor applications, the flavor is needed in a powder or a controlled release form. Spray drying, spray chilling and adsorption on powder are the answers to this need. The products of spray drying and spray chilling also serve as controlled release flavors. In certain flavor applications, flavor oils are used to flavor soft drinks. The flavor oils are not miscible with the sugar solution and they have to be made into an oil-in-water emulsion which can be dispersed in water. Volatile and oxidation prone flavors are protected from evaporation or oxidation by encapsulation into microsized capsules. Microencapsulation also serves to control the flavor release for specific applications. Microencapsulation processes include spray drying, spray chilling, extrusion, molecular inclusion, coacervation, co-crystallization, and liposome formation, etc. Therefore, in the preparation of flavor products from flavor compounds for use in food products many technologies are involved. These flavor technologies may be summarized as:

- Compounding
- Emulsion /Microemulsion
- Spray drying
- Spray chilling
- Extrusion
- Adsorption
- Molecular inclusion
- Coacervation
- Co-crystallization
- Liposome formation

Physical chemistry principles play important roles in these processes.

I. Compounding

Compounding of flavors from basic flavor materials or chemicals is an age old traditional method to create flavors. It is the basic process of preparing a flavor for food uses. Compounding is to mix flavor materials together at a special ratio in which they compliment each other to give the desirable aroma and taste (*1*). A typical artificial black cherry flavor formula is shown in Table I.

Table I. A Typical Artificial Black Cherry Flavor Formula

Ingredients	Composition (g)
Aldehyde, C16	0.25
Rose oil	0.75
Ethyl vanillin	1.00
Balsam of Peru	1.25
Heliotropin	1.25
Aldehyde, C-14	1.25
Cinnamic aldehyde	1.25
Oil of cloves	2.50
Vanillin	5.00
β-Ionone	5.00
Amyl valerate	5.00
Anisyl acetate	7.75
Benzyl acetate	10.25
Amyl acetate	12.25
Tolyl aldehyde	25.00
Ethyl butyrate	25.00
Ethyl acetate	90.00
Benzaldehyde	125.75
Ethyl alcohol (95%)	173.50
Propylene glycol	506.00
Total	1000.00

In compounding, the flavor component materials should be compatible in solubility. They should not be chemically reactive to each other. Miscible to each other is essential. For compounding purposes, many solid flavor ingredients are dissolved in a proper solvent to facilitate the mixing with other liquid components. The finished flavor product has to be in one phase. If a compounded flavor has two immiscible liquid phases, it can be made into a homogeneous solution by adding a co-solvent, homogenized into an emulsion, or converted into a microemulsion.

In a compounded flavor, the perceptional intensity which is caused by odor depends

on its vapor pressure, which is connected with its concentrations in aqueous or oil solutions corresponding to Raoult's law and Henry's law. Once the flavor is diluted in water, Henry's law states that the partial pressure of a particular component in the vapor above a solution is directly proportional to the component's concentration in that solution. This can be expressed as:

$$\rho = C \times N \qquad\qquad\qquad (1)$$

where ρ is the solute's partial pressure above the solution, C is a constant, and N is the molar fraction of the solute in the solution.

A convenient factor which follows Henry's law is the air/water partition coefficient. This is the ratio of the concentration of the solute in the vapor over its concentration in the solution at equilibrium:

$$\text{Air/water partition coefficient} = K = \frac{\rho}{N} \times 0.97 \times 10^{-4} \qquad (2)$$

where ρ is the partial pressure of the solute in the vapor and N is the concentration of the solute in the solution (1). Buttery presented the calculated air/water partition coefficient and plot volatilities against carbon number for homologous series of paraffin, ethers, ketones, alcohols, and acids in diluted water solution. Their calculation showed an increase in volatility with increasing carbon number, for several homologous series. Table II shows the air/water partition coefficient of a series of normal aliphatic alcohols.

Table II. Air/Water Partition Coefficients of Normal Aliphatic Alcohol at 25°C (Reprinted from ref. 1)

Alcohol	Air/Water Partition Coefficient
Methyl	1.8×10^{-4}
Ethyl	2.1×10^{-4}
Propyl	2.8×10^{-4}
Butyl	3.5×10^{-4}
Pentyl	5.3×10^{-4}
Hexyl	6.3×10^{-4}
Heptyl	7.7×10^{-4}
Octyl	9.8×10^{-4}

II. Flavor Emulsion

In many flavor applications, flavors in oil form are required to be dispersed in water to flavor beverages or gravies. To assure homogeneous distribution of the flavor in a product

which has a high viscosity, high speed mechanical mixing is required to distribute the flavor in the product. When the food product is low in viscosity or watery, the oil form flavors are usually first made into an emulsion by the addition of an emulsifier with or without a stabilizer. The emulsifier reduces the intersurface tension of the system and facilitates the homogenization. The addition of a stabilizer increases the viscosity of the water phase to slow down the movement of oil droplets. A hydrocolloid is usually used as the stabilizer in the water phase. In some applications a solute is also added to the water phase to reduce the water activity to control the microbiological stability.

Beverage flavor emulsions are a unique class of flavor emulsions. These emulsions are different from other flavor emulsions in that they are used in a highly diluted form. Good stability is required in both the original concentrated emulsion and the diluted form (2). Citrus oil base flavors are commonly used in these emulsions for preparing citrus flavored beverages. Citrus oils are not water miscible and have a density lower than water. Because of these two natural physical properties it is impossible to add the citrus oil flavors directly into water, especially into sugar sweetened beverages. under these conditions, separation of the oils from water is inevitable due to the density difference. For this type of flavor oil applications, the flavor oils have to be made into an oil-in-water (O/W) emulsion which is water dispersible. If the flavor oil emulsion is not properly formulated and processed, instability may incur. The instability of flavor emulsions can be observed in three stages as described in the following:

1. **Creaming** - At this stage, it can be considered as a separation of the emulsion into two emulsions. The upper portion is richer in the oil phase than the original emulsion, and the lower portion is richer in the water phase.

2. **Flocculation** - It occurs when oil droplets of the dispersed phase form aggregates or clusters without coalescence. At this stage, the droplets still retain their original identities.

3. **Coalescence** - In this stage, there is localized disruption of the sheaths around neighboring droplets of the aggregates, and the oil droplets merge together to form a large droplet. It eventually leads to the breakdown of the emulsion.

To prepare a stable beverage flavor emulsion, the following principles have to be observed at both the concentrated and diluted states of the emulsion:

Stokes' law - This law rules the basic performance of the emulsions:

$$v = \frac{2 \, g \, r^2 \, (\rho_1 - \rho_2)}{9 \, \eta_2} \qquad (3)$$

In Eq. (3), v is the rate of oil droplets separation (creaming), g is the acceleration of gravity, r is the droplet radius, ρ_1 is the density of the oil phase, ρ_2 is the density of the water phase, and η_2 is the viscosity of the water phase. Stokes' law shows that the velocity of a droplet, v, is directly proportional to the density difference between the oil phase and the water phase, and to the square of the radius of the droplet. It is also inversely proportional to the viscosity of the water phase, η_2. The equation clearly shows that the approaches to make a stable emulsion in beverages are to reduce the density difference between the oil phase and the water phase as close to zero as possible, and to make the

particle size as small as possible. The viscosity of the water phase is related to the sugar concentration in water and is considered as a constant.

Electrostatic Interaction - In an oil-in-water emulsion, dispersed oil droplets may acquire electric charge through the ionization of an adsorbed surface charged group. In beverage emulsions, gum Arabic is often used in the water phase. Gum Arabic is an acidic polysaccharide. The carboxyl group (COO-) ions are at the periphery of the molecule and are very active in creating an anionic environment (*3,4*). Surface charge may also be acquired through the adsorption of dissolution of small ions in the water phase. Oppositely charged ions are preferentially attracted towards the surface and ions of the same charges are repelled from the surface. The region of unequal counter-ion and co-ion concentrations near the charged surface is called the electrical double-layer. At some point out in the double layer region, corresponding more or less to the potential at the zone of shear, the electrical potential is called zeta potential. The determination of zeta potential is important in the study of the stability of emulsions. It is an important parameter for both achieving emulsion stability and destroying emulsion stability.

Adsorption at Interfaces - It has been known for many years that gum Arabic solution produces a visco-elastic film at the oil-water interface (*5*). Other hydrocolloids, such as modified starch, are attracted to the oil-water interface and form a film about the oil droplets (*6*). The formation of the interfacial film by hydrocolloid polymers on the oil droplets also help to stabilize the emulsion. It is the hydrocolloid material adsorbed on the surface of the oil droplets that prevents oil droplets from coalescing and forming larger droplets. Coalescence may eventually lead to emulsion break down. It may be described as the adsorbed materials keeping the droplets far enough apart such that the van der Waals attraction force is minimized (*7*).

In many classic emulsions where emulsifiers are used, the emulsifiers are adsorbed on the interfaces of oil droplets as a closely packed monomolecular film and reduce the surface tension (*8,9*). Once the surface tension is reduced, the oil droplets can be broken down to small size particles. Thus, the emulsion will be more stable.

Another contribution of the surface adsorption to the emulsion stability is that the adsorbed film on the droplets also provides an additional weight to the droplets as a whole. The smaller the particle the larger the gain of the weight from the surface adsorption to the droplet. Applying Stokes' law, the weight increase reduces the density difference between the oil droplets and the water phase and thus, increases the emulsion stability (*10*).

III. Flavor Microemulsion

Flavor microemulsions are mostly used in clear mouth washes and clear beverages (*11,12*). Microemulsions can be defined as the clear, thermodynamically stable dispersion of two immiscible liquids, oil-in-water or water-in-oil. They are formed spontaneously and stabilized by an interfacial film of one or more surfactants (*13*). The selection of the components and amounts of the surfactants are very critical in order to produce the stable microemulsion. That is, a stable microemulsion is very specific in the ratio of surfactant/cosurfactant used to disperse A in a continuous phase B. Usually a phase diagram design of the components is followed to prepare a microemulsion as shown in Figure 1 (*14*).

There are many distinct differences between microemulsions and conventional emulsions or macroemulsions. Microemulsions form spontaneously or with only slight agitation and are thermodynamically stable, assuming there are no changes in composition, temperature or pressure. On the other hand, macroemulsions require vigorous agitation to form and, although they may be stable for long period of time, eventually phase separation occurs as the system tries to attain a minimum free energy. The droplets of macroemulsions have minimum diameter of 0.15 to 100 μm. and microemulsions have diameter of 1.5 nm to 0.15 μm with many only slightly larger than micellar system. Therefore, microemulsions are clear, while macroemulsions are turbid and often milky dispersions (*15*). In term of thermodynamic properties, the formation reaction of microemulsions are entropy-driven and thus it is quite different from the formation of macroemulsions (*16*). These differences are summarized in Table III.

Table III. Characterization of Emulsions and Microemulsions (Source: Adapted from ref. 17)

	Emulsion	Microemulsion
Appearance	Turbid	Transparent
Droplet size, μm radius	0.15-100	0.0015-0.15
Formation	Mechanical or chemical energy added	Spontaneous
Thermodynamic stability	No	Yes (No)

The free energy of micellization is a balance of the free energy change associated with the transfer of the surface hydrophobic tail from water to the micellar core and the free energy associated with the electrostatic charge repulsion of the polar head groups at the micelle-water interface. Therefore, microemulsions are very stable (18).

IV. Spray Drying

Spray drying is one of the most popular methods to prepare powder flavor products from liquid flavors and to encapsulate flavors for controlled release purposes (*19*).

Spray drying involves three basic steps: 1) preparation of a carrier or protective matrix solution, 2) mixing the flavor into the carrier solution and homogenizing to make an emulsion, 3) atomization of the emulsion into the drying chamber to evaporate away the water from the water phase of the emulsion droplets.

The important factors to the flavor industry are the flavor oil loading level, retention and the stability of the flavor oil in the dried powder, and the rate of solution of the powder in water. Generally, the oil content in the powder is 20%. The loading and the stability of the flavor oil in the spray dried powder are closely related to the property and quality of the

flavor oil/carrier emulsion (*20*). The principles for achieving flavor emulsion stability as discussed in the section on Emulsions also apply here to the flavor emulsion for spray drying. It is important to have a stable emulsion to prevent oil separation from the emulsion before and during spray drying. Higher oil retention in the spray dried powder are obtained from a well made stable emulsion where the oil droplets are small. Flavor oil stability in the spray dried powder depends very much on the carrier properties, however, when same carrier is used, the smaller the oil particles the better the flavor oil stability in the powder. Reineccius has made an extensive review on the various factors which influence the quality of spray drying flavor products (*21*).

In flavor spray drying, usually the flavor consists of many components. The flavor emulsion spray drying process is not as straightforward as evaporating water in spray drying of foodstuffs. During flavor spray drying, each of the flavor components in the flavor behaves differently inside the emulsion particles. They have different vapor pressures, boiling points, latent heats of vaporization, specific heats of liquid and vapor. They may have different partition coefficients between the flavor solvent and the water of emulsion. Table IV shows the partition coefficient difference of the flavor components of an artificial cherry flavor. Some of the flavor components may even form azeotropes with water of the emulsion. Because of the different physical properties of the flavor components, some of the flavor components will be lost to some degree during spray drying. This is why a spray dried flavor always has a slightly different flavor profile from the original flavor.

Table IV. Partition Coefficient of Components of Artificial Cherry Flavor

Gram	Ingredients	Partition Coefficient
1.75	Eugenol	2.595
4.50	Cinnamic aldehyde	1.875
6.25	Anisyl acetate	1.430
9.25	Anisic aldehyde	2.200
12.50	Ethyl heptanoate	3.410
15.50	Benzyl acetate	1.725
25.00	Vanillin	2.295
25.00	Aldehyde C16	2.751
37.25	Ethyl butyrate	1.790
50.00	Amyl butyrate	3.280
125.00	Tolyl aldehyde	2.150
558.00	Benzaldehyde	1.485
130.00	Ethyl alcohol, 95%	-2.100

Thijssen and Rulkens studied the quantitative aspects of this problem (*22*). They proposed a "Selective Diffusion Theory". They found that the retention of volatile

compounds in spray dried foods is much higher than would be expected only from equilibrium considerations. They attributed this to the rate limiting effect of liquid-phase diffusion of the volatile compounds to the droplet surface. As the water concentration decreases, the diffusion coefficient of these compounds decrease more rapidly than that of water. Below a certain water content the outer layers of the drying droplet become impermeable to the volatile compounds, while still selectively transmitting water.

Further works by Rulkens and Thijssen found an increase in the retention of volatile compounds with increasing dissolved-solids content of the feed emulsion (*23*). The effect of dissolved-solids content can be interpreted through the selective diffusion theory.

Very extensive studies on spray drying on the concentration of solute, retention of volatile and on conditions of dehydration, cooling have been reviewed by Karel and Flink (*24*), Etzel and King (*25*), King et al (*26*) and Toei (*27*).

V. Spray Chilling

Spray chilling is also known as spray congealing. It is similar to spray drying in that both processes rely on formation of droplets containing a suspended material. The action of spray drying is primarily that of evaporation, while in spray chilling it is that of a phase change from a liquid to a solid. The difference between these two processes is the energy flow direction. In the case of spray drying, energy is applied to the droplets forcing evaporation of the media with both energy and mass transfer through the droplets. While in spray chilling, energy is removed from the droplet forcing the melted media to solidify (*28*). The equipment used are similar in principle and design. They are different in the temperature of the air used in the chamber and in the type of coating materials applied. Spray drying uses heated air to vaporize the solvent from the coating dispersion, and spray chilling uses ambient or chilled air to solidify a melted fat or wax coating. In spray drying, the coating materials are commonly low viscosity hydrocolloids. In spray chilling, the coating substance is typically hydrogenated vegetable oils and high melting point edible waxes with melting points in the range of 42° to 90° C.

Spray chilling has been used primarily for the encapsulation of solid food additives, and solid flavors, as well as for moisture sensitive materials. Liquid and water containing flavors may also be encapsulated following their conversion to semi-solid or pasty form (*29*). Liquid flavors which are miscible with the fat may be converted into powder form. The flavor liquid is occluded or trapped in the crystallized fat particles. The end products of spray chilling are water insoluble but release their contents by heat at the melting point of the coating materials. The process is suitable for protecting many water soluble materials including spray dried flavor powders.

Due to the nature of triglycerides, polymorphism plays an important role in spray chilling. Polymorphism may be described as the ability of a fat to exist in more than one crystalline modification. It is related to molecular configuration manifested physically by changes in density and melting point of the different polymorphs: $\alpha \rightarrow \beta' \rightarrow \beta$ (*30*). Figure 2 shows the transition between the liquid state and the various polymorphs of fat.

In spray chilling, rapid cooling of a melted fat produces crystals first in the alpha state, then at ambient temperature they change to beta prime, and ultimately to the most stable beta form. A differential scanning calorimetric curve of hydrogenated soybean oil during cooling is shown in Figure 3. These transformations are accompanied by changes
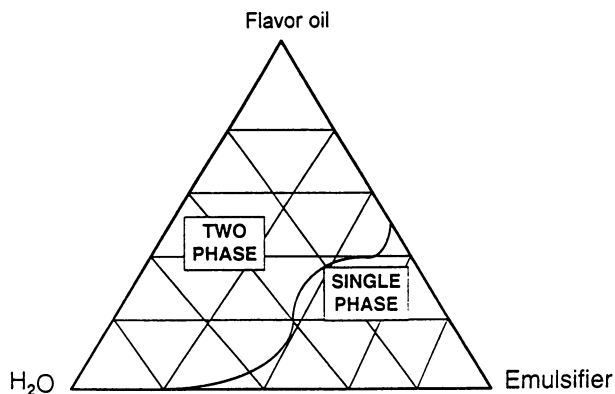
Figure 1. Phase Diagram: Flavor Oil/Water/Emulsifier at 25°C showing the single microemulsion phase region.
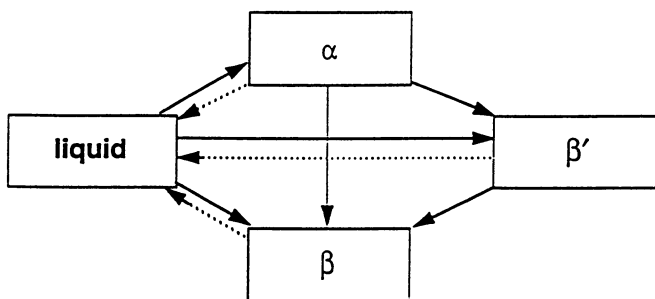
Figure 2. Possible transition between the liquid state and the various polymorphs of triglycerides. —— exthothermal, ········ endothermal transition. (Reprinted from ref. 33)

in density, and generation of heat.   Therefore, it is important to maintain optimum temperature during spray chilling in order to obtain the stable form of fat in the product. Aronhime studied the effect of additives on polymorphism of mixture of fats and reported that emulsifiers may act as a seeding agent and as a dynamic controller of polymorphic transformation (*31*).   Extensive reviews on the thermodynamic stability and crystallograph of lipid polymorphism were made by Sato (*32*), crystallization of fat, by Wasltra (*33*) and Timms (*34*), and fat crystal polymorphic transformation by Garti (*35*), and Aronhime (*36*).

Spray chilled flavor products release the flavor by heat, protect the flavor from moisture and prevent interaction with food ingredients.   They are used in bakery products, dry soup and gravy mixes and in microwaveable foods.

VI. Extrusion

The process of preparing encapsulated flavors by extrusion is different from the extrusion cooking and expansion of cereal products.   The process involves, first, premixing the flavor materials as the core material into a molten carbohydrate mass.   Then, extruding the mixture through a die into a bath of chilling medium to harden the molten carbohydrate. Finally, the extruded filaments are cut to proper size, washed, and dried.   The pressure used in this process is typically less that 100 psi with temperature about 120°C.

The basic concept of protecting an oxidation sensitive citrus oil in a molten carbohydrate mass was originated in 1956 by Schultz et al (*37*).   The industrial production process utilizing extrusion was developed by Swisher (*38,39*) and corn syrup solids (42 DE) was used as the encapsulating matrix.   Antioxidants, such as butylated hydroxyanisole was added to citrus oil to protect it during the high temperature mixing.   Emulsifiers were also added to facilitate the emulsification of the oil in the molten carbohydrates.   The flavor oil load in this encapsulated product is 8-10%.   To improve the hygroscopicity of the encapsulated flavor in corn syrup solids (42 DE) Beck (*40*) replaced the corn syrup solids with a combination of sucrose and maltodextrin (10 DE) in the ratio of 55% to 41%. Miller and Mutka (*40,41*) further modified the process with the use of sucrose as the encapsulation agent to reduce the hygroscopicity of the product.

The basic technology behind extrusion encapsulation of flavor oil in molten carbohydrate is straightforward.   Sucrose and most other sugars normally exist in the stable crystalline state.   By melting the crystals their regular structure is destroyed and when this is rapidly chilled, it becomes a clear transparent glass where the molecules of sucrose are set in an amorphous non-crystalline form.   The melting process is facilitated by addition of water, which reduces the inter-molecular forces holding the rigid crystalline structure intact and thus helps the formation of the liquid melt.   The water is behaving as a solvent but can also be considered as a plasticizer for extrusion (*42*).   Mixtures of sugars and other carbohydrates lose their crystalline structure at different temperatures depending on their composition and the proportion of water that is present.   When chilled rapidly, the molecules do not have time to reorganize themselves into crystals and the system locks them into a glassy amorphous state.   This glass is metastable and as such will revert to a less energetic, more stable form if molecular freedom becomes sufficient to allow crystals to form.   Thus, the critical point is reached by increasing the temperature allowing the trapped molecules to regain sufficient freedom of movement to crystallize.   This is usually referred to as the glass transition temperature, (Tg).   In general, when the product is in the glassy state, the lower the temperature relative to Tg, the more stable it will be.
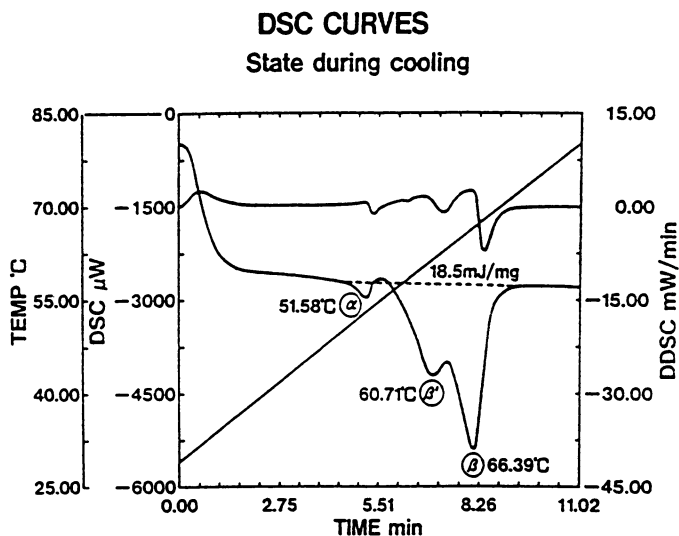
DSC CURVES
State during cooling

Figure 3. DSC curves of hydrogenated soybean oil during cooling state.

Chemical structure   **Molecular shape**
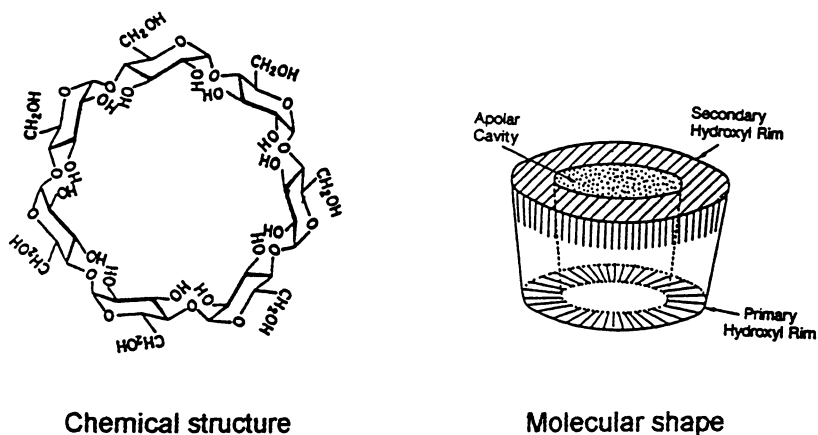
Figure 4. Chemical structure and molecular shape of β-cyclodextrin

The extrusion encapsulation in sugar glasses provides outstanding protection of the flavor against oxidation. A shortcoming is that it is a high temperature process. The flavors for encapsulation have to be subjected to 110-120°C for a substantial period of time. Extrusion encapsulated flavors are soluble in cold or hot water, making them suitable for use in a variety of food applications such as beverage mixes, cake mixes, dessert mixes, cocktail mixes and direct use in baked goods.

VII. Molecular Inclusion

Molecular inclusion of flavors is accomplished through the use of beta-cyclodextrin. A cyclodextrin glycosyl transferase enzyme (CGTase) acts on starch, producing alpha-, beta- and gamma-cyclodextrins, consisting, respectively, of six, seven, and eight glucose monomers bound together in a torus shaped ring. The molecular structure is relatively rigid and has a hollow cavity of a specific volume. Polar hydroxyl groups are oriented to the outside of the ring. The primary polar hydroxyl groups project from one outer edge, and the secondary polar hydroxyl groups from the other. While the outer surfaces have a hydrophilic nature, the internal cavity has a relatively high electron density and hydrophobic nature due to the hydrogens and glycosidic oxygens oriented to the cavity interior as shown in Figure 4.

Due to the hydrophobic nature of the cavity, molecules of suitable size, shape and hydrophobicity are able to interact to form stable complexes. For instance, a beta-cyclodextrin is able to form inclusion complexes with flavor substances of typical molecular mass between 80 and 250 (*44*).

As a rule the more hydrophobic the guest molecule, or more insoluble in water the more readily it will complex. That is, the molecules less soluble in oil will complex in preference. Complexes are normally less soluble than the cyclodextrin itself. The majority will crystallize out of solution at ambient temperature. The dry crystalline complex will not release its guest molecule unless it is either dissolved or heated above 200°C. (*45*).

The complex formation is affected by the following three factors:

1) loss of water from the inner surface of the torus accompanied by reduction in energy.

2) the ability of whole or part of guest molecule to fit into BCD torus.

3) the reduction of energy state on transfer of guest from solution to environment.

The binding forces contribute to the formation of cyclodextrin inclusion complexes in aqueous solution are summarized by Matsui et al (*46*) as follows:

1) hydrophobic interaction

2) van der Waals interaction

3) hydrogen bonding

4) the relief of high energy water from the cyclodextrin cavity upon substrate inclusion.

5) the relief of conformational strain energy in a cyclodextrin-water.

However, the importance of several of these binding forces are still controversial. The molecular, structural and the physical factors influencing the inclusion complexation of cyclodextrin can be found in the reviews prepared by Saenger (*47*).

Cyclodextrin inclusion provides flavor stability. It protects flavors from oxidation,

evaporation and light induced changes. However, there is a specificity of cyclodextrin. Small molecules are poorly retained by cyclodextrin while larger molecules are well retained. This variable retention property will result in an unbalanced flavor, typically lacking in the fresh light notes provided by the low molecular weight volatiles. However, essential oils, such as garlic and onion oils, and so on, may be completely retained in the complexes (*48*). Cyclodextrin is acceptable for food uses in several countries in Europe and Japan, but as of now it is not yet approved in the United States.

VIII. Adsorption

The adsorption of flavor liquid on fine powder to convert liquid flavor to powder form is an age old practice and is still in use. It is the "plating" process. The solid powder is called "carrier". Salt (sodium chloride), dextrose, sugar, maltodextrins and starches are commonly used as the carriers. This process is a pure physical action of solid-liquid intersurface tension and surface adsorption. Flavors commonly adsorbed on these carriers are oils containing no water or solvent which will hydrate starch and starch derivatives. To increase the adsorption capacity puffed micro bulb like maltodextrin and dextrin were produced by starch companies. The major disadvantage of plating oil on powders is excessive surface exposure to air which results in the loss of volatile flavor components and flavor oxidation.

Silicon dioxide or microparticulate silica and microsized edible fibers are another group of carriers used for flavor adsorption. The high porosity of these materials provides a large surface area for liquid adsorption. Since they are inert and water insoluble they are suitable for converting aqueous flavors to powder form. Water soluble flavors adsorbed on silica or fibers also exhibit flavor loss and oxidation but it is not as serious as with the oil flavors. However, flavor powders of some aqueous flavors with high water content will have microbial growth problem. Controlling water activity is important to prevent microbial growth. Bolton and Reineccius recently studied the oxidative stability and retention of a limonene-based model flavor plated on amorphous silica and other carriers (*49*). They reported that amorphous silicas are more effective flavor carriers in the plating process compared to the other traditional carriers. It is not clear how the silica influences limonene oxidation stability. It is possible that there are hydrogen bonding and hydrophobic interactions taking place in the adsorption of limonene on the silica surface.

In food application of amorphous silicon dioxide, the surface chemistry and ratio of silanol or hydroxyl group to siloxane groups, surface charge, pH, and hydrophilicity of the solvent media play an important role in the silica to give the desired functional properties. A very thorough review on the recent food applications and the toxicological and nutritional implications of amorphous silicon dioxide was given by Villota and Hawkes (*50*).

IX. Coacervation

Coacervation encapsulation is also called complex coacervation. It is a three steps process: 1) particles or droplets generation; 2) coacervative wall formation; and 3) capsule isolation. Each step involves a distinct principle of physical chemistry.

The principle of complex coacervation is mutual coagulation of positive and

negative hydrocolloid sols. The hydrocolloids commonly used are gelatin and gum Arabic. A typical complex coacervation encapsulation starts in first forming microsized flavor oil droplets dispersed in a hydrocolloid, such as gum Arabic, which is negatively charged. Then, gelatin solution is added to the dispersion with the pH of the system adjusted to below the isoelectric point of gelatin. At this pH, gelatin is positively charged. Coaservation of the two hydrocolloids takes place at this step and the oil is encapsulated by the coacervates. The capsule walls are insolubilized by the addition of glutaraldehyde or other crosslinking hardening agents. Finally, the microcapsules are washed and dried to a free-flowing powder form product. This type of flavor microcapsules are used mostly in the "Scratch and Sniff" strips. The food applications of coacervation encapsulated flavor is limited because of their limited number of crosslinking agents acceptable in food products. The principles of coacervation are well described by Versic (*51*).

X. Liposomes

The use of liposomes to deliver flavor is a very recent development. Liposomes are formed when phospholipid films hydrate and swell in an aqueous medium. Simple agitation produces large uncharacterized multilamellar bilayer vesicles of heterogeneous sizes. Multilamellar vesicles (MLV) are onion like structure with many lipid bilayers that are separated by fluid compartments. Unilamellar vesicles (UV) consist of a single fluid core, and they may be small (SUV) or large (LUV), ranging from 250 angstrom to several micrometers in diameter. Molecular cargo can be carried in different places within a liposome. Hydrophilic molecules are carried inside the core of the liposome, whereas hydrophobic molecules are embedded inside the lipid bilayer. Molecules with more complex chemical characteristics may be wholly or partly intercalated among the lipids in the bilayer. The use of liposome in flavor delivery is still limited. The short shelf-life of liposomes is a problem for flavor use at this moment. Progress in preserving liposomes has been reported (*52*). Nevertheless, it is a promising flavor delivery system.

XI. Cocrystallization

In cocrystallization of flavor in sucrose, the sucrose structure is modified from a single monoclinic spherical crystal to a microsized, irregular, agglomerated form. At this modified form, the void space and surface area are increased to provide a porous base for flavor incorporation. The process involves spontaneous crystallization, which produces aggregates of micro-crystals ranging from 3 to 30 nm while causing the inclusion of non-sucrose material within or between sucrose crystals (*53*). As an example, acetaldehyde fixed in sucrose is well known process in the flavor industry. The limitation of cocrystallization is that the encapsulated material is less than 0.5% by weight.

Conclusion

In the processing of flavor products for different specific uses, physical chemistry principle plays an important role in these processes. These processes have been successfully applied to produce a variety of flavor products. However, the physical chemistry principles involved in each of these processes is still not fully understood. Most of the research has

been carried out in model systems which have provided the valuable basic understanding of these processes. Research work using real compounded flavor systems will shed more light toward the progress of flavor product processing.

Acknowledgment

The author greatly appreciates the constructive comments on the preparation of this chapter by Dr. Ira Katz, Director of Research, International Flavors & Fragrances. Inc.

Literature Cited

1.   Buttery, R. G.; Bomben, J. L.; Guadagni, D. G.; Ling, L.C. *J. Agric. Food Chem.* **1971**, *19*, 1045.
2.   Tan, C. T.; Holmes, J. W. *Perf. Flavor.* **1988**, *13 (1)*, 1.
3.   Thevenet, F. In *Flavor Encapsulation*, Risch, S. J.; Reineccius, G. A. Eds.; ACS Symp. Ser. No. 370; American Chemical Society: Wahsington, D. C., 1988; p. 37.
4.   Silber, D.; Mizrahi, S. *J. Food Sci.* **1975**, *40*, 1174.
5.   Charma, S. C. *Food Technol.* **1981**, *35 (1)*, 59.
6.   Shotton, S. E.; White, R. F. In *Rheology of Emulsions,* Sherman, P. Ed.; Pergamon Press: Oxford, UK, 1963; pp 59-71.
7.   Trubiano, P. C. In *Modified Starches: Properties and Uses;* Wurzburg, O. B., Ed.; CRC Press: Boca Raton, FL, 1986; pp 131-147.
8.   Tardos, T. F. ; Vincenet, B.; In *Encyclopedia of Emulsion Technology;* Becher, P. Ed.; Marcel Dekker: New York, NY, 1983; Vol. 1, pp 1-56.
9.   Kaufman, V. R.; Garti, N. *J. Dispersion Sci. Technol.* **1981**; *2*, 475.
10.   Tan, C. T. In *Food Emulsions;* Larrson. K.; Friberg, S, Eds.; Marcel Dekker: New York, NY, 1990; p. 445.
11.   Chung, S. L. ; Tan, C. T.; Tuhill, I.; Scharpf, L. G. U. S. Patent No. 5,283,056, 1993.
12.   Wolf, P. A. U.S. Patent No. 4,835,002. 1989.
13.   Prince, L. M. *J. Soc. Cosmet. Chem.* **1970**, *21*, 193-204.
14.   Friberg, S. E. *J. Dispersion Sci. & Tech.* **1985**, *6*, 317.
15.   Jachowicz, J.; Berthiaume, M. D. *Cosmetics & Toiletries* **1993**, *108*, 65-72.
16.   Rosano, H. L.; Cavallo, J. L.; Huang, D. L.; Whittam, J. H. *J. Soc. Cosmet. Chem.* **1988**; *39*, 201.
17.   Friberg, S. E.; Kayali, I. In *Microemulsions and Emulsions in Foods*; El-Nokaly, M.; Cornell, D., Eds.; ACS Symp. Ser. No. 448; American Chemical Society: Washington, D. C., 1991; p 7.
18.   Cavallo, J. L.; Rosano, H. L. In *Food Flavors: Generation, Analysis and Process Influence*; Charalambous, G., Ed.; Elsevier Science B. V.: Amsterdam, The Netherlands, 1995; pp. 1101-1117.
19.   Dziezak, J. D. *Food Technol.* **1988**; *42 (4)*, 135.
20.   Risch, S. J.; Reineccius, G. A. In *Flavor Encapsulation*; Risch, S. J.; Resineccius, G. A., Eds.; ACS Symp. Ser. 370; American Chemical Society: Washington, D.C., 1988; pp. 67-77.
21.   Reineccius, G. A. *Food Rev. Internat.* **1989**, *5*, 147.

22. Thijssen, H. A. C.; Rulkens, W. H. *Delngenieur*. **1968**, *80*, 45.
23. Rulkens, W. H.; Thijssen, H. A. C. *J. Food Technol*. **1972**, *7*, 95.
24. Karel, M.; Flink, J. *Advances in Drying II*. Hemisphere Press: New York, NY, 1983; p.103.
25. Etzel, M. R.; King, C. J. *Ind. Eng. Chem. Process Res. Dev*. **1984**, *29*, 705.
26. King, C. J.; Kieckbusch, T. G.; Greenwald, C. G. In *Advances in Drying*; Mujimdar, A. S., Ed.; Hemisphere Press: New York, NY,1987; Vol. 3, 71.
27. Toei, R. In *Drying '86*; Mujumdar, A.S., Ed. Hemisphere Press: New York, NY,1986; Vol. 2, 880
28. Killeen, M. *Pharma. Eng*. **1993**, July/Aug. 56.

29. Tan, C. T.; Kang, Y. C.; Sudol, M.; King, C. K.; Schulman, M. U.S. Patent No. 5,064,669, 1991.
30. Wong, D. W. S. *Mechanism and Theory in Food*; Van Nostrand Reinhold: New York, NY, 1989.
31. Aronhime, J. S.: Sarig, S.; Garti, N. *J. Amer, Oil Chem.Soc*. **1988**, *65*, 1144-1150.
32. Sato, K. In *Food Microstructure*, Scanning Microscopy International, Chicago, **1987**, *6*, 151.
33. Walstra, P.; In *Food Structure and Behaviour*; Blanshard, J. M.; Lilliford, P. Eds.; Academic Press: New York, NY,1987; pp 67-85.
34. Timms, R. *Chem. & Ind*. **1991**, *5*, 342.
35. Garti, N.; Wellnerand, E.; Sarig, S. *J. Amer.Oil Chem. Soc*. **1982**; *59*, 181.
36. Aronhime, J.S.; Sarig, S.; Garti, N. *J. Amer. Oil Chem. Soc*. **1987**; *64*, 529-533.
37. Schultz, T. H.; Dimick, K. P.; Makower, C. *Food Technol*. **1956**, *10*, 57-60.
38. Swisher, H. E. U.S. Patent 2,809,895. 1957.
39. Swisher, H. E. U.S. Patent 3,041,180. 1962.
40. Beck, E. E. U.S, Patent 3,704,137. 1972
41. Miller, D. H..; Mutka, J. R. US Patent 4,499,122. 1985
42. Miller, D. H..; Mutka. J. R. US patent 4,610,890. 1986.
43. Blake, A. *IFI*. 1994, nr.3, 30-34.
44. Duxbury, D. *Food Processing*, 1990. Sept. 89.
45. Anonymous. *Food Technol*. **1988**, *42 (1)*, 96.
46 Pagington, J.S. *Perf. Flavor*. **1986**, *11 (1)* 49.
47. Matsui, Y.; Nishioka, T.; Fujita, T. In *Topic in Current Chemistry*; **1985**; *116*, 61.
48. Reineccius, G. A.; Risch, S. J. *Perf. Flavor*. **1986**, *11 (4)*, 1.
49. Bolton, T. A.; Reineccius, G. A. *Perf. Flavor*. **1992**, *17 (2)*, 1.
50. Villota, R.; Hawkes, J. G. CRC Criti. Rev. Food Sci. Nutr. **1986**, *23*, pp. 289-321.
51. Versic, R. J. In *Flavor Encapsulation*, Risch, S. J.; Reineccius, G. A.; Eds. ACS Symp. Ser. No. 370; American chemical Society: Washington, D.C., 1988, pp. 126-131.
52. Crowe, J. N.; Lois Crowe; M.; Carpenter, J.F. *Biopharm, Part 2*. **1993**, May , 40.
53. Chen, A. C.; Veiga, M. F.; Rizzuto, A. B. *Food Technol*. **1988**, *42 (11)*, 87.

Chapter 2

Kinetics of Formation and Degradation of Morpholino-1-*deoxy*-D-fructose

Alexis Huyghues-Despointes and Varoujan A. Yaylayan[1]

Department of Food Science and Agricultural Chemistry, McGill University, Quebec H9X 1C0, Canada

The kinetics of the reaction of glucose with morpholine to produce morpholino-1-*deoxy*-D-fructose (Amadori product) was studied under experimental conditions that minimize side reactions and maximize Amadori product formation (pH 3.0, T=100°C, 90% methanol-water, 6 hr). Glucose (0.1 M) was reacted in sealed vials with a series of morpholine solutions (0.1 - 0.3 M) and similarly morpholine (0.1 M) was reacted with different concentrations of glucose (0.05 - 0.2 M). At specific time intervals, the samples were analyzed for the presence of reactants and Amadori product by a multidetector HPLC system (diode array and pulsed amperometric detector). Under the experimental conditions, morpholine alone (in the presence of glucose equivalent of sorbitol) and glucose alone (in the presence of morpholine equivalent of triethylamine) did not degrade. Similarly, the degradation of Amadori product (0.02 M) was also studied in the presence of excess glucose. The data obtained were used to calculate the rate constants for the formation and degradation of Amadori product.

Kinetics of the early Maillard reaction (Scheme 1) can be divided for convenience into two phases; one, generating the Amadori rearrangement product (ARP) (rate of formation) and the other, reactions leading to its destruction (rate of loss). However, the measured concentration of ARP at any time is the concentration of accumulated Amadori product. The factors that complicate the kinetic analysis are the side reactions of amino acid and sugar, and the regeneration of amino acid from the Amadori product. Thus, the rate of loss of either sugar or amino acid does not necessarily indicate the rate of formation of ARP. General kinetic models have been proposed for the Maillard reaction by Debrauwer et al., (*1*), Vernin et al., (*2*), Baisier and Labuza (*3*) and Yaylayan and Forage (*4*). Most of these

---

[1]Corresponding author

models agree with a general scheme in which the reducing sugar (S) reacts with the amine (A) to produce a Schiff base which undergoes the Amadori rearrangement to produce the Amadori product (ARP), which itself degrades to a set of reactive compounds and free amines that recycle. In addition, the sugar may react with the Amadori product to produce diglycated Amadori products. These reactive intermediates then further react to produce fluorescent compounds and brown polymers.

The second order rate equation for the formation of ARP can be written as shown below:

$$\frac{\partial [ARP]}{\partial t} = k_o [S][A]$$

However, the observed or measured rate of the formation of ARP (which will be referred to as the rate of accumulation) is given by the following rate law:

$$\text{Rate of accumulation} = \frac{\partial [ARP]}{\partial t} = k_o[S][A] - k_{1+2}[ARP] - k_n[ARP] - \cdots$$

where, k_1, k_2 and k_n are the rate constants for different decomposition reactions of Amadori product.
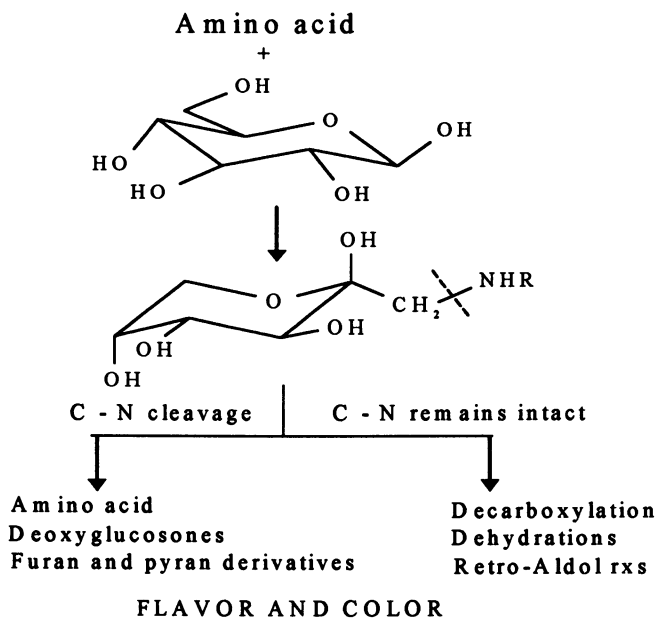
Generally, the rate constants of reactions that follow second order kinetics of the type shown below, depend on the initial concentrations of the reactants and the first order rate loss of each reactant will increase when the concentration of the second reactant is increased.

$$\frac{\partial [X]}{\partial t} = k[A][B]$$

This has been observed at 37°C in the reaction of glycine with glucose (*3*). However, at 60 °C, Vernine et al (*2*) using computer simulated kinetic analysis of data obtained from the reaction of glucose with three different amino acids have observed that irrespective of the initial ratio of the reactants the observed rate of glucose disappearance was always faster than the amino acids (except proline), if these results can be trusted it may mean glucose is undergoing other side reactions (such as forming diglycated products and amino acid catalyzed decompositions) more extensively than amino acids and that the rate of amino acid release from Amadori product is not negligible. In addition, the rate of sugar loss was also depended on the type of amino acid. Glucose disappeared ten time slower in presence of proline than in presence of valine or methionine, however, this rate was approximately the same as the rate of loss of proline at various sugar to

proline ratios between 50 and 65°C (which can be explained by the fact that proline being a secondary amine its ARP cannot react with glucose). However, the thermal degradation of the Amadori product of methionine and proline was much slower (10,000 time slower) compared to valine (*1,2*).

Glucose was reacted in sealed vials with a series of morpholine solutions and similarly morpholine was reacted with different concentrations of glucose. At specific time intervals, the samples were analyzed for the presence of reactants and Amadori product by a multidetector HPLC system (diode array and pulsed amperometric detector). The preliminary analysis of the kinetic data of the reaction between glucose and morpholine to produce morpholino-1-*deoxy*-D-fructose (Amadori product) is presented here. Statistical analysis will be reported elsewhere.

Amino acid
+

OH

HO

HO   OH

OH

O

CH₂   NHR

OH

OH

OH

C - N cleavage   C - N remains intact

Amino acid   Decarboxylation
Deoxyglucosones   Dehydrations
Furan and pyran derivatives   Retro-Aldol rxs

FLAVOR AND COLOR

Scheme 1. General scheme of Maillard reaction

MATERIALS AND METHODS

Reagents and Chemicals.

All reagents were purchased from Aldrich Chemical Company (Milwaukee, WI). HPLC solvents were filtered and degassed (ultrasound/vacuum) prior usage. The Amadori compound of morpholine was purchased from Sigma Chemical Company (St. Louis, MO).

Kinetic Runs

D-glucose (0.05 M - 0.2 M, final concentrations) and morpholine (0.1 M - 0.3 M, final concentrations) solutions (pH $\cong$ 3, adjusted with phosphoric acid) in 90 % methanol/water (see Table I for relative ratios) were incubated in sealed tubes at 100°C for 6 hr. The progress of the reaction was monitored at specific time intervals. Glucose degradation alone was performed in the presence of triethylamine and morpholine degradation alone was performed in the presence of sorbitol (both solutions were at pH $\cong$ 3, adjusted with phosphoric acid). The results represent the average of doublicate analysis.

TABLE I. Final concentrations (M) of reactants in different kinetic runs

Experiment product	Sugar	Amine	Amadori
a	0.1	0.1	0
b	0.1	0.2	0
c	0.1	0.3	0
d	0.2	0.1	0
e	0.05	0.1	0
f	0.1	0	0.02
g	0.1[*]	0	0
h	0	0.1[**]	0

*in the presence of triethylamine, ** in the presence of sorbitol*

HPLC Analysis

Concentrations were determined by a multidetector HPLC system (*5*) which consisted of a programmable solvent module (Beckman, system GOLD, module 126), a diode array detector (Beckman, system GOLD, module 168), an analog interface (Beckman, system GOLD, module 406), and a programmable

electrochemical detector (Hewlett Packard, model 1049A). Glucose was measured by pulsed amperometric detector (PAD) at a gold electrode (E_2 = +0.650 V, t_2 = 50 ms; E_3 = -1.050 V, t_3 = 50 ms; E_1 = +0.10 V, t_1 = 200 ms; vs. Ag/AgCl reference electrode with internal electrolytes). Morpholine and Amadori morpholine were measured by diode array detector, set to monitor the 190 nm to 460 nm region. The carbohydrate dedicated column of Waters (10 mm; 4.6 mm x 30 cm) was used. The mobile phase consisted of 70 % acetonitrile and 30 % phosphate buffer (0.04 M, pH 2.9). The flow rate was set at 1 mL/min.

RESULTS AND DISCUSSION

The mechanism of the reaction of reducing sugars with amino acids and subsequent decomposition of the Amadori product is a complex process which depends primarily on the reaction conditions such as temperature, time, water content and the relative ratio of the reactants and their concentrations. In the context of the kinetic analysis certain assumptions should be made regarding the mechanism in order to simplify the mathematical calculations. The assumption that sugar and amino acid alone do not undergo decomposition in our model system consisting of glucose and morpholine holds true under the experimental conditions as verified by heating these reactants separately (see Table I, runs g and h).

The general kinetic model for the reaction of glucose with morpholine as proposed in Scheme 2, stipulates formation of the Amadori product with a rate constant of k_0 and subsequent decomposition by two pathways one initiated by C-N bond cleavage to regenerate the amino group with a rate constant of k_1 and the other decompositions without C-N bond cleavage with a rate constant of k_2.

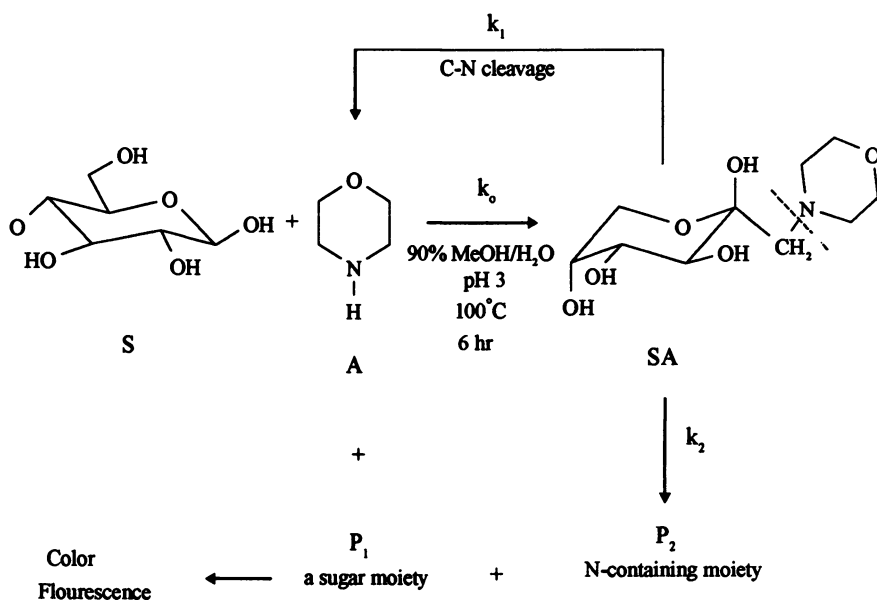### Glucose - morpholine reaction kinetics

In order to calculate the rate constants k_0, k_1 and k_2, it was assumed that at any time $t = t_1$, x moles of sugar react with x moles of amine to produce x moles of Amadori product (SA). A certain fraction of SA (rx moles) decomposes to regenerate the amine, and r'x moles decompose through other pathways (0 < r and r' < 1) therefore:

$$\text{at} \quad t = t_1 \qquad S = (S_0 - x); \quad A = (A_0 - x + rx); \qquad SA = (x - rx - r'x)$$

where S, A and SA are the measured concentrations of sugar, amine and the Amadori product respectively.

By solving simultaneously the above three equations with three unknowns, the following values for x, r and r' can be obtained with either known or experimentally measured values:

$$x = S_0 - S, \qquad r = \frac{A_0 - A + S - S_0}{S - S_0}, \qquad r' = 1 - r - \frac{SA}{S_0 - S}$$

$$k_1$$

C-N cleavage

$$k_o$$

90% MeOH/H_2O
pH 3
100°C
6 hr

S   A   SA

$$k_2$$

+

$$P_1$$ $$P_2$$

Color
Flourescence ← a sugar moiety + N-containing moiety

Kinetic Model

Scheme 2. General kinetic model for the reaction of glucose with morpholine

where S_o and A_o are the initial concentrations of sugar and amine respectively. Knowledge of the fraction of Amadori product undergoing C-N cleavage (rx) and other fragmentations (r'x) under specific conditions, allows the evaluation of their relative importance and contribution to the overall aroma profile. Such analysis can eventually lead to controlled production of Maillard reaction mixtures, enriched with specific types of products for flavor application purposes.

Under the experimental conditions, the absolute value of the rate of loss of sugar is equal to the rate of formation of Amadori compound, and the differential rate law for the second order reaction is given by the following equation:

$$\frac{\partial[x]}{\partial[t]} = -ko[So - x][Ao - x]$$

Solving the above equation will generate the rate law for second order reactions as shown below:
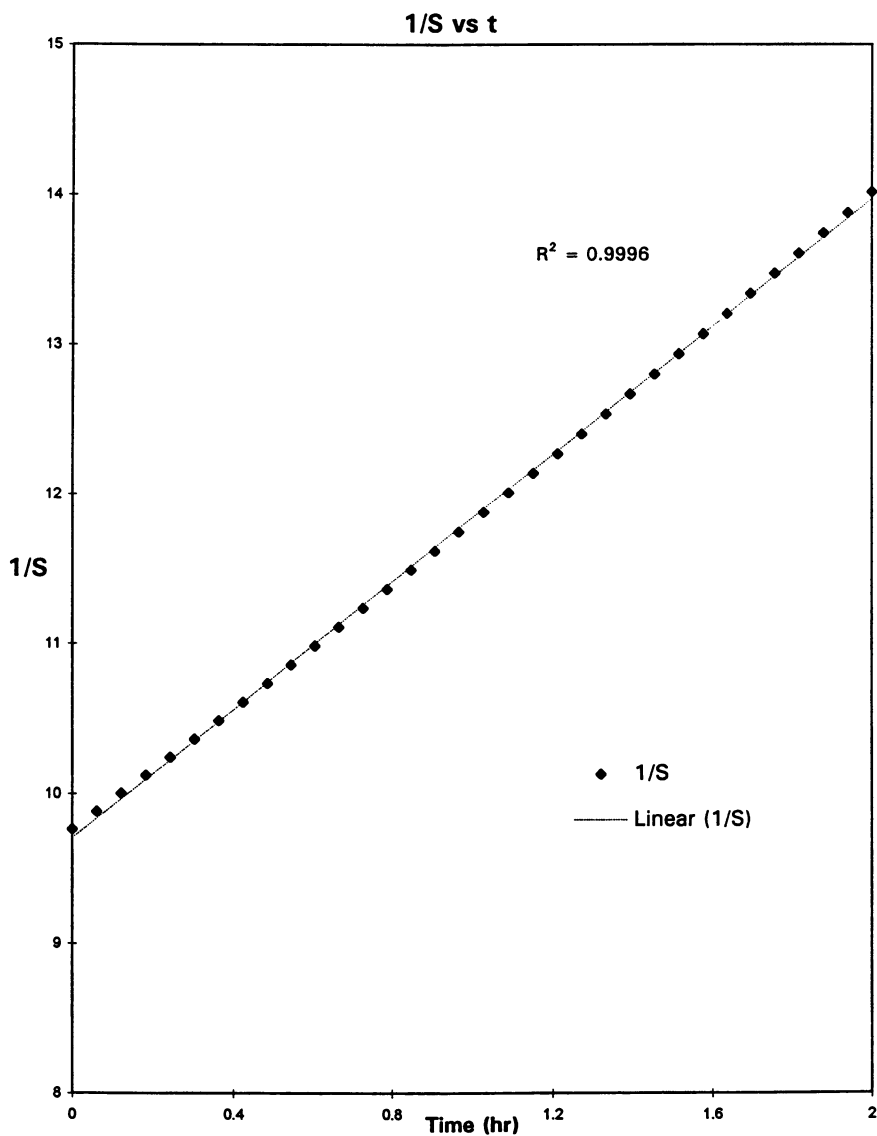
1/S vs t

Figure 1. Plot of 1/S vs time for model system of glucose : morpholine (1:1 molar ratio)

$$\frac{1}{S} = \frac{1}{So} + ko\,t$$

If the reaction is indeed second order then plotting 1/S vs. t will be a straight line with a slope of k_o and intercept $1/S_o$. Figure 1 shows the plot of 1/S vs. t for the sugar/amine ratio of 1:1. Table II lists the calculated initial rates for other model systems in which the ratio of reactants is not 1:1, using the following equation (*6*):

$$\frac{1}{b - ra}\left\{\ln\left(\frac{a}{a - x}\right) - \ln\left[\frac{(b\,/\,r)}{(b\,/\,r) - x}\right]\right\} = kt, \quad r \neq 1$$

where, r is the ratio of reactants, a and b are the initial concentrations of the reactants and x is the number of moles/liter of reactant which have reacted at time t. The data obtained indicate that the reaction of glucose with morpholine to form Amadori product follows second order kinetics and that highest amount of Amadori product was accumulated when the starting amine concentration was three times in excess to that of glucose. A detailed statistical analysis of the data will be published elsewhere.

TABLE II. Calculated initial rate constants (0 - 2 h)

System	k_0 ($M^{-1}h^{-1}$)	k_1 (h^{-1})	k_2 (h^{-1})	R^2
3A : 1S	1.2			0.9987
1A : 2S	0.6			0.9981
1A : 1S	2.1			0.9996
1A : 0.5S	1.0			0.9999
2A : 1S	0.8			0.9927
5S: 1SA		0.35	0.32	

S = glucose; A = morpholine; SA = Amadori product

Kinetics of decomposition of morpholine Amadori compound

To calculate k_1 and k_2 the rate constants for the different decomposition pathways of the Amadori product, the decomposition of the morpholino-D-fructose (final concentration of 0.02 M) was studied under the same reaction conditions in five
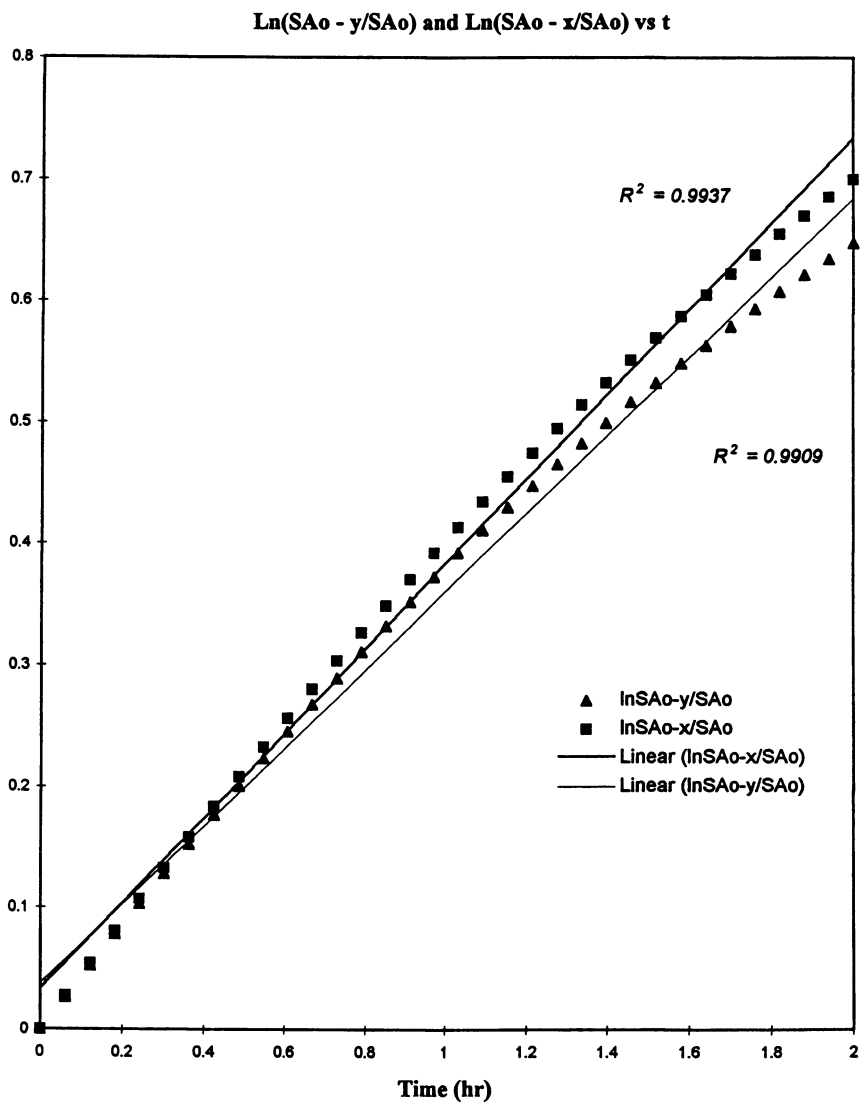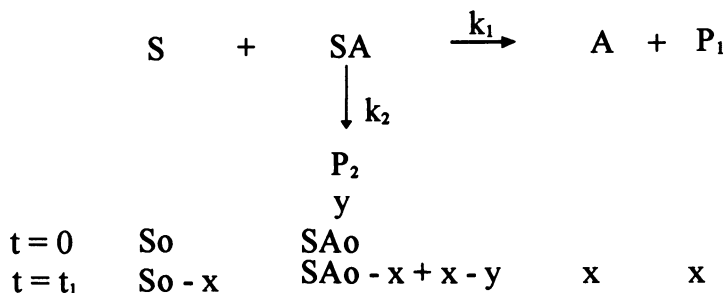
Figure 2. Plots of $Ln(SA_o - y / SA_o)$ and $Ln(SA_o-x / SA_o)$ vs time for morpholine Amadori : Glucose model system.

molar excess of glucose (final concentration of 0.1 M). Assuming that at any time $t = t_1$, x moles of the Amadori product decomposes through C-N bond cleavage and y moles through other pathways then the values for x and y can be calculated as shown below.

$$S \quad + \quad SA \quad \xrightarrow{\;k_1\;} \quad A \; + \; P_1$$

$$\downarrow k_2$$

$$P_2$$
$$y$$

t = 0	So	SAo		
t = t_1	So - x	SAo - x + x - y	x	x

During the reaction of Amadori product in the presence of excess glucose, the concentration of the sugar diminished, indicating a reaction with the amine, since it has been established that sugar alone, under the experimental conditions, do not decompose and that the Amadori product being a tertiary amine cannot react with the sugar. However, the concentrations of the amine produced through C-N cleavage were below the detection limits of the system, indicating that in the presence of excess sugar the released amine reacted quickly with the sugar to form Amadori product. Hence the measured concentration of the sugar (S) and measured Amadori concentration (SA) are given by the following equations:

$$S = So - x\,; \qquad\qquad SA = SAo - x + x - y$$

Rearranging these equations will yield the values for x = So - S, and for y = SAo - SA, where So and SAo are the initial sugar and Amadori concentrations respectively.

For a first order decomposition of Amadori product plotting $\mathrm{Ln}\,\dfrac{SAo - x}{SAo}$ vs. t should generate a straight line with a slope of k_1 similarly plotting $\mathrm{Ln}\,\dfrac{SAo - y}{SAo}$ vs. t should generate a straight line with a slope of k_2. Figure 2 shows the above plots during the initial two hour period. These plots deviate slightly from linearity at the later stages of the reaction due to the regeneration of the Amadori product. The calculated values for the decomposition rate constants (k_1 and k_2) from these plots are listed in Table II.

Conclusion

The kinetic data indicate that the reaction of morpholine with glucose to form the Amadori product follows a second order kinetics and that the relative importance of the decomposition pathway of the resulting Amadori product depends on the sugar amine ratio in the reaction mixture.

Acknowledgments

Literature Cited

1. Debrauwer, L.; Vernin, G.; Metzger, J.; Siouffi, A.M.,; Larice, J.L. *Bull. Soc. Chim. Fr.* **1991**, *128*, 244-254.
2. Vernin, G.; Debrauwer, L.; Vernin, G. M. F.; Zamkotsian, R-M.; Metzger, J.; Larice, J. L. and Parkanyi, C. In *Off-flavors in foods and beverages*, Charalambous, G., Ed.; Elsevier, 1992; pp. 567-623.
3. Baisier W.M.; Labuza, T.P. *J. Agric. Food Chem.*, **1992**, *40*, 707-713.
4. Yaylayan, V.; Forage, N. *Food Chem.* **1992**, *44*, 201-208.
5. Huyghues-Despointes, A.; Yaylayan, V. *Food Chem.* **1994**, *51*, 109-117.
6. Castellan, G. W. In *Physical Chemistry*, Addison-Wesley, 1973; pp. 738-739.

Chapter 3

Kinetics of the Formation of Oxygen-Containing Heterocyclic Compounds via the Maillard Reaction

B. S. Mistry, P. D. Wilson, and G. A. Reineccius

Department of Food Science and Nutrition, University of Minnesota, 1334 Eckles Avenue, St. Paul, MN 55108

The purpose of this study was to investigate the kinetics of formation of seven oxygen-containing heterocyclic compounds via the Maillard reaction. Several variables relating to the composition of the model system were examined. These include the influence of using a phosphate buffer vs no buffer and the amino acid used in the system. Both the buffer and the type of amino acid in the model system had an effect on the rates of formation of certain flavor compounds. Activation energies of the flavor compounds ranged from 25 to 59 kcal/mole.

Maillard browning is a complex reaction involving several steps leading to the production of important odor and color in foods. The contribution of the Maillard reaction to flavor is often studied by identifying the volatile products formed from a model reaction system of amino acid/s and a monosaccharide. Then the results are used to explain the formation of flavors in heated foods.

Classification of Flavor Compounds from Maillard Reactions

Nursten (*1*) classified aroma compounds produced in the Maillard reaction into three groups:
1. "Simple" sugar dehydration/fragmentation products:

    furans   carbonyl compounds

    pyrones   acids

    cyclopentenes
2. "Simple" amino acid degradation products:

    aldehydes

    sulfur compounds (eg. hydrogen sulfide, methanethiol)

    nitrogen compounds (eg. ammonia, amines)
3. Volatiles produced by further interactions:

    pyrroles   thiazoles

    pyridines   thiophenes

    pyrazines   di- and tri-thiolanes

    imidazoles   di- and tri-thianes

    oxazoles   furanthiols

    compounds from aldol condensations

Group 1 includes compounds formed by the breakdown of the glycosylamine in the early stages of the reaction. Group 2 comprises mostly of compounds from the Strecker degradation of amino acids and dicarbonyl compounds. All these Maillard products are capable of further reactions and interact with each other to give Group 3 of the Maillard aroma compounds.

The Maillard reaction is responsible for both pleasant (bread, popcorn, coffee, chocolate) and undesirable (staling of dry potatoes) flavors in foods. The differences between these desirable and undesirable flavors is partly due to the kinetics of formation of these aroma compounds. Although there have been studies on flavor formation via the Maillard reaction (2 - 5), most of these studies have been limited to postulating mechanisms for flavor formation or evaluating sensory characteristics of the compounds. There are not many studies which have focused on determining reaction kinetics of formation of flavor compounds via Maillard reaction. Once we understand the reaction kinetics of certain flavor compounds we can better control the production of desirable and undesirable flavors via the Maillard reacion.

The purpose of this paper was to obtain kinetic data of the flavor compounds formed in model systems via Maillard reaction. This paper will examine the variables related to the composition of the model system. These variables include the effects of phosphate buffer vs. no phosphate buffer and amino acids (glycine vs. cystine) in the model system on the formation of furans and pyranones via the Maillard reaction.

Materials and Methods

Four sugar-amino acid model systems were selected. Glucose (Sigma Chemical Co., St. Louis, MO) was used at 0.5 moles (90.00 g) and glycine or cysteine at 0.1 moles (7.51 g or 12.12 g, respectively). The four model systems were comprised of: glucose + glycine in 400 mL distilled water, glucose + glycine in 400 mL 0.1 M phosphate buffer, glucose + cysteine in 400 mL distilled water, and glucose + cysteine in 400 mL 0.1 M phosphate buffer. Phosphate buffer was prepared at 0.1 M and pH 7 (8). The ratio of sugar to amino acid was deliberately high because excess sugar would increase the rate of the Maillard reaction.

Initial temperature and pH of the reaction mixtures were recorded. Each of the four reaction mixtures was placed in a 600 mL Parr Bomb pressure reactor (Model Series 4563, Parr 4842, Parr Instruments Co., Moline, IL). The Parr Bomb was then sealed and the heating and stirring units were started. During the experiments, the stirrer was set at 60%. Five temperatures, 95, 105, 115, 125 and 135°C, were selected for the study. Six data points were selected for each temperature. The time at which the reactor system reached the desired temperature was time t = 0 for the experiment. At predetermined time intervals listed below for each temperature, 50 mL of the reaction sample was withdrawn from the pressure reactor via a sampling port. Heating times for the samples were chosen to avoid buildup of carbon in the reactor as it took a long time to clean it off.

Temp. (°C)	Time Intervals for Sample Withdrawal from the Parr Bomb (min)
95	120, 180, 240, 300, 360, 420
105	30, 60, 90, 120, 150, 180
115	20, 40, 60, 80, 100, 120
125	5, 10, 15, 20, 25, 30
135	5, 10, 15, 20, 25, 30

After cooling the withdrawn sample to 25°C, the pH was measured. The sample was then extracted in a 125 mL separatory funnel three times with 5 mL aliquots each of methylene chloride containing 45 ppm of octane as an internal

standard. The lower layer containing the methylene chloride extract was then dried with anhydrous magnesium sulfate, filtered and concentrated under a nitrogen flow to ca. 0.5 mL.

Gas Chromatography. The flavor extracts were run on a 5890A HP gas chromatograph (Hewlett Packard, Avondale, PA) equipped with a flame ionization detector. A 1.0 μm film thickness DB-5 fused silica capillary phase column (J&W Scientific, Folsom, CA), 30 m x 0.32 mm i.d. was used. The temperature program used for the analyses was 40°C, temperature held for 1 min., ramped 5°C/min. to 250°C and held at 250°C for 10 min. The column pressure was 15 psig. A 20:1 split was used. Sample size injected was 2 μL. Helium was used as a carrier gas.

Compound identification was carried out by cochromatography with authentic compounds (except for 5-methyl-2 (3H)-furanone and di (H) di (OH) 6-methyl-pyranone which were identified by mass spectrometry).

Mass Spectrometry. The compounds were identified by mass spectrometry using a 5890A HP gas chromatograph interfaced with a 5970 HP (Hewlett Packard, Avondale, PA) mass selective detector. The capillary column was interfaced directly into the mass selective detector operating at 70 eV ionic potential with an ion source temperature of 220°C and a scan threshold of 750, scanning from m/z 29 to 400 at 0.86 s/cycle. The gas chromatographic conditions were the same as above, column head pressure was 7 psig. Mass spectra were compared with those on the NBS and flavor libraries.

Data Analysis. Since the flame ionization detector of the gas chromatograph responds differently to different compounds, the response factor of the compounds of interest was compared and corrected against that of the internal standard to give the quantities of each compound (ppm in the reaction mixture). The data obtained for 5-methyl-2 (3H)-furanone and di (H) di (OH) 6-methyl-pyranone were normalized with respect to the internal standard, octane.

The Macintosh program, "Water Analyzer Series - Reaction Kinetics Program" (9) was used for calculation of reaction rate constants (k, ppm min^{-1}) and activation energies (E$_a$, kcal/mole) at 95% confidence limits. This program is based on the equations from kinetic rate determinations using the integral method (10). The equations used in the program have been discussed by Labuza (10) and Labuza and Kamman (11). For a zero order reaction, a plot of formation of flavor compounds (ppm) vs reaction time (min), would yield a straight line, the slope of which would be the reaction rate constant, k (ppm min^{-1}). One can compare the statistical significance of the rate constants between the experimental conditions by doing linear regression on the data over time for a large change in concentration and calculating the 95% confidence limits of the slope (10). In comparing the rate constants, if their confidence limits do not overlap, the rate constants are statistically different over that time period for that 95% confidence limit.

The observed temperature dependence of the Maillard browning reaction was modelled using the Arrhenius concept of interrelating reaction rate constant with temperature. The Arrhenius relation is $k = k_0 e^{-Ea/RT}$; where k = reaction rate constant, k_0 = preexponential constant, E_a = reaction activation energy, T = absolute temperature and R= gas constant. A semi-log plot of k (log scale) vs 1/T gives a straight line with a negative slope of E_a/R.

Results and Discussion

Seven oxygenated heterocyclic compounds formed from the model system via Maillard reaction were chosen for the study. These compounds were furfural, furfuryl alcohol, 2-acetylfuran, 5-methylfurfural, 5-(hydroxymethyl) furfural, 5-methyl-2 (3H)-furanone and di (H) di (OH) 6-methyl-pyranone.

Effects of Buffer, Time and Temperature on pH of Model Systems. The initial pH of model systems in phosphate buffer was 7.00 ± 0.05. In the absence of phosphate buffer, the initial pH of the model systems was lowered, as expected. Initial pH of the glucose-glycine-water systems was 5.30 ± 0.1 and that of glucose-cysteine-water systems was 4.6 ± 0.1. Figures 1 and 2 show the change in pH of model systems over time with and without buffer at 105°C and 125°C.At any given temperature, the initial drop in pH of the system was greatest, then the pH decreased gradually. In the presence of buffer, the pH of the glucose-cysteine system decreased at a slower rate compared to the glucose-glycine system. In the absence of buffer in the glucose-cysteine system, the initial pH and pH at all reaction temperatures was lower than in the glucose-glycine system.

Formation of Flavor Compounds. Formation of all seven flavor compounds increased with time and temperature of the reaction. Generally, the concentration of 5-(hydroxymethyl) furfural was highest in model systems containing water. In model systems containing phosphate buffer, concentrations of di (H) di (OH) 6-methyl-pyranone and 5-(hydroxymethyl) furfural were generally the highest. Formation of flavor compounds was strongly dependent on reaction temperature, some compounds were not formed at 95 or 105°C. At low reaction temperatures of 95 and 105°C, there was formation of slight amount of furfural in the glucose-cysteine-water system; however, in the glucose-cysteine-buffer system, three to five flavor compounds (di (H) di (OH) 6-methyl-pyranone, 2-acetylfuran, furfural, 5-methylfurfural and 5-(hydroxymethyl) furfural) were formed. The type of amino acid in the model system (cysteine vs glycine) also affected the concentration of the seven flavor compounds. In the cysteine system, concentration of furfural was generally middle to lowest of the seven compounds; in the glycine system, furfural concentration was typically higher (after 5-(hydroxymethyl) furfural and di (H) di (OH) 6-methyl-pyranone). Hence, formation and concentration of flavor compounds was strongly dependent on temperature, type of amino acid and presence or absence of buffer in the model system. Reineccius (*13*) indicated that low reaction temperatures (eg. during storage) produce stale, gluey notes whereas high reaction temperatures produce roasted, toasted notes.

Kinetics of Model Systems Undergoing Maillard Reaction

Order of Reaction. Formation of the seven flavor compounds followed a pseudo zero order reaction (concentration vs time). The term "pseudo zero order" should be used because formation of Maillard products is not a single reaction but a culmination of many reactions with reactive intermediates that are extremely hard to quantify. The order plots did not have the intercept going through the origin. This may be due to trying to fit zero order to the model system when the actual reaction order is not known. This is also caused by some of the products being formed during the time it took the reactor to reach the desired reaction temperature.

Effect of Phosphate Buffer on Reaction Rate Constants. In the glucose-glycine model system, there was a definite impact of phosphate buffer on reaction rate constants, k (ppm min^{-1}), of flavor compounds. The rate constants of all flavor

compounds increased in the presence of phosphate buffer compared to the glucose-glycine-water system. This indicates that phosphate buffer enhanced formation of flavor compounds in the glucose-glycine system (Table I). Dihydrogen phosphate is known to act as a base, abstracting a proton during the Amadori rearrangement, resulting in an increase in rate of conversion of starting materials. Also, the conversion of the Amadori rearrangement products is increased, resulting in increased formation of flavor compounds (*12*). Table I compares the reaction rate constants in glucose-glycine systems at two temperatures, 95 and 125°C. Similar trends were observed at 105, 115 and 135°C.

Table I. Reaction Rate Constants, k (ppm min^{-1}), in Glucose-Glycine Systems

Temp (°C)	Compound	Glucose-Glycine-Buffer	Glucose-Glycine-Water
95	Furfural	$5.199e^{-3}$	$1.502e^{-3}$
	Furfuryl alcohol	$8.139e^{-3}$	$1.333e^{-4}$
	2-acetylfuran	$1.668e^{-3}$	$3.35e^{-4}$
	5-methylfurfural	$2.045e^{-3}$	*
	5-(hydroxymethyl)furfural	$9.455e^{-2}$	$1.303e^{-2}$
	5-methyl-2 (3H)-furanone	$1.577e^{-2}$	*
	di (H) di (OH) 6-methyl-pyranone	$3.881e^{-2}$	$3.75e^{-4}$
125	Furfural	$2.861e^{-1}$	$5.007e^{-2}$
	Furfuryl alcohol	$1.870e^{-1}$	$4.542e^{-3}$
	2-acetylfuran	$8.775e^{-2}$	$6.423e^{-3}$
	5-methylfurfural	$3.976e^{-2}$	$2.300e^{-3}$
	5-(hydroxymethyl)furfural	$6.848e^{0}$	$1.355e^{0}$
	5-methyl-2 (3H)-furanone	$1.065e^{-3}$	*
	di (H) di (OH) 6-methyl-pyranone	$1.430e^{0}$	$4.145e^{-2}$

* not enough data points to calculate k (ppm min^{-1})

In the glucose-cysteine-phosphate model system, at lower reaction temperatures of 95 and 105°C, the formation of flavor compounds was enhanced compared to glucose-cysteine-water systems (Table II). At higher temperatures, no trends were observed in the rate constants of flavor compounds in the glucose-cysteine model system.

Effect of Amino Acids on Reaction Rate Constants. The type of amino acid/s in model systems affected rate of formation of the flavor compounds. In model systems containing glycine, the reaction rate constants for all flavor compounds (except 5-methylfurfural in the water system) were consistently higher compared to the systems containing cysteine. This data shows that glycine enabled greater formation of flavor compounds compared to cysteine.
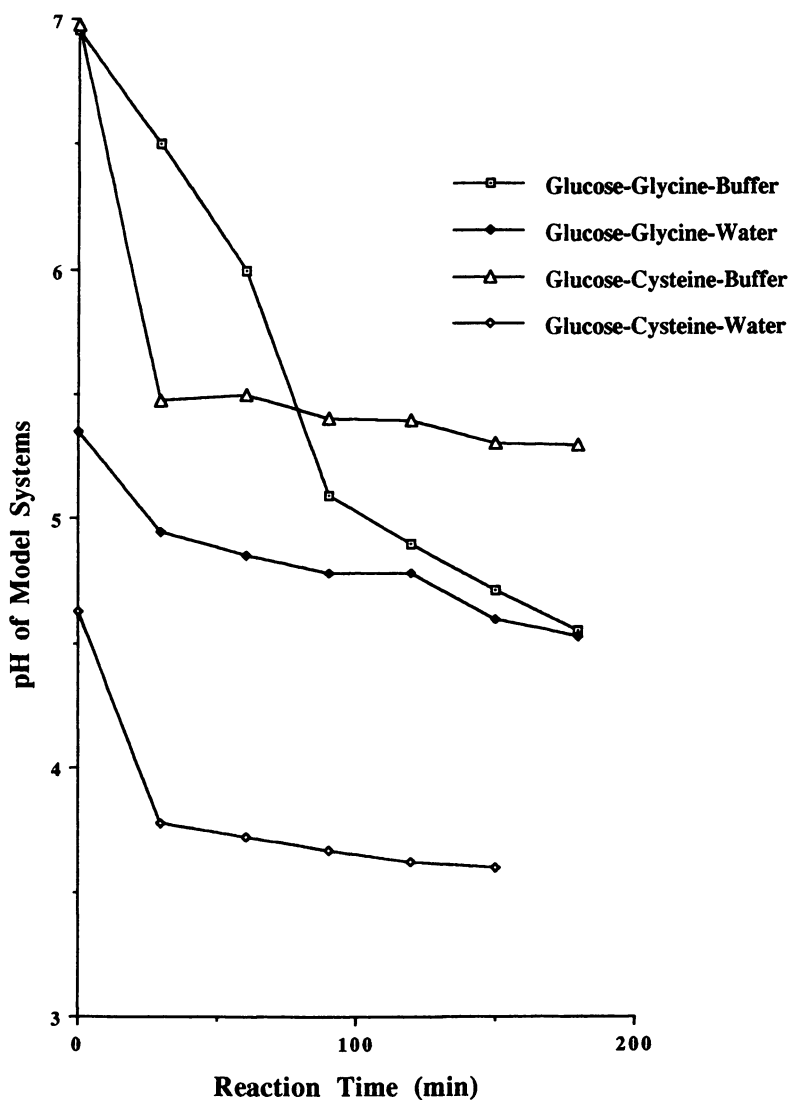
Figure 1. pH profiles of model glucose-amino acid systems with and without buffer at 105°C.
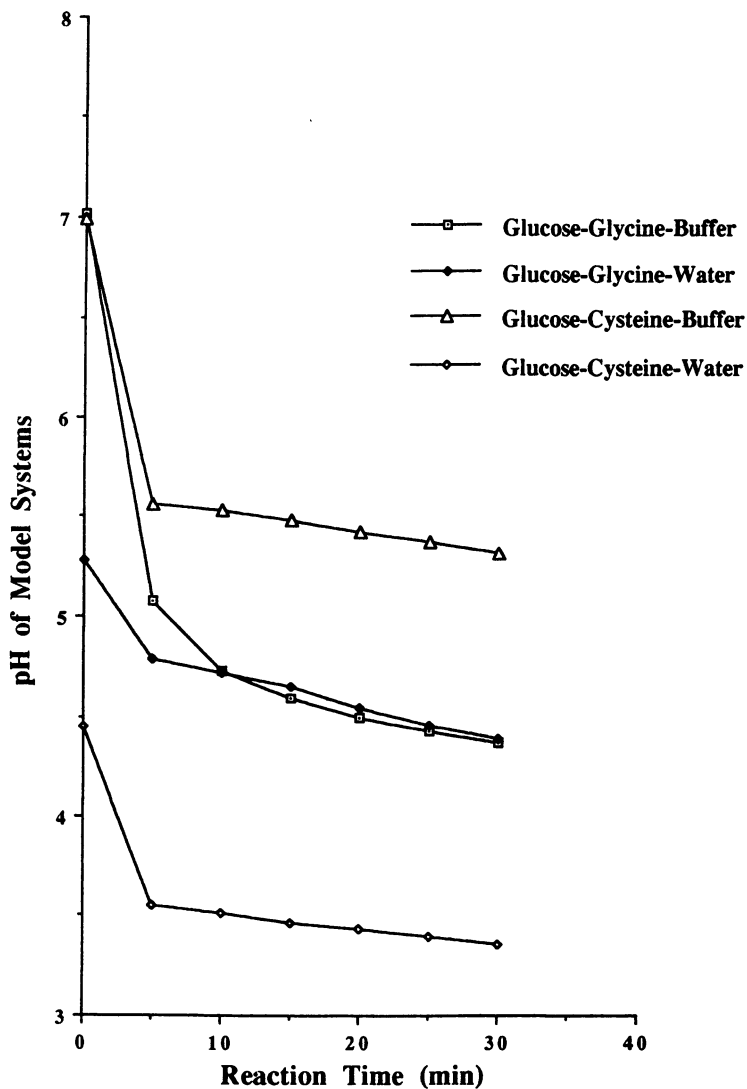
Figure 2. pH profiles of model glucose-amino acid systems with and without buffer at 125°C.

Activation Energies, E_a (kcal/mole) of Flavor Compounds. Activation energies of the seven flavor compounds in the four model systems are presented in Table III.

Table II. Reaction Rate Constants, k (ppm min^{-1}), in Glucose-Cysteine Systems

Temp (°C)	Compound	Glucose-Cysteine-Buffer	Glucose-Cysteine-Water
105	Furfural	6.095e^{-5}	1.524e^{-5}
	Furfuryl alcohol	*	*
	2-acetylfuran	1.963e^{-3}	*
	5-methylfurfural	1.500e^{-4}	*
	5-(hydroxymethyl)furfural	1.717e^{-3}	*
	5-methyl-2 (3H)-furanone	*	*
	di (H) di (OH) 6-methyl-pyranone	2.733e^{-2}	*
125	Furfural	8.600e^{-4}	2.554e^{-3}
	Furfuryl alcohol	2.820e^{-3}	*
	2-acetylfuran	1.595e^{-2}	6.140e^{-3}
	5-methylfurfural	3.700e^{-3}	1.868e^{-2}
	5-(hydroxymethyl)furfural	1.134e^{-2}	1.482e^{-1}
	5-methyl-2 (3H)-furanone	*	2.154e^{-3}
	di (H) di (OH) 6-methyl-pyranone	2.302e^{-1}	*

* not enough data points to calculate k (ppm min^{-1})

Table III. Activation Energies, E_a (kcal/mole) of Flavor Compounds (Assuming Zero Order Reaction)

Compound	E_a (kcal/mole) (r^2)			
	Glucose-Glycine-Buffer	Glucose-Glycine-Water	Glucose-Cysteine-Buffer	Glucose-Cysteine-Water
Furfural	39.75 (0.97)	36.23 (0.87)	50.26 (0.95)	52.42 (0.84)
Furfuryl alcohol	28.16 (0.93)	32.33 (0.92)	48.10 (0.70)	*
2-acetylfuran	40.38 (0.96)	25.96 (0.83)	40.79 (0.92)	55.14 (0.95)
5-methylfurfural	33.22 (0.93)	*	55.50 (0.83)	42.15 (0.86)
5-(hydroxymethyl)furfural	42.86 (0.91)	41.80 (0.85)	46.03 (0.95)	43.59 (0.95)
5-methyl-2 (3H)-furanone	25.47 (0.92)	*	*	58.80 (0.98)
di (H) di (OH) 6-methyl-pyranone	36.09 (0.90)	31.40 (0.70)	35.80 (0.90)	*

* not enough data points to calculate E_a (kcal/mole)

Activation energies of the seven flavor compounds ranged from 25 to 59 kcal/mole. Activation energies for 2-acetylfuran and di (H) di (OH) 6-methyl-pyranone in model sugar-amino acid systems have been previously reported (*6, 7*). The activation energies for 2-acetylfuran are 18 (*7*) and 36.2 (*6*) kcal/mole; those for di (H) di (OH) 6-methyl-pyranone are 16 (*7*) and 30.73 (*6*) kcal/mole for model systems following zero order reactions. The values reported by Fai and Reineccius (*7*) are lower than our values or those reported by Schirle-Keller and Reineccius (*6*). Fai and Reineccius (*7*) used a combination of glucose and a mixture of amino acids (methionine, phenylalanine, proline and leucine) in their model system. In their system (*7*), different reactants may be formed from the degradation of different amino acids. Further, a very reactive amino acid in a model system will rapidly give many reactive fragments which will change the kinetics of formation of secondary volatile compounds or sugar degradation products. Amino acids have been known to act as catalysts for sugar degradation making the kinetics observed for sugar fragmentation products very system dependent. Oxygen-containing heterocyclic compounds such as furans and pyranones are sugar fragmentation products. Hence, the formation of furans and pyranones would be catalyzed by amino acids and their rate of formation would depend on the reaction rate of sugar with the most reactive amino acid. Schirle-Keller and Reineccius (*6*) used different concentrations of glucose and cysteine and no phosphate buffer in their study.

Literature Cited
1. Nursten, H. *Food Chem.* **1980**, *6*, pp.263-277.
2. Finot, P; Aeschbacher, H.; Hurrel, R and Liardon, R. In *The Maillard Reaction in Food Processing, Human Nutrition and Physiology*. Birkhauser Verlag, Switzerland, 1990.
3. *Thermal Generation of Aromas;* Parliment, T.; McGorrin, R. and Ho, C., Ed.; ACS Symposium Series 409; ACS: Washington, D.C., 1989.
4. Bessiere, Y. and Thomas, A. In *Flavor Science and Technology;* Wiley & Sons, N.Y., 1990.
5. Maarse, H. and Vischer, C. In *Volatile Compounds in Foods. TNO-CIVO; Vol.I-III;* Netherlands, 1989.
6. Schirle-Keller, J. and Reineccius, G. In *Flavor Precursors;* Teranishi, R.; Takeoka, G. and Guntert, G., Ed.; ACS Symposium Series 490; ACS: Washington, D.C., 1989.
7. Fai, T. and Reineccius, G. In *The Maillard Reaction;* Labuza, T., Reineccius, G. and Monnier, V., Eds. Royal Chemical Society of London, London, 1994 (in press).
8. *A Guide for the Preparation and Use of Buffers in Biological Systems;* Gueffroy, D., Ed.; Calbiochem: La Jolla, CA, 1975.
9. Labuza, T.; Nelson, K. and Nelson, G. *Water Analyzer Series - Reaction Kinetics Program Version 2.09;* Dept. Food Sci. and Nutrition, Univ. Minnesota, 1991.
10. Labuza, T. *J. Chem. Ed.* **1984**. *61 (4)* , pp. 348-388.
11. Labuza, T. and Kamman, J. In *Computer Aided Techniques in Food Technology,* Sangy, I., Ed.; Marcel Dekker, N.Y., 1983.
12. Potman, R. and van Wijk, Th. In *Thermal Generation of Aromas;* Parliment, T.; McGorrin, R. and Ho, C., Ed.; ACS Symposium Series 409; ACS: Washington, D.C., 1989.
13. Reineccius, G. In *The Maillard Reaction in Food Processing. Human Nutrition and Physiology;* Finot, P.; Aeschbacher, H.; Hurrell, R. and Liardon, R., Ed.; Advances in Life Science; Birkhauser Verlag Basel, Boston, Berlin. 1990.

Chapter 4

Effect of Water Content and Amino Acids on Maillard Browning Kinetics in Propylene Glycol Based Model Systems During Microwave Heating

Guangyuan Lu, Chao-Hsiang Tong, Bruce I. Peterson, and Chi-Tang Ho[1]

Department of Food Science, Cook College, Rutgers University, P.O. Box 231, New Brunswick, NJ 08903–0231

The browning kinetics of the glycine-xylose, proline-xylose and glycine-proline-xylose model systems in propylene glycol were studied during microwave heating. In all systems, the browning rates followed zero-order kinetics at different temperatures (from 110 to 150°C) and different water contents (from 0 to 5 %) after an induction period. The browning rate of the glycine-xylose system was 3.0-3.7 times faster than that of the proline-xylose system, depending upon the water content. The activation energies for the glycine-xylose and the glycine-proline-xylose systems were 31.26 and 35.27 kcal/mol respectively, independent of water content. The browning rates were drastically reduced as the water content increased. The effect of water on the browning rate was most likely due to the change of the properties of the solvent system instead of the change of the activation step. Preliminary results indicated that the effect of amino acids on the browning rate in the glycine-proline-xylose system was additive.

Maillard browning is one of the major chemical reactions responsible for producing the brown color in foods. Such a reaction may or may not be desirable for a particular food and should be adequately controlled. In the past few decades, kinetic studies on Maillard browning in either authentic foods or model systems have been extensively conducted in order to provide the knowledge necessary for the design and control of food processing. These studies have investigated the effects of amino acids, sugars, ratio of amino acid to sugar, pH, temperature, moisture content or water activity, and oxygen on the Maillard browning in different model systems (1-13). Nevertheless, the overwhelming majority of these studies were done in a conventionally heated system.

Recently, the use of microwave ovens has become popular in the food industry and household food preparation due to its fast mode of heat transfer- microwave irradiation. While microwave cooking has its advantages over conventional cooking

[1]Corresponding author

such as convenience and cleanness, there are some problems with microwave-cooked foods (MCF). For example, the desirable crust, flavor, and color are difficult to form in MCF (*14*), which are normally developed in conventionally cooked foods (CCF) via the Maillard reaction. The chemical reactions responsible for such qualities in the CCF and the MCF may be different not only qualitatively but quantitatively. Thus, production of MCFs with such desirable qualities demands a new spectrum of knowledge in the chemistry of microwave food processing. A few browning kinetic studies have been done in microwave-irradiated systems (*10-11,15*)

   A new microwave reaction kinetic reactor ("MWKR") has been recently developed in our lab and used to study the browning kinetics of a proline-xylose containing model system (*10*). MWKR has some advantages for the kinetic study of this kind. First, it overcomes the difficult maintaining a constant water content in the reaction, which otherwise will result in a significant experimental error. Second, the reactor is so designed that it has realized the on-line measurements and/or control of temperature and optical density in a browning system.

   Previously, propylene glycol was used by Peterson et al. (*10*) to mediate the Maillard reaction and found to be a good vehicle for brown color formation. They studied the effect of moisture content on the browning kinetics of a xylose-proline reaction system during microwave heating and found that water content has a significant effect on browning kinetics. The purpose of the present study was to examine the effect of water content and amino acids on browning kinetics of two propylene glycol-mediated model systems, one consisting of glycine and xylose, and the other glycine, proline and xylose during microwave heating. Glycine was selected because it is a common primary amine which is assumed to have a different effect on browning kinetics compared to proline a secondary amine. The glycine-proline-xylose system was used with the intention of examining if there were any significant synergistic effect of amino acids on the kinetics of Maillard browning.

Materials and Methods

Sample preparation: Pre-grounded glycine, L-proline and D-xylose (Sigma Chemical Co., St Louis, MO) were weighed and dissolved in propylene glycol (purity >99%, Aldrich Chemical Co., Inc., Milwaukee, WI) in a volumetric flask by mechanical stirring for 12 hours to give a solution with 0.02M solute, either 0.02M glycine, 0.02M xylose or a combination of 0.01M glycine plus 0.01M proline. Pre-determined amounts of deionized distilled water were mixed with propylene glycol in 0.02M xylose solution so that it contained 0%, 5%, or 10% water. For browning reactions in the glycine-xylose system, equal volumes of 0.02M glycine and 0.02M xylose were mixed to give a reaction solution with 0.01M glycine and 0.01M xylose, which was subjected to microwave-heating at a constant temperature. Similarly equal volumes of 0.02M glycine-proline and 0.02M xylose stock solutions were mixed to obtain a reaction solution with 0.005M glycine, 0.005M proline and 0.01M xylose. The water content in the reaction solution depended on the water content of the xylose stock solution. The preparation of the 0.005M glycine-0.01M xylose browning solution was the same as other systems.

Apparatus: The microwave system used in the study was the same as that used by Peterson et al. (*10*).

Experimental procedure: Four model systems were used as shown in Table I. And the browning conditions were tabulated in Table II. To begin the experiment, the temperature-sensing advice was calibrated at 100°C against the boiling point of distilled water in the microwave oven. The microwave system was assembled and the flow rate was adjusted to 3 ml/min at room temperature. The temperature-controlling and data-acquisiting commands were then set on the computer for a specific run. The reaction solution was prepared just before the experiment started. The initial temperature of the solution was maintained at room temperature. Once prepared, the reaction solution was poured into the reactor which was immediately sealed. The agitator was set at 240 rpm. Then Magnetron power was set at the maximum of 120v so that the coming-up time would be shortest (around 1.5 minutes). The computer then initiated the operation of the system and just before the temperature reached the desirable one, the magnetron power was reduced manually to approximately 80% of the maximum available voltage. The browning reaction was stopped when the O.D. reading was close to 1.2. Each experiment was performed in duplicate under the same conditions.

Table I. Composition of the Model Systems

Model system[*]	Components
1[**]	0.01M Proline + 0.01M Xylose
2	0.01M Glycine + 0.01M Xylose
3	0.005M Glycine + 0.01M Xylose
4.	0.005M Proline + 0.005M Glycine + 0.01M Xylose

[*] All the systems are in propylene glycol with 0, 2.5, 5% water
[**] From Peterson et al. (*10*)

Table II. Experimental Conditions for the Model Systems

Water content (%)	Temperature (°C)
0	110, 120, 130
2.5	120, 130, 140
5	130, 140, 150

Kinetics studies: The kinetic studies followed the procedures used by Peterson et al. (*10*).

Results and Discussion

The plots of optical density (O.D. at 420 nm) versus time (min) at 0%, 2.5%, and 5% added water contents for both the glycine-xylose and glycine-proline-xylose systems followed a similar pattern. Figures 1 and 2 represented the Maillard browning kinetics of these two systems in propylene glycol with 5% added water. From all of the plots, an induction period was observed under every reaction condition and shortened as the reaction temperature increased. The browning rates at each temperature in all the systems studied followed a pseudo-zero-order reaction kinetics after the induction period. Similar phenomena with regard to the induction period and reaction order have been observed by other researchers (*7,10-11,16-17*).

It was also noticed that both temperature and water content influenced the induction period. This phenomenon was the same as that observed by Peterson et al. (*10*). The effect of temperature and water content on the induction period has been discussed by Warmbier et al. (*7*), Labuza and Baisier (*18*), Nelson (*19*). Generally, the higher the temperature used, the shorter the induction period was. With respect to the water content, the higher the water content, the longer the induction period. These results were apparently related to the browning rates.

Water affected not only duration of the induction period, but also the browning rate after the induction period as shown in Table III. Table III shows that the browning rate was drastically reduced as the water content increased. Similar results were found by Peterson et al. (*10*) and by Eichner and Karel (*9*). The browning rate of the glycine-xylose system was more sensitive to the change of water content than that of the glycine-proline-xylose and proline-xylose systems. When the water content increased from 0% to 5%, then the browning rate of the glycine-xylose system dropped 0.392 (O.D./min) and that of the proline-xylose system 0.104 (O.D./min). In other words, water has more inhibitory effect on the glycine-xylose system. Again from Table III, it was found that the exponential factor (k_o) of the proline-xylose browning is much larger than that of the glycine-xylose browning, indicating that the solvent systems were more favorable for the browning reaction of proline and xylose. Water as a strong polar solvent reduced the browning rates by at least three possible mechanisms. The first is that the involvement of water in the solution could form a more structured liquid which impeded the collision of reactants by the interaction (hydrogen bonding and dipole interaction) between water molecules and the reactants or intermediates. Second, the activation step may be involved in dispersing electrical charge in the reactive molecules and thus when the content of the more polar molecule water increased, the browning rate decreased. Unfortunately, the activation step could hardly be localized because of the complexity of Maillard browning reaction. The final possibility was that water functioned as the product of the condensation steps involved in Maillard reaction as mentioned by Eichner and Karel (*9*).
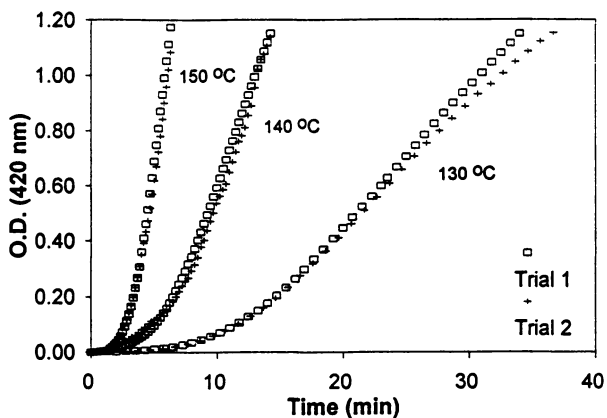
Figure 1. Maillard browning rates of 0.01M glycine and 0.01M xylose in propylene glycol as a function of time and temperature at 5 % water content.
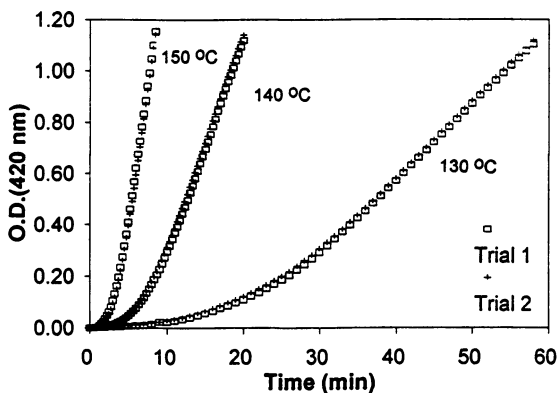
Figure 2. Maillard browning rates of 0.005M proline, 0.005M glycine and 0.01M xylose in propylene glycol as a function of time and temperature at 5 % water content.

Table III. Effect of Amino Acids and Water Contents on the Browning Rate at 130°C

Water Content (%)	System	k^b (O.D./min)	$k_{gx}/k_{px}{}^c$	$k_o{}^d$ ($\times 10^{16}$, O.D./min)
0	Proline/Xylose[a] (1)[e]	0.120		165
	Proline/Glycine/Xylose (4)	0.303	3.68	-
	Glycine/Xylose (2)	0.441		3.99
2.5	Proline/Xylose[a] (1)	0.030		41.3
	Proline/Glycine/Xylose (4)	0.051	3.33	-
	Glycine/Xylose (2)	0.100		0.906
5.0	Proline/Xylose[a] (1)	0.016		22.0
	Proline/Glycine/Xylose (4)	0.029	3.06	-
	Glycine/Xylose (2)	0.049		0.444

a. From Peterson et al. (*10*); b. Average value from the duplicate runs. r^2 for each k is larger than 0.980; c. k_{gx} and k_{px} are the rate constants of glycine-xylose and proline-xylose systems respectively; d. k_o is the pre-exponential factor in Arrehnius equation. e. System code in Table I.

With regard to the effect of different amino acids, it was found that glycine is more reactive than proline in the studied systems. The lower activation energy of the glycine-xylose browning determined to a large degree the chemical activity of glycine in the browning because the solvent system was much more favorable to the proline-xylose browning than the glycine-xylose browning as mentioned above. The ratio of the browning rate of the glycine-xylose system to that of the proline-xylose system was affected by the water content. The higher the water content, the lower the ratio, indicating that the change of the browning rate of the glycine-xylose system was more drastic than that of the proline-xylose system. However, the difference in the browning rates of the glycine-xylose and proline-xylose systems became smaller as the water content increased (see Table III). That indicated that the difference in the effect of these two amino acids on the browning rate was not practically significant at higher water contents. Examining Table III again, it was found that the browning rate of the proline-glycine-xylose system was almost equal to the average of the browning rates of the proline-xylose system and the glycine-xylose system. The effect of different concentrations of glycine on the browning rates was shown in Table IV. It was found that the browning rate constant was related to the initial concentration of glycine and browning rate of the system with 0.005M glycine was nearly half that of the system with 0.01M glycine. All these evidence indicated that at relatively low temperature
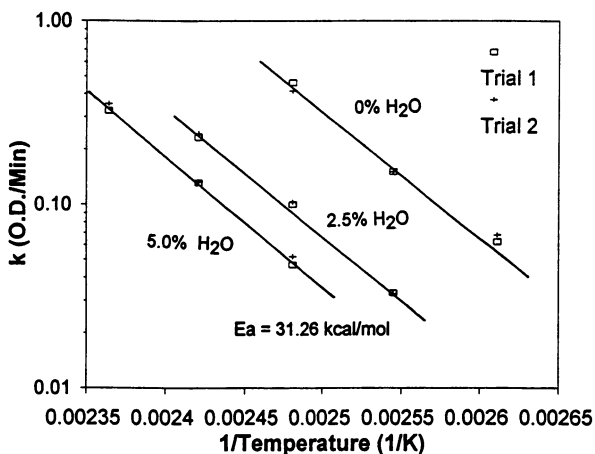
Figure 3. Arrhenius plot of Maillard browning of 0.01M glycine and 0.01M xylose in propylene glycol at different water contents.
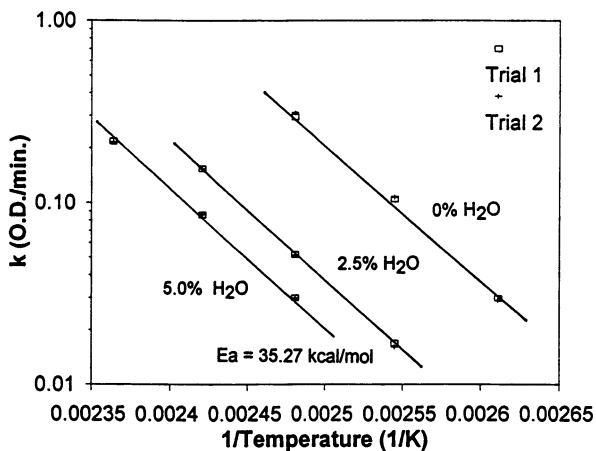
Figure 4. Arrhenius plot of Maillard browning of 0.005M glycine, 0.005M proline and 0.01M xylose in propylene glycol at different water contents.

there was a strong possibility that the effect of these two amino acids on the browning rates in the glycine-proline-xylose system was additive and not synergistic even though more evidence is needed to fully confirm this assumption.

Table IV.   Effect of Glycine concentration on the Browning Rate at 0% Water Content

Temperature (°C)	k (O.D./min)	
	0.05M Glycine	0.01M Glycine
110	0.023	0.054
120	0.076	0.155
130	0.137	0.441

The activation energies of the glycine-xylose browning (Ea = 31.27 kcal/mol) and the proline-glycine-xylose system (Ea = 35.27 kcal/mol) was calculated and shown in Figure 3 and 4. It was found that the activation energies were independent of the water content. The independence of Ea on water content has been observed also for the proline-xylose system (*10*). Thus the effect of water on the activation step of the browning reaction was less likely. In other words, the effect of water on the browning rate was most likely through the change of the solvent properties.

Literature cited

1.   Spark, A. A. *J. Sci. Food Agric.* **1969**, *20*, 308-316.
2.   Wolfrom, M. L.; Kashimuri, N.; Horton, D. *J. Agric. Food Chem.* **1974**, *22*, 796-800.
3.   Burton, H. S.; McWeeny, D. J.; Bilcliffe, D. O. *J. Sci. Food Agric.* **1963**, *14*, 911-20.
4.   Nicoli, M. C.; Amese, M.; Lerici , C. R. *Ital. J. Food Sci.* **1993**, n.2, 139-146.
5.   Anese, M.; Pittia, P.; Nicoli, M. C. *Ital. J. Food Sci.* **1993**, n.1, 75-79.
6.   Warmbier, H. C.; Schnickels, R. A.; Labuza, T. P. *J. Food Sci.* **1976**, *41*, 981-983.
7.   Warmbier, H. C.; Schnickels, R. A.; Labuza, T. P. *J. Food Sci.* **1976**, *41*, 528-531.
8.   Petriella, C.; Resnik, S. L.; Lozano, R. D.; Chirife, J. *J. Food Sci.* **1985**, *50*, 622-626.
9.   Eichner, K; Karel, M. *J. Agric Food Chem.* **1972**, *20*, 218-223.
10.   Peterson, B. I.; Tong, C-H.; Ho, C-T.; Welt, B. A. *J. Agric.Food Chem.* **1994**,

11.   Peterson, B. I. M.S. These, Rutgers University, 1994.

12.   Kato, H.; Yamamoto, M.; Gugimaki, M. *Agric. Biol. Chem.* **1969**, *33*, 939-940.

13.   Underwood, J. C.; Lento, H. G.; Willits, C. O. *Food Res.* **1959**, *24*, 181-184.

14.   Risch, R. K.; Lund, D. B.; Buelow, F. H. *J. Food Sci.* **1983**, *48*, 939-944.

15   Yeo, H. C. H.; Shibamoto, T. *J. Agric. Food Chem.* **1991**, *39*, 1860-1862.

16   Mizrahi, S.; Labuza, T. P.; Karel, M. *J. Food Sci.* **1970**, 799-803.

17.   Franzen, K.; Singh, R. K.; Okos, M. R. *J. Food Eng.* **1990**, *11*, 225-239.

18.   Labuza, T.P.; Baisier, W.M. in *Physical Chemistry of Foods*. Schwartzenburg, H. G.; Hartel, R. W. Eds. Marcel Dekker, Inc.: New York, 1992, pp 595-649.

19.   Nelson, V. *J. Dairy Sci.* **1948**, *31*, 415-419.

Chapter 5

Kinetics of Tetramethylpyrazine Formation under High Hydrostatic Pressure

Tzou-Chi Huang[1], Hui-Yin Fu[2], and Chi-Tang Ho[2,3]

[1]Department of Food Science and Technology, National Pingtung
Polytechnic Institute, Pingtung, Taiwan
[2]Department of Food Science, Cook College, Rutgers University,
P.O. Box 231, New Brunswick, NJ 08903−0231

A significant enhancement of the tetramethylpyrazine (TMP) formation at high pressure was observed in the 3-hydroxy-2-butanone/ammonium acetate model system. In a water system an activation volume of TMP formation under high pressure was found to be -6.82 ml/mole. A mechanism was proposed to elucidate the formation of TMP in a weak acidic condition and high hydrostatic pressure. Solvents such as PG, glycerol, methanol, ethanol, propanol, and butanol were found to enhance the TMP formation. Kinetic analyses indicated that TMP formation in aqueous, 80% PG, and ethanol systems followed pseudo-zero-order reaction kinetics. The activation energies were found to be 18.84±1.3 kcal/mole, 14.19±7.1 kcal/mole, and 13.09±4.7 Kcal/mole respectively.

High hydrostatic pressure has recently become the subject of renewed interest in the food industry. This high pressure treatment causes inactivation of microorganisms, denaturation of protein, and gelatinization of starches at ambient temperature, with little effect on covalent bonds. Compared to conventional thermal processing, high hydrostatic pressure preserves the natural flavor, color, vitamins, and taste of foods. The use of high pressure could provide a new method which would sterilize foods without off-flavor and deterioration of the components and nutrients, and would also give the food a unique texture. Hydrostatic pressures of 1,000 to 10,000 kg/cm^2 were successfully applied to various foods in food processing (*1*).

Pressure can influence most biochemical reactions, since they often involve a change in volume. Volume-increasing reactions will tend to be inhibited by pressure, while reactions leading to a decrease in volume will tend to be promoted. High hydrostatic pressure is of great value in organic synthesis and especially useful for those compounds which cannot be synthesized at ambient pressure due to steric

---

[3]Corresponding author

hindrances or other reasons. Matsumoto et al. (*2*) has reviewed many published papers concerning the pressure effect on the organic synthesis. They reported that high pressure could increase organic synthesis reactions, such as aldol condensation, Michael reaction, alkylation of aldehydes, Diels-Alder reaction, Mannich reaction, etc.

Pyrazines are nitrogen-containing potent heterocyclics that are characteristic flavorants found in a wide range of raw and processed foods (*3*). The odor of TMP was described as pungent, walnut, and green.

Most of the alkylpyrazines are formed in foods which are processed at high temperatures. The activation energies for pyrazine formation are relatively high. Rizzi (*4*) postulated that 3-amino-2-butanone is a reaction intermediate in the formation of TMP. Aminocarbonyls, like 3-amino-2-butanone, are known to dimerize (Schiff base formation) to dihydropyrazine and oxidize (dehydrogenation) to TMP as shown in Figure 1. Schiff base formation is believed to be the critical step in the pyrazine synthesis.

Most of the published pyrazine formation mechanisms are studied at high temperatures using model system. However, Rizzi (*4*) reported that alkylpyrazines were formed by reactions of acyloins and ammonia at acidic pH and low temperature. The pyrazine formation at ambient temperature under high hydrostatic pressure has not been previously studied.

The objectives of this research are to study the effects of temperature and pressure on TMP formation and to investigate the mechanism of TMP formation in a weak acid condition and under high hydrostatic pressure.

Material and methods

Material.   3-Hydroxy-2-butanone and tetramethylpyrazine (TMP) were purchased from Aldrich Chemical Co.(Milwaukee, WI), ammonium salts (acetate, formate, oxalate, hydroxide, carbonate, bicarbonate, sulfate, chloride), propylene glycol (PG) and the solvents for HPLC were chemical grades and obtained from Fisher Chemical Co. Ammonium glutamate was obtained from Ajinomoto Co.

Reaction Procedure.   Reaction mixtures composed of 0.01 mol of 3-hydroxy-2-butanone and 0.03 mol of ammonium salts dissolved in 4 ml of deionized water or solvent. The vials were shaken regularly to assure all the reactants were dissolved. The reactions were run in a water bath at the required constant temperature. The amount of TMP was analyzed by HPLC.

HPLC analysis.   Reaction mixtures were routinely analyzed by HPLC using Waters Associate Liquid Chromatograph Model 6000A and a Model 440 absorbance detector (280 nm) with a 25 x 0.46 cm RP Partisphere C-18 column (Whatman) under isocratic conditions at ambient temperature. Solvent was 50/50 (v/v) methanol-water (1.0 ml/min) for all separations. Tetramethylpyrazine standards were prepared for 0.02, 0.04, 0.06, 0.08 and 0.10 mg/ml in methanol. Quantitation was done on baseline-resolved peaks vs external standards on a Varian 4270 integrator.

High Hydrostatic pressure experiments.   The reactions were done by putting the reactants into small plastic vials (polyethylene bottles with a screwed lid with approximately 4.5 ml capacity) which were filled with water or propylene glycol. High pressure was applied to the plastic vials with a hand-type pressure generator (Type K-P5-B, Hikari, Koatsu Co., Hiroshima, Japan) using water as the pressure medium. The temperature was maintained by immersing the pressure vessel in the water bath.

The effect of different nitrogen sources on TMP formation.   Different ammonium salts (acetate, bicarbonate, carbonate, hydroxide, oxalate, glutamate, chloride, sulfate) were set up to study the influence of nitrogen sources on TMP formation.

The effect of water content on TMP formation.   Different percentages of PG (0, 20, 40, 60, 80, and 100% in water) were used to investigate the water content on TMP formation at 1 and 5,000 kg/cm^2 respectively.

The effect of solvents on TMP formation.   Solvents such as methanol, ethanol, propanol, butanol, and glycerol were used to investigate the solvent effect on TMP formation at 25°C for 1 hour.

Kinetic analysis.   The rate of TMP formation in 3-hydroxy-2-butanone ammonium acetate in water, 80% PG, and ethanol systems at the four reaction temperatures (25°C, 35°C, 45°C, and 55°C) were analyzed by HPLC in the reaction mixture every hour. All kinetic studies were carried out in duplicate.

The kinetics of formation of pyrazines were determined using the basic equation for the rate of change of A with time.

$$dA/dt = K\,A^n$$

where A = concentration, t = time, K = rate constant and n = reaction order. Slopes and intercepts were calculated by the linear least-square method. The activation energies for formation of the TMP were calculated by the Arrhenius equation from the slope of the line generated by plotting the log value of the rate constant versus the reciprocal of the absolute temperature (*5*).

The effect of pressure on pyrazine formation.   The rate of TMP formation in 3-hydroxy-2-butanone ammonium acetate in the water system was obtained at 1, 3000, 4000, 5000 kg/cm^2 and 25° C for 1, 3 or 5 hours. Activation volume was calculated according to the basic relationship between pressure and rate.   The equation originally proposed by van't Hoff is as follows,

$$\Delta V^{\ddagger} = -RT\, \delta \ln K / \delta P$$

where, $\Delta V^{\ddagger}$ is the change in volume per mole when the activated complex is formed

(1) Schiff base formation
(2) dehydrogenation
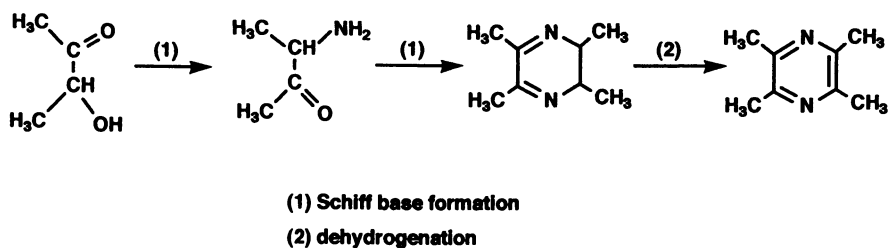
Figure 1. Proposed overall Schiff base formation mechanism for TMP synthesis.

1-1 Ad$_E$3 Condensation
1-2 proton transfer
1-3 general acid catalyzed β-elimination
1-4 proton transfer
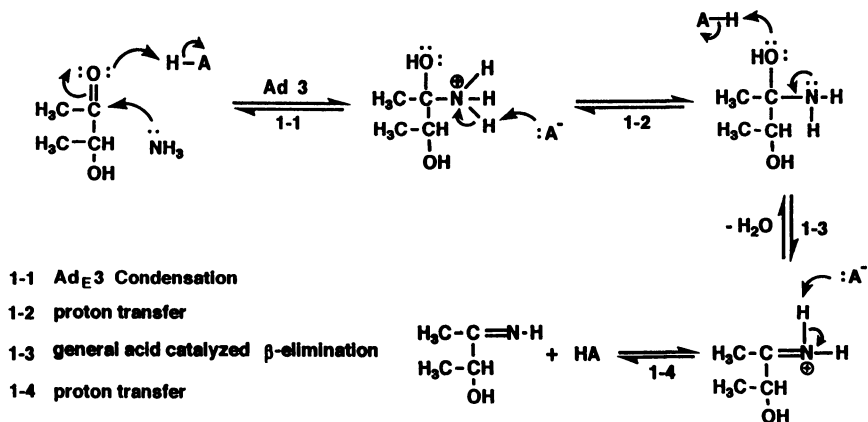
Figure 2.   Detailed Schiff base formation mechanism in 3-hydroxy-2-
butanone/ammonium acetate system.

from the reactants. $\Delta V^{\ddagger}$ can be obtained from the plot of pressure verus rate constant. Various methods have been proposed and used to calculate $\Delta V^{\ddagger}$. The most realistic method is fitting by least squares. Among all the equations proposed and used, the most popular is the parabolic one

$$\ln K = a + bp + cp^2,$$

so that then, at p = 0, $\Delta V^{\ddagger} = bRT$,
where R is the gas constant, 82 $cm^3 \cdot atm.K^{-1} \cdot mole^{-1}$ (6). The pressure units used are 1 atm = 1.01325 bar = 1 kg/cm^2 = 0.101325 MPa. These equation are similar to those classically calculated for temperature as a variable at constant pressure.

Results and Discussion

TMP formation in different ammonium salts. At ambient pressure, the amount of TMP was influenced by the type of ammonium salt. As shown in Table I, among the nitrogen sources tested, the ammonium acetate produced the most TMP. The pKa values for acetic acid and ammonium are 4.76 and 9.25 respectively. An equimolar solution of ammonia and acetic acid had the maximum buffering capacity at pH 7.0.

Table I. The effect of ammonium salts on TMP formation

Ammonium salts	TMP concentration (mg/ml)
ammonium acetate	5.40
ammonium bicarbonate	0.56
ammonium carbonate	0.21
ammonium formate	0.14
ammonium hydroxide	0.06
ammonium glutamate	0.06
ammonium chloride	[a]_
ammonium oxalate	-
ammonium sulfate	-

[a] no product was detected due to the poor solubility of the ammonium salts.

According to Scudder (7), Schiff base formation could be separated into four sequential steps. These steps, as shown in Figure 2, trimolecular addition (AdE3), a proton transfer, general acid catalyzed β-elimination (EgA), followed by proton transfer. The first proton transfer increased the polarization of the carbonyl group. This resulted in the increase of nucleophilic activity of ammonia and led to the

formation of the positively charged transition state. For Schiff base formation to occur, both the hydroxyl group and the hydrogen on the nitrogen must be released. The second proton transfer was necessary in order to remove this hydroxyl group, which is converted to a molecule of water. This proton transfer not only made the hydroxyl group a better leaving group but also made the nitrogen lone pair push the hydroxyl group out. The third proton transfer led to the elimination of the hydrogen atom on the nitrogen atom. The acetic acid/ammonia buffer systems served as either a proton donor or acceptor, which led to the completion of the Schiff base formation. The important role of buffer systems in promoting Schiff base formation in the ammonium acetate/3-hydroxy-2-butanone model system reconfirmed the concept discussed by de Kok and Rosing (8). Similar evidences have been reported by Miyashita et al.(9) and Lin et al.(10). However, in their studies no detailed mechanistic elucidation of the role of buffer salts on Schiff base formation were discussed.

The effects of high pressure on TMP formation. As shown in Table II, in the 3-hydroxy-2-butanone/ammonium hydroxide system, the amount of TMP was 0.01 mg/ml at ambient pressure, it increased to 0.04 mg/ml at the pressure of 500 kg/cm^2. However, when the pressure was increased to 1000 or 2000 kg/cm^2, the amount of TMP did not increase. This may be due to the high pH of the reaction system.

Table II. The effect of different ammonium salts on TMP formation at 22°C under different pressures

Ammonium salts	Concentration (mg/ml)			
	Pressure (kg/cm^2)	1	500	1000	2000
acetate		12.44	14.35	14.29	22.05
carbonate		0.27	0.34	0.37	0.45
hydroxide		0.01	0.04	0.04	0.03
oxalate		[a]-	-	-	-

[a] undetectable

In the 3-hydroxy-2-butanone / ammonium carbonate system, the amount of TMP increased with increasing pressure. The amounts of TMP were 0.27 and 0.34 mg/ml at 1 and 500 kg/cm^2 respectively. When the pressure increased to 1000 kg/cm^2, the amount of TMP increased to 0.37 mg/ml. When a pressure of 2000 kg/cm^2 was applied, the amount of TMP increased to 0.45 mg/ml. These results showed that high pressure could enhance TMP formation.

No TMP was detected in the oxalate system due to the low solubility of ammonium oxalate.

A significant pressure effect of TMP formation was observed in the 3-hydroxy-2-butanone/ammonium acetate system. The amounts of TMP at the pressure of 500 kg/cm² and 1000 kg/cm² was 14.35 and 14.29 mg/ml respectively. When the pressure was increased to 2000 kg/cm², the amount of TMP increased to 22.05 mg/ml. The amount of TMP increased 1.2 folds under 1,000 kg/cm² and 1.8 folds under 2,000 kg/cm² for the sample pressurized at 22 °C for 24 hours.

The effects of propylene glycol on TMP formation in 3-hydroxy-2-butanone/ammonium acetate system Figure 3 shows the different percentages of PG used for TMP formation in the 3-hydroxy-2-butanone ammonium acetate system. At ambient pressure, the amount of TMP increased with the increasing percentage of PG up to 80%. The concentration of free ammonia increased the nucleophilic attack on the carbonyl group of 3-hydroxy-2-butanone and accelerated the formation of TMP. However, a percentage of PG higher than 80% did not increase the TMP formation due to high viscosity. The trend was the same at 5000 kg/cm². An increase in PG up to 80% showed an increase in TMP. In the 80% PG system, a significant increase was observed indicating that at this water activity, the proximity of the two reactants was enhanced at higher pressure. The amount of TMP was about 1.5 folds higher than that of TMP at 1 kg/cm². But in 100% propylene glycol, even at 5000 kg/cm², the low amount of TMP was also obtained due to the high viscosity of PG. PG has long been utilized as a water activity lowering agent. The water activities of 20%, 40%, 60%, and 80% PG in water are 0.96, 0.91, 0.88, and 0.84 respectively (*11*). The water holding capacity of PG shifts the Schiff base reaction to the final product.

The effect of protic solvents on TMP formation. A significant solvent effect on TMP formation in the ammonium acetate/3-hydroxy-2-butanone model system was observed. Protic solvents such as methanol, ethanol, propanol, butanol, PG, and glycerol were used to replace water in our model system. The amount of TMP increased 27, 57, 53, 36, 4, and 2 folds respectively as shown in Figure 4.

Kinetic studies of TMP formation

The effect of temperature on reaction rate. The plots of TMP concentration (mg/ml) versus time for water, 80% PG, and ethanol are shown in Figures 5, 6, and 7 respectively. The rates of TMP formation at each temperature followed pseudo-zero-order reaction kinetics as shown by the linear plot of TMP concentration versus time. This indicates that pyrazine formation in all systems tested is relatively complex. Rate constants were calculated from the slope using the least square fit method.

The natural log of the rate constant as a function of the reciprocal of temperature was shown in the Arrhenius plot (Figure 8). Linear regression data summarizing the effects of temperature on TMP formation were shown in Table III. The activation energies were found to be 18.84±1.3 Kcal/mole (R^2 = 0.999),
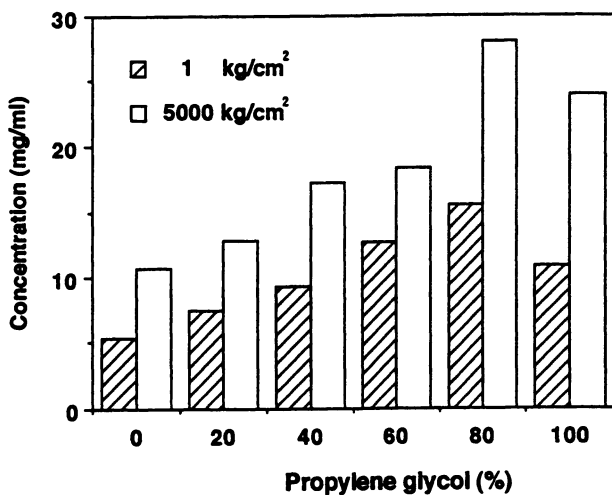
Figure 3. The effect of propylene glycol on TMP formation at the pressure of 1 and 5000 kg/cm².
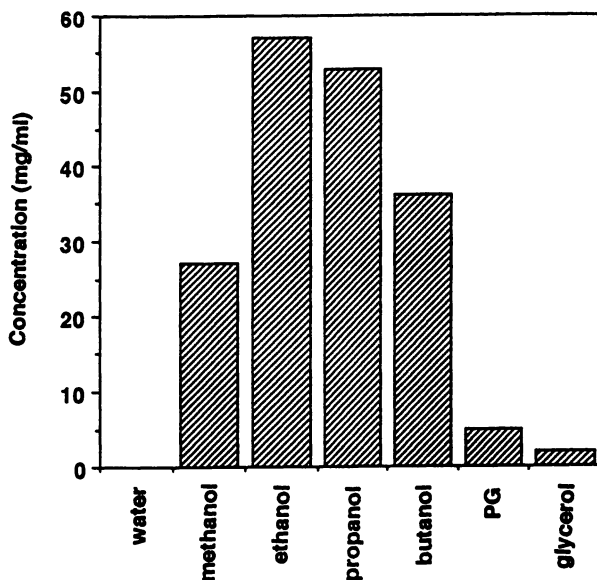
Figure 4.   Solvent effect on TMP formation.
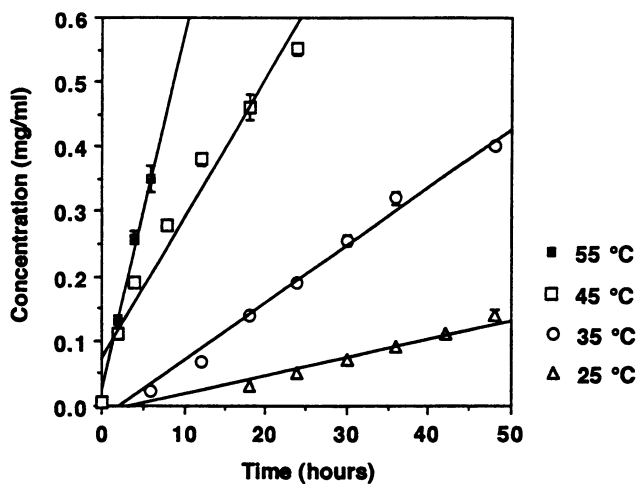
Figure 5. TMP formation at different temperatures in a water system.
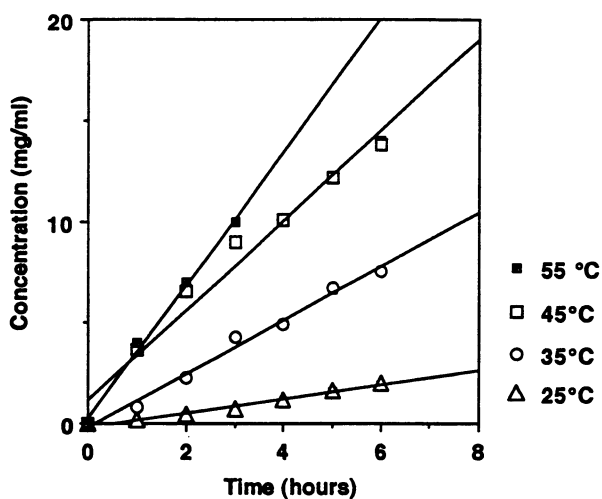
Figure 6. TMP formation at different temperatures in an 80% propylene glycol system.
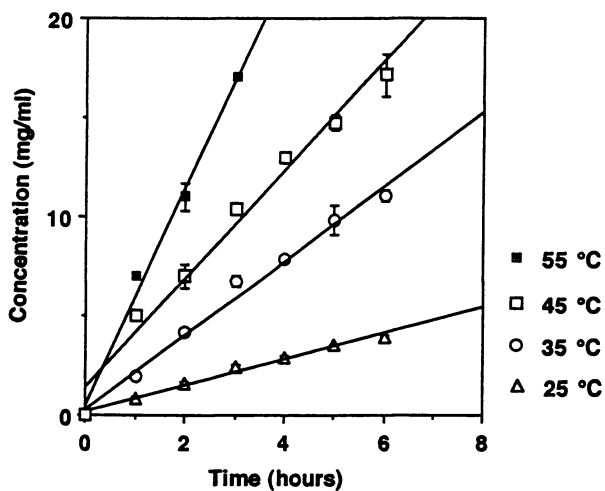
Figure 7. TMP formation at different temperatures in an ethanol system.
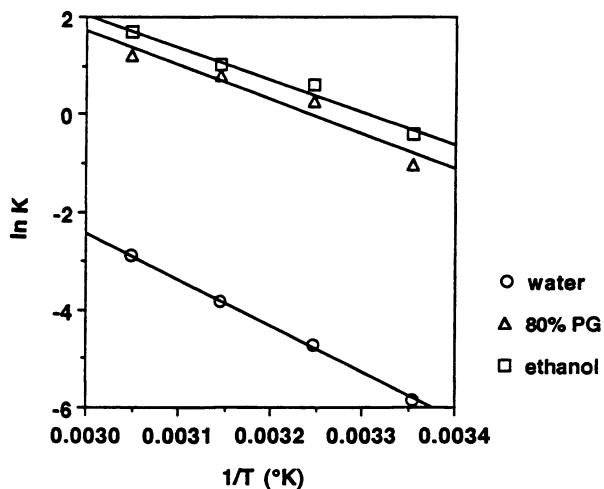
Figure 8. Arrhenius plot of TMP formation in water, 80% PG, and ethanol system respectively.

14.19±7.1 Kcal/mole (R^2 = 0.929), and 13.09±4.7 Kcal/mole (R^2 = 0.967) in water, 80% PG, and ethanol respectively.

Table III. Zero-order constants (K) and corresponding regression coefficients (R^2) of TMP formation from 3-hydroxy-2- butanone/ammonium acetate in water, 80% PG, and ethanol systems

Condition	Temperature	K (mg/ml hr)	R^2
water	25°C	0.003	0.984
	35°C	0.009	0.989
	45°C	0.022	0.953
	55°C	0.055	0.989
80% PG	25°C	0.350	0.983
	35°C	1.331	0.989
	45°C	2.226	0.972
	55°C	3.300	0.995
ethanol	25°C	0.657	0.989
	35°C	1.876	0.995
	45°C	2.652	0.965
	55°C	5.500	0.990

Pressure dependence on reaction rate.   The plot of TMP concentration (mM) versus time for water system is shown in Figure 9. The activation volume can be obtained from the plot of pressure versus a natural log of the rate constant (Figure 10). The apparent activation volume of TMP formation was found to be -6.82 ml/mole. Negative activation volume of TMP formation indicated that high hydrostatic pressure could accelerate TMP formation. Hamman (*12*) proposed that those reactions in which the transition state is more highly ionic and hence more extensively solvated than the initial state are greatly accelerated by pressure. Those in which the transition state is less ionic and less solvated than the initial state are retarded by pressure. The positive pressure effect of TMP formation was caused by an ionic intermediate. Binding solvent molecules to the more highly charged activated complex resulted in a decrease in the volume of the system. For the AdE3 addition mechanism, the three reactants, the nucleophile, acid, and carbonyl group must be roughly coplanar. High hydrostatic pressure can facilitate mutual collision, and thus promote the formation of the transition state intermediate.

Mechanism of TMP formation at a weak acidic condition.   As shown in Figure 11, a mechanism for the formation of TMP under a weak acidic condition was
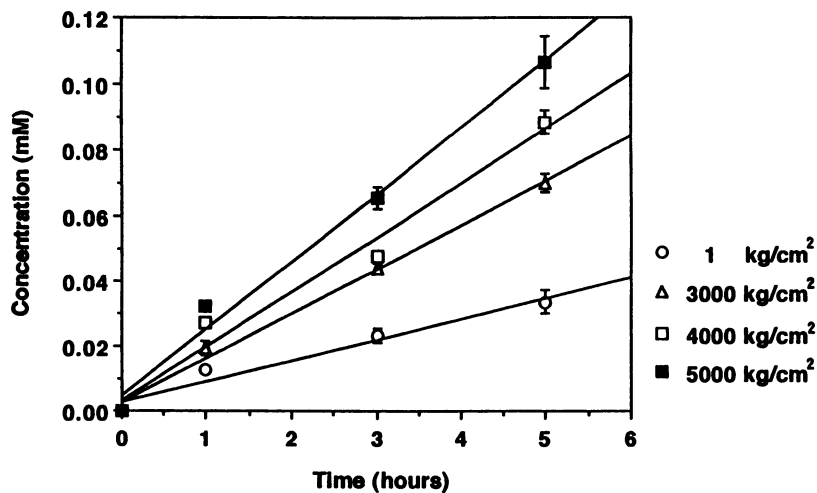
Figure 9. TMP formation in a water system under high hydrostatic pressure.
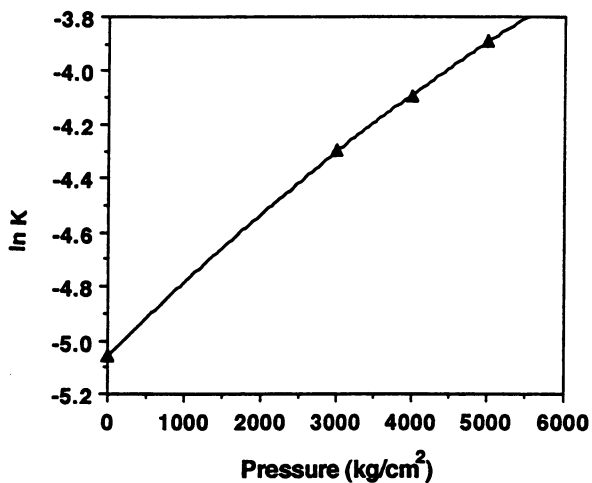
Figure 10.   Effect of pressure on the rate of TMP formation.
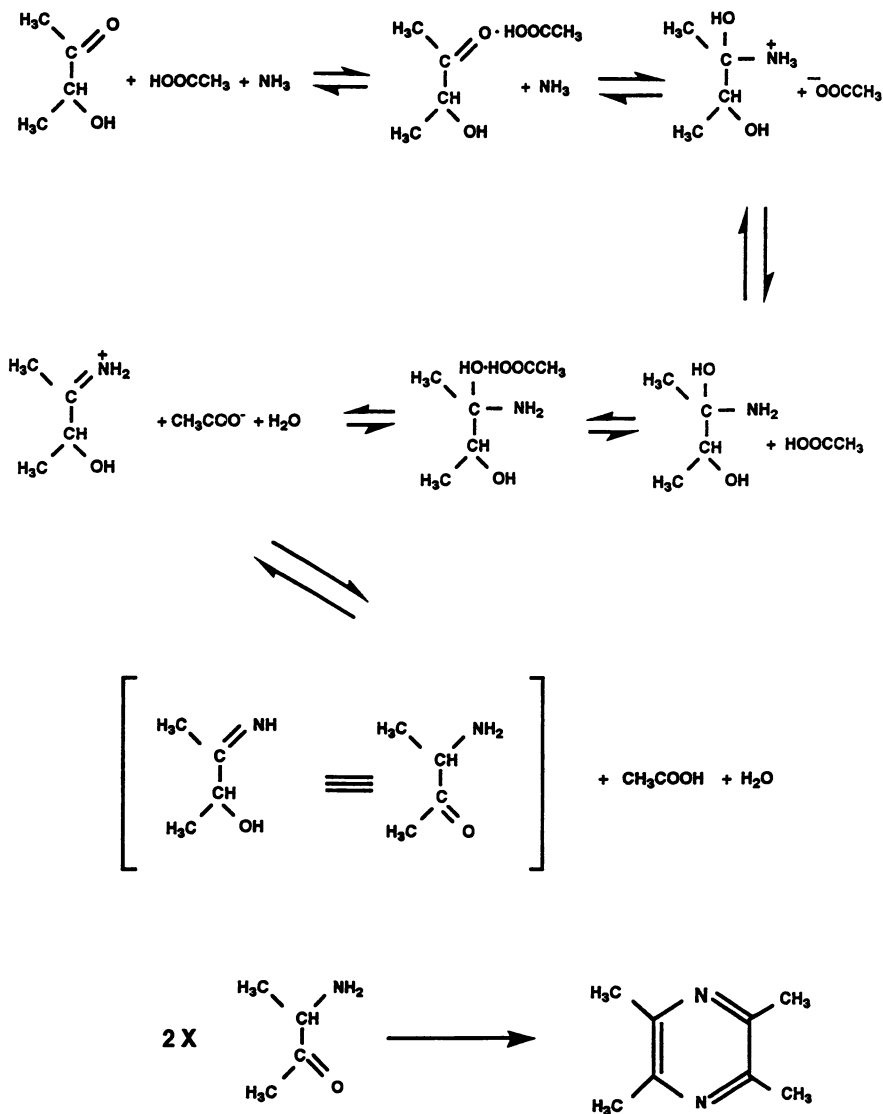
Figure 11. Proposed mechanism of TMP formation in a weak acidic condition under high pressure.

proposed. The proton from acetic acid protonated the carbonyl carbon of 3-hydroxy-2-butanone which facilitated the formation of an ionic intermediate. This was confirmed by the high pressure experiments. Subsequent rearrangements of the intermediate were catalyzed by the acetate ion and led to the formation of amino ketone. Condensation of two molecules of amino ketone produced one molecule of TMP.

Conclusion.   Application of high hydrostatic pressure could enhance the formation of tetramethylpyrazine in the 3-hydroxy-2-butanone/ammonium acetate system. The negative activation volume for this reaction explained the reason for the observed pressure effect. The mechanism proposed in this paper could be applicable to other reactions which involve Schiff base formation.

Literature Cited

1.   Hayashi, R. In *Engineering and Food*; Species, W.E.L.; Schubert,H., Eds.; Elsevier Applied Sci.: London, 1989; *vol.2*; pp 815-826.
2.   Matsumoto, K.; Sera, A.; Uchida, T. In *Organic Synthesis Under High Pressure I. Reviews. Synthesis*; 1985, pp 1-26.
3.   Maga, J.A. Food Rev. Internat. **1992**, *8*, 479-558.
4.   Rizzi, G.P. *J. Agric. Food Chem.* **1988**, *36*, 349-352.
5.   Labuza, T.P. In *Computer-Aided Techniques in Food Technology;* Saguy, I. Eds.; Marcel Dekker, Inc.: New York, NY, 1983; Vol.*1*; pp 71.
6.   Asano, T.; Le Noble, W.J. *Chem. Rev.* **1978**, *78*, 407-439.
7.   Scudder, P.H. *J. Org. Chem.* **1990**, *55*, 4239-4240.
8.   de Kok, P.M.T.; Rosing, E.A.E. In *Thermally Generated Flavors: Maillard, Microwave and Extrusion Process*;   Parliment,T.H.;   Morello,   M.J.; McGorrin, R.J., Eds.; ACS   Symp. Ser. 543; American Chemical Society.: Washington, D.C., 1994, pp 158-179.
9.   Miyashita, K.; Kanda, K.; Takagi, T. *J. Ameri. Oil Chem.Soc.***1991**, *68*, 748-751.
10.   Lin, T.F.; Yakushijin, G.H.; Buchi, G.H.; Demain. *J. Indust. Micro.* **1992**, *9*, 173-179.
11.   Alzamora, S.M.; Chirife, J.; Gerschenson, L.N. *Food Rev. Internat.* **1994**, *27*, 65-67.
12.   Hamman,S.D. In *Physico-chemical Effects of Pressure;* Academic press, Inc.: New York, N.Y. 1957.

Chapter 6

Modeling Maillard Browning in Dehydrated Food Systems as a Function of Temperature, Moisture Content, and Glass Transition Temperature

Raivo Karmas and Marcus Karel[1]

Department of Food Science, Cook College, Rutgers University, P.O. Box 231, New Brunswick, NJ 08903-0231

Browning in dehydrated food systems is influenced by a combination of factors including temperature, moisture content, composition, and physical changes in the matrix of the food during storage. The glass transition concept was studied as a potential way to combine the above factors so that a simplified model for browning could be developed based on temperature above the glass transition temperature (T-Tg). Six freeze dried model systems were studied over a range of moisture contents and temperatures. Arrhenius equation based models were developed for each system. Acceptable models were obtained when any two of the three following parameters were used: temperature, moisture content, and (T-Tg). The best models included all three parameters. Although glass transition does influence browning, there are separate effects of temperature and moisture which cannot be accounted for by the (T-Tg) term.

Non-enzymatic browning (NEB) is an important set of reactions in foods. It often causes quality loss in dehydrated foods containing reducing sugars and amino compounds. It is responsible for the off-flavors, discoloration, and nutritional loss limiting the shelf-life of products such as dry milk and whey powders, dehydrated eggs, meat and fish, cereals, cake mixes, and concentrated juices (1). The reaction is strongly dependent on water content and temperature (2,3,4). It is also dependent on physical changes in the system which may occur during storage (5,6). Physical and chemical changes which can occur simultaneously, are sensitive to temperature and composition, especially water content. Much research has focussed on determining a predictable "critical point" where physical and chemical changes start (7,8).

Low and intermediate moisture foods may contain a significant portion of their constituents in an amorphous state. It has been proposed that in such systems the glass transition may be considered a critical point for stability (9,10,11,12,13). The glass transition temperature (Tg) is the temperature at

[1]Corresponding author

which an amorphous system changes from a relatively immobile and stable glass to a system where molecular mobility is increased and changes, both physical and chemical, may be expected. Because the Tg of a system depends on moisture content and composition, the term (T-Tg) may combine some of the effects of temperature (T), moisture (M), and composition on stability. Whether (T-Tg) accounts for them completely is not resolved by literature, and is one of the questions posed in this research. The relationship between physical stability and glass transition has already been demonstrated (9-13). This investigation will address the influence of the glass transition on chemical changes, specifically, on NEB in freeze-dried food models.

Experimental Approach and Methods

The objectives of this research was to characterize the kinetics of the non-enzymatic browning (NEB) reaction in the vicinity of the glass transition of food models. The experimental approach involved using dehydrated model systems of reactants dispersed in a matrix of inert or relatively inert material(s). Experiments were carried out at a several combinations of moisture contents and temperature. The range of water activities, (0-0.44) were chosen so that diffusion limitations would be expected.

Samples were prepared by making a 20% aqueous solution containing browning reactants (amino compound and reducing sugar) and a matrix material. The amino compound, in all of the experiments was L-lysine monohydrochloride (Alfa Division of Ventron, Danvers, MA) and the reducing sugar in most of the experiments was xylose (Fisher Scientific). These compounds were chosen because they are considered very reactive, so that some level of browning in the eventual dehydrated systems could be detected, especially at low temperature and low moisture conditions. In most of the model systems studied the reactants were at relatively low concentration so that diffusional effects could be expected. Some experiments were done with lactose or maltose as both the reacting sugar and as the matrix material.

0.5ml aliquots of the solutions were filled into 2 ml vials. The vials were then stored 24 hours at -30 to -35°C, followed by 3 hours over dry ice [as recommended for amorphous glass formation by Roos and Karel (1991b)], and freeze dried (48 hours, Vertis Benchtop, 3L). After freeze drying samples were equilibrated over saturated salt solutions in vacuum desiccators for one week to obtain desired moisture contents.

Differential Scanning Calorimetry (DSC) Differential scanning calorimetry was used to determine the glass transition (onset of endothermal change of specific heat) of the model systems at the various moisture contents. DSC was also helpful to determine the tendency of samples to crystallize. A Mettler TA4000 thermal analysis system with a TC11 TA processor and a DSC30S cell were used. The instrument was calibrated for heat flow and temperature using n-hexane (m.p. 29.8°C, ΔHm 151.8Jg^{-1}), water (m.p. 0°C, ΔHm 334Jg^{-1}), gallium (m.p. 29.8°C, ΔHm 79.3Jg^{-1}), and indium (m.p. 156.6°C, ΔHm 28.5Jg^{-1}). Samples were prepared by weighing of the test material in 40ml aluminium DSC pans (Mettler) which were then hermetically sealed. An empty aluminium pan was used as the reference for all measurements. The samples were rapidly cooled to a temperature below the expected Tg in the DSC cell. After cooling

the samples were scanned at 5°C/minute to an end temperature above the expected glass transition enset. The Tg onset was determined using Mettler GraphWare TA72PS.1. Results from an average of three replicate samples were used to determine the mean.

Isotherms The freeze dried samples in vials were dehydrated to a "zero" moisture content by holding in vacuum desiccators over P_2O_5 for one week. The samples were then rapidly weighed (Mettler AE240 digital balance) and rehumidified to varying moisture contents for at least one week over saturated salt solutions in vacuum desiccators at 20°C. After equilibrating samples were reweighed and the moisture content calculated from the weight gained. An average of at least three samples were used to determine the moisture content

Browning The samples were freeze dried, equilibrated in vacuum dessicators to desired water activities and moisture contents, sealed, and heated in dry baths over a period of time. Samples were then solubilized with 2 ml water and optical density was determined at 420nm. Zero order rate constants were determined. Data were used to model browning as a function of (T-Tg).

Arrhenius-type Models: Mathematical models were obtained using JMP software for the Macintosh. The following example were the output of the linear model created when the natural logarithm of the browning rate constants for the PVP10/xylose/lysine (98:1:1) system were modeled as a function of the reciprical of absolute temperature (1/T), moisture content (M), and (T-Tg).

Summary of Fit

Rsquare	0.979268
Root Mean Square Error	0.31772
Mean of Response	-3.31121
Observations (or Sum Wgts)	48

Parameter Estimates

Term	Estimate	Std Error	t Ratio	Prob>ltl
Intercept	15.090951	2.7595	5.47	0.0000
1/k	-6070.271	977.172	-6.21	0.0000
M	-0.241538	0.04714	-5.12	0.0000
T-Tg	0.0864535	0.008	10.81	0.0000

Sample output of the linear model created by JMP software.

The coefficients of the equation appear in the parameter estimates results. The resulting model is therefore:

$$\ln k = 15.09 - 6070\left(\frac{1}{T}\right) - 0.24M + 0.086(T - Tg)$$

Models were generated for various systems where moisture content, temperature, and (T-Tg) were variables. Models with 2 and 3 of the parameters were obtained. The systems and conditions studied are listed:

    1) Temperature range: 30-145°C

2) a_Ws: 0, 0.12, 0.23, 0.33, 0.44
3) Sample compositions of systems
PVP10/xylose/lysine   98 : 1 ; 1
PVP40/xylose/lysine   98 : 1 : 1
maltose/lysine   80 : 20
amioca/maltose/lysine   20 : 70 : 10
amioca/lactose/lysine   20 : 70 : 10
amioca/lactose/lysine   20 : 79 : 1

Results and Discussion

Figure 1-3 show the results of the browning experiments plotted as a function of (T-Tg) Each data point on the (T-Tg) plots represents a browning rate at a unique temperature and Tg. Below a (T-Tg)= 0 the systems are in the highly viscous and immobile glassy state while above a (T-Tg)=0 the systems are in a more mobile rubber-like condition. Reaction rates of all the systems were low in the general region below a (T-Tg)=0. Above (T-Tg)=0 the rates started to increase noticeably. The curves for the different moisture contents of a given system separated above (T-Tg)=0. The divergence of the curves above (T-Tg)=0 indicates that there are other temperature and moisture effects not accounted for by the (T-Tg) term. If the glass transition temperature served as a all-encomposing and unifying parameter, the curves for all the moisture contents would have superimposed above (T-Tg)=0.

The Arrhenius-type models are shown in Table I. Moisture, temperature, and glass transition temperature were all important in browning. Using any two of the three variable produced acceptable correlations. The best correlations were obtained when all three variables were included. The models show that any two parameters can be conveniently used to predict browning in the systems. It should be pointed out that the three parameters are not independent, since Tg depends on moisture content. Because the correlations of the models improved with the inclusion of the Tg term, glass transition does have an effect on browning. The effect is not as significant as crystallization. Physical processes have been well described as functions of (T-Tg)(*9-13*). Chemical changes are more complex in that beyond influencing the mobility of a system, temperature and moisture can have other effects on the chemistry. Moisture can be involved as a product or reactant in a reaction(*14*). In browning, water is formed at various condensation steps, including the initial reaction of the amino acid and sugar. Moisture affects the mobility of the matrix, but may also be involved in dissolution of the reactant (*15-18*). Temperature can have an important effect on mechanism of the reaction. It is well known that the browning products obtained are very temperature dependent. In a compex set of reaction such as browning, it would be an over simplification to assume that temperature and moisture have a one sided effect, that of controlling viscosity.

Equation 1 describes the relationship between diffusion and the observed reaction rate constant (k') for a chemical reaction (*19,20*). If there are no diffusional limitations k'=k, where k is typically dependent on temperature and can be described with the Arrhenius equation. So it is evident that the reaction rate constant should depend on separate temperature effects anyway. If diffusion of the reactants through the system becomes a limiting factor, and D is a function of (T-Tg), the ratio of the numerator to the denominator of equation 1 determines if the effect of the glass transition will be an overriding influence on k'. k' would only deviate from the Arrhenius relationship to the degree that the
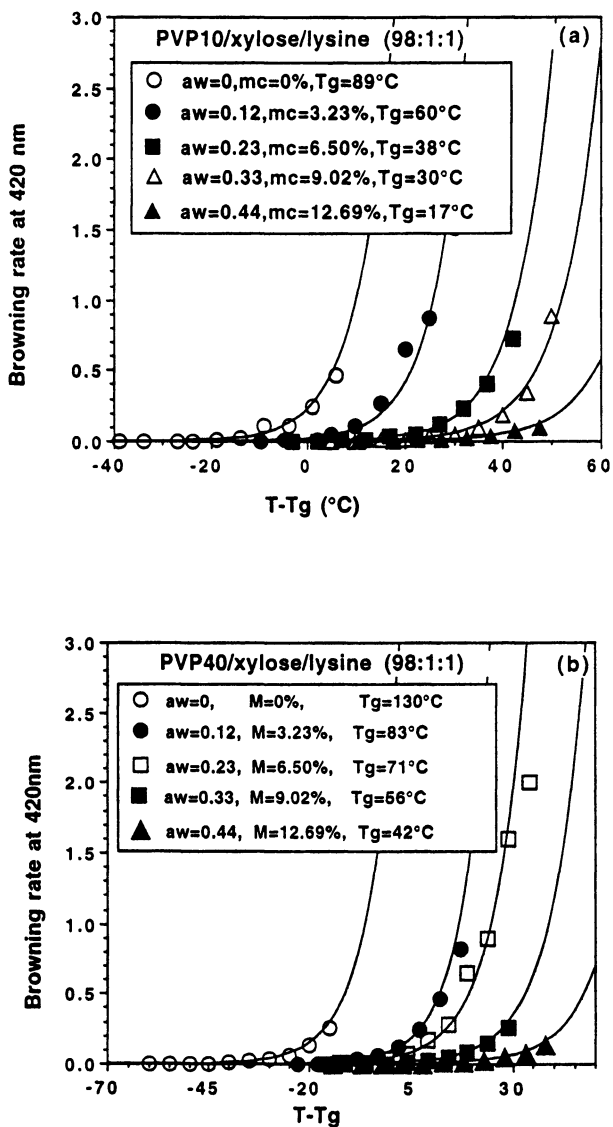
Figure 1. Browning in systems based on PVP/xylose/lysine as a function of (T-Tg). Figure 1a shows results for PVP 10 which has a lower glass transition temperature than PVP 40 the results for which are shown in figure 1b. The corresponding Tg values are indicated in the inset in each figure. Figure 1a is reproduced with permission from Thermochimica Acta, reference 9, copyright 1994.
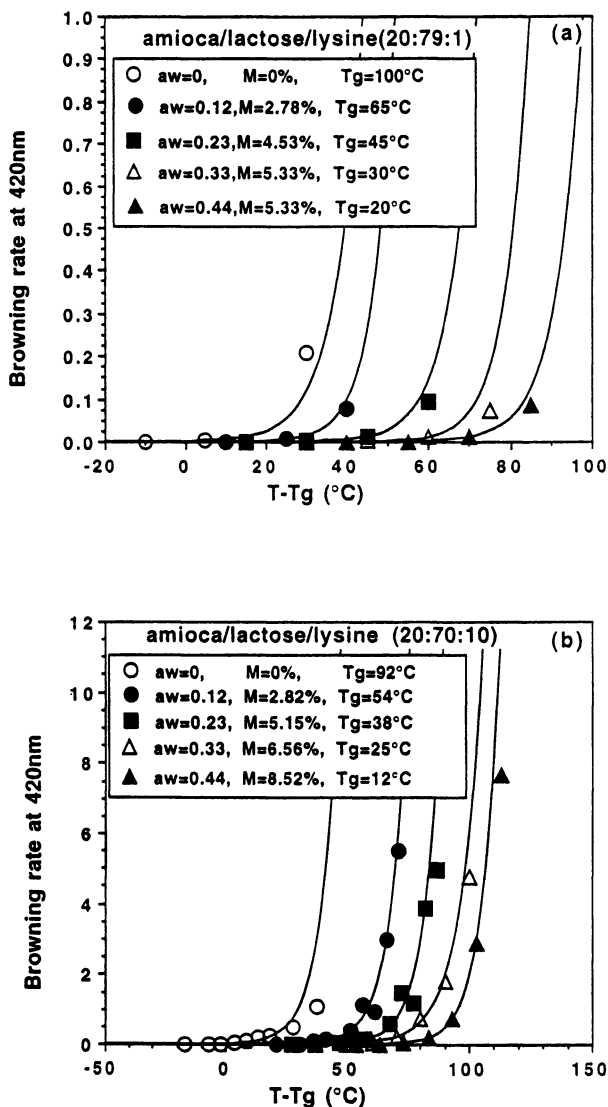
Figure 2. Browning in systems containing maltose and lysine as reactants. In the results shown in figure 2a the matrix is composed of the reactants without any additional solids, in 2b amioca starch has been added resulting in increased Tg values as shown in the inset.
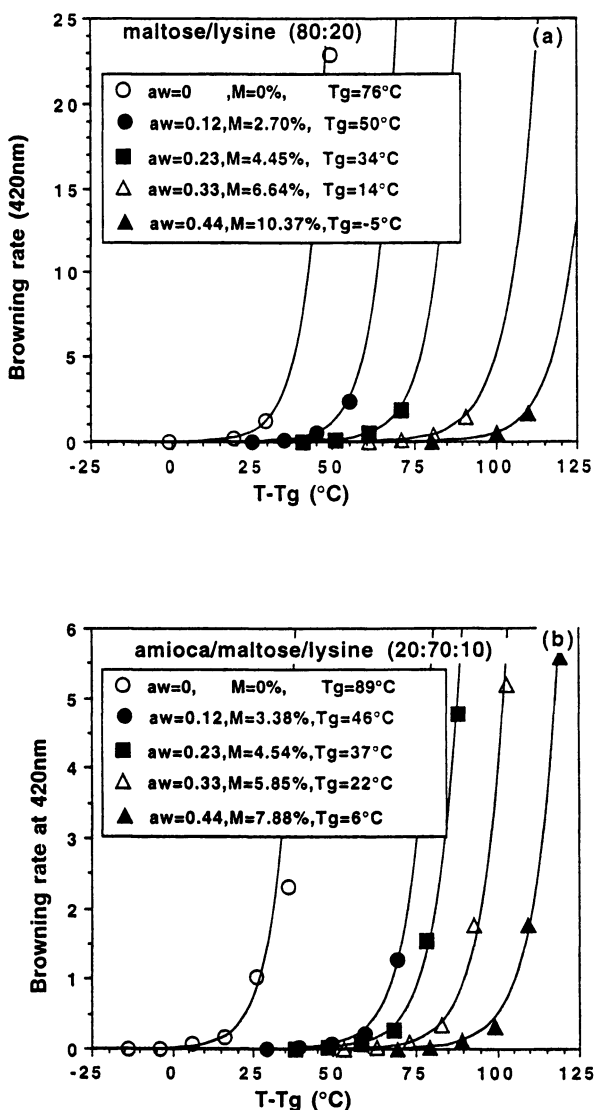
Figure 3. Browning in systems based on reactants lactose and lysine. The matrix is based on 70 to 79 parts of lactose and 20 parts of amioca starch. The concentration of lysine was increased in experiments shown in figure 3b tenfold over the level used in experiments shown in figure 3a, resulting in more rapid browning at the same (T-Tg) level.

Table I. Kinetic models for browning in matrix/xylose/lysine systems

PVP10/xylose/lysine (98:1:1)
2 parameter models:

$$\ln k = 42.71 - 15884\left(\frac{1}{T}\right) + 0.25\,M \qquad r^2 = 0.92$$

$$\ln k = 28.38 - 10764\left(\frac{1}{T}\right) + 0.045(T - Tg) \qquad r^2 = 0.96$$

$$\ln k = -2.044 - 0.52\,M + 0.13(T - Tg) \qquad r^2 = 0.96$$

3 parameter model:

$$\ln k = 15.09 - 6070\left(\frac{1}{T}\right) - 0.24\,M + 0.086(T - Tg) \qquad r^2 = 0.98$$

PVP40/xylose/lysine (98:1:1)
2 parameter models:

$$\ln k = 41.47 - 16091\left(\frac{1}{T}\right) + 0.22\,M \qquad r^2 = 0.96$$

$$\ln k = 28.41 - 10960\left(\frac{1}{T}\right) + 0.043(T - Tg) \qquad r^2 = 0.98$$

$$\ln k = 0.053 - 0.44\,M + 0.12(T - Tg) \qquad r^2 = 0.97$$

3 parameter model:

$$\ln k = 18.42 - 7111\left(\frac{1}{T}\right) - 0.16\,M + 0.072(T - Tg) \qquad r^2 = 0.98$$

Other 3 parameter models:
amioca/lactose/lysine (20:79:1)

$$\ln k = 27.08 - 12257\left(\frac{1}{T}\right) - 0.18\,M + 0.055(T - Tg) \qquad r^2 = 0.88$$

amioca/lactose/lysine (20:70:10)

$$\ln k = 32.47 - 13333\left(\frac{1}{T}\right) - 0.18\,M + 0.045(T - Tg) \qquad r^2 = 0.96$$

maltose/lysine (80:20)

$$\ln k = 41.16 - 15785\left(\frac{1}{T}\right) - 0.18\,M + 0.030(T - Tg) \qquad r^2 = 0.99$$

amioca/maltose/lysine (20:70:10)

$$\ln k = 42.22 - 16754\left(\frac{1}{T}\right) - 0.074\,M + 0.19(T - Tg) \qquad r^2 = 0.98$$

T, Tg in K
k in O.D. units/hour
M in %d.b.

dependence of D on (T-Tg) becomes significantly great relative to the value of k. Therefore, one would not expect the dependence of chemical reactions on (T-Tg) to be a simple one. If the additional influences of moisture are also considered, it is easy to see how the results of our work indicated that (T-Tg) could not account for all the temperature and moisture effects on browning.

$$k' = \frac{k}{\left(1 + \dfrac{k}{\alpha D}\right)} \qquad (1)$$

Conclusions:
Models were developed which describe browning rates as a function of T, M, and (T-Tg). Acceptable models were obtained when and two of the above three variables were used. The best models were obtained when all three parameters were included. Chemical changes in the vicinity of the glass transition are more complex than physical changes. Besides affecting mobility of the system, temperature and moisture have separate and important influences on chemical changes.

Literature Cited
1. Labuza, T.P. Shelf-life dating of foods. Food and Nutrition Press, Westport, CT, **1982**; 30-70.
2. Franzen, K.; Singh, R.; Okos, M.R. Kinetics of nonenzymatic browning in dried skim milk. *J. Food Engin.* **1990**;*11*, 225-239.
3. Labuza, T.P. and Baiser, W.M. The kinetics of nonenzymatic browning. In: *Physical Chemistry of Foods*; H.G. Schwartzberg and R.W. Hartel (eds.), Marcel Dekker, NY, **1992**.
4. Labuza, T.P. and Saltmarch, M. The nonenzymatic browning reaction as affected by water in foods. In: *Water activity: Influences on food quality.* Academic Press, San Francisco,**1981**; 605-649.
5. Karmas, R. and Karel, M. The Effect of Glass Transition on Maillard Browning in Foods. In: *Maillard Reactions in Chemistry, Food and Health*; T.P. Labuza, G.A. Reineccius, V.M. Monnier, J. O'Brien and J.W. Baynes (eds.) Royal Society of Chemistry, Cambridge, England, **1994**; pp. 182-187.
6. Karmas, R., Buera, M.P., and Karel, M. Effect of Glass Transition on Rates of Nonenzymatic Browning in Food Systems. *J.Agric.Food Chem.*, **1992**; *40*:, 837-879.
7. Salwin, H. Defining minimum moisture contents for dehydrated foods. *Food Technol.*, **1959**; *13*, 534.
8. Labuza, T.P., Tannenbaum, S.R., and Karel, M. Water content and stability of low-moisture and intermediate moisture foods. *Food Technol.*, **1970** ;*24*: 543-544, 546-548, 550.

9. Karel,M., Anglea, S.A., Buera,M.P., Karmas, R., Levi, G., and Roos, Y. *Stability Related Transitions of Amorphous Foods.* Thermochimica Acta **1994**; *246*:249-269.

10. Roos, Y. and Karel, M. Applying state diagram to food processing and development. *Food Technology,* **1991**;Dec. 66-71, 107

11. Slade, L. and Levine, H. Beyond water activity: Recent advances based on an alternative approach to the assessment of food quality and safety. In *CRC Critical Reviews in Food Science and Nutrition.* **1991**; 30/2,3 115-360.

12. Williams, M.L., Landel, R.F. and Ferry, J.D. The temperature dependence of relaxation mechanisms in amorphous polymers and other glass-forming liquids. **1955**. *77*:3701-3707.

13. White G.W., and Cakebread, S.H. The Glassy State in Certain Sugar Containing Food Products. *J. Food Technology* , **1966**; 1:*73*

14. Hodge, J.E. Chemistry of browning reaction in model systems. *J.Agric.Food Chem.,* **1953**; *1*, 928-943.

15. Duckworth, R.B. Solute mobility in relation to water content and water activity. In: *Water Activity: Influences on Food Quality*; R.B. Rockland and G.F. Stewart (eds.), Academic Press, New York, **1981**; 295-318.

16. Duckworth, R.B. and Kelly, C.E. Studies of solution processes in hydrated starch and agar at low moisture levels using wide-line nuclear magnetic resonance. *J.Food Technol.* **1973**;*3*, 105-113.

17. Duckworth, R.B. and Smith, G.M. Diffusion of solutes at low moisture levels. In: *Recent Advances in Food Science-3;* J.M. Leitch and D.N. Rhodes (eds.), Butterworths, London, **1963**; 230-238.

18. Karel, M. Effects of water activity and water content on mobility of food components and their effect on phase transition in food systems. In *Properties of Water in Foods.* D Simatos and J.L. Multon (Eds.), Martinus Nijhoff Publishers, Dordrecht, Holland. **1985**; 153-169.

19. Karel, M. Temperature-dependence of food deterioration processes. *J. Food Sci.* **1993**; *58* (6) ii.

20. Karel, M. and Saguy, I. Effects of water on diffusion in food systems. In: *Water relationships of foods*; H. Levine and L. Slade, (eds.). Plenum Press, N.Y. **1991**; 157-173.

Chapter 7

Modeling the Maillard Reaction

A Computer Simulation and a Discussion of Its Application to Maillard Reaction Analysis and Design

Patrick S. Lee

Nestlé Food Company, 800 North Brand Boulevard, Glendale, CA 91203

> The Maillard reaction is mathematically modeled on the computer. The kinetics of the Maillard reaction are described by a set of ordinary differential equations. The ODE's are then mathematically integrated using a Runge-Kutta method. Simulation of the reaction were made under various conditions. The simulation runs are done on a computer using a relatively simple spreadsheet program. The results are presented in the form of time-concentration profiles of key compounds generated or consumed during the reaction. Temperature, reactant concentrations, reactant ratios, pH and pH adjustments are some of the variables tested. These simulations allow a comparative analysis of the Maillard reaction under different conditions. The program can be used as a tool for analyzing the Maillard reaction and for simulating novel processes. This tool allows investigators to design processes and to optimize output. The methodology used in the simulation is discussed along with an analysis of how kinetic parameters may be derived from experimental data. A discussion is made on future experiments to improve the model and to refine key parameters.

The objective of this paper is to present a computational tool that was developed for the dual purpose of "analysis" and "design." As an analytical tool, investigators can use this software to analyze experimental data, to verify consistency of data, to simulate experiments, and to model complex chemical pathways. As a design tool, users can model processes, to predict results of chemical processes, to design process conditions for commercial purposes. Use of this computational tool is in the form of computer simulations. When a set of selected variables is properly inputted, a user can observe the effect of a designed chemical pathways at the specified conditions by running a simulation.

Introduction

The overall Maillard reaction is a rather complex reaction. It is not a single reaction but a whole series of reactions each proceeding in parallel and in series. Attempts to describe the Maillard reaction have been made by many others (1,2,3,4,5) and will not be repeated here. Modeling the entire Maillard process can be difficult at best and is made more so when accurate data is insufficient. This paper will *not* model the entire Maillard reaction. Instead it will focus on a few key chemical steps. The purpose is to demonstrate that such an approach is reasonable and the results can be useful. If successful, the model can be expanded to include more of the individual steps in the complex reaction.

Presented below is a relatively simple model of the Maillard reaction, consisting of several key chemical steps. The purpose of this model is to illustrate how simulations can aid in the analysis of proposed processes. As part of the example, the effect of pH on a key reaction pathway is demonstrated. As a point of focus, it will be shown how pH can affect the overall reaction. But more importantly, it will be shown that this pH effect can be altered dependent on *how* it is introduced into the process. This implies that by controlling the pH precisely, one can design a process that can optimize the outcome of the Maillard reaction.

The model is formally described as a set of kinetic equations and is expressed in the form of ordinary differential equations (ODE). Each kinetic equation is specified by its associated set of kinetic parameters, including activation energies and Arrhenius constants. When diagrammed out in its entirety, the Maillard reaction is illustrated as a set of chemical pathways, occurring in series and in parallel. Kinetics equations are written in the form of ODE's. Integration of these ODE's generate the concentration profile of various compounds of interests as a function of time, including those of intermediary compounds. Since these differential equations do not all have analytical solutions, numerical methods have to be employed to solve them mathematically.

For the purpose of simplicity, a 4th-order Runge-Kutta integration method was used to solve the ODE's. While 4th-order Runge-Kutta is not a sophisticated mathematical tool, it is a well established and well understood method. And it is fairly easy to implement. As a first attempt, this method is more than adequate. The accuracy of the method will be demonstrated. Other methods can easily be substituted and implemented. For more complicated differential equations, e.g. partial differential equation models, much more sophisticated methods need to be used. A discussion on the object-oriented approach will show how this is feasible.

The platform chosen to implement this software is a readily available spreadsheet program (Microsoft EXCEL) that works on commonly available PC's (either IBM compatibles or Apple Macintosh). The reason for this selection is the
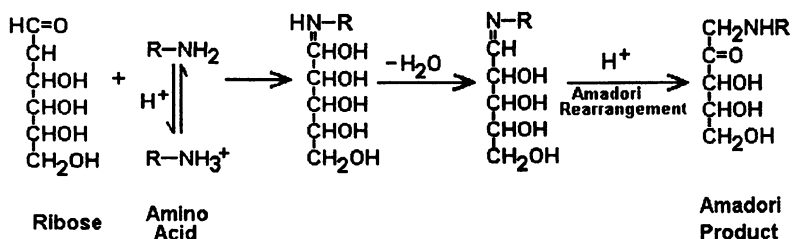
Figure 1. Early Stages of the Maillard Reaction (reprint with permission, ref.2)
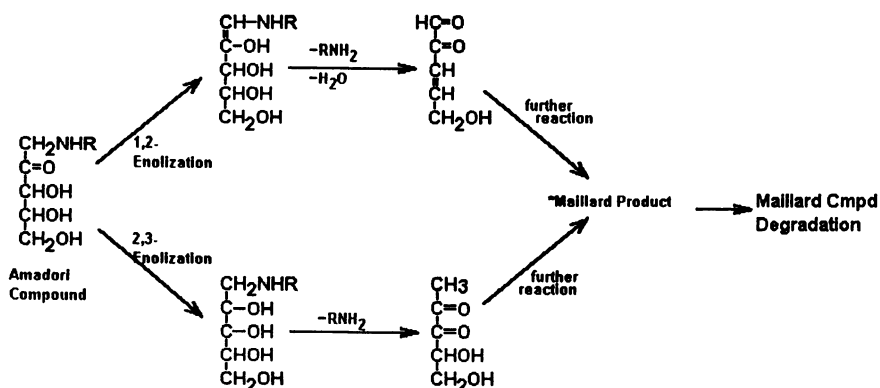
Figure 2. The Two Enolization Pathways. (reprint with permission, ref.2)
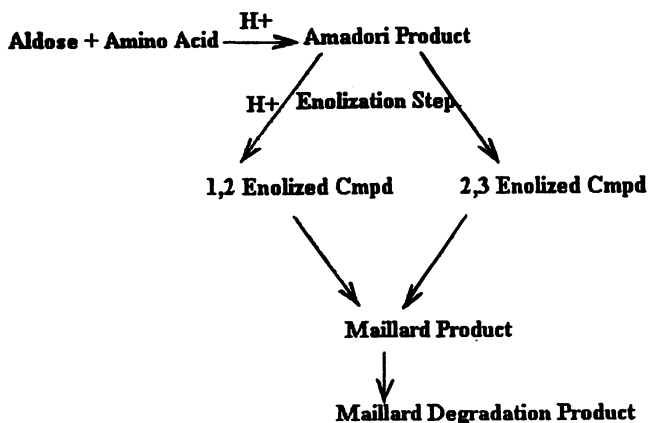
Figure 3. Reaction Pathways Used in Model of the Maillard Reaction.

belief that a useful software package must be easy to use and easy to port between machines. The format of the spreadsheet allow easy modification by the user. The data is readily transportable from one machine to another. Speed of execution is not an issue -- provided that the model is concisely maintained. The user-interface is superior to that of a mainframe and this is an important feature for the user.

Methodology

The kinetic model. A very simple model is adapted to describing the overall Maillard product formation. Recognizing that this is *not* a complete model of the Maillard reaction, its intent is to illustrate the use of simulation. In this special case, focus is placed on the effects of pH on several key steps in the overall reaction. The chemical pathways suggested here have been proposed by earlier investigations by others (2,3). The emphasis is placed on the effect of several key parameters in the generation of the final Maillard product. The two reaction paths of interest are the Amadori rearrangement (illustrated in Figure 1) and the enolization of the Amadori Compound (illustrated in Figure 2).

Figure 1 shows the reaction of an amino acid with an aldose into the formation of Amadori compounds in the Amadori rearrangement. The Amadori rearrangement is actually inhibited by a high [H+] concentration or (low pH). In this model, a proportionality function is added to the reaction step. According to this proportionality function, the Amadori rearrangement is facilitated at higher pH's and is slowed down at lower pH.

Figure 2 shows that Amadori compounds undergoing further reaction. In this case it either undergoes a 1,2 enolization step to yield 3-oxyosones or a 2,3 enolization step to yield 1-deoxyosones. In both of these reaction steps, pH plays a role. The enolization step is affected by the presence of H^+. The 1,2 enolization path is favored by low pH, and is also favorable in the formation of selected Maillard products. Whereas the 2,3 enolization path is favored by higher pH, and is less reactive in the formation of Maillard products.

This model allows proteins as precursors along with pure amino acids. With the presence of proteolytic enzyme, amino acid or longer chain polypeptides may be generated by hydrolysis. The overall reaction pathway being modeled is presented in Figure 3. The Amadori compounds are key components in the model. Its dependence on pH and its subsequent degradation into one of two possible reaction steps is a major factor in the extent of Maillard product generation. The reaction of Amadori compound into the two potential enolization product is also affected by pH.

Reactions leading to the Maillard product are simplified by expressing the subsequent reactions as single stage 1st-order reactions. Each of the enolization

compounds reacts further to form the final Maillard compound. Both enolized compounds have a different kinetic rate but both are in the same range value.

The final Maillard product is also presumed to degrade to further non-detectable compounds. The kinetics of the degradation is assumed to be slow compared with the other reactions but is significant in controlling the final Maillard concentration.

The set of reactions describing the model can be as follows:

$$\text{Protein} + \text{Enzyme} \xrightarrow{\ k_1\ } \text{Amino Acid} \qquad\qquad\qquad\text{(R1)}$$
$$C_1 \qquad\qquad\qquad\qquad C_2$$

$$\text{Amino Acid} + \text{Aldose} \xrightarrow{\ k_2\ } \text{Amadori Rearrangement Cmpds} \qquad\text{(R2)}$$
$$C_2 \qquad\quad C_3 \qquad\qquad C_4$$

$$\text{Amadori Compound} \xrightarrow{\ k_3\ } \text{1,2 Enolization} \quad \text{(favored by low pH)} \qquad\text{(R3)}$$
$$C_4 \qquad\qquad\qquad\qquad C_5$$

$$\text{Amadori Compound} \xrightarrow{\ k_4\ } \text{2,3 Enolization} \quad \text{(favored by higher pH)} \qquad\text{(R4)}$$
$$C_4 \qquad\qquad\qquad\qquad C_6$$

$$\text{1,2 Enol. Compound} \xrightarrow{\ k_5\ } \text{*Maillard product} \qquad\qquad\qquad\text{(R5)}$$
$$C_5 \qquad\qquad\qquad\qquad C_7$$

$$\text{2,3 Enol. Compound} \xrightarrow{\ k_6\ } \text{*Maillard product} \qquad\qquad\qquad\text{(R6)}$$
$$C_6 \qquad\qquad\qquad\qquad C_7$$

$$\text{*Maillard Product} \xrightarrow{\ k_7\ } \text{Degradation products} \qquad\qquad\qquad\text{(R7)}$$
$$C_7 \qquad\qquad\qquad\qquad C_8$$
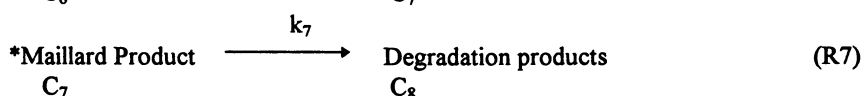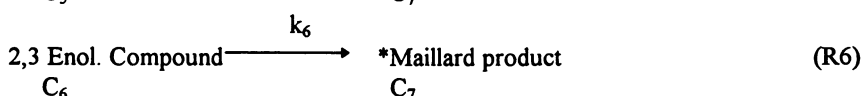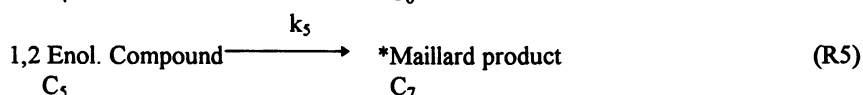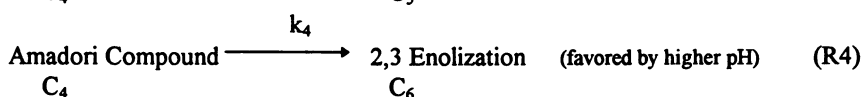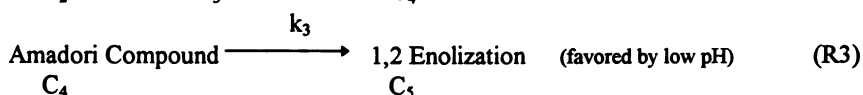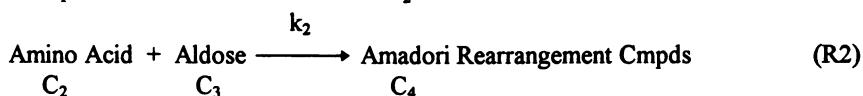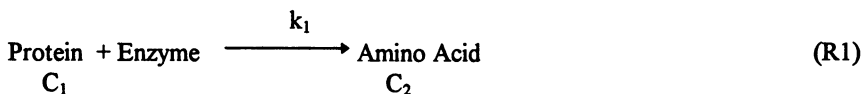
Overall, there are 7 reactions and 8 compounds of interest. The "*Maillard" product referred to here is a pseudonym for a collection of some selected Maillard compounds. The end product of the Maillard reaction could be any of a number of compounds (4,5), it would not be useful to isolate any one compound for this paper/ The main objective of this paper is to introduce a mathematical technique to investigate the generation of *any* Maillard end product. Since it is difficult to identify any one specific compound that could clearly characterize the Maillard reaction, a model (*) compound is used to referred to *all* of them collectively.

Kinetic equation   Each reaction rate equation is expressed in the form of $dC_i / dt = f(x_1, x_2, \ldots x_i, t, \text{pH, T, etc.})$. For example, for the simple reaction

$$C_1 \xrightarrow{\ K_1\ } C_2 \qquad\qquad\qquad \text{(a1)}$$
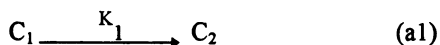
the kinetic equation describing the concentration C_1 may be

$$\frac{dC_1}{dt} = -K_1 C_1$$

where K_1 is the reaction constant for the reaction $C_1 \longrightarrow C_2$. If species C_2 undergoes another reaction such as

$$C_2 \xrightarrow{\quad K_2 \quad} C_3 \qquad\qquad (a2)$$
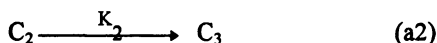
the kinetic equation describing C_2 may be:

$$\frac{dC_2}{dt} = K_1 C_1 - K_2 C_2$$

where K_2 is the reaction constant for the second reaction. The equation describes the production of C_2 from reaction (a1) and the disappearance of C_2 from reaction (a2). These kinetic equations are all of the first order. Most simple reactions can be described as first order with respect to each reactant. However, this model can accommodate any number of kinetic equation each of which may be of any order.

The set of ODE describing the appearance and disappearance of each of the eight compounds of interest is as follows:

$$\frac{dC_1}{dt} = -k_1 C_1 \qquad\qquad (E1)$$

$$\frac{dC_2}{dt} = k_1 C_1 - k_2 C_2 C_3 \qquad\qquad (E2)$$

$$\frac{dC_3}{dt} = -k_2 C_2 C_3 \qquad\qquad (E3)$$

$$\frac{dC_4}{dt} = k_2 C_2 C_3 - k_3 C_4 f(pH) - k_4 C_4 g(pH) \qquad\qquad (E4)$$

$$\frac{dC_5}{dt} = k_3 C_4 f(pH) - k_5 C_5 \qquad\qquad (E5)$$

$$\frac{dC_6}{dt} = k_4 C_4 g(pH) - k_6 C_6 \qquad\qquad (E6)$$

$$\frac{dC_7}{dt} = k_5 C_5 + k_6 C_6 - k_7 C_7 \qquad\qquad\qquad (E7)$$

$$\frac{dC_8}{dt} = k_7 C_7 \qquad\qquad\qquad\qquad\qquad (E8)$$

where k_i has the Arrhenius kinetics model form of $k_i \cong k_{0i} \exp(-\Delta E_i / RT)$, k_{0i} is the pre-exponential constant, $-\Delta E_i$ is the activation energy, R is the universal gas constant, T is the absolute temperature.

Assumptions

The functions f (pH) and g (pH) describe the effects of pH on reactions (R3) and (R4). Instead of expressing pH as $[H^+]$ concentration, a functional expression relates other effect proton ions may have besides concentration, i.e. it is an indirect effects of [H+] concentration. For example, there is a buffering effect due to the presence of protein and amino acids. Therefore, the f() and g() functions are very specific for each individual system. For illustrative purposes, simple first order algebraic expressions are used for discussion in this paper. The pH functions are: f (pH) = (9-pH)*0.55 and g (pH) = (pH-1)*0.25.

All of these ODE's are first order with respect to each reactant. The assumption made here is that each of the reactions understudied is a basic reaction involving uni-molecular reaction and therefore must be first order. In addition, it has been widely reported in literature that the generation of Maillard compounds follows a zero order or first order kinetics (6,7,8,9,10). It will be demonstrated that regardless of the order of the individual reactions, the Maillard concentration profile is largely a function of the last few reaction steps.

Numerical method   A fourth-order Runge Kutta method was adapted for the numerical integration. Since the Runge-Kutta family of numerical methods have been well documented elsewhere (11,12), only a brief review will be offered here.

To solve these ordinary differential equations (ODE's), a 4th order approximation algorithm uses an equation of the general form $y_{i+1} = y_i + h(ak_1 + bk_2 + ck_3 + dk_4)$, where y_{i+1} is the approximated value of the function $f(x)$ at x_{i+1}, y_i is the current value of $f(x)$, h is the step interval from x_i to x_{i+1}, and k_2, k_2, k_3, and k_4 are approximate derivative values computed on the interval $x_i \le x \le x_{i+1}$. More specifically, the set of approximations are:

$$y_{i+1} = y_i + \frac{h}{6}(k_1 + 2k_2 + 2k_3 + k_4)$$
$$k_1 = f(x_i, y_i),$$

$$k_2 = f(x_i + \tfrac{1}{2} h, \ y_i + \tfrac{1}{2} h \, k_1),$$

$$k_3 = f(x_i + \tfrac{1}{2} h, \ y_i + \tfrac{1}{2} h \, k_2),$$

$$k_4 = f(x_i + h, \ y_i + h \, k_3)$$

The accuracy of these approximations can be verified by running a known function f(x) using the approximation and comparing the results with the analytical solution. An example is done for the simple reaction $C_1 \longrightarrow C_2$, which is described by the kinetic equation $dC_1 / dt = K \, C_1$. The analytical (exact) solution to this ODE is as follows

$$C_2 = C_2 (t_0) + C_1(t_0) \exp (-K \, t)$$

Using a time step size of 0.1 and a K value set to 5, the Runge-Kutta solutions are compared to the analytical solutions and are shown in Table I below. The results clearly show that even with a step size of $\Delta t = 0.10$ the error difference was at worst 0.03% and at longer integration time, the error falls to 0.00%. With smaller step sizes, the approximation gets more accurate yet. However, note that with very small step sizes, for example at $\Delta t = 0.0001$, the approximation becomes mathematically "unstable" and the results get irrational. A discussion of choosing the correct step size and how to control stability is made later.

Table I: Analytical Vs Runge-Kutta Values of a Test ODE Solution

	Analytical Solution		Runge-Kutta Solution		Error=1-(C2/C2')
t	C1	C2	C1'	C2'	% Error
0.00	0.6000	0.3000	0.6000	0.3000	0.00%
0.10	0.3639	0.5361	0.3641	0.5359	-0.03%
0.20	0.2207	0.6793	0.2209	0.6791	-0.03%
0.30	0.1339	0.7661	0.1340	0.7660	-0.02%
0.40	0.0812	0.8188	0.0813	0.8187	-0.02%
0.50	0.0493	0.8507	0.0493	0.8507	-0.01%
0.60	0.0299	0.8701	0.0299	0.8701	-0.01%
0.70	0.0181	0.8819	0.0182	0.8818	-0.01%
0.80	0.0110	0.8890	0.0110	0.8890	0.00%
0.90	0.0067	0.8933	0.0067	0.8933	0.00%
1.00	0.0040	0.8960	0.0041	0.8959	0.00%
1.10	0.0025	0.8975	0.0025	0.8975	0.00%
1.20	0.0015	0.8985	0.0015	0.8985	0.00%
1.30	0.0009	0.8991	0.0009	0.8991	0.00%
1.40	0.0005	0.8995	0.0006	0.8994	0.00%
1.50	0.0003	0.8997	0.0003	0.8997	0.00%

Microsoft Excel - BASE.X

File Edit View Insert Format Tools Data Window Help

Times New Roman

F15

	Label =	Base Case: 175F: Initial Reactants at 0.02					dt = 0.2			
		f(pH) =	(9-ph)^0.55 =	2.2000						
		g(pH) =	(ph-1)^0.25 =	1		steps = 50				
Kinetics rates	Pre-exp constant	Activation Energy	Protein n1	Amino Ac n2	Aldose n3	Amadori n4	1,2 enol n5	2,3 enol n6	"Maillard & n7
59.6E+6	2.50E-08	1.00	1	0	0	0	0	0	0
44.8E+0	7.50E-07	10.00	0	1	0	0	0	0	0
41.8E-3	7.00E-04	10.00	0	0	1	0	0	0	0
59.8E-3	1.00E+05	10.00	0	0	0	1	0	0	0
51.4E-3	8.60E-04	10.00	0	0	0	0	1	0	0
88.9E-3	6.23E-05	11.00	0	0	0	0	0	1	0
59.8E-3	1.00E+05	10.00	0	0	0	0	0	0	1
		dC/dt	0.000	0.005	0.005	0.000	0.00E+00	0.00E+00	0.00E+00
	Runge-Kutta k1:		0.000	0.000	0.000	0.000	1.01E-04	-2.36E-05	9.02E-05
	Runge-Kutta k2:		0.000	0.000	0.000	0.000	0.000	0.000	0.000

Figure 4. Screen Dump from EXCEL Showing Main Page of the Spreadsheet.

Hardware and Software   A IBM compatible computer (Compaq Elite) using an Intel 486 chip, with Windows 3.1 and DOS 6.0 as the operating system, was the basic platform. The spreadsheet used for computation was a Microsoft EXCEL version 5.0 for Windows. It should be noted that the very earlier version of this model was developed on the Apple Macintosh computer (IIsi) using System 6.0 and Microsoft EXCEL version 2.2a for Macintosh. The macros which were written to run the simulation was written in EXCEL 2.2 format, but it is upwardly compatible with higher versions of EXCEL. Basically, the early Macintosh version is still usable and is upwardly compatible except for some minor modifications. And by using Access PC, a Mac/PC file exchange program, Macintosh and PC files are basically interchangeable.

A illustration of the spreadsheet is shown in Figure 4 from a computer screen dump. This is the main page on which all of the run variables are entered, including kinetic parameters, interval step size, number of intervals, and most importantly the ODE for each reaction to be traced, etc. Each run of the simulation takes less than 1 minute but can be longer if the number of steps is large or if the step size is small. The difference in speed between using an Intel 486 and 386 chip is insignificant. The only difference in using a higher version of software or hardware is to have access to better graphic features, which is a nicety but not a necessity.

Results and Discussion

Results of the simulation runs are presented in the form of concentration profiles. Each run is presented in one figure and contains the concentration profiles of 5 compounds of interest. In each case, the y-axis is scaled differently to more clearly represent the range of values of concentration. The x-axis is always kept constant for a typical run of 10 hours. The legend for each of the 5 compounds is given and is consistent for all of the figure presented hereafter. The profiles collectively illustrates the evolution of each of the key component of the Maillard reaction.

Base Case: A base case condition run is made and the results are presented in Figures 5 to 7. The set of kinetic values used are given in table II below. This is an hypothetical situation assuming an initial reactant concentration of amino compound and aldose each at 0.02 weight fraction (or 2% by weight). The reaction is held at 175°F constantly for a period of 10 hours. The pH is initialized set at pH=6.7, and allowed to drop to a moderate low of 6.2. The step size is 0.2 hour and the total number of steps is 50, resulting in a total simulated run time of 10 hours. The pH functions are assumed to be a simple linear relationship and is shown as part of Figure 4.
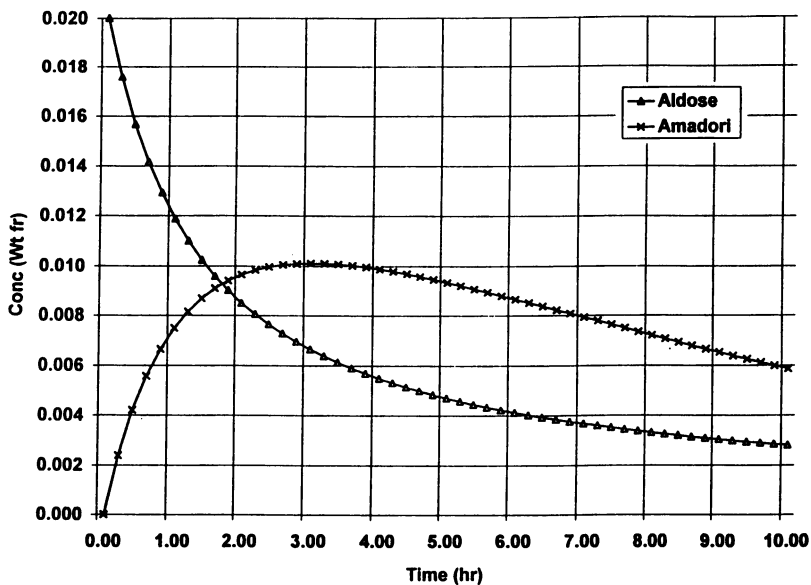
Figure 5. Concentration Profiles of Aldose and Amadori Cmpds (Base case).
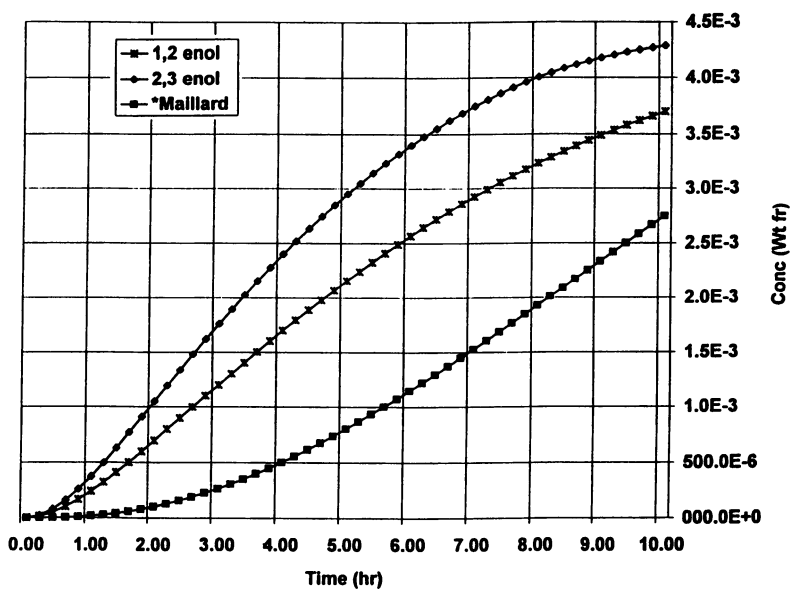
Figure 6. Profiles of Enolization and *Maillard Compounds (Base Case)

Table II: Kinetic Values of Base Case Simulation: k = A exp(-ΔE / RT)

Reaction	Pre-exponential Value A	Activation Energy - ΔE (kcal/mol)
R1	2.5 E +8	1
R2	7.5 E +7	10
R3	7.0 E +4	10
R4	1.0 E +5	10
R5	8.6 E +4	10
R6	6.2 E +5	11
R7	1.0 E +5	10

Initial Reactions. The initial steps in the Maillard reaction consists of the depletion of the reactants and the subsequent generation of the Amadori compound. The reaction concentration profile is shown in Figure 5. By observing the depletion of the aldose and the subsequent generation of the Amadori compound, the initial reaction kinetics can be followed. The aldose is consumed at the same rate as amino compounds and therefore has the identical profile as the amino compound. The aldose concentration is representative of both reactants. The Amadori concentration profile illustrates the appearance and disappearance of an intermediate compounds. The shape of the Amadori curve is typical of an intermediate compound -- rising to a peak, then decreases as the reaction progresses. Where the maxima occurs depends on a number of variables including temperature, reactant concentration, and pH. In general, the shapes of these two curves do not change significantly with reaction conditions. Only the relative positioning, size, and concentrations differ when conditions are changed.

Later Reactions   The later reactions refer to the enolization step, the Maillard product generation step, and the Maillard product degradation step. Concentration profiles of the three compounds of interests are shown in Figure 6. Representative of the Maillard reaction are the relative competitive nature of the 1,2 and 2,3 enolization step. Recall that 1,2 enolization is favored by a higher pH. In this base case simulation, the pH varies from a high of 6.7 to a low of 6.2 towards the end of the 10 hour period. Since 1,2 enolization is also slower in generating the target Maillard product, its concentration curve is positioned higher than that of the 2,3 enolization.

The Maillard product itself exhibits a relatively linear concentration profile. The Maillard production does have a lag time of approximately 90 minutes. The kinetics is indicative of a zero order or a pseudo first order reaction, consistent with what has been reported in literature (6,7,8,9,10). Kinetically, the final Maillard step is relatively slow, and therefore its concentration profile is proportionally slower and smaller. The final concentration of the Maillard is in the range of 2,000 to 3,000 ppm, and is similar to values reported in literature. The actual concentration values are quite sensitive to initial conditions, i.e. reactant concentrations. Since only
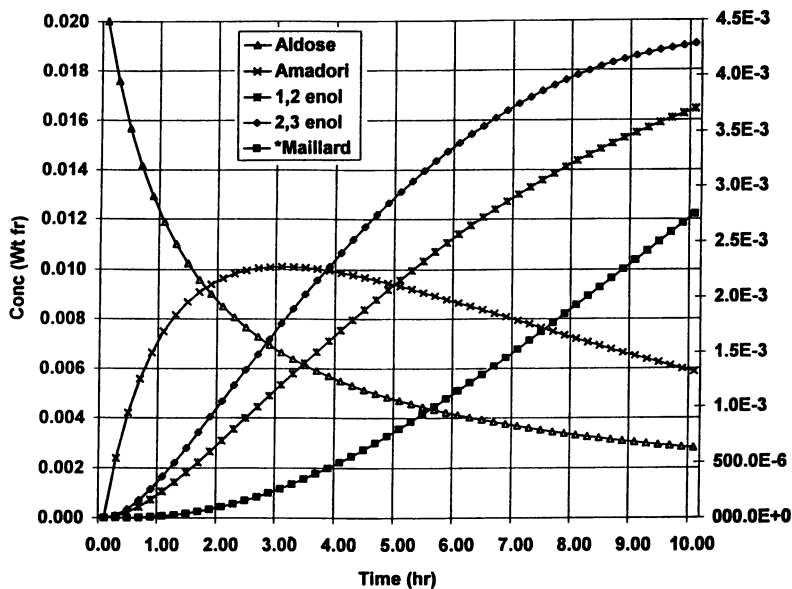
Figure 7. Combined profiles of all 5 compounds (combining figures 5 and 6)
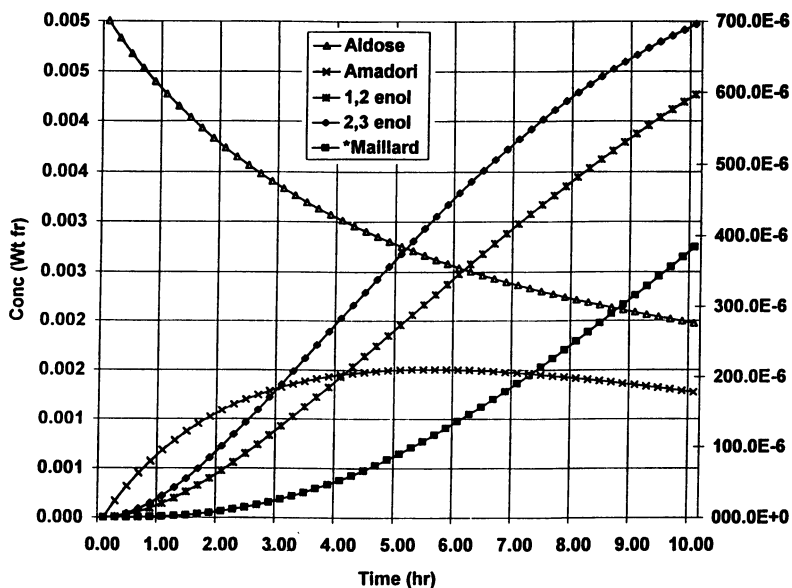
Figure 8. Run With Both Initial Reactant Concentrations of 0.005 (wt fraction)

"assumed kinetic values" are used, these curves should only be examined qualitatively.

Combined Profile   The combined profiles of all 5 compounds are presented in Figure 7 (combining Figures 5 and 6).   Figure 7 is typical in illustrating the relationships among the various compounds.   The Amadori compounds, for examples, drive the later generation of enolization products. If the Amadori rearrangement is slow, then all of its subsequent steps are proportionally slower. It can be shown that even though the kinetic values (Table I above) were estimates, the shape of the various curves remain similar.   The major difference observed if the kinetic parameters were changed are the relative positioning of these curves to each other.   Other differences are seen in the range of concentration values, the location of the maxima, and the asymptotic values.   In general, the concentration profiles have the following features:

- a slowly decreasing reactant concentration until ultimately reaching zero
- intermediate compounds follow a 1st order kinetics: rises to a maxima then slowly decreases in concentration
- 1,2 enolization and 2,3 enolization closely follow one another
- a lag time (typically 30 - 90 minutes) for the generation of Maillard product
- the Maillard profile follows a linear rise, exhibiting a zero order or pseudo 1st order kinetic

Reactant Concentration.   The effects of varying the initial reactant concentration is examined by modifying the base case conditions of 0.02 wt fraction. Initial concentrations have a direct effect on the overall kinetics. As Figure 8 shows, when the reactant concentrations are lower to 0.005, the reaction progresses slower and the end product also reaches a much lower level.   The final Maillard concentration of 400 ppm, when compared with 2,500 ppm in the base case, is much lower than expected.   A conclusion is that the extent of the reaction is not proportional to the reactant concentration. This observation is confirmed when the initial concentrations are raised 4 fold to 0.08. The result is shown in Figure 9. In this case, the final Maillard concentration is 14,000 ppm, much more than 4 times the 2,500 ppm in the base case.   Both simulation shows that as the reactant concentration increases, the reaction proceeds faster.

The changes in reaction rate could be attributed to a driving force behind one of the reaction steps. Which one of the reaction step(s) is the controlling step for the overall reaction? Is it one of the initial steps or the later steps? The kinetics parameters indicate that the Amadori rearrangement is much faster than the other subsequent steps. This means a higher initial concentration would drives the earlier reactions forward faster.   The resulting Amadori product in turn drives the rest of the reaction towards a higher final Maillard concentration.
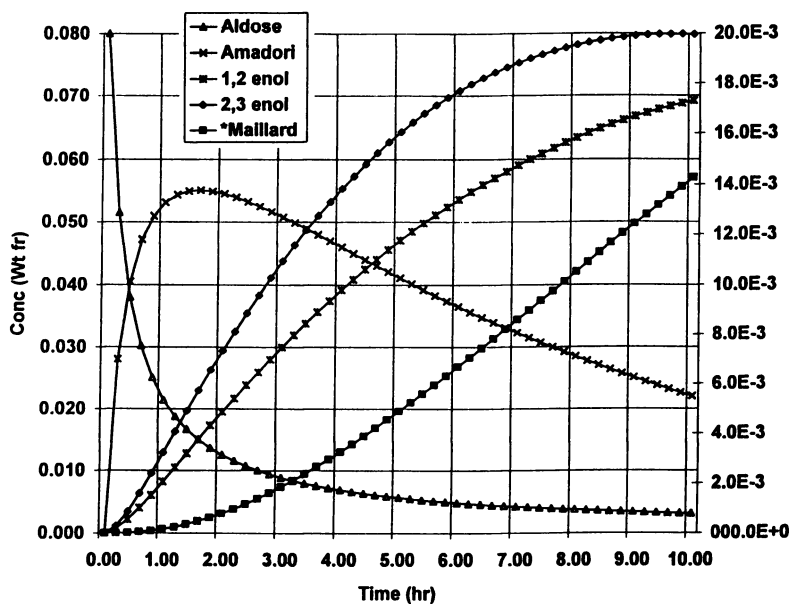
Figure 9. Run With Both Initial Reactant Concentrations of 0.08 (wt fraction)
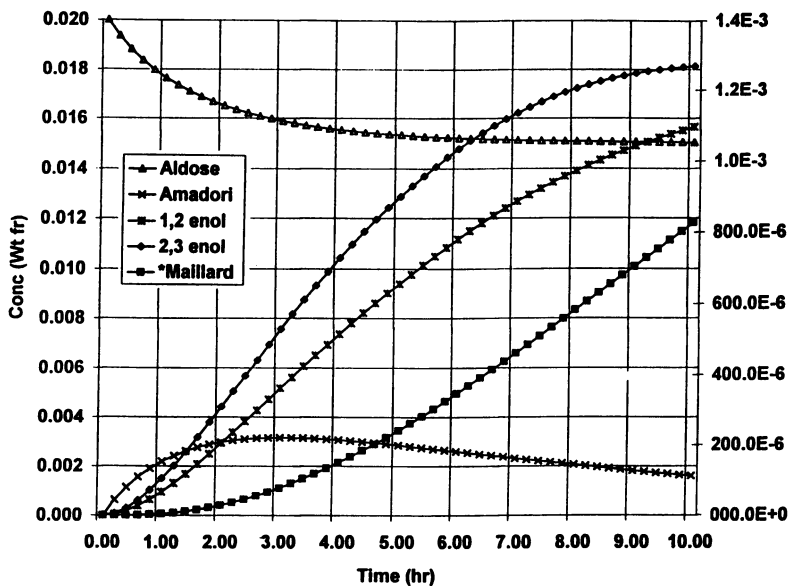
Figure 10. Amino Compound at 0.005 and Aldose at 0.020 Initially (wt fr)

Reactant Ratio. The effects of varying the reactant ratios are made and the results are presented in Figures 10 and 11. The reactant ratio may affect the overall reaction rate. The base case ratio of amino compound to sugar was 1:1 (initial concentrations of both 0.02 wt fraction). . In these two simulations, the ratio of amino compound to sugar is changed to 1:4 and 4:1 respectively. The results show that while the concentration profiles of the initial reactants are changed dramatically, the final Maillard Compound concentration is identical in both test cases at 800 ppm. It appears that a faster initial reaction does not necessarily drive the later reaction. The limiting factor is the reactant at the early part of the reaction, but it exerts its effects early on only. By the time the later reactions become active, the slightly lower intermediate compound concentration is no longer a significant factor.

Compared with the base case, the Maillard formation does show a decrease in final concentration but not as much as if both reactants were reduced in concentration. At a final concentration of 800 ppm, the Maillard concentration is lower than the 2,500 ppm observed in the base case, but higher than the 400 ppm than when both reactants were lowered equally (to 0.005). As the enolization compound profiles show, it is not the later reactions that drives the overall process. Regardless of the initial ratio of reactant, the final concentrations are the same. Neither the amino compound nor the aldose determines the final extent of the overall reaction.

Temperature effect. The effects of temperature on the reaction system is examined by varying the temperature of the reaction. The result is shown in Figure 12. The rate of reaction is highly dependent on the system temperature. It has been reported that the rate of the Maillard reaction doubles for every 10°C rise in temperature. Figure 12 shows part of this temperature effect. The base condition of 175°F was ran against 4 other temperatures. No definitive pattern is observed other than the expected result that the reaction proceed faster at higher temperatures. As far as the rate of reaction is concerned, a doubling effect can be seen for every 10°C rise only seen at certain time frame (e.g. 4 hours). At these conditions, the reaction actually reaches a maximum if the system temperature is 250°F. This implies that the reaction rates can only be meaningfully reported if the reaction time, concentration, and temperature are specified.

Effect of pH. The effect of pH on the overall reaction was run and the results are shown in Figure 13 to 15. The rate of reaction is directly affected by pH. pH plays a significant role in the overall reaction in three places: pH affects the initial Amadori step (favored by a higher pH), pH also favors the 2,3 enolization step where a lower pH favors the 1,2 enolization step.

If the reaction were to take place in a system at a constant pH of 9.0, the overall Maillard reaction would rise to a final concentration of 3,500 ppm. This effect is shown in Figure 13. The higher pH stopped the 1,2 enolization completely. But, the high pH facilitated the initial Amadori step and the 2,3 enolization step. The net effect is favorable to a high Maillard production.
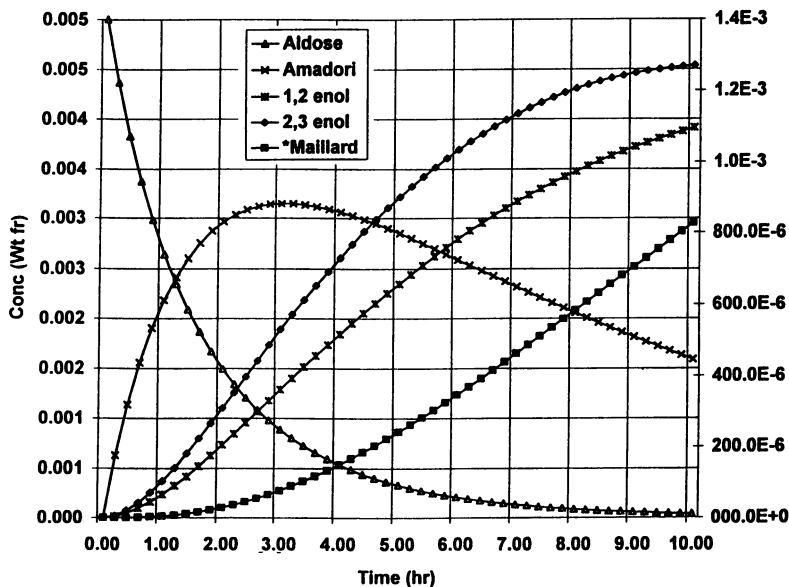
Figure 11. Amino Compound at 0.020 and Aldose at 0.005 Initially (wt fr).
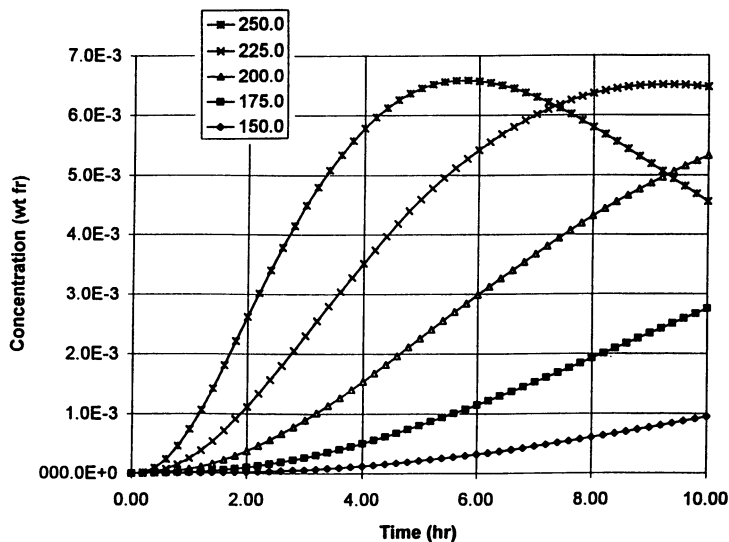
Figure 12. Maillard Profiles As Function of Time at Various Temperatures.
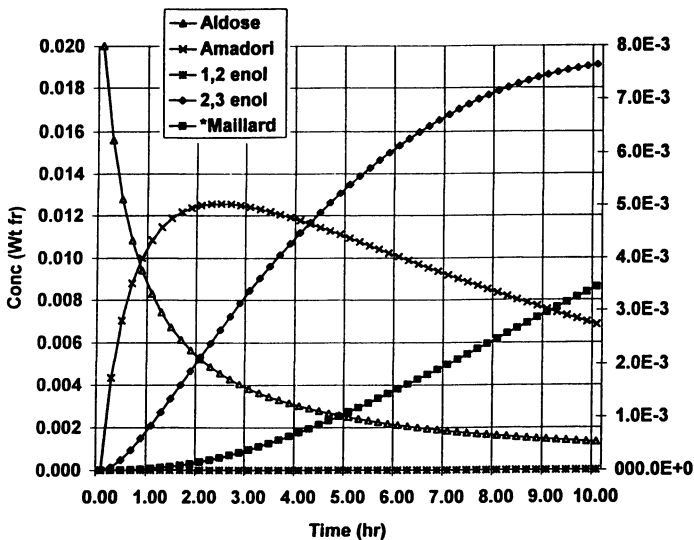
Figure 13. Concentration Profiles of Run at Constant pH of 9.0 Throughout.
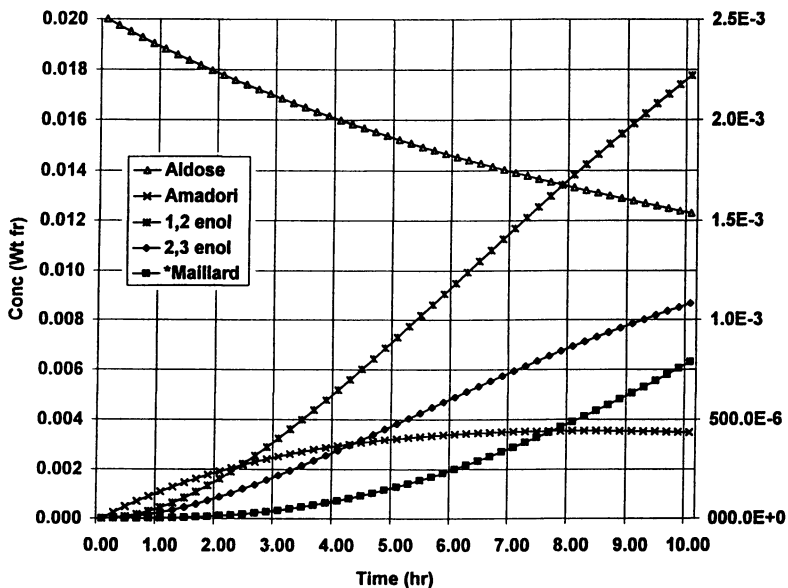
Figure 14. Concentration Profiles of Run at Constant pH of 4.7 Throughout.
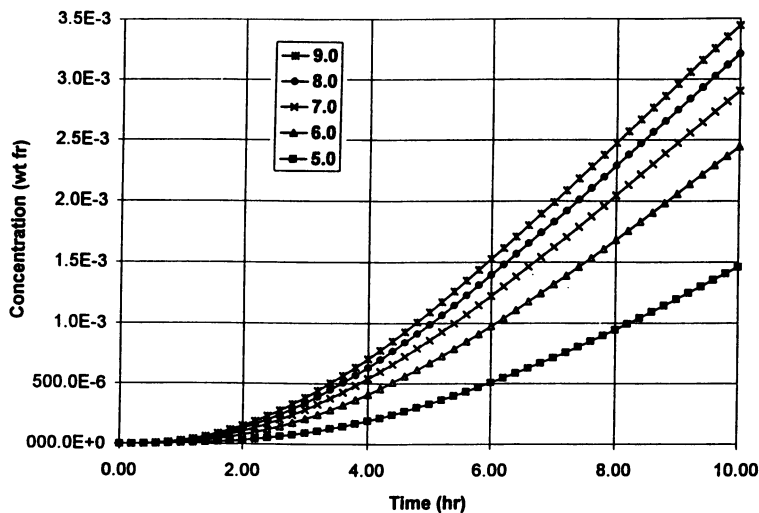
Figure 15. Maillard Concentration Profiles As Function of Time at Various pH
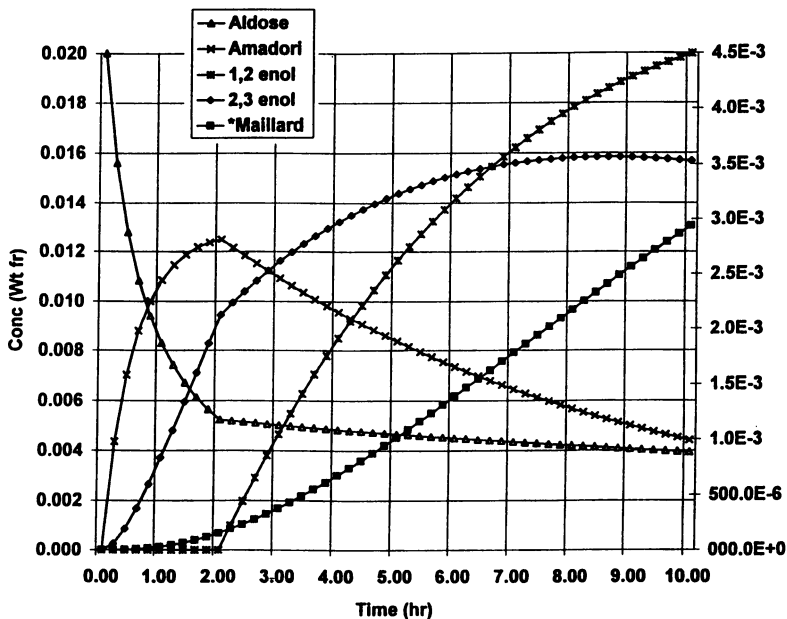
Figure 16. Run of pH Initially at 9.0 Adjusted to pH of 5.0 at Time t=2.0

If the reaction were to take place in a system of pH 4.7 (shown in Figure 14), the overall Maillard generation would fall to only 760 ppm. The major effect of a low pH was on the initial step. As Figure 14 shows, the Aldose concentration falls very slowly throughout the reaction. Consequently, there are limited concentrations of Amadori compound to proceed to the final Maillard steps. This observation agrees well with most reports of the inhibiting effects of acid on the overall Maillard reaction.

Figure 15 shows the effect of pH from 5.0 to 9.0 on the overall Maillard reaction. As the curves indicate, the effect is not proportional. As very low pH, the effect is definitive, Maillard production is severely limited. In fact, at a pH of 4.0, there would not be any Maillard product generated at all. As the pH rises, the rate of Maillard production is only rising 50% for every 100% rise in pH. At a pH of 9.0, the rate has basically reached its maximum. If pH is a controlling factor in the Maillard reaction, then the time of acid addition (or adjusting the pH somehow during the reaction) can be used a control point for the overall Maillard reaction.

Other pH Effects   There is more than one way to use pH to control the reaction. Several simulations were ran to examine the effect of adjusting the pH *during* the course of the reaction and the results are shown in Figures 16 and 17. The objective is to use pH to control the overall reaction but without affecting the reaction time. By adding an acid to lower the pH to 5.0, the Maillard reaction can be slowed down at any point during the reaction. Figure 16 shows the effect of spiking the reaction system with an acid at time t=2.0 into the reaction to change the pH to 5.0. The addition of acid abruptly changes the rate of most of the reactions. Especially affected are the enolization steps. The two enolization profiles actually cross each other. From t = 5.2 onward, the 1,2 enolization that was initially inhibited now dominates the 2,3 enolization reaction and is driving the overall reaction. The overall reaction is promoted on and eventually ending in a final Maillard concentration of 3,000 ppm, almost the same as if the entire reaction was ran at a pH of 9.0.

Figure 17 shows the relative effect of adjusting the pH during the reaction at different times. The initial pH was set to 9 and was adjusted to 5 during the run at time t. A run with the pH set at 9 throughout the reaction is made, and is shown as the top curve. A run with pH set to 5 throughout the reaction is made and is shown as the bottom-most curve. Simulations were made to run with pH adjustment to 5.0 at various times (at t =0.2 to 2.0). As the graph shows, by adjusting the pH, the rate of the overall reaction is significantly changed. An important observation is that the effect is most dramatic if the pH adjustment was made early into the reaction, for example at t < 1.0. After t = 2.0, the effect is less significant. In fact, when spiked at t=2.0, even after another 8 hours of reaction time, the final Maillard reaction is not too different than when pH was maintained constant at 9 throughout the entire reaction.

The implication of the pH adjustment effect is that the final Maillard profile can be affected by precisely adjusting the pH at the right time. If, for example, a low pH and a high Maillard concentration is desired, a reaction can be made to
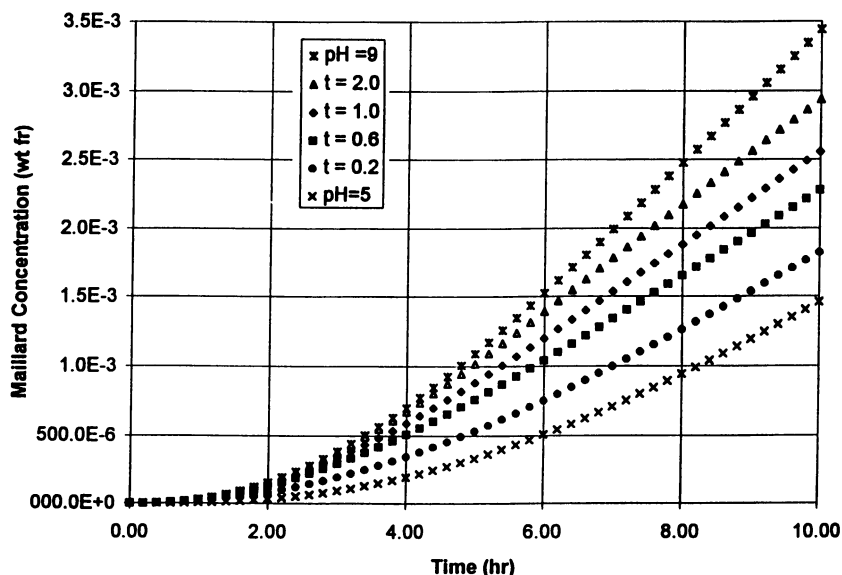
Figure 17. Adjustment to pH 5.0 at Various Time t And At Fixed pH of 5 and 9

proceed fast by initially setting the pH to 9, then some time into the reaction the pH is brought back down to 5 to slow down the process and to achieve the desired pH.

Discussion

An analysis tool. It is proposed that these simulations can be used as an analysis tool. Assuming only a limited set of kinetics data is available, computer simulations can be used to derive the key kinetics parameters by an iterative process. Each iteration of a simulation run uses an improved set of estimated kinetics values. Each set of resultant concentration values will approximate closer to the actual data values. The set of kinetic parameters that generates the *closest* resultant concentration values is the kinetic parameters for that particular reaction.

Example: suppose a set of experimental data is available for a particular *Maillard product formation under a fixed set of laboratory condition. The fixed conditions being those of temperature, pH dependence, and initial concentrations, etc. And the data are in the form of concentration profiles of the *Maillard product. If the quantity of data is sufficient, then a "base" model can be established by using this iteration process. By sufficient data, it is meant that there are enough experimental data points to be evaluated against predicted values and it a way that allow the repeated estimation of new test values. The goal is to reach a unique set of estimated values.

In this model, there are 14 variables (7 kinetic rate variables, k_i, each of which has 2 components, a pre-exponential constant and its associated activation energy) described in each of equations E1 to E7. Therefore, in order to establish a most basic of reaction model, an investigator should have a minimum of 14 data points in order to generate a "unique" solution to the equations E1 to E7. A model can be said to be unique when it, and only it, can generate a set of values corresponding to the observed data.

To generate the unique solution, a user would guess an initial set of kinetics values, k_i. When the kinetic values are put into the model, a simulation run can be made. This simulation run will generate a set of predicted concentration values. This result can then be compared to the experimental data. The investigator estimate new kinetic values based on an approximation method that will yield a new set of predicted values, ones that are closer to the observed data. The new kinetic values are put into the model, replacing the last set. This iteration process repeats until a satisfactory sets of data is generated. Ideally, a final set of simulation result will emerge that matches exactly the experimental data.

Several problems can be expected. The main one is the accuracy and precision of the experimental data. If the initial data are inconsistent or are grossly imprecise, then the usefulness of any simulation run is limited. The issue of measuring Maillard formation is a very difficult one and have been discussed elsewhere (3,4,5). This paper assumes that the investigator has or will have an adequate measurement method and that the experimental values are meaningful.

A second problem is how to *guess* and *estimate* new kinetic values. How much effort is required to converge to an acceptable set of kinetic values? In most cases, the initial estimates are the most difficult. However, if the judgment of the investigator is keen, the initial iterations can be relatively productive in reaching the right order of magnitude estimates.   For example, reactions E5 and E6 are similar and yet competing reactions, they are likely to have the same order of magnitude kinetic values.   Therefore, once one of the two kinetics values is nearly approximated, the other one can be easily converged. If each iteration brings a variable 50% closer to its true value (i.e. doubling of accuracy per iteration), then it would require 224 ($= 2^4$ x14) iterations to converge to a solution set that is within 94% accuracy.   Realistically, additional runs need to be made since the equations are not independent, i.e. each of E1 to E7 affects each other.

Mathematical Efficiency: It should be recognized that the finite difference method is not the only and certainly not the best numerical method for integrating differential equations.   It is possible that a set of non-ordinary differential equations is used to describe the kinetics, say a set of partial differential equations. Then a better method would be to use one of the finite-element methods. There is a plethora of such methods, many of which is described in literature (11,12). The choice of finite difference is because of its simplicity and easy implementation on a spreadsheet format.   Other issues in using numerical methods is the fact that there

are limits to the "stability" and accuracy of the result. In finite difference, for example, one can not use too small a step size. Otherwise, the result can fluctuate wildly, sometimes assuming a sinusoidal curve that will not stablize. The user has to experiment step sizes to verify the meaningfulness of the result and adjust accordingly.

Qualitative Application: Even when very little experimental data is available, these simulation can be used qualitatively. As demonstrated in the example runs above, very general observations can be made from an assumed set of kinetic parameters. For example, if only the effects of one of the reactant is of interest, then simulations can be run by fixing the remaining parameters and run only the single reactant concentration as a variable. Other effects such as pH and temperatures can be simulated at combinations of conditions expensive or not possible under experimental conditions. In these cases, the simulation serves as an extrapolation tool.

A design tool. Finally, it is desired that this computational approach is useful as a design tool. While the simulations presented in this paper are all theoretical runs. The outputs may be useful as general guidelines. For example, it can be concluded that certain pH effects contribute certain sensitivity to the overall reaction. Given this information, a design engineer can design processes that reduces sensitivity to pH, perhaps by using a buffering system. Or, an engineer may choose to utilize certain effect to his advantage. For example, if high temperature is proven to be beneficial only at the initial stages of a process, then cost savings can be realized by minimizing the reaction hold time, or using an energy efficient heating system, or varying the reactor size.

Conclusion

Computer simulation allows the predictive estimation of process output. The main benefit of computer simulation is cost. It could allow an experimenter to test various scenario of proposed processes without wasting valuable resources. Simulations can add to the precision of a process design. Another use are the sensitivity studies of various conditions on the final outcome, including process condition, equipment configuration, initial concentrations, yield factors, and so on. Again, it should be stated that the output of any computer simulation is only as good as the data inputted to the program. So it is imperative that the user is aware of the accuracy and appropriateness of the design data.

Computer simulation can be useful in predicting results of chemical reactions, assuming that the data used to run the simulation is representative. The reaction kinetics are highly dependent on the kinetic parameters. The overall reaction kinetics are dependent on a number of variables including: reactant concentration, reactant ratio, temperature, pH, and duration of reaction.

Adjustment of any one of the above *during* the reaction can also affect the overall rate. The simulations presented are theoretical. Nonetheless, certain observations can be made. Some of the very useful ones are the sensitivity analyses done on the simple variables such as temperature and pH. These simulations should be used as a tool and be experimented by the user for as far as the user can imagine.

References

1.   Hodge, J.E. *Journal of Agric. Food Chemistry.* 1953, 1, 928-943
2.   Mottram, D.S. *Thermally Generated Flavors.* ACS Symposium Series 543, The American Chemical Society: Washington, D.C., 1994. Chapter 10.
3.   Eichner, K., Reutter, M. And Wittmann, R. *Thermally Generated Flavors.* ACS Symposium Series 543, The American Chemical Society: Washington, D.C., 1994. Chapter 5.
4.   Bailey, M.E. *The Maillard Reaction in Foods and Nutrition.* ACS Symposium Series 215, The American Chemical Society: Washington, D.C., 1983. Chapter 11.
5.   Nursten, H.E. *Flavor Chemistry*, 1980-81 Vol. 8, pp 263-277
6.   Barbanti, D., Mastrocola, D., and Lerici, C.R. *in Leansmittel-Wissenschaft unde-Technologie*, 1990 Vol. 23, pp 494-498
7.   Leahy, M. and Reineccius, G. Flavor Chemistry*: ACS Symposium Series 388*, , The American Chemical Society: Washington, D.C., 1989, Chapter 7.
8.   Lerici, C.R., Manzano, M., and Cherubin, S. *Lebansmittel-Wiseenschaft und-Technologie*, 1990 Vol 23, pp. 289-294
9.   Ramaswamy, H., Shazala, S., and van de Voort, F. *Journal of the Canadian Institute of Food Science and Technology*, 1990 Vol 23, # 2/3, pp. 125-130
10.   Sensidoni, A., Munari, M. and Lerici, C.R. *Lebansmittel-Wiseenschaft und-Technologie*, 1991 Vol 24, pp. 218-225
11.   Carnahan, B., Luther, H.A. and Wilkes, J.O. *Applied Numerical Methods.* Halsted Press, John Wiley & Sons, New York, 1974. Chapters 6 and 7.
12.   Rose, L.M. *The Application of Mathematical Modelling to Process Development and Design.* Halsted Press, John Wiley & Sons, New York, 1969.

Chapter 8

Implementation of Process Kinetics To Scale Up Automated Thermally Reacted Flavor Processes

Chwan Kong King

International Flavors & Fragrances, Inc., 1515 Highway 36, Union Beach, NJ 07735

Batch reaction flavor processing represents a specific time-temperature treatment of mixed natural ingredients through a series of heating, holding, and cooling phases. In this study, process kinetics was sequentially developed from laboratory, pilot plant, and scale up in production. The objective was to integrate among process design parameters, process control strategy, and intrinsic properties of the formulation into a semi-empirical process model. Based on this model, an adaptive control strategy was designed to improve the system control responsiveness, and to generate a more uniform reacted product for heat sensitive formulations. When the process scaled up to the production scale, both the knowledge and correlation developed from the laboratory/pilot scale model system were found to be applicable to the actual formulations. Patterns of process kinetics were found to be identical to pilot plant runs. An adaptive control scheme containing the non-linear correlation between the virtual reaction temperature with the apparent probe temperature is proposed.

Batch thermal processing is one of the most common unit operations applied to food, flavor, and fine chemical processes (*1-2*). Process flavors, enzymatic reactions, fermentation, pasteurization, and aseptic processing of particulate are examples which require following a specific time-temperature relationship to achieve the desired colors, flavors, textures, residual enzyme or microorganism limits (*3-8*). Generally, the starting feed material in flavor applications is a viscous homogeneous mixture containing several natural food ingredients. The mixture is usually processed in a closed jacketed scraped surface vessel through a series of time-temperature treatments, including heating, holding, and cooling phases as shown in Figures 1. Within the batch cycle, five process variables, namely, the final heating target temperature, heating rate, holding time, cooling

rate, and final target cooling temperature, are the process control variables. By changing the various combination of those variables, different product characteristics can be derived from the same formulation.

Development of batch thermal processing from laboratory, through the pilot plant, then to the production environment can be summarized in Table I. Predictions of the end product profiles from literature or other resource are not readily available. Formulation often changes frequently, for example, natural ingredients often change their supply sources to meet the specific sensory or regulatory requirements. Interactions of the active components in the formula can produce a series of complicated intermediates. Up to several hundred different compounds have been identified and reported by flavor researchers (*9-10*). The increasing demand for improving product quality, process efficiency, and safety, calls for a better understanding of the kinetic behavior during the course of a multi-product batch processing system. Therefore, a semi-empirical process model was developed to study such a complex reaction kinetics in processing environment. This model was based upon comparisons between both the intrinsic kinetics in the laboratory and process kinetics in a pilot plant (*11*). It was found that process variables such as agitation speed, reactor heating/cooling media temperatures, vessel configurations, and process control strategy can change the path of the time-temperature relationship and affect the product quality factors. As a result, different time-temperature histories, non-linear temperature probe response time, system characteristics, and process operating procedures are the contributing factors for inconsistent qualities between batches. A comparison between manual operation with automated batch processing in a five gallon reactor is illustrated in Figure 2. In a manually operated batch (Figure 2A), a process temperature profile can be significantly deviated from the set point temperature profiles, based upon the operator who had run the process. The automated batch (Figure 2B) demonstrates that temperature overshoot and undershoot during the entire cycle can be minimized(*11*).

As a formulation it generally contains water, carbohydrate, and protein. Upon heating, carbohydrates will undergo gelatinization and protein molecules will form intermolecular bindings with carbohydrate molecules. Thus, within the batch cycle, thermophysical and transport properties of the mixed ingredients change from one batch phase to another. For a viscous, non-Newtonian fluid, flow regime can shift with processing time from turbulent / transient to laminar regime. In laminar regime, mixing of heated scraped film with bulk fluid becomes difficult (*12*). Therefore, the observed process kinetic behavior in a processing environment can be significantly different from that of intrinsic reaction kinetics obtained from an ideal laboratory environment. Heating a viscous non-Newtonian fluid in a batch jacketed reactor can be achieved either by using heat transfer fluid or steam. When applying a narrow driving force such as circulated water bath through the jacket, there is a narrow temperature difference within the vessel, and the reaction tends to be uniform throughout the batch reactor. Disadvantages is that longer time is required to reach the final equilibrium temperature. Therefore, the processing environment often uses steam or hot oil as the heating media. When high pressure steam is used, a wider temperature difference and time delay exists between the reactor wall surface and the inner bulk material. The degree of deviation depends solely upon mixing, heat transfer, and process control.
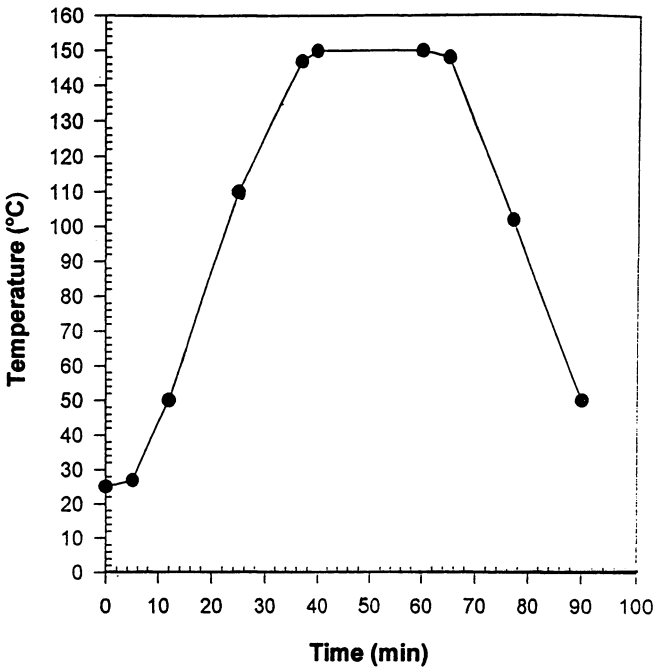
Figure 1. Batch process cycle for a typical reaction flavor process.
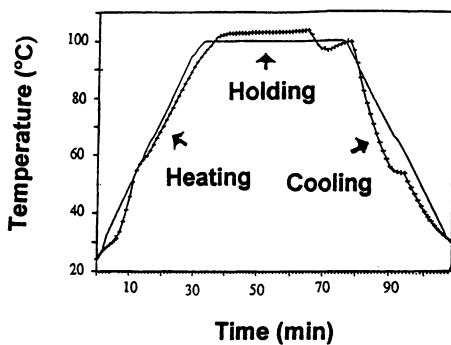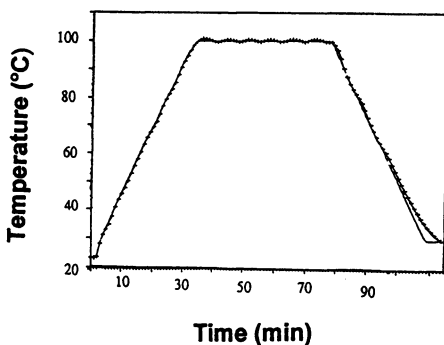
Figure 2. Comparison of manual operation (A) with automated batch processing (B). Both processes were operated in a pilot scale closed scraped surface reactor and using the model system formulation.

Table I. Process identifications for a batch thermal processing

---

I. Intrinsic properties study (5 gram Laboratory Scale)

1. Formulation variables,
2. Time-temperature-concentration dependent thermophysical properties, and
3. Intrinsic reaction kinetics.

II. External factors study (5 gallon Pilot Plant Scale)

1. Mixing,
2. Heat transfer,
3. Equipment design,
4. Process operating procedures:
    Batch process cycle consists of the following phases:
    a. Heating,
    b. Heating to holding,
    c. Holding to cooling phases,
    d. Cooling,
    e. Discharge the material.
5. Process operating conditions.

III. Design a process kinetics based adaptive control strategy
(Both 5 gallon pilot plant scale and 500 gallon production scale)

1. Identify the critical transient regimes between the batch phases,
2. Correlate the virtual reaction temperature with the probe temperature,
3. Derived the lead or lag constant for the batch system, and
4. Scale-up.

It was found that in a batch thermal cycle, three non-linear transient phases, namely, the initial heating, heating to holding, and holding to cooling, exist between those batch phases. It was also observed that the instantaneous probe temperature measured from the specific location of the reactor does not represent the virtual reaction temperature of the bulk fluid. For a heat sensitive reaction formulation, this deviation becomes a challenge in achieving consistent product qualities between different batches. When applying a simple feedback or cascade control scheme, a linear lead or lag time constant was usually added to the controller for improving the system's response. However, those linear lead/lag constants are often obtained by trial and error, and applied to the entire regime of the batch phases. Therefore, there is a need to design an adaptive control strategy that is based upon process kinetics to effectively control the temperature profile in individual transient phase. The reproducible temperature profiles in the transient phases, without overshoot or undershoot, have a significant impact on the product quality factors between batches.

The objective of this study was to implement a process kinetics model previously established in laboratory/pilot studies, to the batch process control system in production. The scale-up batch automated system generates a reproducible, precise and smooth time-temperature profile for multiple formulations. A process implementation scheme initiated from laboratory, through pilot plant, to production, and then finally returning to laboratory and pilot plant is illustrated in Figure 3.

Process Kinetics

A process kinetic study is to provide a process efficiency index for a time, concentration, and temperature dependent batch process operating under a non-ideal environment. This index is based upon a comparison between the intrinsic reaction kinetics of a model system in an ideal laboratory environment with the same formulation in a pilot and production environment. The deviation illustrates the level of external processing conditions that can influence the conversion of the reaction as well as the variation of the product. The prerequisites of the study were based upon :

(1) An on-line non-sensory, quantifiable measuring index that can correlate the extent of both reaction accurately and immediately in the processing environment.

(2) A robust automated batch control system whereby batch experiments must be reproducible for comparison.

In a typical Maillard reaction, the overall reaction involving four reactants can be expressed as follows:

$$A + B + C + D \longrightarrow E + F + \text{etc.} \qquad (1)$$
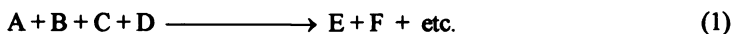
Where   A : 2,3 butanedione

B: ammonium acetate

C: defatted soy flour

D: de-ionized water

E: pyrazine (s)

F: oxazole(s)
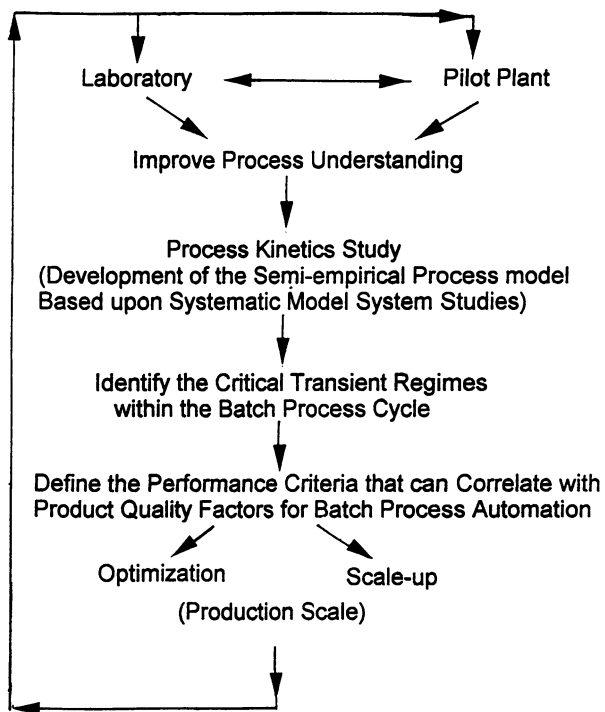
Figure 3. A process implementation cycle from laboratory, through pilot plant, to production, and then finally returning to laboratory for continuous improvement.

Limitations and assumptions are taken into consideration prior to the development of the empirical kinetic model as described in the guidelines by Labuza (*13*). A batch reaction at constant pressure, volume and temperature, if the reaction is irreversible, the rates of reaction can be written as:

$$r = k'[C_A]^n [C_B]^o [C_C]^p [C_D]^q = k[C_A]^n \tag{2}$$

where n, o, p, and q can be determined from experimental results under isothermal conditions. Five different initial concentration levels on C_A, C_B, C_C, and C_D were tested in the laboratory (Table II). It was found that different initial concentrations of C_B, C_C, and C_D did not significantly affect the color formation during the reaction. They are in a large excess that $C_B \gg C_A$, $C_C \gg C_A$, and $C_D \gg C_A$ in this model system. Therefore, C_A becomes the only rate limiting reactant in the model system. The reaction rate constant k', C_B, C_C, and C_D can be regarded as constants during the course of the reaction. Thus, Equation. (2) can be combined into an empirical pseudo n-th order reaction and an effective rate constant k as:

$$r = -\frac{d[C_A]}{dt} = k[C_A]^n \tag{3}$$

where $k = k'[C_B]^o [C_C]^p [C_D]^q$

The experimental result indicated that this is a pseudo-first order reaction with an Arrhenius temperature dependence the rate constant k is given as:

$$\int_{C_{A,0}}^{C_{A,t}} \frac{dC_A}{C_A} = \ln(\frac{C_{A,t}}{C_{A,0}}) = -\int_0^t k \, dt = -k_0 \int_{T_0^*}^{T^*} \exp(-\frac{E_a}{RT^*}) dT^* \tag{4}$$

where $k = k_0 \exp(-\frac{E_a}{RT^*})$, T^* is the virtual reaction temperature.

The temperature integral, $\int \exp(-E/RT) dT$, is obtained when the temperature is increased at constant rate (β). The temperature integral is not analytical integrable due to variation of temperature of T^* with the reaction time t. Various approximations for solving the exponential integral have been reported in the literature. Integral approximation for the non-isothermal pseudo-first order reaction kinetics in the linear constant temperature ramp (β) was given by Agrawal and Sivasubramanian (*14*) :

$$\int_0^{T^*} \exp(-\frac{E_a}{RT^*}) dT^* = \frac{RT^{*2}}{E_a} \left[\frac{1 - 2(\frac{RT^*}{E_a})}{1 - 5(\frac{RT^*}{E_a})^2} \right] \exp(\frac{E_a}{RT^*}) \tag{5}$$

Table II. Experimental set-up for laboratory and pilot plant experiments

System Variables	Laboratory Experiments	Pilot Plant Development Work
Testing Apparatus	Two glass slides (75 x 25 x 1 mm) with 2 mm spacing, three sides sealed with Epoxy resin	A batch scraped surface reactor, closed vessel with 40 pound /batch capacity
Formulations (gram/liter)	(A) 2,3 Butanedione Five concentration levels: (0, 0.176%, 0. 271%, 0.407%, 0.542%) (B) Ammonium Acetate Five concentration levels (0, 0.365%, 0.729%, 0.1094%, 0.1458%) (C) Defatted soy flour Three concentration levels (15%, 20%, 22.5%) (D) De-ionized water Make up quantities other than the above.	(A) 2,3 Butanedione 0.271% (B) Ammonium Acetate 0.729% (C) Defatted Soy Flour 20.0% (D) De-ionized Water 79.0%
Heating Media Temperature ($^{\circ}C$)	Isothermal Water Bath (70, 75, 80, 85, 90)	(A) Isothermal water bath circulate through the reactor jacket (90, 95, 100). (B) Steam (150 psig) and batch computer control of temperature ramp (3.3 $^{\circ}C$/min)
Agitation	None	20, 60, 100 rpm
Seeking Parameters	Intrinsic kinetic parameters: 1. Reaction order, n'. 2. Activation energy, E. 3. Pre-exponential of Arrhenius equation, K_0. 4. Thermophysical properties.: C_p, K , μ, α .	A. Process kinetic parameters: 1. Average virtual reaction temperature, T^{*}. 2. Transfer efficiency, E_m. 3. Scraped-film heat transfer coefficient, h_i. B. Performance criteria.

Thus,

$$\ln(\frac{C_{A,t}}{C_{A,0}}) = -\frac{k_0}{\beta}\left(\frac{RT^{*2}}{E_a}\right)\left[\frac{1-2(\frac{RT^*}{E_a})}{1-5(\frac{RT^*}{E_a})^2}\right]\exp(-\frac{E_a}{RT^*}) \qquad (6)$$

In the above expression, the constant linear heating ramp (β) can be accurately estimated from the heating curve when the processing system was under a precise on-line computer control. The intrinsic parameters (E_a, k_0) can be obtained from a series of laboratory experiments. The initial concentration ($C_{A,0}$) and residual concentration ($C_{A,t}$) of the samples were obtained from a color-concentration correlation curve.

Thus, from in-line conversion data from pilot plant batches and intrinsic kinetic parameters from laboratory experiments, the virtual reaction temperature (T^*) at a linear heating ramp rate (β) can be calculated from Equation 6 by the Newton's perturbation procedure (*11*).

Implementation of Process Kinetics for Scale-up

Implementation of process kinetics to production scale involves several integrated steps. Starting from the laboratory, the initial task is to screen and convert various qualitative descriptions and mechanisms to a quantifiable and measurable performance parameters. By designing an economical model system, laboratory testing requires only a small amount of material, which cover a wide range of formulation and processing variables. Experimental set-up for both the laboratory and pilot plant are summarized in Table II. Five different levels of reactant's concentration and temperature were tested to define the model system's intrinsic kinetic parameters.

During scale up at the pilot plant, a forty pound per batch of the model system was first tested under different combinations of control variables and experimental design. Those tests were monitored and controlled by a process computer. Five other representative formulations with different viscosity, solid contents, and thermophysical properties were selected for testing the robustness of the designed control strategy. Those formulations were chosen because they were frequently used in production and have a broad range of thermophysical and transport properties. An overall performance criterion and correlation were established between the model system and the five representative formulations. Product quality factors for the five representative formulations from pilot scale were accepted by sensory evaluation. The performance criteria (APD, equation 14) was defined at 2 °C. The pilot scale batch control system was thoroughly tested and thus allowing allowed flexibility to adapt to the necessary change in production environment.

When scale up from pilot five gallon to production five hundred gallon batch, the model system became economically unfeasible. Only the five previously tested representative formulations correlated with the model system from the pilot plant were selected as the scale-up formulations. Control strategy and performance criteria were further modified for adaptation to the real system. Only after the production batch

quality was accepted by the quality control team, a repeated developmental process will then return to the laboratory scale for continuous improvement (Figure 3).

Laboratory Experiments A glass apparatus containing two glass slides (75 x 25 x 1 mm) with 2 mm spacing was used to develop the intrinsic reaction model. Heating and cooling time for the homogeneous reactants within a thin space took only 30 to 50 seconds. The short period does not contribute significantly in comparison to the processing batches which generally take one to three hours.

A typical homogeneous, viscous model system contains 2,3-butanedione ($CH_3COCOCH_3$, diacetyl) (0.27%), ammonium acetate (0.73%), defatted soy flour (20%) and water (79%). This formulation has a 3 to 1 molar ratio of ammonium acetate to 2,3-butanedione. After ammonium acetate has been dissolved in water with a dispersator in a container, the defatted soy flour was added and pre-mixed well. Then 2,3-butanedione was added and homogenized for two minutes before use in laboratory or pilot tests.

The procedure to build up the correlation between the extent of coloration of the formulation mixture during heating and the residual volatile reactant concentration is described as follows. In the laboratory, the residual volatile reactant (2,3-butanedione) concentration was analyzed by gas chromatography after the sample has been collected by the steam distillation method. The extent of coloration of thermally reacted samples was measured by a colorimeter. A different gradient of red coloration was observed when the model system was heated from 70 to 90 °C during the initial 10 to 50 minutes. The color index is expressed in Hunter L, a, b system in a tri-dimensional scale (*15*). The "a" value of the Hunter measurement scale was used to correlate with the residual volatile concentration since a reddish color was developed. The correlation provides a basis for immediate determination of the residual reactant concentration in a processing environment.

Pilot Plant Experiments Both the five gallon pilot scale, and the five hundred gallon production scale batch scraped surface reactors were used in this study. Both vessels were insulated and equipped with a single motion anchor agitator. Teflon scraper blades were located on the two sides and the bottom of the reactor (Figure 4). Steam and city water were used as the heating/cooling media. A thermocouple was installed in the jacketed reactor, located at a point about 1/4 radius of the vessel. The thermocouple was used for the control of the whole process. Since the jacketed vessel was heated by steam from the outside, a temperature gradient of the bulk fluid form throughout the vessel. Thus, the instantaneous temperature reading from thermocouple probe could not represent the average bulk fluid temperature. In order to effectively determine the temperature at which the accumulated reaction has taken place, namely, the virtual reaction temperature (T^*), a small portion of the mixture was withdrawn periodically from the bottom of the vessel. Then, color development of the reacted product was quenched to ice water bath, and color was measured by the colorimeter to correlate its residual reactant concentrations that was previously established.

Unsteady State Scraped-film Transfer Coefficient. Figure 5 illustrates the unsteady state heat transfer across viscous non-Newtonian fluid in a scraped surface reactor which consists of (A) the scraped surface film region where heat conduction across the reactor wall and the renewable film was heated by conduction, and (B) the bulk fluid region where forced convection of the bulk fluid mixes with the heated film material by mechanical agitation. For viscous food material, the overall heat transfer coefficient depends on both the scraped-film heat transfer and bulk fluid heat transfer.

The following unmodified stagnant film penetration model has been used to estimate the heat transfer in a scraped vessel with 2 scrapers (*16-18*):

$$h_{i,stagnant} = 2\sqrt{\frac{C_p \rho K}{\pi \theta}} \tag{7}$$

where h_i is the scraped-film heat transfer coefficient ,
K is thermal conductivity, θ is the contact time between two scrapings.

$$\theta = \frac{1}{60NZ} \tag{8}$$

where N is in r.p.m, and Z is the number of scrapers.
The scraped-film heat transfer coefficient can be expressed as:

$$h_i = 2\sqrt{\frac{60}{\pi}}\sqrt{C_p \rho KNZ} = 8.74(C_p \rho KNZ)^{\frac{1}{2}} \tag{9}$$

Since two scraper blades are used for the current study, the above equation can be simplified as below:

$$h_i = 12.36(C_p \rho KN)^{\frac{1}{2}} \tag{10}$$

This is a theoretically derived heat transfer coefficient, defined only by heat capacity, density, thermal conductivity and the contact time of the process fluid which neglect to incorporate the changes of viscosity in both the thermal boundary layer built between two scrapings, and the bulk fluid homogeneity, scraper design, and vessel design. Therefore, this theoretical model generates an over-estimated value (*18*).

To improve the representation of this parameter for the material in the testing vessel, contact time, θ, was replaced by an empirically defined batch thermal mixing time, t_{mix}. Thermal mixing time has the advantage that it incorporated the mixer and vessel design parameters as well as the fluid viscosity during the operating temperature ranges. To determine t_{mix} , a small amount of process material was pre-cooled in a refrigerator. After the process temperature in the reactor has reached equilibrium, the pre-cooled process material, or simply ice cube if the viscosity difference is not significant, was added to the bulk fluid. Thus, temperature of the bulk fluid had a sudden temperature drop, and the batch thermal mixing time (t_{mix}) is the time required to
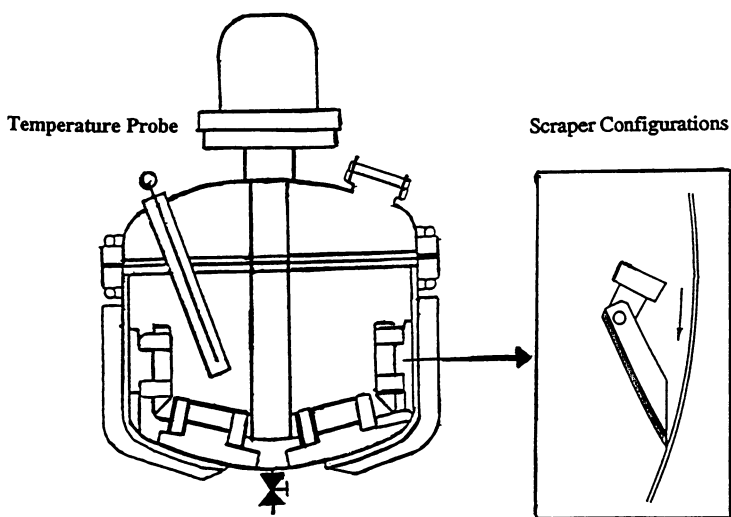
Figure 4. A pilot scale batch scraped surface reactor.
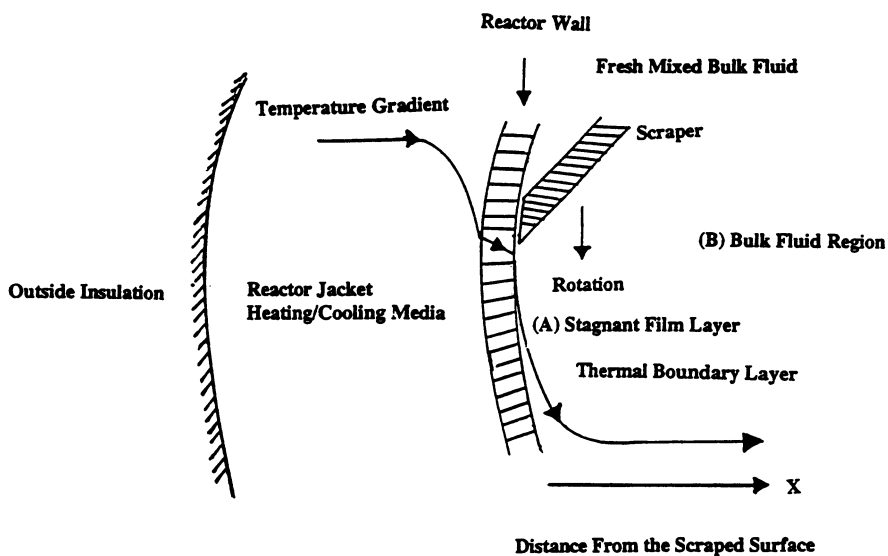
Figure 5. Stagnant film-penetration model for heat transfer in a batch scraped surface reactor.

decrease 90% of the temperature difference between the temperatures before and after adding the pre-cooled material.

An improved heat transfer coefficient can be written as follows:

$$h_{i,stagnant,improved} = 2\sqrt{\frac{C_p\rho k}{\pi t_{mix}}} \tag{11}$$

Scale-up   The approach to scale-up was based upon maintaining the identical controlling mechanism (*19-20*). In this study, unsteady state heat transfer coefficient ($h_{i,\text{ transient phase}}$) at the constant linear heating ramp rate (β) , based upon process kinetics study, can be expressed as follows:

$$h_{i,\text{ transient phase}} = E_m \left[2\sqrt{\frac{C_p\rho K}{\pi t_{mix}}} \right] = \left[\frac{(T_s - T_{App})}{(T_s - T^*)} \right] 2\sqrt{\frac{C_p\rho k}{\pi t_{mix}}} \tag{12}$$

Where E_m is the dimensionless efficiency ratio, $E_m = \left[\dfrac{\left(T_s - T_{App}\right)}{(T_s - T^*)} \right]$

T_s :   heating media temperature.

T_{app}: apparent probe temperature.

T^*:   virtual reaction temperature from process kinetic study in Equation 6.

t_{mix} : batch thermal mixing time by thermal equilibrium method, an experimental value for thermally reacted product in the processing system.

Three separate performance criteria for initial transient phase, transient phase I, and transient phase II (Figure 9) are listed as follows:

$$APD_{\text{initial transient phase}} = \sqrt{\frac{ISE}{n}} = \sqrt{\frac{\sum_{i=1}^{n}\left(T_{App,n} - SP(T_n)\right)^2}{n}} < Y_{\text{initial}} \tag{13}$$

$$APD_{\text{transient phase, 1}} = \sqrt{\frac{ISE}{n}} = \sqrt{\frac{\sum_{i=1}^{n}\left(T_{App,n} - SP(T_n)\right)^2}{n}} < Y_{\text{transient phase, 1}} \tag{14}$$

$$APD_{\text{transient phase, 2}} = \sqrt{\frac{ISE}{n}} = \sqrt{\frac{\sum_{i=1}^{n}\left(T_{App,n} - SP(T_n)\right)^2}{n}} < Y_{\text{transient phase, 2}} \tag{15}$$
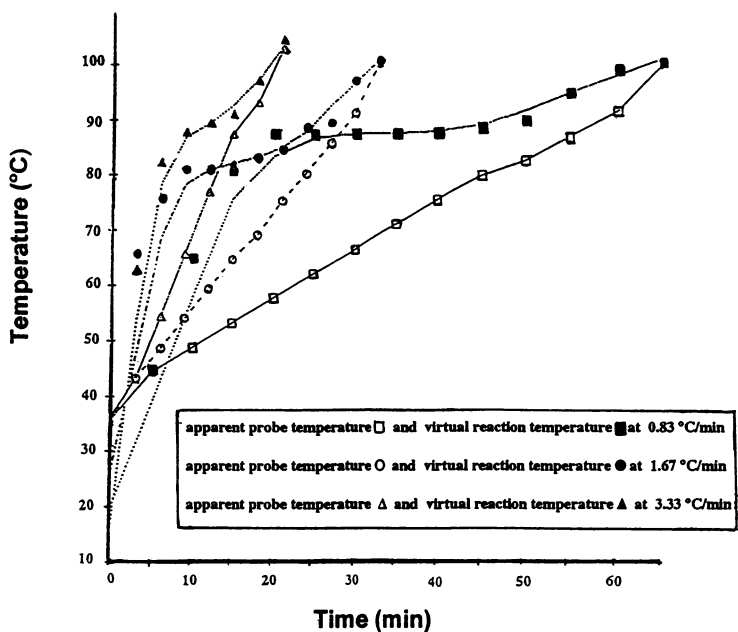
Figure 6. Comparison of apparent process temperature (T_{app}) with virtual reaction temperature (T^*) at different heating rates. Those batches operated in a five gallon pilot scale reactor and using 150 psig steam as the heating media.
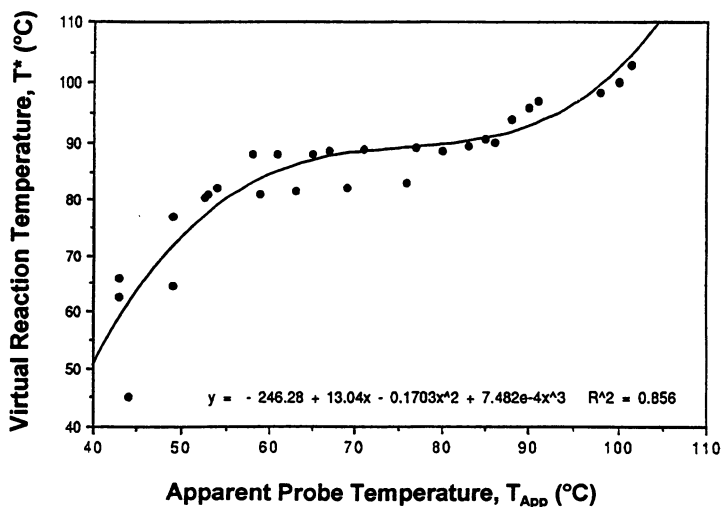
Figure 7. Correlation between virtual reaction temperature (T^*) and apparent probe temperature (T_{app}) from the pilot scale model system study.

Where APD is the Average of Process Deviation (°F), ISE is Integral of the Square Error, n is the number of temperature measuring points, $SP(T_n)$ is each set point temperature, Y is the individual product acceptance criterion, a range between 2.0 to 5.0 °C, which is defined by the product sensory or other quality control standards. In a highly nonlinear batch processing system, those separately defined performance criteria became the quantitative process efficiency measuring index for continuous improvement of the product quality factors.

Results

The reaction kinetics for the model system in the laboratory scale, after an initial induction period, exhibits a pseudo-first order kinetics over a temperature range of 75 to 90 °C, and reaction time of 10 to 50 minutes, with an initial 2,3-butanedione concentration of 2.72 g/kg in the model system. The intrinsic activation energy based on Arrhenius-type dependence over the experimental regime was calculated to be 23 kcal/mole (*11*). This value is within the range of the browning reaction (10-30 kcal/mole), as reported by Hallström et. al. (*1*).

The composition of defatted soy flour includes 31% carbohydrate, 52% protein, 3% fiber. 6% ash and 1% fat. Upon heating, carbohydrates will undergo gelatinization, and protein molecules will form intermolecular bindings with each other and also react with carbohydrate molecules in the Maillard reaction. As a result, the viscosity of the mixture increases rapidly. Viscosity of the starting material is 1,650 centipoise (Brookfield viscometer), and the reacted model system's viscosity is 7,250,000 centipoise. The viscosity increases drastically during the heating process. Based upon Reynolds number, flow regime changes from the transient to the laminar flow regime. In the laminar flow regime, mixing becomes very difficult. Partially segregated fluid in the scraped surface film regime may have an over-reacted product due to in-sufficient mixing of the surface film layer. As a result, the average bulk fluid becomes a heterogeneous mixture containing both over reacted and under reacted fluid.

Figure 6 as shown is the pilot plant test whereby the process system was under computer control with a different heating rate (0.83, 1.67, 3.33 °C/min). At a higher heating rate (3.33 °C/min), first, the virtual reaction temperature lead the apparent process temperature, and then gradually rejoined the apparent process temperature. The virtual reaction temperature had a non-linear correlation with the probe temperature. The regression of the two temperatures, as demonstrated in Figure 7, follows a third-order polynomial equation:

$$T^* = -246.28 + 13.04 \, T_{app} - 0.1703 \, T_{app}^2 + 7.482 \times 10^{-4} \, T_{app}^3 \qquad (16)$$

where T^* is the virtual reaction temperature and T_{app} is the apparent probe temperature.

Heating Phase
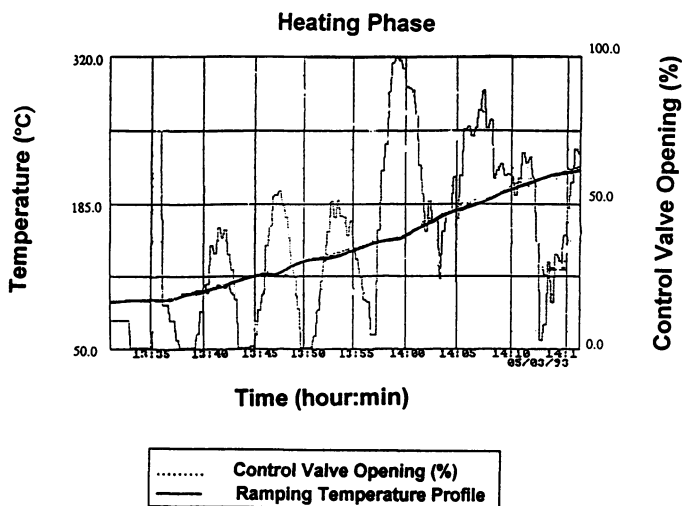
Figure 8. Process dynamics for control valve opening to ramp the apparent
          probe temperature. This batch operated in a production scale 500
          gallon reactor and using 100 psig steam as the heating media.
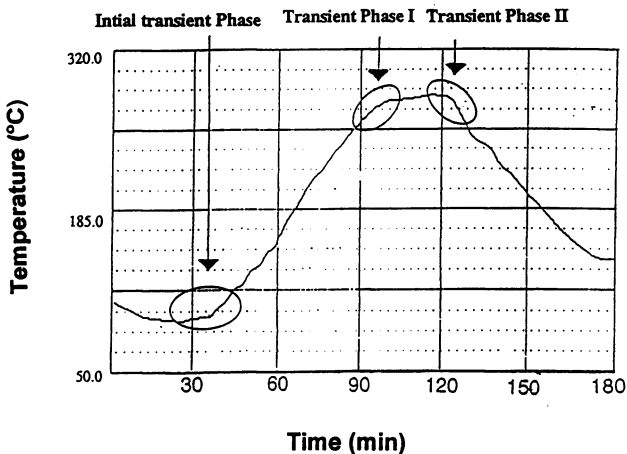
Figure 9. In 500 gallon production batch, three transient regimes existed in a
          batch thermal process cycle. Those phases have significant impact on
          the product quality factors and consistency between the batches.

Figure 8 illustrates process dynamics in a 500 gallon production system. This batch was operated in a process mini-computer. During the heating ramp, 100 to 150 psig steam entered the jacket. The set points in the ramp phase are constantly updating and the probe temperature appears to follow a smooth pathway to the defined set points. The batch process appears to be in good control. However, the control valve opens and closes dynamically to correct the deviations feedback from the probe temperature. When the control valve is in a full open position, the jacket wall temperature can significantly have a higher magnitude of driving force to heat the wall material than probe temperature shown. When the control valve is in a closed position, the probe temperature still indicates a ramp profile. Thus, the bulk fluid consists of a mixture of partially over-reacted and partially under-reacted product. For a heat sensitive formulation, this distribution of the partially segregated fluids contributes to the distinguishable characteristics of the product quality.

Figure 9 illustrates production batch in the corresponding transient regime (Equations 13,14,15). Having correlated with the product quality factors from quality control, 5 °C was found to be an acceptable limit. However, control of those three regimes are not as robust as the previous pilot plant result of 2 °C (Figure 2 B). Therefore, those transient regimes require further optimization.

Conclusions and Recommendations

In haste of transferring R&D processes to manufacturing, a systematic model system study is an effective implementation tool for avoiding the expensive remedial costs. Though it is a time-consuming process, it reveals the degree of the product quality factors influenced by processing conditions, and thus locates the critical regimes in a batch cycle for further process optimization.

It is found that virtual reaction temperature is a continuous function, which has followed the specific time-temperature relationship since the reaction start. Thus it represents the mixed bulk fluid reaction temperature in the processing environment. On the other side, the probe temperature is simply a snap shot of the apparent process temperature which is independent of the pathway of the reaction. Therefore, proposed is an improved adaptive control scheme that is based on a non-linear correlation from the process kinetics study (Figure 10). The unique feature of the process model is that it incorporates not only the processing system characteristics, but also its intrinsic kinetic characteristics of the formulation from a model system study. A lead or lag time constant can be derived from the process kinetics model for feedforward control of the control valve position in the heating phase. This control strategy will minimize the distribution of over and under reacted segregated viscous fluid. To implement the system to production environment, one can set up a data base to group the different formulation's thermophysical and transport properties as compared to that of the established model system. Then one establishes the corresponding correlation between virtual reaction temperature and probe temperature. It is predicted that the process kinetics based model control system will further improve the system's responsiveness, and thereby provide more uniformly reacted products for heat sensitive formulations.
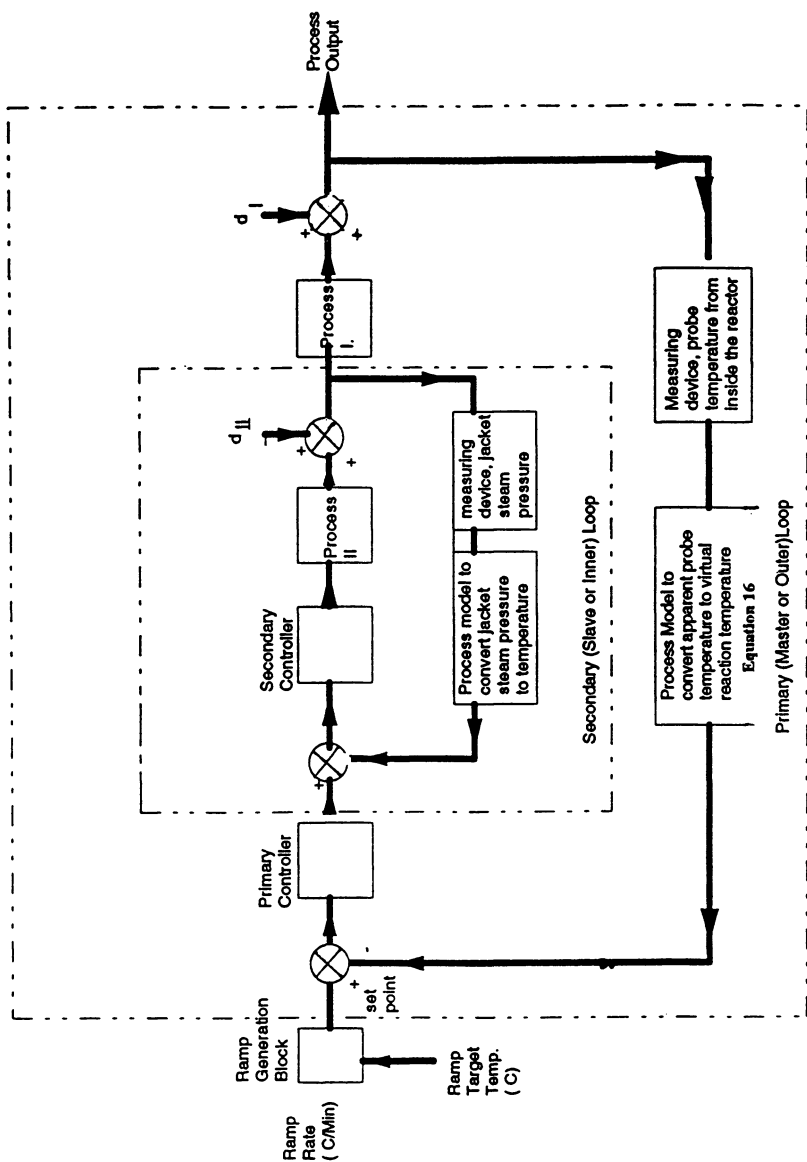
Figure 10. Schematic representation of a process kinetics based batch control strategy.

Acknowledgments

Nomenclature

E_0 = pre-exponential (absolute) rate constant

E_a = activation energy in cal/mole

R = gas constant, 1.987 (Kal/(mole)(K)).

T = absolute temperature in Kelvin.

$[C_A]$ = 2,3-butanedione concentration.

$[C_B]$ = ammonium acetate concentration.

$[C_C]$ = defatted soy flour concentration.

$[C_D]$ = de-ionized water content.

n, o, p, q= order of reaction for 2,3-butanedione, ammonium acetate, defatted soy flour, and de-ionized water.

k' = the reaction constant, time $^{-1}$(concentration)$^{1-n}$

r = the rate of reaction.

h_{i_L} = scraped-film heat transfer coefficient.

$$E_m = \left[\frac{\left(T_s - T_{App}\right)}{(T_s - T^*)} \right. \quad \text{transfer efficiency, dimensionless.}$$

T_s = temperature of the heating media in the jacket.

T_{app} = apparent process temperature from probe.

T^* = average virtual reaction temperature.

t_{mix} = batch thermal mixing time by thermal equilibrium method, an experimental value for thermally reacted product in the processing system.

K = thermal conductivity.

θ = contact time between scrapings (sec).

ρ = density.

C_p = heat capacity

α = thermal diffusivity, (K /(ρ C_p)).

β = linear heating or cooling rate.

Literature Cited

1. Hallström, B.; Skjöldebrand, C.; Trägårdh, C. Heat Transfer and Food products; Elsevier Applied Science.:London, 1988.

2. Manley, C. H. In: *Thermally Generated Flavors Milliard, Microwave, and Extrusion Processes*; Parliment, T. H.; Morello, M. J.;McGorrin, R. J. Eds. American Chemical Society: Washington, DC. 1994; pp. 16-25.

3. Thijssen, H. A. C.; Kerkhof, P. J. A. M. In: *Physical, Chemical and Biological Changes by Thermal Processing*. Applied Science Publisher: London, 1976; pp. 142-157.

4. Labuza, T. P.; Baisier, W. M. In: *Physical Chemistry of Foods*; Schwartzberg, H; Hartel, R. W. Eds.; Marcel Dekker, Inc.: New York; 1992; pp. 595-650.

5. Karel, M. In: *Preconcentration and Drying of Food Materials*; Bruin, S. Ed. Elsevier Science Publishers B. V.: Amsterdam, 1988; pp. 217-234.

6. Holdsworth, S. D. *Aseptic Processing and Packaging of Food Products*; Elsevier Applied Science: London, 1992.

7. Lund, D. In: *Food Protection Technology*, Lewis Publishers, Inc.: Michigan, 1987; pp. 377-385.

8. May, C. G. In: *Food Flavorings*; second edition, Chapman & Hall: New York, 1994; Chapter 10. pp. 276.

9. Mega, J. A. In: *Bitterness in Foods and Beverages*; Rouseff, R. L. Ed.; Elsevier Science Publishers: Netherlands, 1990; pp. 81-101.

10. Weenen, H.; Tjan, S. B.; deValois, P. J.; Bouter, N.; Pos, A..; Vonk, H. In: *Thermally Generated Flavors Maillard, Microwave, and Extrusion Processes*, Parliment, T. H.; Morello, M. J.; McGorrin, R. J. Eds. American Chemical Society: Washington, D.C. 1994; pp. 142-157.

11. King, C. K. *Process Kinetics of a Non-Newtonian Maillard Reaction Model System in a Computer-Controlled Batch Scraped Surface Reactor*. Ph.D. Dissertation, New Brunswick, NJ , Rutgers University, 1989.

12. Nagata, S. *Mixing: Principles and Applications*. John Wiley & Sons:New York, 1975

13. Labuza, T. P.; Kamman, J. F., In: *Computer-aided Techniques in Food Technology*. 1990; pp. 71-115.

14. Agrawal, R. K.; Sivasubramanian, M. S; *AIChE J.* **1987**; *33*, 1212-1214.

15. Francis, F. J.; Glydesdale, F. M *Food Colorimetry: Theory and Application*. The AVI Publishing Co.: Westport, Conn, 1975.

16. Härröd, M. *J. Food Proc. Eng.* **1987**; *9*, 1-62.

17. Nauman, E. B. *Chem. Eng. Sci.* **1977**; *32*, 359-367.

18. Skelland, A. H. P. *Non-Newtonian Flow and Heat Transfer*, John Wiley: New York. 1967.

19. Tatterson, G. B, *Scale-up and Design of Industrial Mixing Processes*. McGraw-Hill: New York. 1994.

20. Zolkarnik, M. *Dimensional Analysis and Scale-up in Chemical Engineering*. Springer-Verlag.: New York. 1991.

Chapter 9

Production of Natural Flavors Using a Cold Extrusion Process

M. H. Cho[1,3], X. Zheng[1], S. S. Wang[1], Y. Kim[2], and Chi-Tang Ho[2,4]

[1]Department of Chemical and Biochemical Engineering, Rutgers University, P.O. Box 909, Piscataway, NJ 08855–0909
[2]Department of Food Science, Cook College, Rutgers University P.O. Box 231, New Brunswick, NJ 08903

Cold extrusion of moistened waxy corn starch mixed with methionine or with cysteine produced methional (potato chip flavor component) or hydrogen sulfide (meat flavor component) as key flavors among several other compounds. Cold extrusion process produced those flavors more efficiently than thermal cooking in a heating bomb or hot extrusion process. Shear energy intensity was a critical factor for flavor generation in the cold extrusion process. Natural flavors from cold extrudates were more pleasant than those generated from thermal treatment for these reaction systems.

Conventional extrusion processes are usually operated at high temperature to supply heat energy into the material, even though there is also shear energy input in the extruder. If the operating temperature of the extrusion process is decreased below 60°C, which was called "cold extrusion" by Wang et al. (*1*), the thermal effect might be significantly diminished comparing to the shear effect. The viscosity of rheological material in the extruder can be increased tremendously at low temperature, which creates a high shear energy environment in the extruder. Wang et al. (*1,2*) demonstrated that shear energy alone can cause starch conversion without thermal energy input by using both a capillary rheometer and a single screw extruder. Wang (*2,3*) also suggested that shear energy is more efficient than thermal energy in the conversion of starch material based on activation energy calculations. Recently, Yam et al. (*4*) showed that the conversion of corn meal was achieved by reverse screw elements during twin-screw extrusion below 60°C, in which they also reported that the conversion was due to shear alone, since thermal effects were negligible at these low temperatures.

[3]Current address: Department of Chemical Engineering, Yeungnam University, Gyongsan 712–749, Korea
[4]Corresponding author

The objectives of this study are to produce natural flavors from amino acid-starch mixtures by using cold extrusion processes, and to compare characteristics of flavor generations between thermal treatment and cold extrusion processes. As case 1, the methional formation from L-methionine-starch mixture was performed. Methional has a flavor similar to potato chips, which was already produced by cold extrusion process below 40°C (*1*). But, Lee et al. (*5*) reported that potato chip-like aroma was noticed only when methionine was treated under deep-fat frying conditions above 180°C. And, as case 2, the hydrogen sulfide formation from L-cysteine-starch mixture was performed. Hydrogen sulfide is a basic compound that has been identified repeatedly in meat flavor (*6*), and not only directly contributes to meat flavor also participates as a precursor in the formation of other sulfur-containing volatiles (*7*).

Materials and Methods

The starch used was a waxy corn starch (Amioca). L-methionine and L-cysteine (both minimum 98% grade) were obtained from Sigma Chemical Co.

Extrusion experiments were performed in a Brabender single screw extruder (Model D-3002) with a barrel diameter of 1.9 cm and a barrel length to a diameter ratio of 20:1, and with a die diameter of 0.5 cm. The extrudate temperature was controlled by circulating ice-water at the flow rate of 1.8 l/min through the cooling jacket for cold extrusion or by using an electrical heating jacket for hot extrusion. Thermal treatments were carried out in a cylindrical heating bomb (350 ml) containing 50 g of starting material. The heating bomb was heated in a Fisher Isotope Oven (200 series). The heating bomb was immersed in an ice-water bath to quench the reaction after heating for a certain period time.

Methional and other sulfur compounds formed from methionine-starch mixture were analyzed by GC-Mass spectroscopy. Four grams of sample was treated by purge & trap and direct thermal desorption methods to release volatile flavor compounds from the solid sample, and analyzed by GC/Mass spectroscopy. Hydrogen sulfide formed from cysteine-starch mixture was analyzed by the sulfide/silver electrode method. A standard sodium sulfide solution in sulfur antioxidation buffer (SAOB, consisting of 2N NaOH, 1N EDTA and 4% ascorbic acid) was used for making a standard curve. Five grams of sample was put in 25 ml SAOB buffer solution and was stirred at 300 rpm for 3 hrs at room temperature. The hydrogen sulfide concentration in the samples could be calculated from the electrode potential and the dilution factor.

Results and Discussions

Case 1: Formation of Methional from Methionine-Starch Mixture.   Usually, methional can be formed from methionine with α-dicarbonyl compounds such as pyruvaldehyde, glyoxal, dehydroascorbic acid or 3-deoxyglucosone at high temperatures above 100°C by Strecker degradation (*8*). But, Table I shows that high concentration of methional was formed at the extrudate temperature of 40°C by cold extrusion process, which might be explained differently from the Strecker degradation. We could assume a kind of free radical reaction occurring by shear force in the cold

extrusion process. In addition, the flavor of cold extrudate was a pleasant potato chip-like one. But, that of thermal cooking was like an overcooked cabbage odor, although it has 1.66 ppm of methional in it. This result agreed with that of Elode et al. (9) who also reported that heating an aqueous methionine solution with sugars produced a cabbage-like flavor at temperatures of 100°C and 180°C. And, Lee et al. (5) insisted that the potato chip-like aroma was noticed only when methionine was treated under deep-fat frying conditions, and they thought it was formed from interactions between the thermal oxidative decomposition products of the oil and the thermal degradation productions of methionine. Then, their reaction route for flavor formation is quite different from that of cold extrusion process.

Table I. Comparison of Flavor Compounds Formed by Cold Extrusion and Thermal Cooking (35% Moisture, 1% Methionine Concentration)

Compound	Concentration (ppm)		
	Control (raw material)	Thermal Cooking (150°C, 30 min)	Cold Extrusion (40°C, 40 rpm)
Methional	0.28	1.66	248.2
Dimethyl disulfide	0.02	0.02	28.9
Dimethyl trisulfide	-	0.01	9.5
Propanethiol	-	-	2.2

Table II shows the effect of methionine concentration on the flavor composition in cold extrudates. Methional concentration was slightly decreased with increasing methionine concentration from 1% to 2%, while concentrations of other sulfur compounds such as dimethyl disulfide, dimethyl trisulfide and propanethiol were greatly increased. It means that the methional formation was achieved sufficiently with 1% methionine concentration. More experiments are needed to determine the critical methionine concentration for the sufficient formation of methional flavor.

Table III shows that the shear energy intensity is very critical for the formation of methional from methionine by cold extrusion processes. For the low shear environment (compression ratio = 1:1), there was no formation of methional comparing to the control data (see Table I). And, the flavor of extrudate under low shear environment was not the pleasant potato chip-like flavor. Therefore, there must be a critical shear energy intensity above which tribochemical reactions of methionine-starch mixture are initiated to form methional.

Table II. Effect of Methionine Concentration on the Flavor Composition in Cold Extrudates (35% Moisture, 40°C, 40 rpm)

Compound	Concentration(ppm)	
	1% Methionine	2% Methionine
Methional	248.2	239.2
Dimethyl disulfide	28.9	182.7
Dimethyl trisulfide	9.5	42.1
Propanethiol	2.2	33.8

Table III. Effect of Shear Intensity on the Flavor Composition in Cold Extrudates (35% Moisture, 1% Methionine, 40°C, 40 rpm)

Compound	Concentration (ppm)	
	Low Shear (Comp. Ratio=1:1)	High Shear (Comp. Ratio=3:1)
Methional	0.042	248.2
Dimethyl disulfide	0.076	28.9
Dimethyl trisulfide	0.001	9.5
Propanethiol	-	2.2

Case 2: Formation of Hydrogen Sulfide from Cysteine-Starch Mixture.   The most common method used for developing hydrogen sulfide is through thermal treatment, but it requires hours to obtain a reasonable concentration of hydrogen sulfide. Table IV shows the effect of reaction time on the formation of hydrogen sulfide by using a heating bomb in a conventional oven. At 160°C, it took more than 30 min. to make a considerable concentration of hydrogen sulfide. Furthermore, even though the concentration of hydrogen sulfide for 1 hour was sufficiently high (15.88 ppm), its flavor was not meaty, but a burnt caramel.

Table V shows the effect of screw speed of hot extrusion on the formation of hydrogen sulfide. Temperatures of products were maintained above 90°C, which increased slightly with increasing screw speed. The concentration of hydrogen sulfide in the product was decreased with increasing screw speed due to the decrease of retention time of material in the extruder. Cold extrusion was performed by maintaining

temperatures of products below 55 °C with changing screw speed. As shown in Table VI, the concentrations of hydrogen sulfide in the cold extrudates were around twice as high as those in the hot extrudates, even though the retention times of cold extrudates were smaller than those of hot extrudates.

Table IV. Concentration of Hydrogen Sulfide Formed by Heating Bomb in a Conventional Oven (30% Moisture, 0.5% Cysteine)

Sample	Temperature	Time	H_2S Concentration[*]
	(°C)	(min)	(ppm)
1	160	15	0.154
2	160	30	0.959
3	160	60	15.88

[*] H_2S concentration is measured as ppm based on dry starch.

Table V. Concentration of Hydrogen Sulfide Formed by Hot Extrusion at Different Screw Speeds (30 % Moisture, 0.5 % Cysteine)

Screw Speed (rpm)	Temperature (°C)	Retention Time (sec)	H_2S Concentration (ppm)
25	90	102	1.093
50	94	61	0.412
75	93	45	0.707
100	95	37	0.849
125	98	28	0.486
150	96	24	0.499

Results presented so far are concentrations of the flavor compounds formed. Table VII lists the rates of formations of hydrogen sulfide. The rate of hydrogen sulfide formation increases with increasing shear stress. Another advantage of a cold extrusion process over hot extrusion process is its low temperature which reduces the loss of volatiles during processing.

**Table VI. Concentration of Hydrogen Sulfide Formed by Cold Extrusion
at Different Screw Speeds (30 % Moisture, 0.5 % Cysteine)**

Screw Speed (rpm)	Temperature (°C)	Retention Time (sec)	H_2S Concentration (ppm)
25	35	80	2.131
50	40	45	1.262
75	48	30	1.853
100	50	24	1.427
125	53	20	0.931
150	55	17	0.755

**Table VII. Comparison of Hydrogen Sulfide Formation Rates by
Heating Bomb, Hot Extrusion and Cold Extrusion Processes**

Processing Conditions	Temperature (°C)	Shear Stress $(N/m^2 \times 10^{-5})$	H_2S Formation Rate (ppm/min)
Heating Bomb in an oven	160	0	0.01-0.26
Hot Extrusion 25-150 rpm	90-98	0.13-0.22	0.41-1.38
Cold Extrusion 25-150 rpm	35-55	0.73-1.60	1.54-3.56

Conclusions

We observed two cases of natural flavor productions from amino acid-starch mixture by using heating bomb in a conventional oven, cold extrusion and hot extrusion processes. The first case was the formation of methional which has a potato chip-like flavor from methionine-starch mixture. And, the second case was the formation of hydrogen sulfide which has a meat-like flavor from cysteine-stach mixture. Cold extrusion process produced those flavors more efficiently than the thermal cooking or hot extrusion process in terms of formation rate and flavor quality. Among several variables, shear energy intensity was the critical factor for flavor generation in the extrusion processes. More experiments are needed to investigate the mechanism of flavor formation in the cold extrusion process. Spin trap and electron spinning resonance (ESR) analyses are needed for the proof of intermediate free radicals.

Acknowledgments

Literature Cited

1.   Wang, S.S.; Zheng, X.; Ho, C.T.; Qu, D. Proceedings of The 6th International Congress on Engineering and Food, **1993**, May 23-27, Kyoto, Japan.
2.   Wang, S.S.; Chiang, W.C.; Zheng X.; Zhao B.L.; Cho, M.H.; Yeh, A.-I. *Extrusion Science and Technology*; Kokini, J.; Ho, C.-T.; Karwe, M. Eds.; Marcel Dekker, Inc.: New York, N.Y., 1992; pp 165-176.
3.   Wang, S.S. *Starch*, **1993**, *45*, 388-390.
4.   Yam, K.L.; Gogoi, B.K.; Karwe, M.V.; Wang, S.S. *J. Food Sci.* **1994**, *50*, 113-114.
5.   Lee, S.-C.; Reddy, B.R.; Chang, S.S. *J. Food Sci.* **1973**, *38*, 788-790.
6.   Pippen, E.L.; Erying, E.J. *Food Technol.* **1957**, *11*, 53-56.
7.   Schutte, L; Koenders, E.B. *J. Agric. Food Chem.* **1972**, *20*, 181-184.
8.   Wang, P.-S.; Kato, H.; Fujiimaki, M. *Agric. Biol. Chem.* **1969**, *33*, 1775.
9.   Elode, K.E.; Dornseifeerr, T.P.; Keith, E.S.; Powers, J.J. *J. Food Sci.*, **1966**, *31*, 351-357.

Chapter 10

A Novel Membrane Process for Folding Essential Oils

M. H. Auerbach

Food Science Research and Development, Pfizer Central Research, Eastern Point Road, Groton, CT 06340–5196

Raw (cold-pressed) citrus peel oils contain 89-98% terpene hydro-carbons, which are often undesirable as they oxidize easily and cause cloudiness in aqueous systems. Folded oils are enriched in the more desirable oxygenated components (aldehydes, alcohols, esters). Com-mercial folding is done primarily by vacuum distillation; lesser amounts are also folded by solvent extraction. Such folded products may be ther-mally stressed, contain solvent residues or undesirable component ra-tios, or are too costly.

A novel continuous membrane process has been developed that yields undegraded folded oils free of solvent residues. Three process configu-rations were investigated using combinations of ultrafiltration, reverse osmosis, dialysis and pervaporation operations. A 100 g/day pilot unit was constructed to demonstrate feasibility.

Membrane product component ratios differ from those of convention-ally folded oils, giving the flavorist a new set of natural raw materials. The processes can also be used to recover valuable components from aqueous waste streams from oil processing plants. Although this work was done entirely with cold-pressed orange and lemon peel oils, the processes should also be applicable to other high-terpene essential oils.

Based on published data and information from consultants, worldwide sales of citrus oils were estimated to be 15-20 MM kg/yr worth $100-150 MM in 1988. The leading use for these flavor raw materials is in beverages. Citrus peel oils are produced primarily by aqueous emulsion centrifugation during mechanical juice extraction (1). These oils cost $2.50-25/kg and contain 89-98% terpene hyd-rocarbons (2,3), which are often undesirable as they are easily oxidized and cause cloudiness in aqueous systems. Non-citrus essential oils are also produced by steam distillation (4). Citrus oils contain over a hundred individual components; the leading ones are given in Table I.

Table I - CITRUS OIL COMPONENTS - Hydrocarbons

Monoterpenes		Sesquiterpenes
d-limonene	α/β-pinene	β-caryophyllene
α-thujene	sabinene	α/β-copaene
myrcene	α-phellandrene	α/β-farnesene
p-cymene	terpinolene	valencene
γ-terpinene	Δ^3-carene	δ-cadinene
tr-β-ocimene	camphene	β-bisabolene
α/γ-selinene	α/β-ylangene	tr-α-bergamotene
		sesquicitronellene
		β-cubebbene
		β-elemene
		α-humulene
Oxygenates		longifolene

Aldehydes	Alcohols	Esters
octanal	linalool	octyl acetate
decanal	α-terpineol	neryl acetate
citronellal	octanol	decyl acetate
neral	nerol	geranyl acetate
geranial	geraniol	citronellyl acetate
nonanal	terpinen-4-ol	N-Me,Me-anthranilate
α/β-sinensal	isopulegol	
undecanal	borneol	**Ketones**
dodecanal	fenchol	nootkatone
perillaldehyde	pinol	carvone
2,4-decadienal	p-cymen-8-ol	
hexanal	tr-carveol	**Others**
	thymol	limonene oxides
	elemol	thymyl Me ether
	citronellol	linalool oxide

"Folding" is an imprecise term used in the flavor industry to describe the volume reduction of an essential oil. Folded citrus oils are enriched in the desirable oxygenated components (aldehydes, alcohols, esters). They contain 5-95% oxygenates and sell for $22-990/kg. If a distillate is one-fifth the original volume of the raw feed oil, it is said to be five-fold, even though the oxygenate content of the product may not be five times that of the feed. Folding is done commercially primarily by vacuum distillation (5); smaller volumes are also folded by solvent/countercurrent extraction (6) [ethanol or CO_2 (7)]. Other non-conventional processes for removing

terpenes from essential oils involve adsorption of oxygenates onto a polar particulate solid followed by recovery with supercritical CO_2 *(8)*, or extraction with β-cyclodextrin *(9)*. These processes are not continuous and have limited terpene removal potential.

There is generally no industry-wide consensus or accepted specification for what constitutes a five-fold orange oil. Many unique products are offered by, for example, combining a vacuum-distilled cold-pressed peel oil with an essence oil [organic phase of condensate from juice concentration (evaporation) process] or aroma (aqueous phase of condensate from juice concentration process). Typical compositions of some vacuum distilled orange oils are given in Table II. Such folded materials may be thermally stressed, contain solvent residues or undesirable component ratios, or be prohibitively costly.

Membrane processes offer the potential advantages of low-temperature, organic solvent-free operation, reduced oxidative degradation, and controllable selectivity for certain components. They have been used to a certain extent in juice processing and oil recovery *(10-13)*, but until the present work, a continuous hybrid process for folding essential oils had not been developed. The objective of this work was to investigate possible membrane systems that would yield useful citrus oil flavor materials with improved organoleptic properties vs conventionally folded oils.

Experimental

Three basic process scenarios were investigated for the concentration of oxygenated components from cold-pressed citrus oils *(14)*.

1. DA/PV: Raw citrus oil was recirculated through a dialysis module against water and oxygenated components of the oil were selectively extracted into the water. These components were then removed from the water by pervaporation and condensed, yielding an oil product greatly enriched in oxygenated components.

2. UF/RO/DA: An aqueous suspension of raw citrus oil was prepared and recirculated through an ultrafiltration module, giving a dilute aqueous permeate greatly enriched in oxygenated components. The oil content of the UF permeate was concentrated 15-20x by recirculation through a reverse osmosis module. The oil phase of the more concentrated RO reject was extracted into fresh raw oil by recirculation through a dialysis module, enriching the oxygenate content of the oil.

3. RO/DA: As much as 20% of the peel oil is lost in commercial processing plants in aqueous emulsion clarification centrifuge waste discharges *(10)*. In an attempt to recover a significant portion of this oil, the aqueous waste stream from a commercial processing plant was obtained and concentrated by recirculating through a reverse osmosis module. The oil phase of the RO reject stream was extracted into fresh raw oil by dialysis as in process 2 above.

Table II - VACUUM DISTILLED ORANGE OIL ANALYSES

Sample	RawF1[a]	VDF1[a]	C/F	CPVal[b]	10x[b]	C/F	CP MS[b]	10x[b]	C/F
Oxygenates	1.3%	5.7%	4.4	1.0%	5.8%	5.8	0.73%	3.74%	5.1
Component %[c]									
α-pinene	0.56	0.02	0.04	0.42	0.23	0.55	0.43	0.26	0.60
sabinene	0.51	0.07	0.1	0.24	0.14	0.58	0.34	0.23	0.68
β-pinene	0.14	0.08	0.6	NR	NR	--	NR	NR	--
myrcene/octanal	1.7	0.56	0.33	1.86	1.05	0.56	1.81	1.31	0.72
d-limonene	95.7	93.4	0.97	95.2	79.9	0.84	95.4	82.8	0.87
γ-terpinene	0.17	0.12	0.71	NR	NR	--	NR	NR	--
linalool	0.42	2.0	4.8	0.25	0.52	2.1	0.17	0.37	2.2
citronellal	0.04	0.33	8	0.05	0.14	3	0.04	0.12	3
α-terpineol	0.06	0.16	3	0.03	0.17	6	0.03	0.14	5
decanal	0.42	2.0	4.8	0.28	1.48	5.3	0.18	0.96	5.3
neral	0.14	0.63	4.5	0.07	0.41	6	0.05	0.30	6
geranial	0.19	0.56	2.9	0.10	0.68	7	0.08	0.52	6
other terpenes	ND	ND	--	0.16	1.42	8.9	0.14	0.78	5.6
other oxygenate	ND	ND	--	0.22	2.44	11	0.18	1.33	7.4

C/F = concentration factor; ND = not determined; NR = not reported
a. Raw and 5-fold vacuum distilled oil from commercial source F, 1994
b. Cold-pressed Valencia (Val) and mid-season (MS) raw and 10-fold vacuum distilled oils from Vora et al 1984 (reference 5)
c. Oxygenate and component percent by weight from GC analyses (see text)

The chemical compositions of essential oils are generally determined by capillary column gas chromatography *(15-17)*. The raw citrus oils, intermediate process streams and resulting products were analysed using GC conditions similar to those of Anandaraman and Reineccius *(17)*. In some cases a DB-Wax column (J&W Scientific, Folsom, CA) was used instead of OV-101 or SE-30 silicone to resolve β-myrcene from octanal. Oil samples were prepared for analysis by dilution 1:50 in hexane containing 1000 ppm n-octane as an internal standard. Aqueous samples (10 mL) were vigorously shaken with 1 mL hexane (w/1000 ppm n-octane internal standard) for 1 minute followed by 2 minutes high-speed centrifugation. The hexane phase was then injected into the GC. The method was validated and response factors determined using authentic standards. A representative chromatogram with GC conditions is given in Figure 3.

Results

Results of the investigation of various membrane folding processes are given below.

Process 1: DA/PV - A diagram of this process is given in Figure 1 and compositions of products from cold-pressed orange peel oil in this process are given in Table III. The oil content of the aqueous dialysate was about 30 ppm. Several types of pervaporation membranes were tested; certain types were more selective but gave lower flux than others.

Compared to the vacuum distilled folded oils in Table I, the products from this process were generally richer in linalool, octanal, neral, geranial and α-terpineol, and less rich in decanal. Although the product composition was interesting, process development was discontinued in favor of the systems below because of uneconomically low membrane flux rates and the lack of a commercial source for larger scale pervaporation modules.

Process 2: UF/RO/DA - A diagram of this process is given in Figure 2; compositions of products from cold-pressed orange and lemon oils in this process are given in Table IV. Several types of membranes were tested; some had a tendency to leak oil within a few hours, while for others selectivity for oxygenates declined rapidly. For the pilot scale membrane unit run on orange oil, the aqueous feed emulsion was prepared to contain 8-10% oil and the UF permeate contained 10-16 ppm oil (70-80% oxygenates). The UF reject stream contained 1.2-1.3% oxygenates, confirming membrane selectivity for oxygenates. Recycle of the permeate through the RO module concentrated the RO reject to 150-350 ppm oil (90-96% oxygenates), while the RO permeate contained 0.5-2.0 ppm oil.

Although the proportion of oxygenates in the UF permeate/RO reject recycle stream was quite high, the total oil content was relatively low because the RO unit had to be operated below about 1000 ppm oil content. Above this value a separate oil phase would separate out and foul the membrane, reducing water flux and oil rejection dramatically. Thus direct recovery of oxygenates from the dilute aqueous
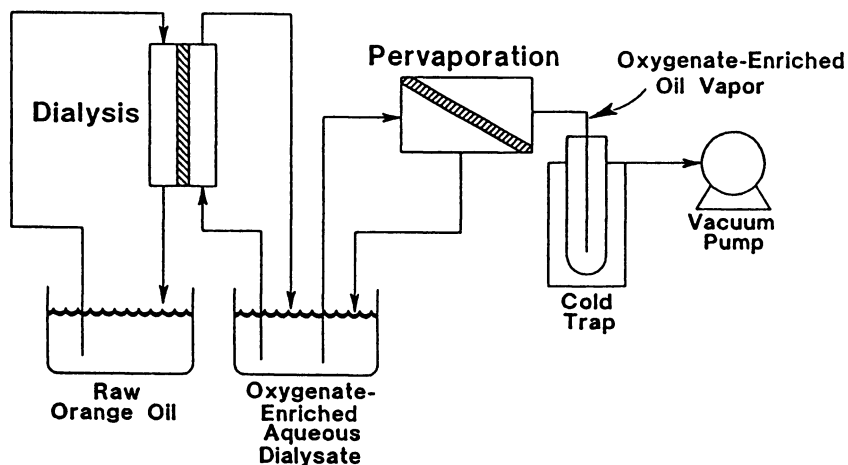
Figure 1 - Combined dialysis/pervaporation system
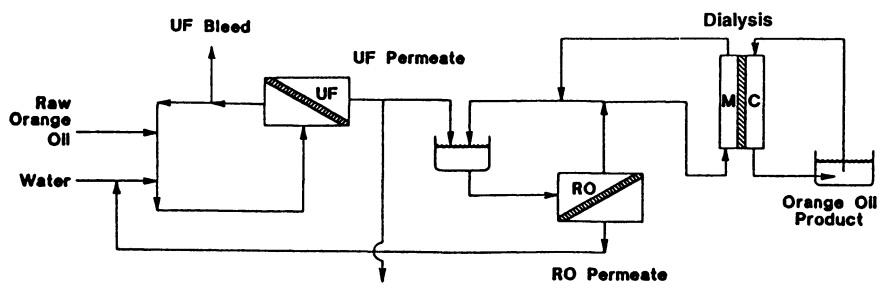
Figure 2 - Combined ultrafiltration/-
reverse osmosis/dialysis system
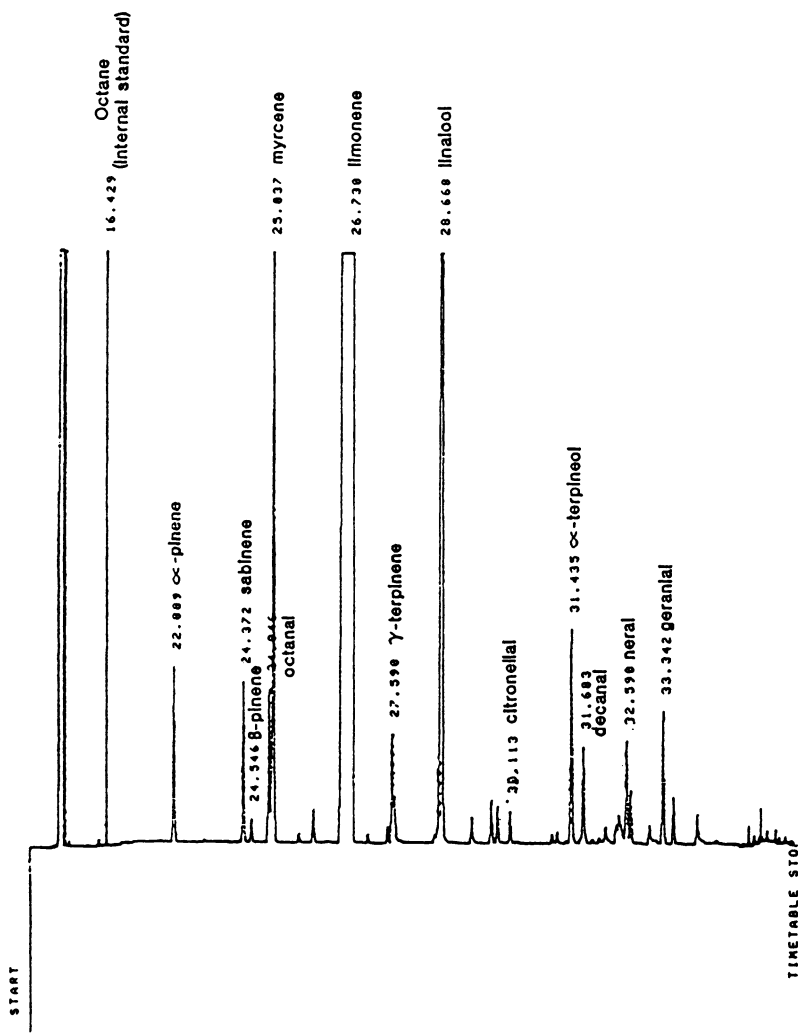
Gas Chromatography Conditions

Instrument: HP 5890A FID GC; HP 7673A automatic injector; HP 3396A integrator

Column: 60 m fused silica 0.25 mm ID capillary, 0.25 μm SE-30 film

Carrier Gas: 1.6 mL/min helium ~30 psig head pressure; 60:1 FID split ratio

Flame Ionization Detector: 70 mL/min hydrogen, 350 mL/min air, 250 °C

Injector Temperature: 200 °C   Injection Sample Size: 3 μL

Oven Temperature Program: 40 °C for 11 min, heat to 200 °C at 6 °C/min, heat to 250 °C at 20 °C/min, hold at 250 °C for 6 min, then cool to 40 °C

Figure 3 - Gas chromatogram of 4-fold orange oil

Table III - ORANGE OIL ANALYSES

Sample	DA/PV Process				RO/DA Process	
	Raw C1[a]	CODP1	PV59P3	C / F	SAR7[b]	VDF1[c]
Oxygenates	1.9%	19.5%	35.9%	10-18	7.5%	5.7%
Component %[d]						
α-pinene	0.37	0.24	0.20	0.5-0.7	0.49	0.02
sabinene	0.19	0.17	0.13	0.7-0.9	ND	0.07
β-myrcene	1.9	1.5	1.2	0.6-0.8	1.9	0.56
octanal	0.68	6.2	4.7	6.9-9.1	0.23	ND
d-limonene	95.6	76.4	59.7	0.6-0.8	90.1	93.4
γ-terpinene	0.01	0.52	ND	50	ND	0.12
linalool	0.53	10.4	24.4	20-46	1.9	2.0
citronellal	0.09	0.21	0.30	2-3	0.06	0.33
α-terpineol	0.07	1.6	3.0	23-43	ND	0.16
decanal	0.40	0.63	1.2	1.6-3	5.1	2.0
neral	0.06	0.82	2.4	14-40	0.13	0.63
geranial	0.11	1.2	2.9	11-26	0.05	0.56

C/F = concentration factor; ND = not determined
a. Raw cold-pressed oil from commercial source C, 1988
b. Feed: commercial source S plant centrifuge waste emulsion, 1989 (80 ppm oil)
c. 5-Fold vacuum distilled oil from commercial source F, 1994 (see Table 2)
d. Oxygenate and component percent by weight from GC analyses (see text)

RO product was not possible. Recovery of oxygenates was first attempted by extraction with fresh raw oil after adding salt to the aqueous phase. This was difficult to perform continuously, however, and involved use of additional chemicals (salt), so was later done by dialyzing the RO reject against fresh raw oil, with product bleed taken off after equilibrium at the target oxygenate concentration had been reached.

Compared to the vacuum distilled folded oils in Table I, the orange oil products from this process were generally richer in linalool, β-myrcene, α-pinene, sabinene and α-terpineol, and less rich in decanal. In the lemon oil sample, the concentrations of linalool, α-terpineol, neral and geranial were significantly boosted.

Process 3: RO/DA - A diagram of this process is essentially the last two stages of Process 2 in Figure 2. However, instead of feeding UF permeate to the RO module as in Process 2 above, an aqueous waste stream from a commercial orange peel oil plant centrifuge was fed. Since this stream was at one time in equilibrium with raw orange oil, it should have been enriched in oxygenates due to selective partition. In

Table IV - UF/RO/DA OIL ANALYSES

Sample	Orange Oil					Lemon Oil		
	Raw S3[a]	SOUR4	C/F	143-1	C/F	Raw S4[a]	SLUR4	C/F
Oxygenates	1.2%	7.0%	5.8	8.8%	7.3	1.7%	22.4%	13
Component %[b]								
α-pinene	0.38	0.54	1.4	0.60	1.6	1.2	0.91	0.76
sabinene	0.37	0.45	1.2	0.55	1.5	0.97	0.77	0.79
β-pinene	0.05	0.07	1.4	0.06	1.2	4.6	3.6	0.78
β-myrcene	1.9	1.8	0.94	3.1	1.6	2.0	1.6	0.80
octanal	0.44	1.1	2.5	1.4	3.2	0.08	0.33	4
d-limonene	96.0	90.0	0.94	86.4	0.90	83.9	66.4	0.79
γ-terpinene	0.04	0.05	1.3	ND	--	5.7	4.3	0.74
linalool	0.33	4.2	13	5.8	18	0.13	3.4	26
citronellal	0.07	0.12	1.7	0.14	2.0	0.07	0.15	2
α-terpineol	0.04	0.56	14	0.42	10	0.22	7.4	34
decanal	0.27	0.31	1.1	0.48	1.8	0.04	0.10	2.5
neral	0.04	0.26	7	0.46	10	0.46	5.2	11
geranial	0.06	0.44	7	0.64	10	0.72	5.9	8.2

C/F = concentration factor; ND = not determined
a. Raw cold-pressed oils from commercial source S, 1989
b. Oxygenate and component percent by weight from GC analyses (see text)

fact, the feed stream oil content was 80 ppm with 30 ppm oxygenates (38% based on oil). This was higher in oil content but lower in oxygenate proportion than Process 2 UF permeate, indicating a tradeoff between throughput/yield and selectivity for the two processes.

The composition of product from this process is shown in Table III. Compared to the vacuum distilled folded oils in Table I, this product was significantly richer in decanal, α-pinene and β-myrcene, and less rich in citronellal, neral and geranial. In this case, linalool content was about the same.

Flavor Characteristics

Folded citrus oils from the above processes were evaluated vs conventional folded oils by trained flavor panels at selected commercial flavor houses as follows:
1. An aqueous solution containing 8% sucrose and 0.025% citric acid was prepared.
2. A solution of 1% citrus oil test sample in ethanol was added to the aqueous sucrose solution at 0.1%, giving a solution with about 10 ppm citrus oil.
3. The aqueous test solutions were then tasted in a triangle test.

In general, the membrane-folded samples were judged to be "juicier" and "fresher" in character than their vacuum-distilled counterparts, although the flavor impact was somewhat less for a given fold.

Discussion

Inasmuch as aqueous partition plays a big role in all of the processes described above, it is not surprising that the alcohols linalool and α-terpineol were generally concentrated to the greatest extent, followed by the unsaturated aldehydes neral and geranial (citral), which are less polar than alcohols but more polar than saturated aldehydes decanal and octanal. However, α-terpineol is not necessarily a desirable component of folded citrus oils. It arises primarily as a result of acid hydrolysis of d-limonene. Its formation could perhaps have been controlled by basic buffering of the aqueous streams in these process, but this likely would have reduced the solubility and throughput of the desirable oil components. It also would have introduced another chemical variable to the process that we were not prepared to evaluate at the time.

Limonene oxide, an oxidation product of citrus oils, was not specifically tracked in this program. The formation of limonene oxides during vacuum distillation was not discussed in Vora et al (5).

In conclusion, the membrane processes described herein yielded folded orange and lemon oils significantly enhanced in linalool and citral content and lower in decanal content than conventionally folded oils. It may be possible to boost the decanal content with product recovered from aqueous waste streams using process 3 above, which was considerably higher in decanal. It is also possible with the UF/RO/DA system to concentrate lemon oil oxygenates via UF/RO and then transfer these into raw orange oil in the dialysis loop, thus yielding another novel, but still natural, citrus oil flavor product.

Literature Cited

1. Matthews, R.F.; Braddock, R.J. Recovery and Applications of Essential Oils from Oranges. *Food Technology* **1987,** *41(1),* 57-61
2. Shaw, P.E. Review of Quantitative Analyses of Citrus Essential Oils. *J. Agr. Food Chem.* **1979,** *27,* 246-257
3. Boelens, M.H. A Critical Review on the Chemical Composition of Citrus Oils. *Perfumer & Flavorist* **1991,** *16,* 17-34
4. Boucard, G.R.; Serth, R.W. A Continuous Steam Stripping Process for the Distillation of Essential Oils. *Perfumer & Flavorist* **1991,** *16,* 2-8
5. Vora, J.D.; Matthews, R.F.; Crandall, P.G.; Cook, R. Preparation and Chemical Composition of Orange Oil Concentrates. *J. Food Sci.* **1983,** *48,* 1197-1199
6. Fleisher, A.; Biza, G.; Secord, N.; Dono, J. Ultra-Tech Citrus Concentrates - a New Series of Deterpenified Citrus Oils. *Perfumer & Flavorist* **1987,** *12,* 57-60
7. Temelli, F.; Chen, C.S.; Braddock, R.J. Supercritical Fluid Extraction in Citrus Oil Processing. *Food Technology* **1988,** *42(6),* 145-150
8. Cully, J.; Schutz, E.; Vollbrecht, H.R. Process for the Removal of Terpenes from Essential Oils. **1981,** US Patent 5,061,502
9. Brose, D.J.; Chidlaw, M.B.; LaChapelle, E.D.; van Eikeren, P. Fractionation of Citrus Oils using Membrane-mediated Cyclodextrin Extraction, in *Proceedings 6th Int'l. Symp. Cyclodextrins,* Hedges, A.R., Ed., Ed. Sante: Paris, 1992, pp 573-8
10. Braddock, R.J.; Adams, J.P. Recovery of Citrus Oils by Ultrafiltration and Reverse Osmosis. *Food Technology* **1984,** *38(12),* 109-111
11. Sperber, R.M. 'Cold concentration' enhances juice quality. *Food Processing* **1989,** July pp 21-22
12. Beaudry, E.G.; Lampi, K.A. Membrane Technology for Direct Osmosis Concentration of Fruit Juices. *Food Technology* **1990,** *44(6),* 121
13. Koseoglu, S.S.; Lawhon, J.T.; Lusas, E.W. Use of Membranes in Citrus Juice Processing. *Food Technology* **1990,** *44(12),* 90-97
14. van Eikeren, P.; Brose, D.J.; Ray, R.J. Selective Aqueous Extraction of Organics Coupled with Trapping by Membrane Separation. **1991,** US Pat. 5,041,227

15. Staroscik, J.A.; Wilson, A.A. Quantitative Analysis of Cold-Pressed Lemon Oil by Glass Capillary Gas Chromatography. *J. Agr. Food Chem.* **1982,** *30,* 308
16. Chamblee, T.S.; Clark, B.C.; Radford, T.; Iacobucci, G.A. General Method for the HPLC Prefractionation of Essential Oils and Flavor Mixtures for GCMS Analysis. *J. Chromatog.* **1985,** *330,* **141-151**
17. Anandaraman, S.; Reineccius, G.A. Analysis of Encapsulated Orange Peel Oil. *Perfumer & Flavorist* **1987,** *12,* 33-39

Chapter 11

Oxidative Stability of Encapsulated Seal Blubber Oil

Fereidoon Shahidi and Udaya N. Wanasundara

Department of Biochemistry, Memorial University of Newfoundland, St. John's, Newfoundland A1B 3X9, Canada

Oils containing a large proportion of polyunsaturated fatty acids, especially the omega-3 type, are highly prone to oxidative deterioration and off-flavor development. Therefore, inhibition of oxidation is a major criterion when such oils are incorporated into food products. Encapsulation of omega-3 rich marine oils would confer better stability to products by preventing contact with air and light. It also provides a free-flowing powder which can be easily incorporated into foods. The present study was undertaken to stabilize seal blubber oil (SBO) by microencapsulation. SBO contains 21-26% long chain omega-3 fatty acids consisting of 6.5-8.5% eicosapentaenoic, 4-6% docosapentaenoic and 8-10% docosahexaenoic acids. Encapsulating materials examined were β-cyclodextrin, corn-syrup solids and maltodextrin. Aqueous solutions containing the encapsulating material, Tween 80 as an emulsifier, and SBO were then spray-dried. The storage stability of these powdered products was determined by monitoring their peroxide and 2-thiobarbituric acid reactive substances values as well as changes of their fatty acid composition. Among the encapsulating materials tested, β-cyclodextrin and corn-syrup solids were found to be good encapsulating agents for SBO.

Until the last few decades, lipids from marine animals and plants or those from fresh water bodies of the World were not considered important to human nutrition. However, studies on Greenland Eskimos, who traditionally consume large amounts of fatty fish and oils from marine mammals, resulted in current interest on biological effects of marine lipids. The Greenland Eskimos have been reported

to have a lower blood clotting tendency, longer bleeding time and a lower incidence of coronary heart disease as compared to the Danes who consumed very little fatty fish or oils from marine mammals.   Other communities which characteristically consumed large amounts of fish (i.e. about 250 g per day), such as Japanese fishermen, also show a reduced blood-clotting tendency and incidence of coronary heart disease. Bang *et al.* (*1*) concluded that the active component of the Eskimo's diet contained long-chain omega-3 polyunsaturated fatty acids (PUFA) such as eicosapentaenoic acid (C20:5ω3, EPA) and docosahexaenoic acid (C22:6ω3, DHA), which are found in fish and marine mammal lipids.

The omega-3 fatty acid family is derived from the 'parent' fatty acid α-linolenic acid. These fatty acids can not be synthesized in the human body and must be provided in the diet; they therefore referred to as essential fatty acids. Neither human nor plant cells can readily convert α-linolenic acid to its long chain derivatives, such as EPA and DHA. The only form of life which can readily synthesize these long chain omega-3 PUFA is algae. Because fish and marine mammals feed on algae, they become richer sources of long chain omega-3 PUFA than land animals or plants. Therefore, the principle sources of high PUFA marine lipids are storage organs of bottom dwelling fish (eg. liver of cod and haddock), body fat of pelagic fish (eg. herring, mackerel and menhaden) and depot fat of marine mammals (eg. blubber of whale and seal).

Blubber of harp seal (*Phoca groenlandica*) contains 90-95% of lipids (*2*) which include considerable amounts of EPA and DHA. It also contains docosapentaenoic acid (C22:5ω3, DPA) which is less abundant in fish oils. The other important factor of SBO is its high content of monoenes which have also been reported as having beneficial effects against cardiovascular diseases. Seal blubber and fish oils differ in the positional distribution of PUFA on their triacylglycerol (TAG) molecules. In the fish oils, EPA, DPA and DHA are located primarily at the 2-position of TAG molecules. In seal blubber oil, however, these three fatty acids are located primarily at the 3-position with some at the 1-position, but little at the 2-position. Thus, omega-3 fatty acids from SBO may be assimilated into the body more effectively than fish oils (*3*).

Our current intake of long chain omega-3 PUFA from fish is only about 1 g per week (*4*). The report of the British Nutrition Foundation Task Force on Unsaturated Fatty Acids recommended that 0.5 per cent of our total energy intake should come from long chain omega-3 PUFA. For an average size woman, this would translate to about 8 g long chain omega-3 PUFA per week, and for an average man to 10 g per week.   Therefore, in order to meet these recommendations a substantial increase in the consumption of omega-3 PUFA is required.

The beneficial effects of long chain omega-3 PUFA have been ascribed to their ability to lower serum TAG and cholesterol (*5*). While DHA is essential for proper functioning of the eye and may have a structural role in the brain, EPA serves as a precursor to eicosanoid compounds (*6*) and has therapeutic benefits in human cardiovascular diseases (*7,8*). The important role of DHA in early stages of fetation means that women who intend to become pregnant should have good dietary intakes of DHA at critical stages in the fetus's development. Infant milk

formulae should include DHA (and also arachidonic acid) in order to resemble human milk as closely as possible (*4,9*).

Oxidative quality of marine oils is known to have significant effects on their nutritional value. Because of the presence of long chain omega-3 PUFA, these oils easily undergo autoxidation during processing and storage, producing a wide array of undesirable compounds including hydroperoxides and their breakdown products such as aldehydes, ketones, alcohols and epoxides (*10*). These latter compounds in turn give rise to the development of unpleasant off-odors in the oil (*11*). Furthermore, products of lipid autoxidation have been shown to be chemical toxicants and are believed to lead to deteriorative processes in the body such as aging (*12*). Deleterious consequences from consuming oxidized marine oils, due to the possible toxic effects of peroxides, have been reported from animal feeding trials. Because these compounds have a strong local irritant action, animals fed oxidized fish oil showed inflammation of the intestinal tract, damage to the mucous membrane of the stomach and intestines and severe ulcerations, as well as decreased cellular respiration and enzyme inhibition (*13*). Therefore, inhibition of oxidation is a major criteria when incorporating these oils into food products.

Oxidation of lipids containing PUFA can proceed via different mechanisms and therefore, devising complementary strategies to minimize it is mandatory. Because oxygen is an essential reactant in the process, control of oxygen availability is a critical variable in minimizing oxidation of PUFA. Microencapsulation of PUFA-rich oils would confer better stability to the product by preventing contact of the oil with oxygen and light. It also produces a free-flowing powder which can easily be incorporated into foods.

Microencapsulation is a technique by which oil is entrapped into a wall matrix and is therefore protected from oxygen, moisture and light. Spray- or freeze-dried powder particles are considered to be of the microencapsuled kind. Gejl-Hansen and Fink (*14*) reported that microencapsulated linoleic acid in a maltodextrin coating was not susceptible to oxidative deterioration even though maltodextrin is not known as being a good encapsulating agent. Ono and Aoyama (*15*) reported that rice bran oil embedded in granules containing corn-syrup solid and pork polypeptone which was vacuum-dried, underwent little oxidation on exposure to air at a high temperature. Recently, Taguchi *et al.* (*16*) reported the oxidative stability of sardine oil embedded in spray-dried egg white powder and use of the product as a source of omega-3 PUFA for fortification of cookies. These authors reported that use of microencapsulated sardine oil in fortified cookies did not affect their sensory quality. In addition, spray-dried egg white powder inclusive of sardine oil was stable during prolonged storage.

The initial step in encapsulating a food ingredient is the selection of a suitable coating or encapsulating material. Coating substances are basically film-forming materials which can be selected from a wide variety of natural or synthetic polymers, depending on the material to be coated and the characteristics desired in the final microcapsules. Therefore, starches and modified starches serve as useful entrapping materials for food applications. The present study was
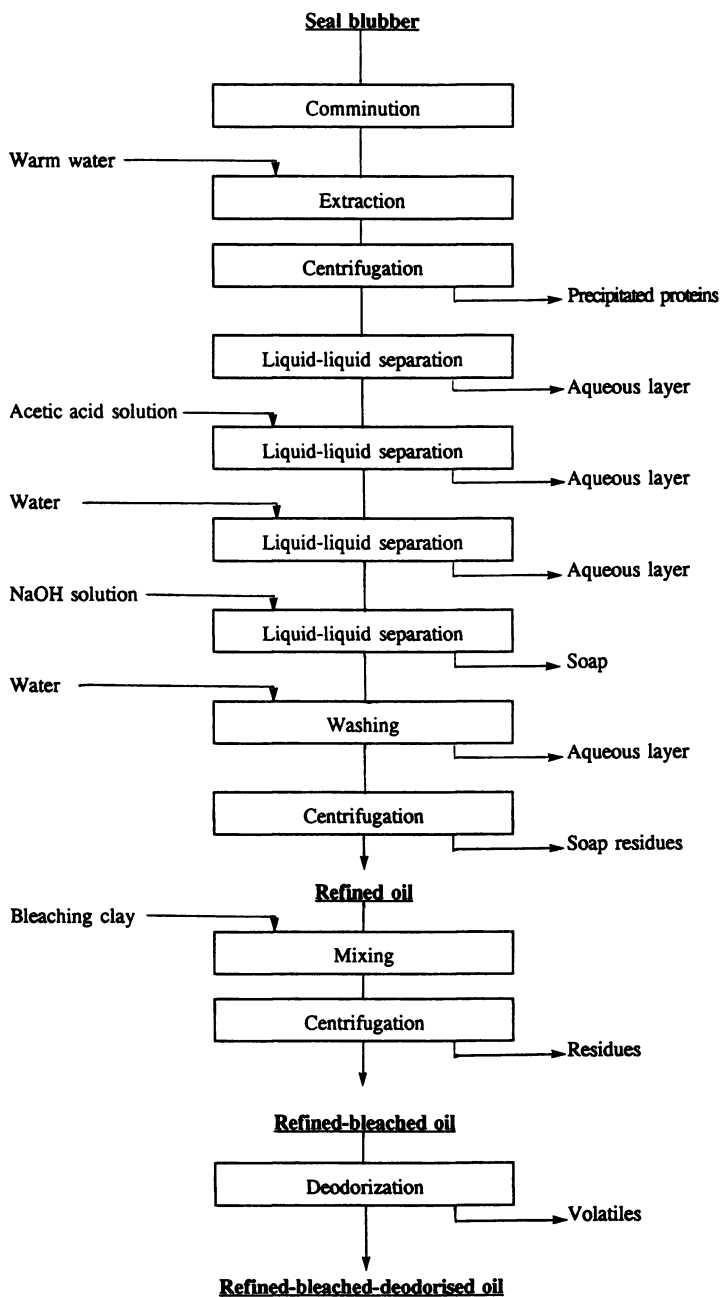
Figure 1.   Preparation of refined-bleached and deodorized seal blubber oil.

undertaken to examine the possible application of starches and modified starches to encapsulate SBO.

Materials and Methods

Materials. Blubber of harp seal (*Phoca groenlandica*) was acquired through local sources in Newfoundland. β-cyclodextrin was obtained from the American Maize-Products Company (Hammond, IN) and corn-syrup solids as well as maltodextrin were obtained from the Grain Processing Corporation (Muscatine, IA). Fatty acid methyl ester standards were purchased from Supelco Canada (Oakville, ON). All other chemicals used in this study were ACS grade or better.

Extraction and refining of SBO. SBO was prepared from raw blubber. Extraction and purification of the oil was carried out according to the scheme given in Figure 1. Small chunks of seal blubber were communited using a Waring Blendor and then heated in water (water:blubber, 3:2, v/w) at 65°C for 10 min. The denatured proteins were removed by centrifugation (10 min at 3300 x g) and oil was recovered using a separatory funnel. A 5% (v/v) acetic acid solution was added to the oil (acid:oil, 3:2, v/v) to precipitate residual proteins. After 5 min, the aqueous layer containing residual proteins was removed to obtain the crude oil. Crude oil was treated with 0.1N NaOH (NaOH:oil, 3:2, v/v) at room temperature to saponify impurities. Saponified materials were washed three times with water (water:oil, 3:2, v/v) and residual soap was removed by centrifugation. Alkali-refined oil was bleached using 4% (w/w) activated clay at 60°C with vigorous stirring for 10 min. Refined-bleached oil was obtained after centrifugation at 3300 x g for 10 min. The deodorization of refined-bleached oil was carried out using a laboratory scale vacuum steam distillation apparatus. The oil was heated to 190°C using steam, while under vacuum. Volatile compounds were then recovered during the deodorization process over a 5-hour period. The prepared refined-bleached and deodorized SBO was stored at -60 °C until encapsulated.

Preparation of encapsulated SBO. Encapsulation of SBO was carried out according to the scheme given in Figure 2. Encapsulating materials (β-cyclodextrin, corn-syrup solids and maltodextrin) were dissolved in distilled water (30%, w/w) with slight heating in a water bath until clear solutions were obtained. For β-cyclodextrin, 2-3 drops of 50% (w/v) NaOH were added to attain complete dissolution. Refined-bleached and deodorized SBO was emulsified in an ice bath with solutions of encapsulating materials (oil:encapsulating material, 3:17, w/w) using a Brinkmann Polytron PT 3000 homogenizer (10 min at 10000 rpm). Tween-80 (9% of the oil phase) was added as an emulsifier during homogenization. The resulting emulsions were then spray dried using a BÜCHI-190 mini spray-drier using nitrogen as the spray flow through gas. The inlet and outlet temperatures were 145 and 80°C, respectively.

Seal blubber oil (SBO)

Encapsulating material
Emulsifier

┌─────────────────────────┐
│   Mixing   │
└─────────────────────────┘

┌─────────────────────────┐
│   Spray drying   │
└─────────────────────────┘

┌─────────────────────────┐
│   Storage   │
└─────────────────────────┘

Stored microencapsulated SBO
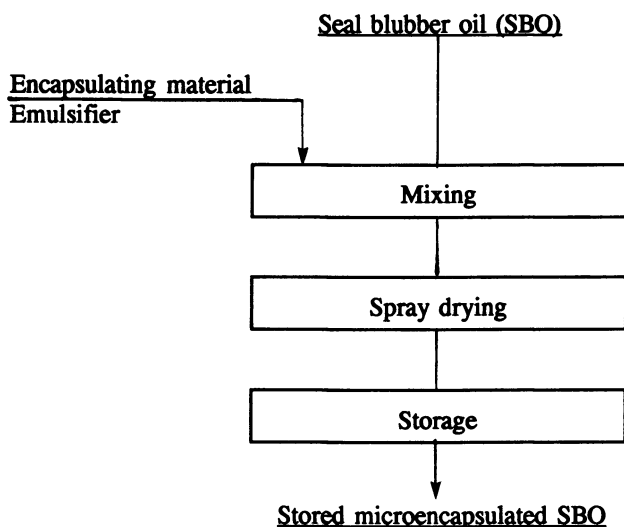
Figure 2. Preparation of microencapsulated seal blubber oil.

Storage condition of unencapsulated and encapsulated oils. Ten grams of unencapsulated or encapsulated SBO (spray-dried) samples were placed in brown glass bottles (40 mm diameter and 60 mm height) and stored under nitrogen at room temperature. To determine the oxidative stability, samples were removed periodically (separate sample containers for each day) for analyses.

Extraction of lipids from encapsulated SBO. The encapsulating materials from 10 g of microencapsulated products were dissolved in 50 mL of a 0.88% (w/v) KCl solution. Then 100 mL of chloroform, 50 mL of methanol and a few crystals of tert-butylhydroquinone (TBHQ) were added. The mixture was then homogenized using the Polytron PT-3000 homogenizer for 2.5 min at 12000 rpm. The mixture was transferred to a separatory funnel, the chloroform layer was separated and then evaporated using a rotary evaporator at 40°C to recover the oil.

Scanning electron microscopy (SEM). Spray-dried starch materials with or without oil inside the particles were attached to the aluminium SEM holders with double sided adhesive tape. The samples were then coated with a thin layer of gold under vacuum and then SE micrographs were observed using a Hitachi S-570 Scanning Microanalyzer operated at 20 kV.

Chemical analyses. Fatty acid composition of oil was determined according to the method of Keough and Kariel (17). Official methods (18) were used for determination of iodine value (IV, method Cd 1-25), free fatty acids (Acid value,

method Cd 3a-63) and the 2-thiobarbituric acid reactive substances (TBARS, method Cd 19-90).   Peroxide value (PV) was determined according to the procedure given by Asakawa and Matsushita (*19*). Cholesterol content of samples was determined as described previously (*20*). Separation of lipid classes was done according to the method described by Christie (*21*). All analyses were carried out in triplicate. Generally total oxidation (TOTOX) value is calculated as 2PV+p-anisidine value. Since both p-anisidine and TBARS values measure the extent of secondary oxidation products of lipids, in this work TBARS values were used to calculate total oxidation (TOTOX$_{TBA}$ = 2PV+TBARS).

Results and Discussion

The content of neutral and polar lipids as well as cholesterol and α-tocopherol in blubber of harp seal is given in Table I.   Approximately 98.9 and 1.1 % of blubber lipids were composed of triacylglycerols (neutral lipids) and polar lipids, respectively. The content of cholesterol in the blubber was 105.7 mg/100g. The total lipid content of raw blubber was 95.5%, of which 84.2% was recovered after aqueous washing. Upon caustic refining and bleaching, 71.1% refined-bleached seal blubber oil (SBO) was obtained.

Table I.   Content of neutral lipids, cholesterol, α-tocopherol and the iodine value of refined-bleached and deodorized seal blubber oil

Constituent/Characteristic	Content
Neutral lipids (g/100g)	98.9 $\pm$ 0.2
α-Tocopherol (mg/100g)	2.8 $\pm$ 0.1
Iodine value (g/100g)	146.3 $\pm$ 1.0
Cholesterol (mg/100g)	105.7 $\pm$ 22.0
Acid value (mg KOH/g)	0.041 $\pm$ 0.0

Table II summarizes the fatty acid composition of SBO. The total unsaturated fatty acid content of SBO was about 84%. A close scrutiny of the results indicates that the content of omega-3 PUFA in SBO was in order of DHA>EPA>DPA. Furthermore, more than 50% of fatty acids of SBO were monoenes. The content of total omega-3 fatty acids was 22%.

The presence of high amounts of PUFA in SBO makes it highly susceptible to oxidative deterioration.   Therefore, several methods may be used to prevent oxidative deterioration of oils rich in PUFA. The commonly practiced industrial

methods include hydrogenation, use of synthetic and natural antioxidants or microencapsulation. Hydrogenation of the oil decreases the content of unsaturated fatty acids and may produce *trans* isomers, therefore, this method is not nutritionally favorable. Use of synthetic antioxidants in food systems has to be reevaluated because of the growing concern over their possible carcinogenic effects (*22*). In this study microencapsulation of SBO was carried out as a means to prevent oxidative deterioration.

Table II. Fatty acid composition of freshly prepared refined-bleached and deodorized seal blubber oil

Fatty acid	Content (w/w %)
C14:0	3.58 ± 0.05
C14:1	1.00 ± 0.04
C16:0	6.21 ± 0.03
C16:1	19.15 ± 0.10
C18:0	0.80 ± 0.00
C18:1ω9	21.31 ± 0.06
C18:1ω7	4.66 ± 0.05
C18:2ω6	1.77 ± 0.02
C18:3ω3	0.38 ± 0.00
C18:4ω3	1.02 ± 0.02
C20:1ω9	11.02 ± 0.02
C20:2ω6	0.19 ± 0.00
C20:4ω6	0.59 ± 0.03
C20:5ω3	7.49 ± 0.02
C22:1ω11	1.94 ± 0.00
C22:5ω3	4.90 ± 0.01
C22:6ω3	8.35 ± 0.09

Changes in fatty acid composition of stored SBO, both in the encapsulated and unencapsulated forms are shown in Table III. The total PUFA content of unencapsulated SBO decreased from 24.69% (day-0) to 11.48% (day-49) but, PUFA of SBO encapsulated in β-cyclodextrin and corn-syrup solid decreased only by 1.80 and 6.14%, respectively. The total omega-3 fatty acids in β-cyclodextrin encapsulated SBO remained unchanged even after 21 days of storage while those for unencapsulated SBO changed from 22.14 to 10.61%.

Table III. Changes in polyunsaturated fatty acids of microencapsulated refined-bleached and deodorized (RBD) seal blubber oil during storage

Fatty acid (w/w%)	Day-0	RBD-Seal blubber oil		β-cyclodextrin		Corn-syrup solids		Maltodextrin	
		Day-21	Day-49	Day-21	Day-49	Day-21	Day-49	Day-21	Day-49
Total Polyunsaturated	24.69	13.06	11.48	23.27	22.18	20.00	17.84	14.97	11.87
EPA (C20:5 ω3)	7.49	3.33	3.02	7.11	7.02	5.86	5.42	3.35	3.00
DPA (C22:5 ω3)	4.90	2.14	2.09	4.24	4.22	3.68	3.49	2.95	2.15
DHA (C22:6 ω3)	8.35	3.75	3.01	8.02	7.19	6.93	5.48	3.86	3.19
Total ω3	22.14	10.61	9.22	21.90	20.79	17.67	15.52	10.72	9.25
Total ω6	2.55	2.45	2.26	2.37	2.34	2.33	2.32	2.26	2.00
ω3/ω6	8.68	4.33	4.10	8.82	8.46	7.58	6.69	4.74	4.62

Figure 3 illustrates progression of peroxide formation in unencapsulated and encapsulated SBO stored at room temperature. Encapsulated samples showed low PV throughout the storage period. Among the encapsulating materials tested, β-cyclodextrin served best in keeping the amount of peroxides produced low, and this was followed by corn-syrup solids. For up to 21 days, the PV of the control samples (unencapsulated oil) increased from 2.08 to 16.98 meq/kg oil. Corresponding values for encapsulated oils in β-cyclodextrin and corn-syrup solid matrices were smaller, changing from 3.01 to 7.32 and from 4.01 to 12.01 meq/kg oil, respectively.

Percentage inhibition of TBARS formation for encapsulated SBO as compared with the unencapsulated oil is presented in Figure 4. The β-cyclodextrin matrix was able to reduce the TBARS formation of SBO by 74%, even after 49 days of storage, when compared with control samples. The corn-syrup solid matrix was also effective in lowering TBARS production after 49 days of storage of SBO. Corresponding changes of TOTOX$_{TBA}$ values of samples are give in Figure 5. The total oxidation or TOTOX$_{TBA}$ values of SBO encapsulated in a β-cyclodextrin matrix were much lower than those of control samples, thereby indicating the effectiveness of β-cyclodextrin as an encapsulating agent to reduce oxidative deterioration of PUFA rich SBO. Corn-syrup solids were also effective as encapsulating materials for use in marine oil microencapsulation. On the other hand, maltodextrin seemed to serve only as a carrier rather than as an effective encapsulating agent for SBO. Its use for the purpose of protection of SBO against oxidation is not recommended.

A close scrutiny of scanning electron micrographs (SEM) of spray-dried encapsulating materials, both in the absence and presence of SBO indicated that while some creases or dents were evident on the surface of encapsulating materials devoid of SBO. However, starch particles containing oil were globular in shape with smooth surfaces and were variable in size. The β-cyclodextrin and, to a lesser extent, corn-syrup solid particles containing SBO were more globular in shape than their counterpart maltodextrin encapsules, thus revealing that the former encapsulating materials were more effective microencapsulating agents. Iwami *et al.* (*23*) reported similar changes of encapsulating material upon entrapment of fatty acids where gliadin particles containing fatty acids exhibited spherical shapes with smooth surfaces. Some creases or dents were seen on gliadin surfaces devoid of fatty acids.

In summary, results of the present study demonstrated that micrencapsulation offers an effective means to prevent oxidative deterioration of SBO and to preserve the integrity of nutritionally important fatty acids from marine oils. β-cyclodextrin was the most effective encapsulating material examined in this study. Therefore, microencapsulation of SBO would confer reasonable stability to PUFA and nutritionally favorable omega-3 fatty acids. The resultant products are free-flowing powders and can be easily incorporated into food formulations.
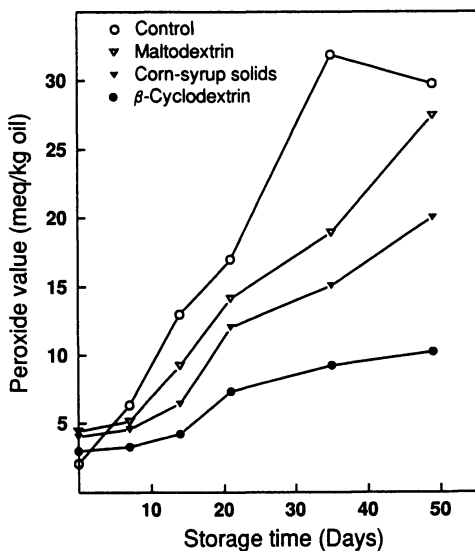
Figure 3. Peroxide values of microencapsulated seal blubber oil during storage at room temperature.
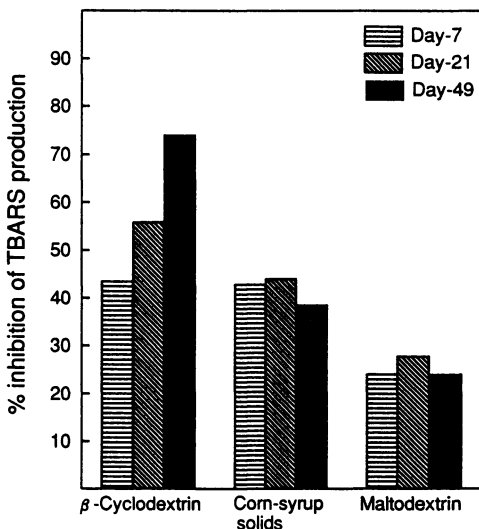
Figure 4. Percent inhibition of TBARS formation of microencapsulated seal blubber oil during storage at room temperature.
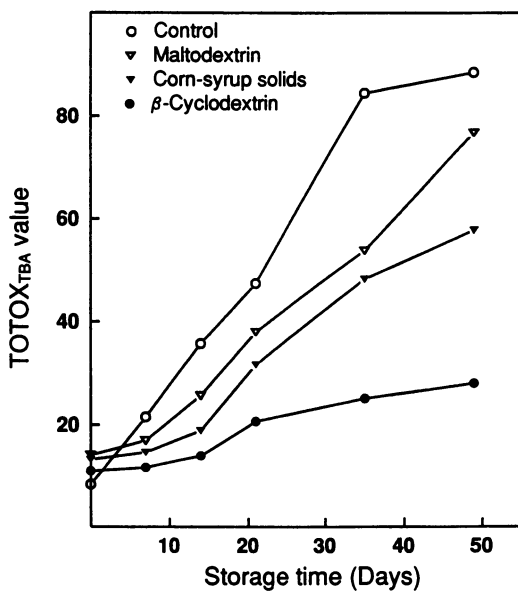
Figure 5.   Total oxidation ($TOTOX_{TBA}$ = 2PV + TBA) of microencapsulated seal blubber oil during storage at room temperature.

Literature Cited

1. Bang, H.O., Dyerberg, J. and Hjorne, N. (1976). *Acta. Med. Scand.* **200**, 59.
2. Shahidi, F., Synowieki, J., Amarowicz, R. and Wanasundara, U.N. (1994). In: *Lipids in Food Falvors*, ed C.-T. Ho and T.G. Hartman. ACS Symposium Series 558, Am. Chem Soc., Washington DC. pp 233.
3. Shahidi, F., Wanasundara, U.N. and Brunet, N. (1994). *Food Res. Int.* **27**, 555.
4. Groom, H. (1993). *Nutr. Food Sci.* No 6 (Nov/Dec), 4-8.
5. Seppanen-Laakso, T., Vanhanen, H., Laakso, I., Kohtamaki, H. and Viikari, J. (1992). *British J. Nutr.* **68**, 639.
6. Branden, L.M. and Carroll, K.K. (1986). *Lipids* **21**, 285.
7. Dyerberg, J. (1986). *J. Nutr. Rev.* **44**, 125.
8. Mehta, J., Lopez, L.M., Lawton, D. and Wargovich, T. (1988). *Am. J. Med.* **84**, 45.
9. Koletzko, B., Thiel, I., Springer, S. (1992). *European J. Vlin. Nutr.* **46**, 545.
10. Labuza, T.P. (1971). *CRC Crit. Rev. Food Technol.* **2**, 355.
11. Ke, P.J. and Ackman, R.G. (1975). *J. Am. Oil Chem. Soc.* **52**, 349.
12. Pearson, A.M., Gray, J.I., Wolzak, A.M. and Horenstein, N.A. (1983). *Food Technol.* **37**(7), 121.
13. Lang, K. (1965). In: *The Technology of Fish Utilization*, ed. R. Kreuzer. Fishing News Books, Landon. pp 223.
14. Gejl-Hansen, F. and Fink, J.M. (1977). *J. Food Sci.* **42**, 1049.
15. Ono, F. and Aoyama, Y. (1979). *J. Jpn. Soc. Food Sci. Technol.* **26**, 13.
16. Taguchi, K., Iwami, K., Ibuki, F. and Kawabata, M. (1992). *Biosci. Biotech. Biochem.* **56**, 560.
17. Keough, K.M.W. and Kariel, N. (1987). *Biochem. Biophys. Acta.* **902**, 11.
18. AOCS. (1990). *Official Methods and Recommended Practices of the American Oil Chemists' Society*, 4th ed. Am. Oil Chem. Soc., Champaign, IL.
19. Asakawa, T. and Matsushita, S. (1980). *Lipids* **15**, 965.
20. Shahidi, F. and Synowieki, J. (1991). *Can. Inst. Food Sci. Technol. J.* **24**, 269.
21. Christie, W.W. (1982). In: *Lipid Analysis*, 2nd ed. Pergamon Press, New York, NY. pp 107.
22. Barlow, S.M. (1990). In: *Food Antioxidants*, ed. B.J.P. Hudson. Elsevier Applied Sci., London. pp 253.
23. Iwami, K., Hattori, M., Nakatani, S. and Ibuki, F. (1987). *Agric. Biol. Chem.* **51**, 3301.

Chapter 12

The Location of Vanillin in a Food Emulsion System

Ibrahim Kayali[1], Christopher C. Heisig, and Stig E. Friberg

Center for Advanced Materials Processing, Clarkson University, Box 5814, Potsdam, NY 13699–5814

The partition of vanillin between the three phases, water, oil and lamellar liquid crystal, in an emulsion of water, lecithin and soybean oil was determined by UV analysis.

With the phases separated, the aqueous phase showed a maximum vanillin solubility of 1.0%, the oil phase 3% and the liquid crystalline phase 8.0%. The partition of vanillin between different phases reflected those maximum solubilities. So was a concentration ratio of 2.8 found for the partition between oil and water in the absence of lecithin. The presence of lecithin significantly changed this ratio because the lecithin formed liposomes in the water carrying higher concentrations of vanillin.

Flavor is the most important part of food; together with appearance (color and form) it forms the primary impression of a dish and is decisive for choice. Hence, the research in the area is extensive as demonstrated by numerous review articles covering general aspects of volatile oils *(1)* as well as their composition, biosynthesis, extraction and analysis *(2)*, protein sweeteners *(3)*, spices and their extracts *(4)* the common fruit and berry flavors *(5)* aroma recovery *(6)*, flavor retention *(7)* as well as perevaporation *(8)*. Flavor recognition *(9,10)* has given rise to sophisticated investigations as has the intricate relationship between structure and aroma *(11,12)*. All these investigations are based on chromatography methods with different detector systems and a review article *(13)* emphasizing the limitations and problems with the methods forms very instructive reading. Most food products are in a dispersed state frequently of colloidal

[1]Permanent address: AL–QUDS University, College of Science & Technology, Abu–Deis, West Bank

dimensions, and it appears reasonable to assume the partition of flavors between different colloidal association structures to be important for flavor perception. However, except for a recent article on the release of butanol from multiple emulsions of the W/O/W type *(14)* no publications were found on this subject.

With this article we present results from an introductory investigation of vanillin partition in a common emulsion system of water, lecithin and a fatty oil. The results were to some extent surprising, because the vanillin compound was strongly partitioned towards the liquid crystal present and small amount of the latter (1%) dispersed as liposomes in the aqueous phase significantly changed the partition between oil and water.

Vanillin was chosen as the flavor substance, because it and its derivatives, especially ethylvanillin, are by for the most important flavor compound with approximately 50% of the entire market *(15)*. In spite of this fact the recent research on the compound is not extensive. The flavor development with arguments in favor of or against the coniferine precursor theory has been reviewed *(16)* and the synthesis of ethylvanillin *(17)* has been described.

Experimental

Materials.

The vanillin, 97% pure, and the oil Blue N dye were supplied by Aldrich, Milwaukee, Wisconsin. The soybean oil was supplied by Hain Pure Food Co., Inc., Los Angeles, California. Lecithin extracted from egg was from Kabi Chem. Stockholm, Sweden, and water was doubly distilled.

Phase Diagrams.

The maximum solubility of vanillin in water and oil, and the boundaries for the various phases were established by direct titration using visual and microscopic observation. The liquid crystalline phase was identified from its pattern in an optical microscope between crossed polarizers and its phase limits determined by low angle x–ray diffraction. The oil phase in the three phase region was stained by oil Blue N dye to facilitate microscopic identification of its phase.

Low Angle X–ray Diffraction.

The samples were introduced into a fine glass capillary tube (0.5mm diameter). Low angle x–ray diffraction data were obtained by using a Kiessig low angle camera from Richard Siefert. Ni filtered Cu radiation was used ($\lambda = 1.542\text{Å}$) and the reflection peaks were determined by a Tennelec position sensitive detection system (Model PSD–1100).

Photomicrography.

An Olympus B11 polarizing microscope, attached to an automatic exposure Olympus camera (Model C035A), was used. A small amount of sample was transferred from the sample tube onto the glass slide and was covered immediately with a slide cover. The sample was then sheared between the slide and the cover to a thickness of ˜5 to 10μm. The following samples were observed between crossed polarizers. –1– 66% lecithin, 28% water, 6 vanillin; –2– 64% lecithin, 28% water and 8% vanillin; –3– 57% lecithin, 25% water, 12% soy oil and 6% vanillin; –4– 56% lecithin, 25% water, 12% soy oil and 7% vanillin; –5– 38% lecithin, 57% water and 5% vanillin; –6– 35% lecithin, 58% water and 7% vanillin.

Partition of Vanillin in Soybean Oil/Water

Soybean oil was layered onto aqueous solution containing 0.5% vanillin. The sample was mixed on a vortex mixer for 30 sec. and left to equilibrate on a Barnestead/Thermolyne mixer with gentle mixing for two hours. The concentration of vanillin was determined in each phase by UV spectrometry.

Partition of Vanillin in Soybean Oil/Water/Liquid Crystal

Vanillin, 0.5%, was dissolved in water, layered onto a liquid crystalline phase with the composition of 70% lecithin and 30% water and a third phase, the soybean oil was then layered onto the aqueous phase. The weight ratios of the three phases was 49.5% soybean oil, 49.5% water and 1% liquid crystal.

The sample was mixed on a vortex mixer for 30 sec. and left to equilibrate on a Barnested/Thermolyne mixer for two hours. This resulted in two layers, one with the diluted liquid crystalline phase forming liposomes in the aqueous phase and the other, the oil phase.

The concentration of vanillin in each phase was determined using UV spectrometry.

Results

The results are reported in the following order. The three–component phase diagrams are first described followed by their combination emphasizing the three–phase and four–phase spaces. With this information, the maximum solubility in the three phases experienced in an emulsion is related to the phase equilibria and the partition between phases at less than maximum solubility reported. Finally, the dimensions in the lamellar liquid crystal is calculated from the low angle x–ray diffractograms.

Phase Diagrams

The water rich part of the system water, lecithin and soy oil is shown in Figure 1 revealing the lamellar liquid crystalline phase between 65 and 90% lecithin with a maximum solubilization of soy oil of 14% by weight. The lecithin did not show measurable solubility in the water nor in the soy oil. The essential feature in the diagram is the oil and the aqueous phases being in equilibrium with a lamellar liquid crystal composition containing maximum water but no oil.

This is not the case with vanillin replacing the oil, Figure 2. The three-phase region now comprises vanillin with no solubility of water or lecithin, water with 1% by weight vanillin dissolved and a liquid crystal of 8.7% vanillin, 22.9% water and 68.4% lecithin.

Combining these two diagrams results in the partial phase diagrams according to Figure 3. The two-phase region of water and lamellar liquid crystal in Figure 2 extends towards the oil phase connecting the line 0 to 1 percent vanillin on the water/vanillin axis with a part of the surface of the liquid crystalline phase pointing towards the water corner, Figure 4. A second two-phase space consists of the line between 0 and 3% vanillin on the oil/vanillin axis and a corresponding area on the lamellar liquid crystalline surface, Figure 5. The line separating these two areas on the lamellar liquid crystal forms a three-phase space with the mentioned two lines on the water/vanillin and oil/vanillin axis, Figure 6. With vanillin amounts in excess of these maximal values a four-phase region is found with the three phases of maximum vanillin content in equilibrium with vanillin crystals, Figure 7.

The presence of native vanillin was conspicuous feature of the optical microscope image as demonstrated by the combinations in Figure 8. Figures 8a, b reveal the presence of a large vanillin crystal in the liquid crystalline phase, with a lecithin/water ratio of 2.3 and water contents of 6 and 8% vanillin respectively. The optical pattern in Figure 8a is typical of a lamellar liquid crystal while in Figure 8b the vanillin crystal is easily recognizable. Figure 8c,d show a similar pattern for composition within a liquid crystalline composition with lecithin/water/soy oil ratios of 2.3/1/0.48 with 5%, Fig. 8c, and 7% vanillin, Fig. 8d, added. The same method of detection was useful for the multi-phase regions; Figs. 8e,f show compositions with a lecithin/water ratio of 0.66 and vanillin contents of 5 and 7%.

Determinations of total vanillin content in the two phase range water/liquid crystal, Figure 2, gave a linear relationship according to the phase diagram. It should be noted that the optical pattern of the liquid crystal could not be found except for high content of liquid crystal. The intense stirring from the vibrator/mixer caused the liquid crystal to form vesicles in the water.

Low Angle X-Ray Diffraction

Addition of soybean oil to the lecithin/water liquid crystal increased the slope of the interlayer spacing versus water volume ratio, Figure 9, but left the value extrapolated to zero water content without significant change. Addition of
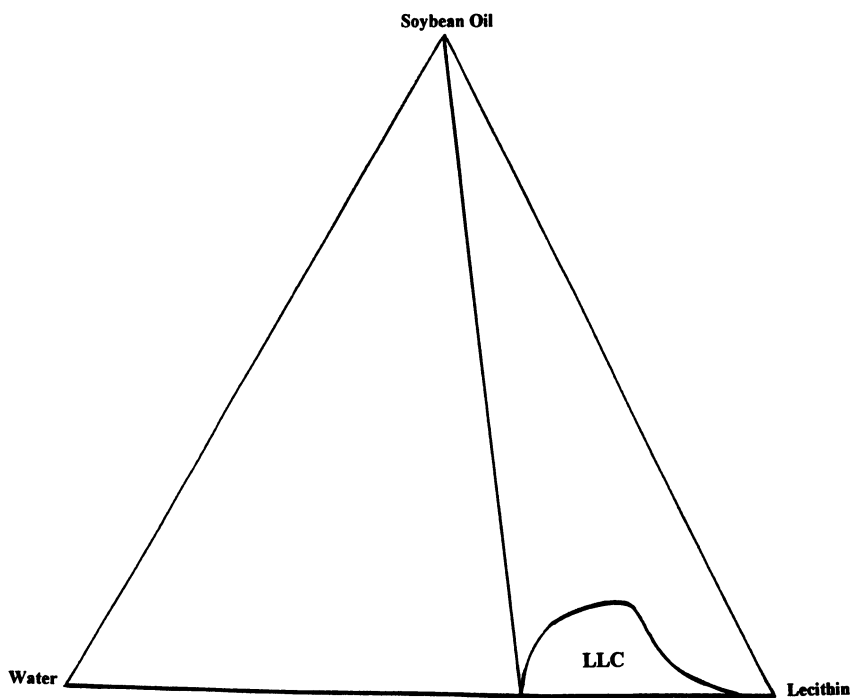
Figure 1. Three component phase diagram of soybean oil, water, and lecithin.
LLC: Lamellar Liquid Crystal
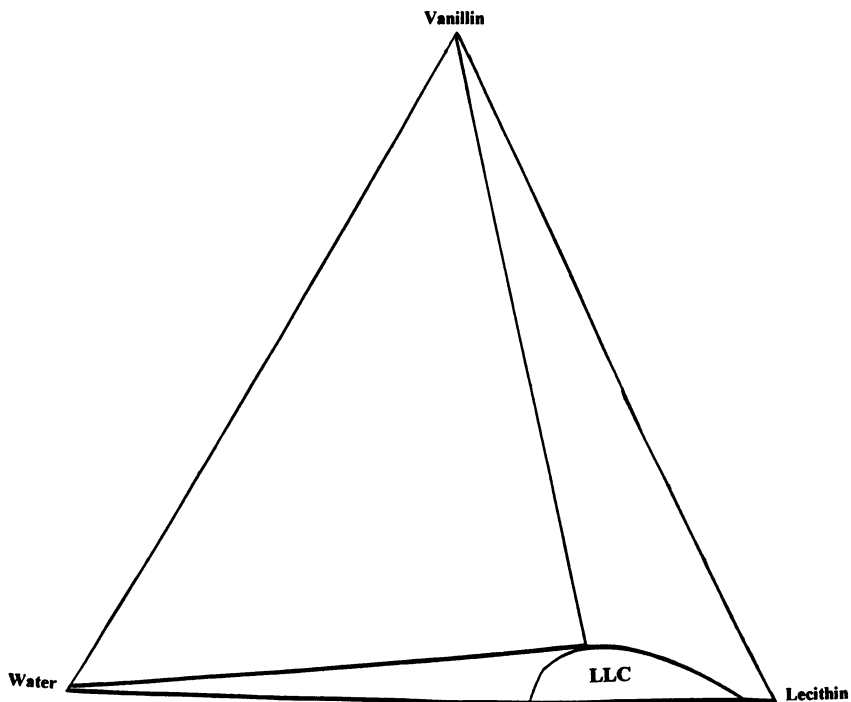
Figure 2. Three component phase diagram of vanillin, water, and lecithin.
LLC: Lamellar Liquid Crystal
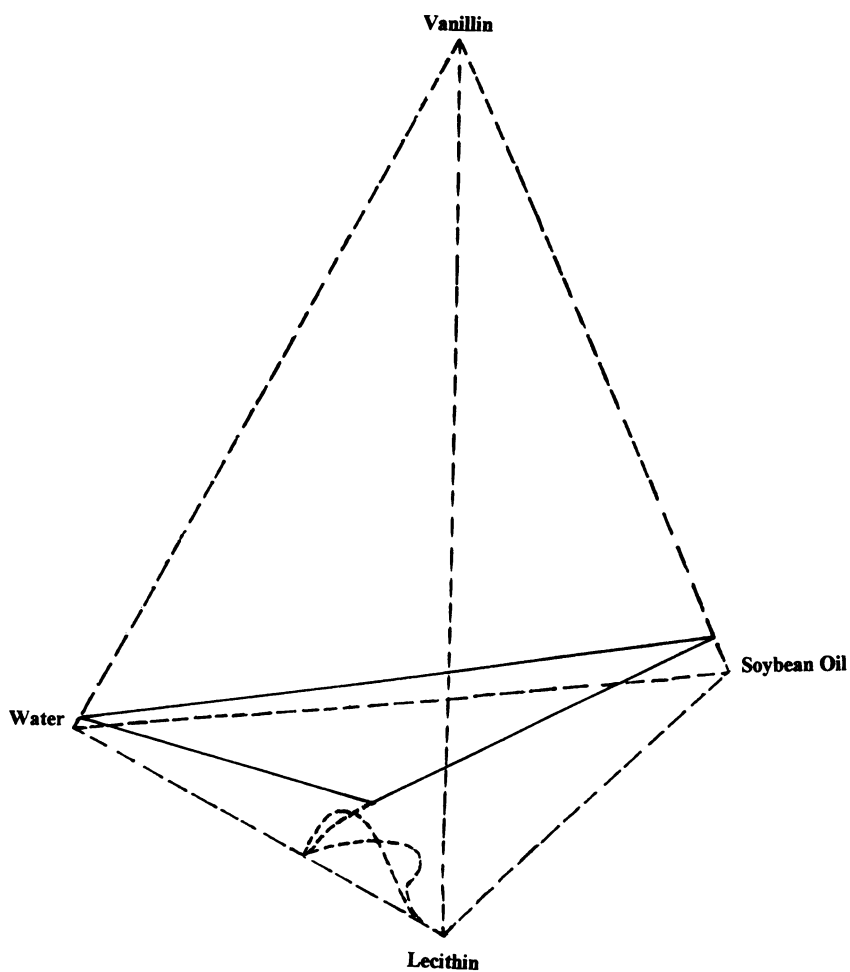
Figure 3. Four component phase diagram of vanillin, soybean oil, water and lecithin.
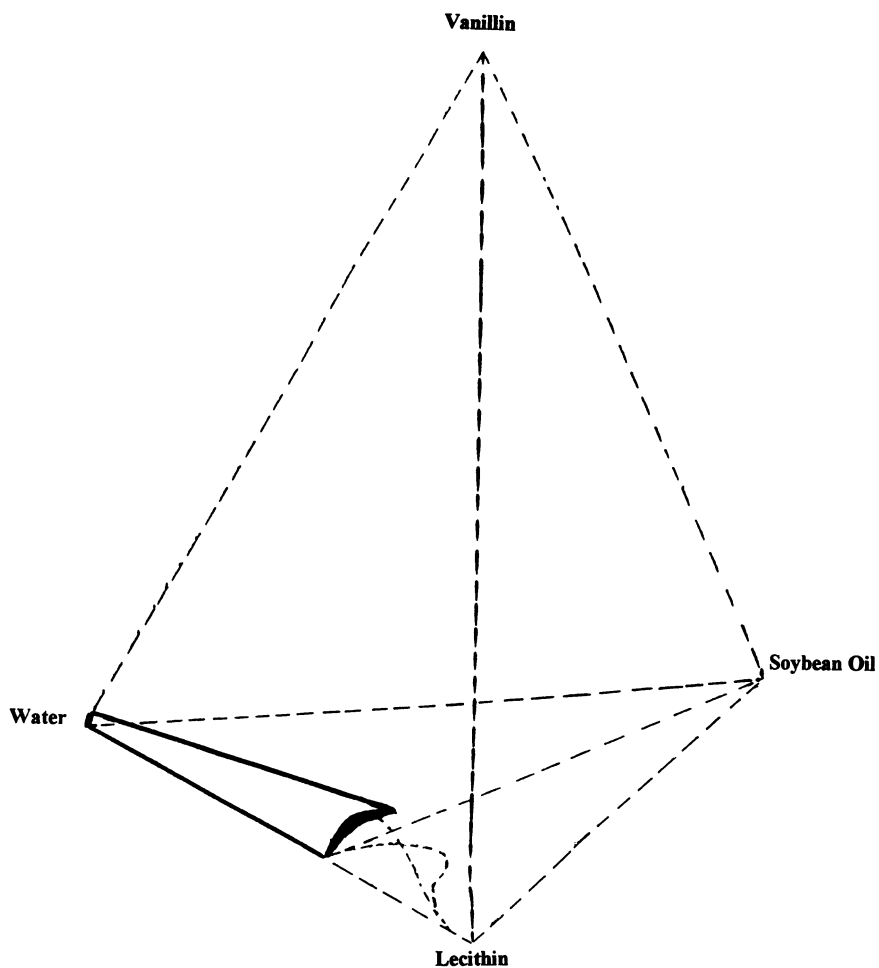
Figure 4. Four component phase diagram of vanillin, soybean oil, water and lecithin. The two-phase region consisting of the aqueous solution and the lamellar liquid crystal is outlined.
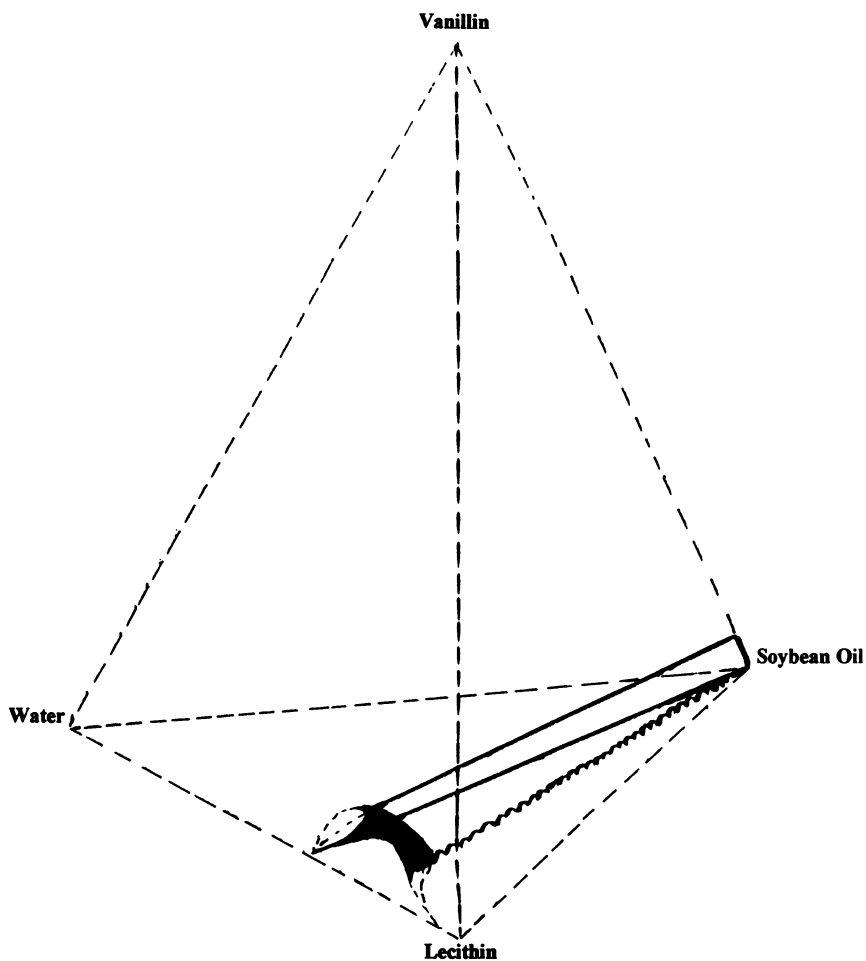
Figure 5. Four component phase diagram of vanillin, soybean oil, water and lecithin. The two-phase region consisting of the soybean oil solution and the lamellar liquid is outlined.
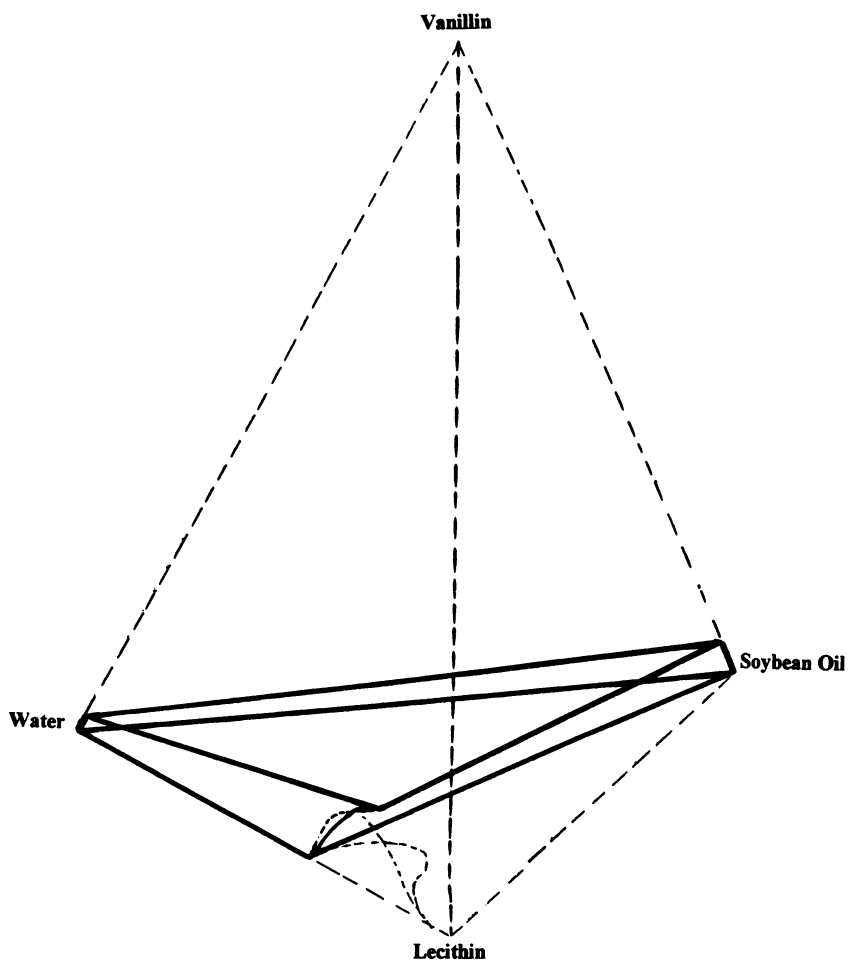
Figure 6. Four component phase diagram of vanillin, soybean oil, water and lecithin. The three-phase region consisting of the aqueous solution, the soybean oil solution and the lamellar liquid crystal is outlined.
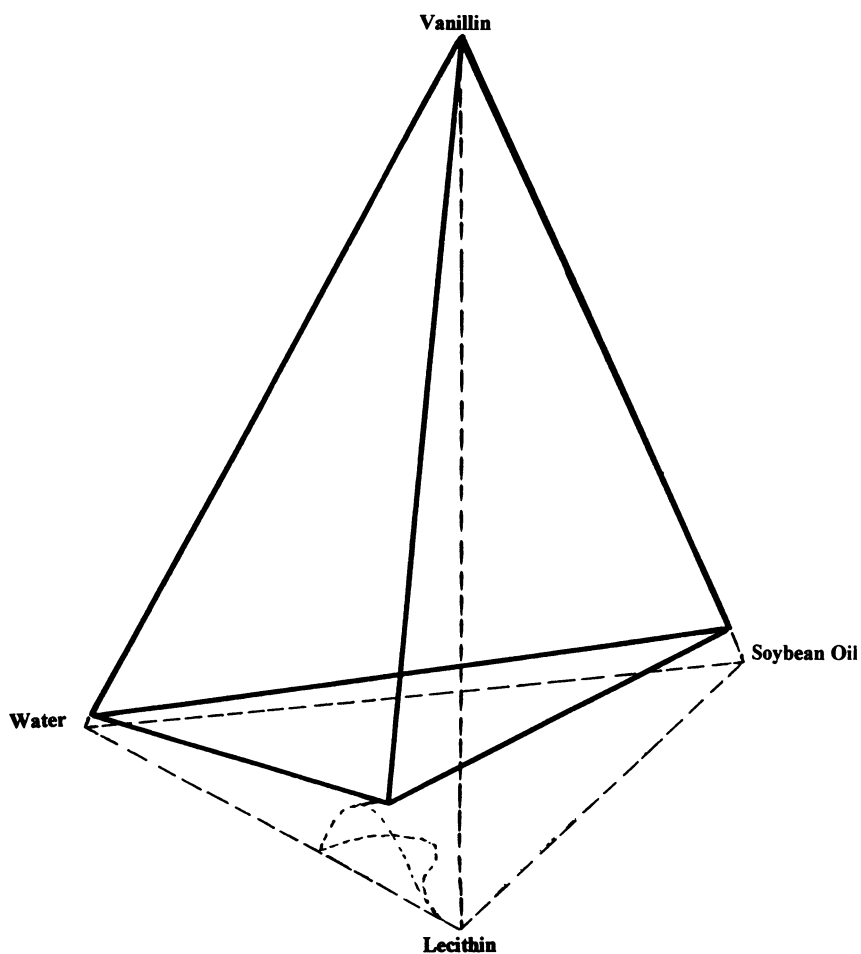
Figure 7. Four component phase diagram of vanillin, soybean oil, water and lecithin. The four-phase region consisting of water, soybean oil, lamellar liquid crystal and vanillin is outlined.

vanillin, on the other hand, Figure 10, gave both a reduction of the extrapolated value for interlayer spacing and an increase of the slope.

Discussion

The results are pertinent for food emulsions stabilized by lecithin showing the third phase, a lamellar liquid crystal, to be formed at low lecithin content at equilibrium in accordance with very early results *(18)*. However, in the present investigation, the lamellar liquid crystal was not detected optically; the adsorbed layers of liquid crystal *(19)* are removed during intensive stirring forming vesicles *(20)*, which serve as stabilizers.

The present results show the maximum solubility of the vanillin flavor molecule to vary in the order aqueous phase, oil phase, liquid crystalline phase with 1, 3, and 8% by weight respectively. The maximum solubility may, hence, be expressed as a linear function of weight fractions of the three phases, because of the fact that the vesicles formed in the aqueous phase added to the total solubility of vanillin as if an intact liquid crystalline phase had been present. Furthermore, realizing that the lamellar liquid crystal contains 35% water the following expression is obtained

$$S_{tot}^{van} = 0.010w + 0.03\sigma + 0.114\ell \qquad [1]$$

in which w, σ and ℓ are weight fractions of water, oil and lecithin, while S_{tot}^{van} is the maximum solubility of vanillin as weight fraction. The formula is, of course, valid only within the following limit

$$W \geq 0.35 \ [1-\sigma/(\sigma+\ell)] \qquad [2]$$

The comparatively high solubility of vanillin in the liquid crystal compared to the two other phases is related to the location of the vanillin molecule in the lamellar liquid crystalline structure. The organization of the mesogen molecules may be described as in Fig. 11 with three parallel layers. A is the water layer and polar parts dissolved in it, B is the hydrocarbon chains except the terminal methyl group, which forms the layer C.

The location of the solubilized molecule is estimated from the dimensions of the three layers. A location between the methyl groups, C, Fig. 11, will increase the combined thickness of layers B and C, while a localization of an added molecule within zone B leads to no change in this value, but to a reduction of the distance across layer A due to the lateral expansion in layers B and C.

The location of the added molecule may only be estimated from the interlayer spacing extrapolated to zero water content; for other compositions the partial penetration of water from zone A to zone B, Figure 11 makes the interlayer spacing, d, Figure 11, irrelevant to an evaluation of that kind.

The calculation of the location of the soybean oil molecule is, hence, made from the d_0 values from Figure 9. If a volume fraction of added oil, α, enters B
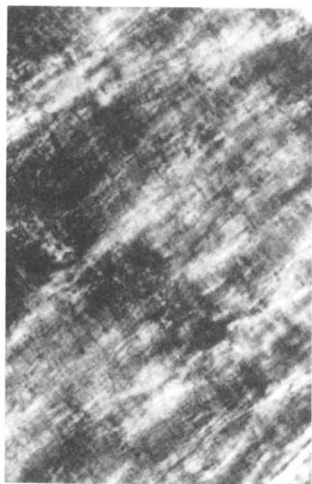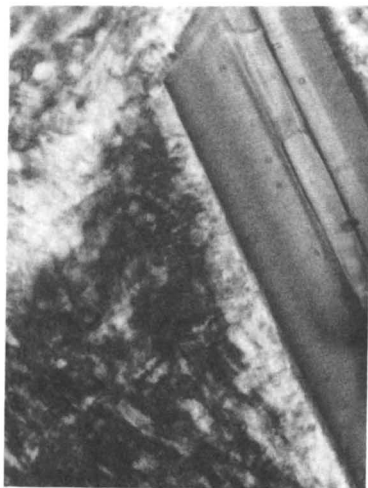
Figure 8a

Figure 8b
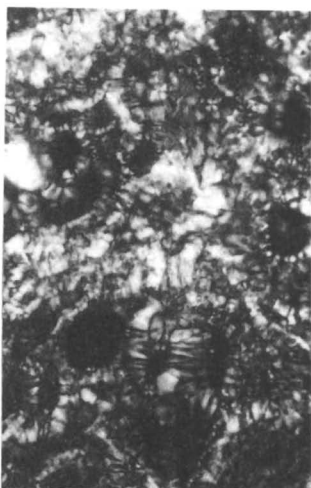
Figure 8c

Figure 8d

Figure 8. Photograph with the sample between crossed-polarizers
a. LLC (lecithin / water) with 6% vanillin
b. LLC (lecithin / water) with 8% vanillin
c. LLC (lecithin / water) + soybean oil with 6% vanillin
d. LLC (lecithin / water) + soybean oil with 7% vanillin
e. multiple phases, 38% lecithin, 57% water, 5% vanillin
f. multiple phases, 35% lecithin, 58% water 7% vanillin

Figure 8e

Figure 8f

Figure 8. *Continued*
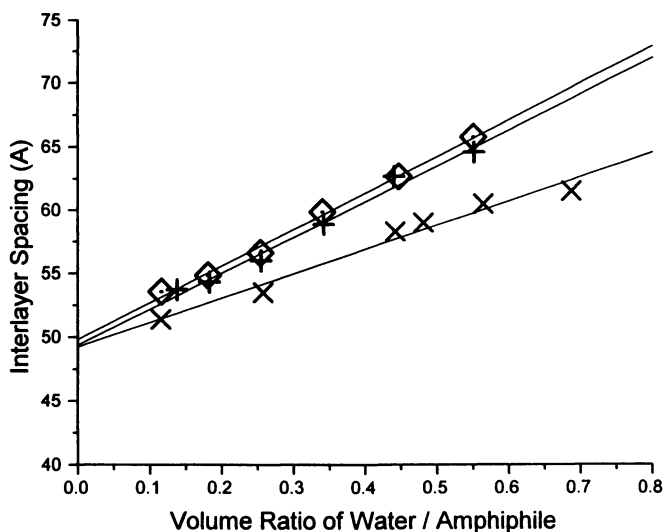
Figure 9. Plot of interlayer spacing vs. volume ratio of water for the system of water, lecithin and soybean oil.

◇ 90% lecithin / 10% soybean oil
+ 95% lecithin / 5% soybean oil
X 100% lecithin
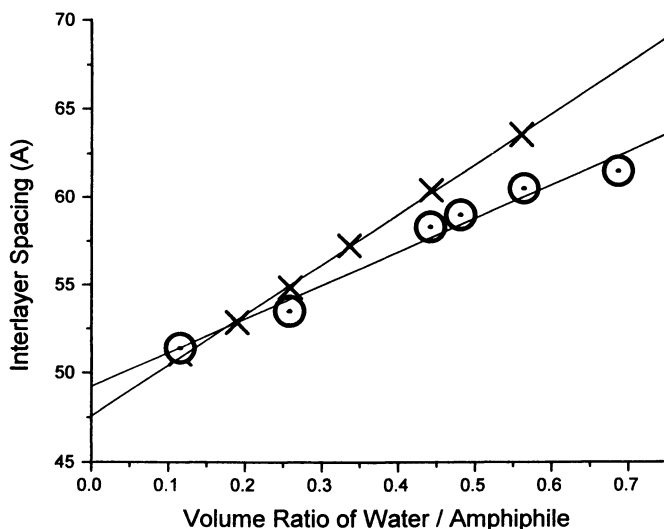
Figure 10. Plot of interlayer spacing vs. volume ratio of water for the system of water, lecithin and vanillin.

o 100% lecithin
X 95% lecithin / 5% vanillin
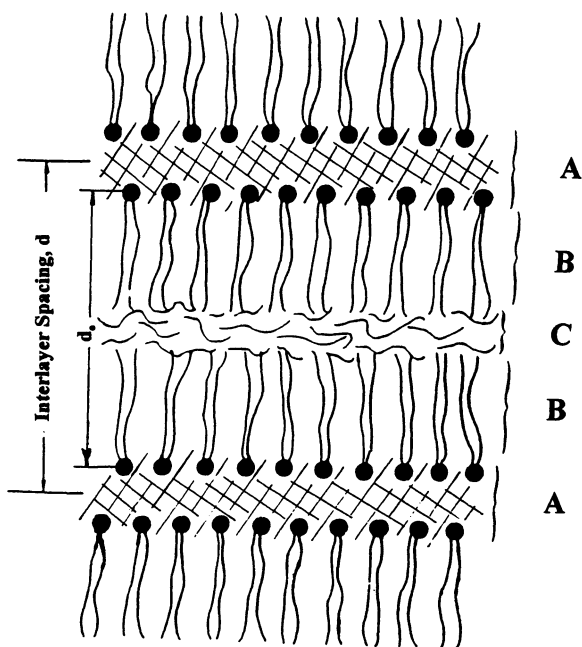
Figure 11. Schematic representation of the different layers in a lamellar liquid crystal.

from C, Figure 11; a relation between the d_o values with oil = d_o^o and without oil = d_o becomes

$$d_o^o = d_o (1+R)/(1+\alpha R) \qquad [3]$$

in which R is the volume ratio of oil to lecithin.

The extremely minuscule increase in d_o after addition of oil enables only one conclusion; close to all of the added oil is located in zone B, Figure 11. Addition of vanillin caused an actual reduction of interlayer spacing showing the vanillin molecules to concentrate towards the interface A/B, Figure 11. An approximate estimation of the number of vanillin molecules so anchored may be obtained by the following calculation. 5% vanillin and 95% lecithin correspond to molfractions of 0.20 and 0.80. Assuming a height of vanillin of 7.5Å while that of lecithin is 24.5Å according to the results in Figure 5 and 6 and calculating their volume of the molecules from density values (ρ_{van} = 1.056 V_{van} = 239Å^3, ρ_{lec} = 1.04 V_{lec} = 1300Å^3) the following relation is obtained, if mol fraction x_v of vanillin is anchored at the interface while 0.20–x_v mol fraction is in region B, Figure 11

$$h_{av} = V_{tot} / A_{tot} \qquad [4]$$

in which h_{av} = 24.5 from x-ray, V_{tot} is the volume of all molecules involved while A_{tot} is the added areas of the molecules at the interface A/B, Figure 11.

$$23.5 = (0.8 \cdot 1{,}300 + 0.2 \cdot 239) / (x \cdot 32 + 0.8 \cdot 53) \qquad [5]$$
$$x = 0.12$$

Whereas this number is extremely approximate it indicates that the significant fraction of more than one half of the vanillin molecules is anchored at the polar interface.

This attachment caused a difference in the next characteristic property of the liquid crystal; the amount of added water penetrating from zone A to zone B, Figure 11. Equation [3] is valid also for this evaluation, but the α value will be reduced with increased water addition, because of the almost constant thickness of layer B + C, Figure 11. It is, hence, to be preferred to use the limiting value of α when R approaches zero.

$$\alpha = 1-(\partial R/\partial d)/d_o \qquad [6]$$

The lamellar liquid crystal of lecithin, Figure 5,6, has an α value of 0.6. Adding soybean oil reduces that value to 0.4, but adding vanillin causes a reduction to 0.05. Obviously the vanillin molecule being to a significant part anchored to the A/B interface, Figure 11, presents a barrier to water penetration into zone B, Figure 11.

It seems reasonable that the anchoring to the interface is one of the essential factors in the comparatively high solubility of the vanillin in the liquid crystal. Another factor is the influence of the Israelachvili–Ninham packing ratio (20). An increase in this value causes an increase in the solubility, because of a structural contribution to the free energy change (21). This factor was early pointed out by Wahlgren (22).

Literature Cited
1. Kobayashi, A. *Nippon Shokuhin Kogyo Gakkaishi* **1994**, 41, 165.
2. Waterman, P.G. In *Volatile Oil Crops: Their Biological and Biochemical Production; Hay, R.K.H., Waterman, P.G.,* Eds.; Longman Publ. Co., Harlow U.K., 1993, pp.47.
3. Kurihara, Y.; Nirasawa, S. *Trends Food Sci. Technol.* **1994**, 5, 37.
4. Marion, J.P.; Andino, A.; Marguial, L.; Brenard, H. *Div. Food Sci.* **1994**, 34, 71.
5. Perez, A.G.; Sanz, C.; Rios, J.J.; Olias, J.M. *Rev. Esp. Cienc. Technol. Alimeat* **1993**, 33, 665.
6. Bohra, P.M.; Vaze, A.S.; Pangarkar, V.G. *J. Chem. Technol. Biotechnol.* **1994**, 60, 97.
7. Coumans, J.W.; Kerkhat, P.J.A.M.; Bruin, S. *Drying Technol.* **1994**, 12, 99.
8. Karlsson, H.O.E.; Traegardh, G. *J. Membr. Sci.* **1994**, 91, 189.
9. Kashinayanagi, M. Shoji, K. Kurihara, K. *Supramol. Chem.* **1993**, 1, 199.
10. Nakamura, M.; Tsujii, K.; Katsuragi, Y.; Kurihara, K.; Sumamuto, J. *Biochem. Biophys. Res. Comm.* **1994**, 201, 415.
11. Kashiwayanagi, M.; Shoji, T.; Kurihara, K. *Supramolecular Chemistry* **1993**, 1, 119.
12. Spreitzer, H.; Kaller, U.; *Z. Lebenson Unters. Forseh.* **1992**, 194, 213.
13. Joulain, D. *Perfum. Flavor* **1994**, 19, 5.
14. Dickinson, E.; Evison, J.; Gramsbow J.W.; Schwape, D. *Food Hydrocolloids* **1994**, 8, 63.
15. Mayler, D. *Chemistry Industry* **Jan. 1991**, 11.
16. Kanisawa, T. *Koryo* **1993**, 180, 113.
17. Li, J.; He, X.; Cao, Z. *Hecheng Huazue* **1993**, 1, 333.
18. Friberg, S.E.; Mandell, L. *J. Pharm. Sci.* **1970**, 59, 1001.
19. Friberg, S.E.; Jansson, P.O., Cederberg, E. *J. Colloid Interface Sci.* **1976**, 55, 614.
20. Israelachvili, J.N.; Mitchell, J.; Ninham, B.W. *J. Chem. Soc. Faraday Trans. II* **1976**, 76, 1525.
21. Mitchell, D.J.; Ninham, B.W. *J. Chem. Soc. Faraday Trans. II* **1981**, 77, 601.
22. Wahlgren, S.; Lindström, A.L.; Friberg, S.E. *J. Pharm. Sci.* **1984**, 73, 1484.

Chapter 13

Methods To Predict the Physical Stability of Flavor–Cloud Emulsion

K. Y. Tse[1] and G. A. Reineccius[2]

[1]Robertet Flavors, 640 Montrose Avenue, South Plainfield, NJ 07080
[2]Department of Food Science and Nutrition, University of Minnesota, 1334 Eckles Avenue, St. Paul, MN 55108

The usefulness of particle size determination, centrifugation and elevated temperature storage for the prediction of the stability of beverage emulsions was evaluated. Based on our results, storing diluted beverage emulsions at elevated temperatures will give the most accurate prediction of emulsion stability. Storing an emulsion at 45 °C would be expected to increase the rate of loss of turbidity by factors of 2.5 to 4 over room temperature storage. While this approach gives an accurate prediction of emulsion stability, the analysis time is too long to be useful in quality control applications. Particle size and centrifugation methods were found to be inaccurate due to their inability to consider emulsion instability caused by coalescence or flocculation. It is suggested that methods to determine Zeta potential be evaluated in the future.

A common problem in the flavor industry is producing a cloud or flavor emulsion which remains stable over the desired shelf life. The particulate phase (e.g. flavor formulations or orange terpenes) generally has a specific gravity of about 0.84 while the aqueous phase will generally range from 1.0 to 1.06 depending upon the amount of solids (most often sugar) in the product. These emulsions are, therefore, inherently unstable once put into the final application (e.g. a beverage) and will tend to undergo phase separation resulting in decreased turbidity of the bulk of the product and the formation of a ring of flavor or clouding agent at the top of the product.

The industry uses a combination of emulsifiers (e.g. modified starches or gum acacias), homogenization (to reduce particle size of the dispersed phase) and the incorporation of weighing agents (e.g. brominated vegetable oil or ester gum) to attempt to stabilize these emulsions. Despite the use of these approaches, the industry still commonly has a problem with the stability of products containing flavor or cloud emulsions.

There is substantial need to be able to rapidly determine whether an emulsion will have the desired shelf life in a particular application for quality control purposes. The most common method to evaluate emulsion stability is to measure particle size of the emulsion at the time of manufacture. The importance of particle size in determining emulsion stability is evident from Stokes' Law:

$$V = \frac{2 \, g \, r^2 (d_1 - d_2)}{9 \, \eta}$$

Where V is velocity of phase separation, r is radius of the dispersed phase, d_1 and d_2 are densities of the dispersed and continuous phase, respectively, g is the acceleration of gravity and η is the viscosity of the continuous phase. One will note that the velocity of separation is related to the square of the radius so small changes in particle size will have profound effects on emulsion stability. Particle size may be determined using a light microscope and visually estimating particle size or determining particle size distribution using some instrumental technique such as light scattering or electrical resistance. Another means of rapidly predicting emulsion stability is centrifugation. Centrifugation increases the g term in the equation which speeds destabilization of the emulsion.

The use of elevated temperature storage on emulsion stability is less evident. It is clear that increasing temperature will decrease the viscosity of the system but the effect is greater than that alone. Elevated temperature provides greater mobility to the system thereby enhancing flocculation and coalescence. Both flocculation and coalescence will occur during aging of an emulsion and greatly increase particle size - thus emulsion instability. The last method to be noted is Zeta potential. Zeta potential, simply put, is a measurement of the rate of migration of the particulate phase in an electric field. In an emulsion, the particles will inherently take on an electrical charge and this charge will influence whether the particulate phase will flocculate and/or coalesce. Riddick (*1*) stated that emulsions with a Zeta potential of at least -40 mV are stable and those with a Zeta potential of less than -15 mV are generally unstable. It is of interest that emulsions based on gum acacia have Zeta potentials of about -23 mV suggesting they are on the border of stability (*2-3*). One should note that neither flocculation nor coalescence are considered in Stokes' Law. Stokes' Law considers only creaming and thus any method for predicting stability which is based on Stokes' Law (e.g. particle size and centrifugation) may not be accurate since these other mechanisms of instability are not considered. Tan and Wu (*4*) have provided a most thoughtful discussion of emulsion stability and suggest Zeta potential as the best predictor of emulsion stability.

The industry currently uses several methods to predict emulsion stability. While Zeta potential may be the best predictor of emulsion stability, the instrumentation to determine Zeta potential is expensive and less expensive alternatives are generally used. Particle size (by light microscope) and absorbance (400 or a ratio of 400/700 or 800 nm) (*5-7*) are thus, very common methods. The purpose of this study was to evaluate several methods of predicting the stability of an emulsion using the more common methodology.

Material and Methods

Materials. Cold pressed orange oil was purchased from Sunkist Growers, Inc. (Ontario, CA). Gum acacia (Spray gum 28830) and Emulgum (BV 25631) were supplied by Colloides Naturels Inc. (Bridgewater, NJ) and Purity gum BE was provided by National Starch Inc. (Bridgewater, NJ). Weighing agent (ester gum 8BG) was provided by Hercules Inc. (Wilmington, DE).

Emulsion Preparation. Emulsifiers (gum acacia, Emulgum and Purity gum) were rehydrated in 60 °C distilled water. In order to get all hydrocolloids fully rehydrated, gum acacia solution was prepared and allowed to stand overnight at room temperature before use while solutions of Emulgum and Purity gum were prepared two to three hour prior to use. It should be noted that ester gum solutions were also prepared in advance since the ester gum took several hour to dissolve in orange oil. Orange oil (with or without ester gum) was added to the gum solutions and emulsified thoroughly using a Waring-type blender (3 min on high speed) or a Microfluidizer (Microfluidics Inc., Newport, Mass) . The Microfluidizer was operated at either low pressure (8,400 psig) or high pressure (12,600 psig). The formulae of emulsions used in this research (Table I) were based on information provided by the gum suppliers in order to optimize the emulsifying properties of each gum.

Emulsion Stability Tests

Preliminary experiments indicated that the data obtained on emulsion stability were very reproducible. Therefore, all data for emulsion stability tests were collected from a single experiment with duplicate determinations.

Centrifugation Stability Tests. Diluted emulsions (0.3% w/v) were freshly prepared by adding 3 g of the original emulsion to a volumetric flask and adding water to make 1000 mL. This diluted emulsion was centrifuged (International centrifuge model UV) at 500 X g for the times noted. After centrifugation, the white cream layer at the top of the emulsion was discarded and sample was pipetted from the remaining emulsion. Emulsion absorbance was measured at 400 nm in a 1 cm path length optical glass cuvette (Bausch & Lomb) using a spectrophotometer (Spectronic 21, Bausch & Lomb) before centrifugation and after 5, 10, 20, 30 and 45 min of centrifugation. Distilled water was used as a blank for absorbance measurement. All data reported are the result of a single experiment with duplicate determinations.

Shelf Life Storage Test. Diluted emulsions (0.3 % w/v) were stored in small test tubes (12 cm x 15 mm) sealed with parafilm at five different temperatures (4, 13, 23, 35 and 45 °C). Samples for absorbance measurement were pipetted from the middle portion of the diluted emulsions. Absorbencies (400 nm in a 1 cm path length cuvette) were measured over a period of 36 days. All data reported are the result of a single experiment with duplicate measurements.

Table I. Formulae of emulsions used in this study

Component	Composition (%)	
	With Weighing	Without Weighing
Gum acacia emulsion		
Gum acacia	20.0	20.0
Orange oil	6.5	6.5 (or 12.5)
Ester gum	6.0	-
Distilled water	67.5	73.5 (or 67.5)
Emulgum emulsion		
Emulgum	3.5	3.5
Orange oil	6.5	6.5 (or 12.5)
Ester gum	6.0	-
Distilled water	84.0	90.0 (or 84.0)
Purity gum emulsion		
Purity gum	12.0	12.0
Orange oil	6.5	6.5 (or 12.5)
Ester gum	6.0	-
Distilled water	75.5	81.5 (or 75.5)

Particle Size Analysis. Particle size distributions and mean particle sizes of freshly prepared and one week old emulsions were analyzed using a particle size analyzer (Brinkmann Instruments, Inc.). The diluted emulsion was put in a 1 cm path length cuvette and a beam of laser light was passed through the emulsion. Mean particle size and particle size distribution were determined through light scattering diffraction and photo imaging. The entire analysis was computerized and the detected range in particle size was from 0.5 to 150 μm.

Results and Discussion

The purpose of this study was to determine the usefulness of absorbance, particle size analysis and centrifugation to predict the stability of flavor/cloud emulsions. The data which are presented and discussed in this paper are a part of a larger study which was done to determine the effect of using different emulsifiers, means of forming the emulsions (equipment) and the effectiveness of weighing agents (ester gum) on emulsion stability. The results of this larger study will be published elsewhere (Tse, K.Y.; Reineccius, G.A. *Perfumer & Flavorist*, submitted).

Influence of Temperature on Emulsion Stability. The influence of temperature on the stability of diluted emulsions is represented by the data provided in Figures 1-4.
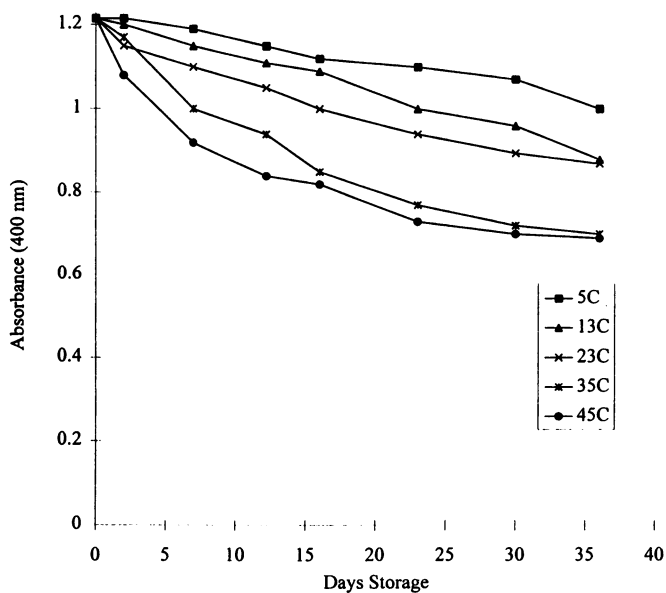
Figure 1. The change in absorption of emulsions based on gum acacia during storage (low pressure Microfluidization).
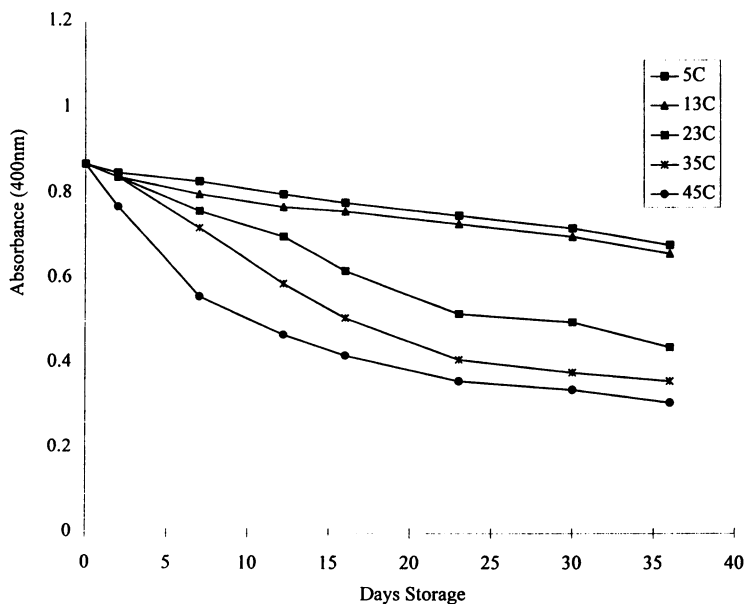
Figure 2. The change in absorption of·emulsions based on Emulgum during storage (low pressure Microfluidization).
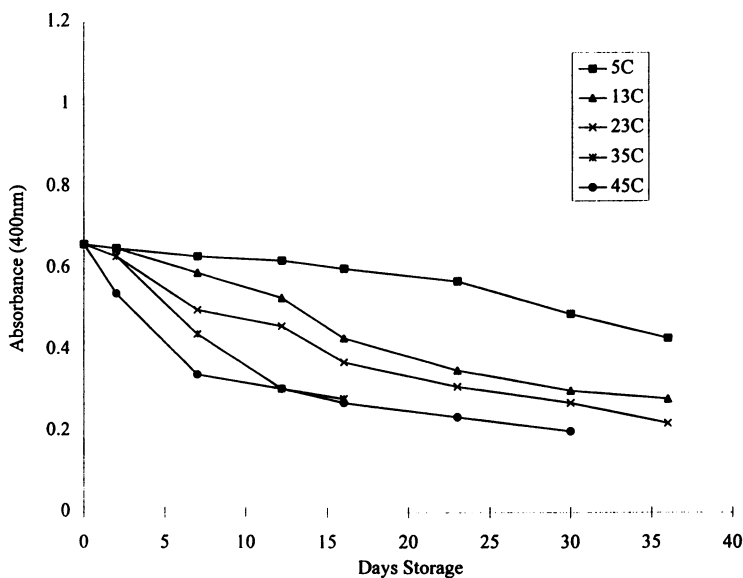
Figure 3. The change in absorption of emulsions based on Purity gum during storage (low pressure Microfluidization).
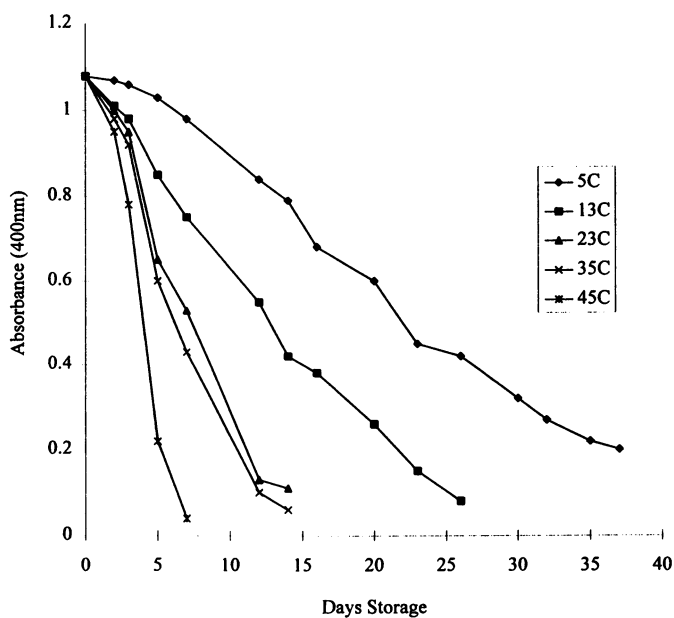
Figure 4. The change in absorption of emulsions based on Purity gum (no weighing agent) during storage (high pressure Microfluidization).

These figures are from emulsions based on gum acacia, Emulgum or Purity gum. Several observations can be made from the data in these figures. The first is that emulsion stability is inversely related to storage temperature. This is not unexpected since, as noted earlier, higher temperatures result in decreased solution viscosity and enhanced rates of collision between emulsion droplets. Decreased solution viscosity increases the rate of creaming while increased incidence of collision enhances flocculation and coalescence.

A second point relates to the effectiveness of increasing temperature to accelerate emulsion instability. It is obvious from these figures and the data in Table II that temperature had a definite effect on the stability of the emulsions and that different emulsions are affected differently by increasing storage temperature. While the effect of temperature on solution viscosity is likely to be reasonably the same for all emulsifiers, the effect on coalescence and flocculation is likely to be different and this is probably why there is a difference in temperature effects for the different emulsifiers. On the average, increasing the temperature 10 °C increased the rate of loss of absorption (or rate of loss of turbidity) by a factor of 1.4, 1.68 and 1.96 for the weighted gum acacia, Emulgum and Purity gum emulsions, respectively. Thus one could make an assumption that the loss of turbidity observed when an emulsion is stored at 45 °C (c.a. 20 °C above room temperature) for 1 month should be about equal to that observed for the same emulsion stored for 2.5 to 4 months at room temperatures (time equivalent depends on the emulsifier used). The data provided on an unweighted emulsion are quite similar to those obtained for the weighted emulsion except that the rates of loss of turbidity are 3-5 times greater (Table II and Figure 4). However, increasing temperature has about the same accelerating effect as observed for the weighted emulsions.

The utility of using accelerated storage temperatures as a quality control procedure suffers from the excessive time required to obtain data. If one is interested in predicting whether a spray dried emulsion (e.g. a dry beverage mix) will last 1 week in the refrigerator following reconstitution, accelerated storage testing may be appropriate. However, if one is interested in determining whether an emulsion will last 6 months, then at least 1 month testing will be required to be assured that it will last the required time. The manufacturer can not keep an emulsion for 1-2 months before shipping to be assured the emulsion is good. A quicker method is required for quality assurance purposes.

Centrifugation to Predict Emulsion Stability. As noted earlier, it is desirable to obtain results faster than can be obtained in accelerated temperature storage studies. The use of centrifugation to increase the rate of creaming appears to be a reasonable means of rapidly evaluating emulsion stability. A major concern is that centrifugation will only measure creaming and not coalescence or flocculation which both occur over time. Thus there is some question as to whether centrifugation will accurately reflect emulsion stability.

The results from this centrifugation study will have some error due to the low level of change that occurred during centrifugation. Most ester gum-containing emulsions lost <10% of their initial turbidity over the period of centrifugation. The emulsions made without ester gum lost a greater amount of turbidity (Figure 5) but did not

provide as good a starting emulsion (i.e. had a low initial absorption) so these data also may not truly representative. However, comparisons will be made with these limitations in mind.

Table II. Effect of temperature on the loss of turbidity in various emulsions
(diluted to 0.3% in water)

	Temperature of Storage (°C)				
	5	13	23	35	45
Emulsifier	----------- Rate of change in absorption[a] --------------				
(with weighing agent)					
Gum acacia	-0.00808	-0.00814	-0.0123	-0.0236	-0.0295
Emulgum	-0.00540	-0.00678	-0.0152	-0.0231	-0.0331
Purity gum	-0.00329	-0.01110	-0.0174	-0.0304	-0.0446
(without weighing agent)					
Purity gum	-0.0264	-0.0401	-0.0763	-0.0768	-0.1650

[a] change in absorbance (400 nm) /day storage.

While there are many ways in which the data could be presented and interpreted (e.g. kinetic or statistical approaches), we will take a simple intuitive approach and look at the total amount of absorbance lost by centrifugation vs the amount lost during shelf life studies. All of the emulsions containing ester gum lost about the same amount of absorption during centrifugation. They would be judged equivalent in terms of stability (one should note that the higher initial absorbance of the gum acacia emulsion makes this emulsion superior to the others despite having about the same stability). The Purity gum and gum acacia emulsions containing no ester gum would be considered about equivalent by centrifugation (Figure 5) while the shelf life studies at room temperature suggest that the gum acacia emulsion is more stable than the Purity gum system (Table II). This disagreement between methods may be explained by considering the particle size data in Table III. The emulsions made using Purity gum and Emulgum underwent substantial coalescence during storage. This would decrease absorption and result in a loss of stability. The gum acacia emulsion did not change in mean particle size and thus was more stable during room temperature storage. This coalescence would not be obvious in centrifugation studies but would affect shelf life. Thus emulsions which will coalesce can not be accurately evaluated by centrifugation methods. This is a danger of using centrifugation as a tool for the evaluation of emulsion stability.

Particle Size to Predict Emulsion Stability. It is quite common to employ some method of measuring particle size to judge emulsion quality and stability. There is little
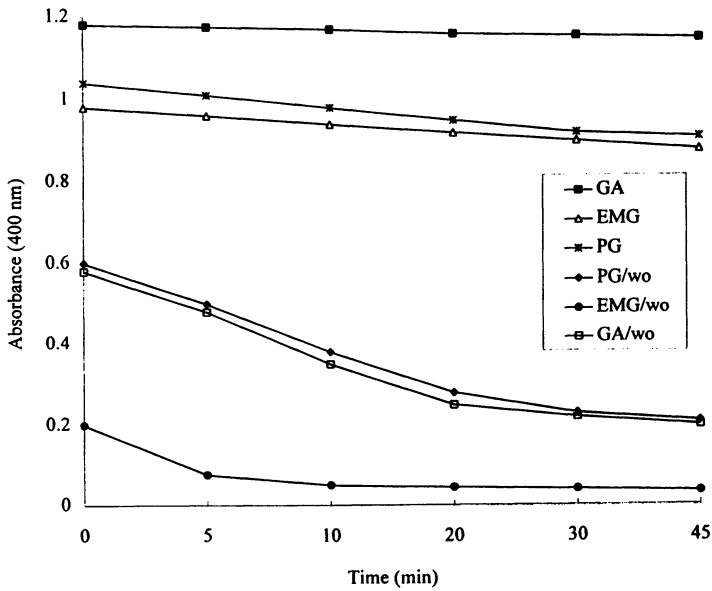
Figure 5. The effect of centrifugation on the absorbance of diluted emulsions (high speed blending) (GA - gum acacia, EMG - Emulgum, PG - Purity gum; wo - no weighing agent).
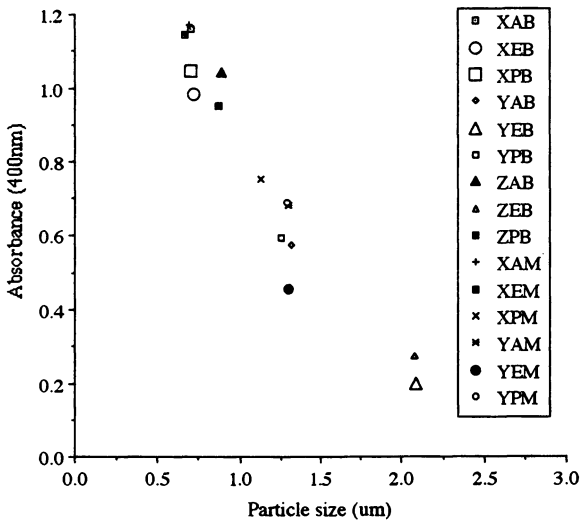
Figure 6. Relationship between absorbance and particle size of emulsions.(X-6.5% oil with 6% ester gum, Y-6.5% oil, Z-12.5% oil; A- gum acaia, E- Emulgum, P- Purity gum; B- blended, M- Microfluidized)

question that there is a good relationship between turbidity (or clouding effect) and particle size. Emulsions having an average particle size between 0.5 and 1.5 μm are preferred since they give maximum turbidity and the desired white color. Despite this knowledge, the quality of relationship between particle size and absorption at 400 nm found in this study was somewhat surprising to us (Figure 6). The data presented in Figure 6 show a very linear relationship between particle size and absorption despite the system composition (type of emulsifier, amount of oil phase and the presence or absence of ester gum). These data suggest that we can get a very good estimate of particle size simply by using absorption at 400 nm - we do not need to purchase an expensive instrument to determine particle size. A simple measure of the absorption of a diluted emulsion may suffice to replace particle size data.

The use of particle size to predict emulsion shelf life suffers from the same disadvantage as centrifugation i.e. it will not consider emulsion instability due to coalescence or flocculation. Thus an emulsion may be produced which has a very small mean particle size and would be judged acceptable but that undergoes coalescence during storage and later becomes unstable.

Table III. Changes in mean particle size of emulsions made without ester gum

	Particle size (μm)			
	Blended		Microfluidized	
	initial	stored [a]	initial	stored
Gum acacia	1.28	1.37	1.27	1.95
	1.34[b]	1.39	1.33	1.99
Emulgum	2.07	2.51	1.29	2.28
	2.11	2.53	1.31	2.30
Purity gum	1.24	1.50	1.26	2.45
	1.26	1.54	1.32	2.45

[a] Stored 7 days at room temperature.
[b] Duplicate sample.

Conclusions

Based on the methods evaluated in this study, storage tests at elevated temperatures are considered to be the most accurate means to shorten analysis time to determine emulsion stability. The use of centrifugation and particle size determination suffer from not considering coalescence or flocculation effects causing instability and thus, may give inaccurate predictions. This does not mean that particle size or centrifugation data are useless for predicting emulsion stability. If one is making a given emulsion on a regular basis and it is found that these methods correlate well to shelf life (method of

instability is primarily creaming rather than coalescence or flocculation), they are valuable quality control methods and should be used. However, using these methods on a new emulsion may give inaccurate predictions and should be used with caution.

Since storing emulsions at the elevated temperatures used in this study gave limited benefits in terms of saving analysis time, we would suggest extending the temperatures for storage to 60 °C (for example) to further reduce analysis time. The time may still be too long to be acceptable as a quality control method. Thus alternative methods must be found. We feel that methods to determine Zeta potential (rate of migration in an electric field) are most likely to give the best predictions of emulsion stability. Zeta potential will consider particle size and charge which then includes emulsion instability due to creaming, coalescence and flocculation. The ability to coalesce or flocculate is strongly influenced by electric charge. We are in agreement with Tan and Wu (4) who proposed Zeta potential as the preferred method for evaluating emulsion stability. Future work will evaluate Zeta potential for this purpose.

Literature Cited

1. Riddick, T. M. Zeta Meter Inc., New York. **1968.**
2. Sharma, S. C. *Food Technol.* **1981,** *35*, 59-67.
3. Silber, D.; Mizrahi, S. *J. Food Sci.* **1975,** *40*, 1174-1178.
4. Tan, C. T.; Wu, H. *Perfumer & Flavorist.* **1988,** *13*, 23-41.
5. Horie, K.; Tanaka, S.; Akabori, T. *Cosmetics and Toiletries.* **1978,** 93(5), 53-62.
6. Kauffman, V. R.; Garati, N. *J. Dispersion Sci. Technol.* **1980,** *2*, 475-490.
7. Kauffman, V. R.; Garati, N. *J. Food Technol.* **1984,** *19*, 255-261.

Chapter 14

Surface Dilational Rheological Properties of Protein-Adsorbed Interfaces

Relationship to Stability of Food Foams and Emulsions

Q. Jiang and Y. C. Chiew[1]

**Department of Chemical and Biochemical Engineering,
Rutgers University, P.O. Box 909, Piscataway, NJ 08855–0909**

Dilational viscoelasticity of air/water and corn oil/water Lysozyme adsorbed interfaces are measured as a function of the protein concentration and surface age. The coalescence of air bubbles with an air/aqueous lysozyme solution interface and corn oil drops with an corn oil/aqueous lysozyme solution interface are also investigated. Specifically, we measured the half-life times of air bubbles, of varying surface age, coalescing with an aged air/lysozyme solution interface, and that of fresh corn oil drops coalescing with an aging oil/aqueous lysozyme solution interface. We found that the half-life times of air bubbles and corn oil drops seem to correlate with the dilational elasticity of the interface. The techniques for measuring interfacial elasticity and stability of droplets at both air/water and oil/water interfaces are briefly reviewed.

Foams and emulsions are frequently encountered in a great variety of food systems (*1,2,3*); some examples include ice cream, milk, sauces, dressings, mayonnaise and flavor oils. Foams comprise a dispersion of gas bubbles in a continuous liquid phase separated by thin liquid films. Liquid emulsions consist of dispersions of one liquid in another in the form of droplets. In an oil-in-water emulsion, oil droplets are dispersed in the continuous water phase while the opposite arrangement is referred to as the water-in-oil emulsion. In flavor oil systems, oil form flavors are dispersed in an aqueous system as an oil-in-water emulsion. For example, beverage flavor emulsions is a dilute oil-in water emulsion consisting of flavor oil droplets dispersed in water.

Foams and emulsions are thermodynamically unstable and are stabilized by food surfactants and proteins in the gas/liquid (foams) and water/oil (emulsion) interfacial region between the dissimilar phases. Their stability is related to the rate of coalescence of the dispersed phases. When two gas bubbles or liquid droplets approach each other, the thin liquid film separating the two colliding

---

[1]Corresponding author

"particles" must drain. This thin film drainage phenomenon is affected by the thermodynamic and hydrodynamic interaction in the two approaching surfaces (*4,5,6*).

Previous works have suggested that the rate of drainage of a liquid thin film between two approaching fluid surfaces depends on, among other factors, the surface dilational elasticity of the surfaces (*7,8,9*). Earlier studies have focused on examining the effect of interfacial shear viscosity on emulsion stability; however, little work has been done to characterize the effect of dilational elasticity on bubble and liquid droplet coalescence rates. In the present work, we examine and measure the dynamic interfacial dilational viscoelasticities of protein adsorbed gas/liquid and oil/water interfaces, and correlate them with the rate of coalescence of gas bubbles and liquid droplets. The viscoelastic properties of gas/liquid and oil/water interfaces depend on the concentration, type, composition and interactions between surface active food surfactants and proteins at the fluid interface. In this study, we measured the dilational elastic modulus and dilational viscosity of protein adsorbed gas/water and corn oil/water interfaces as a function of bulk protein concentration and surface age. In addition, the characteristic life-times required for bubbles or droplets to coalesce at the air/water and oil/water interfaces, respectively, are measured through the method of Cockbain and McRoberts (*8*).   Correlation between the surface dilational elasticity and coalescence time was established.

This paper is organized as follows. We begin with a brief review of surface dilational viscoelasticity. Experimental techniques used to measure these surface rheological properties and gas bubble and liquid droplets coalescence times are described. Results obtained will be presented, followed by a discussion section.

Interfacial Dilational Elasticity and Viscosity

Fluid/fluid (air/water or oil/water) interfaces with adsorbed amphiphillic surfactants and proteins exhibit viscoelastic behavior. The dilational viscoelasticity ε of an interface is a characteristic measure of its resistance to surface deformation. The quantity ε is defined as the change of surface tension relative to a fractional change in surface area deformation,

$$\varepsilon = \frac{d\sigma}{d\ln A} = \varepsilon_d + i\omega\eta_d = |\varepsilon|e^{i\theta} \tag{1}$$

Here ε_d and η_d represent the dilational elasticity and viscosity, respectively; $|\varepsilon|$ is referred to as the elastic modulus; θ is the loss angle; σ is the interfacial tension; ω is the frequency of area deformation; and A denotes the area of the interface.

The dilational viscoelasticity ε is a complex quantity with real part ε_d and imaginary part $\omega\eta_d$. The complex behavior of the dilational elasticity is a consequence of the coupling between the interchange of matter between the bulk

phase and the interface. When an interface is subjected to expansion, the equilibrium between the interface and the bulk phases is disturbed; this results in a decrease in the surface concentration and the creation of a local surface tension gradient in the interface. Consequently, surfactants and/or proteins are transported onto the interface by diffusion (or, convection). If the characteristic diffusion time for the surfactant or protein is slower than the frequency of deformation, the surface tension response will lag behind the area change and leads to a viscous behavior characterized by the imaginary part of the dilational viscoelasticity ε in eq. (1). If the surface deformation frequency ω is much greater than the characteristic diffusion frequency ω_{diff}, there is negligible mass transfer between the bulk and the interface. In this case, the interface will behave as if it is insoluble, and the resulting elasticity will become independent of frequency ω.

Methods for measuring surface dilational elasticity at the air/liquid interface

Capillary Waves. In our laboratory, three techniques, namely, capillary waves, longitudinal waves and modified Langmuir trough, are used to measure surface viscoelasticities at an air/liquid interface covering a wide frequency range. At high surface deformation frequencies (100 Hz ~ 1000Hz), surface elasticities are measured through capillary waves. This apparatus has been described in detail earlier (*10*). Briefly, capillary waves are generated by applying a high AC voltage and DC offset voltage between a sharp blade and the solution under study, and detected by reflection of a focused laser beam to a position sensitive photodiode. The surface wave can be scanned over a distance of 8 cm by a computer-controlled linear translation motor, and the wave amplitude and phase angle are recorded as a function of distance from the wave generator through lock-in technique. Capillary wavelength λ_c and spatial damping constant β_c are therefore measured. By using the capillary wave dispersion equation, surface dilational viscoelasticity can be calculated with the measured λ_c and β_c. By using a sharp needle, instead of a long blade, we can generate a propagating cylindrical capillary wave. Our study has shown that even through plane and cylindrical transverse waves possess different geometry, both can be used to obtain surface dilational properties effectively (*11*).

Longitudinal Waves. At intermediate frequencies (1 Hz to 10 Hz), surface dilational properties are measured through longitudinal waves. In contrast to capillary waves, longitudinal waves can be generated by oscillating a barrier parallel to and in the plane of the interface. Two basic techniques have been employed to detect longitudinal waves: (i) a method that involve the use of a barrier touching the surface to measure the wave (*12*) and (ii) the use of a capillary wave (*13-16*). The capillary wave generation and detection are done without mechanically contacting the surface as described earlier. Therefore the second technique, first used by Lucassen and van Temple (*13*) and recently improved by

Miyano et al. (*14*), has a distinct advantage over the first technique in the sense that the detection avoids mechanical disturbance of the surface.

The apparatus we have set up earlier (*16*) is similar to that reported in reference (*14*). The major modification is that we use the "double loci-in" technique: both capillary and longitudinal waves are detected with two different lock-in amplifiers. The longitudinal wavelength and damping coefficient can be measured simultaneously by scanning the surface within a short period of time. Experimentally, our apparatus is more convenient than that of data fitting (*14,15*), and it is more suitable for the study of dynamic systems.

The propagation of longitudinal wave is accompanied by dilation and compression of the surface monolayer, which in turn produces a propagating oscillation in the surface tension $\Delta\sigma$. Detection of longitudinal waves is based on Kelvin's equation,

$$\omega_c^2 \lambda_c^3 = (2\pi)^3 \sigma / \rho \qquad (2)$$

which relates surface tension σ to wavelength λ_c and wave angular frequency ω_c, where ρ is the density of the liquid. A capillary wave superimposes upon the longitudinal wave but in the orthogonal direction. The phase angle ϕ_c of the capillary wave is monitored at a distance away l from the capillary wave generator. At this point, $\phi_c = 360l / \lambda_c$. Therefore, the change in capillary wave phase angle, $\Delta\phi_c$, due to surface tension change, $\Delta\sigma$, is

$$\Delta\phi_c = -120 \frac{l}{\lambda_c} \frac{\Delta\sigma}{\sigma} \qquad (3)$$

Hence, the oscillation of surface tension due to longitudinal waves is proportional to capillary wave phase angle change. The phase angle ϕ_c of the capillary wave at the detection line, which is parallel with the capillary wave generator, can be written as

$$\phi_c = \phi_{c0} + \Delta\phi_c \qquad (4)$$

where ϕ_{c0} is the capillary wave phase angle in the absence of longitudinal waves, and $\Delta\phi_c$ is the change in the phase angle caused by the propagation of longitudinal waves and can be written as

$$\Delta\phi_c(x,t) = \Delta\phi_{c0} e^{-\beta_l x + i\omega_l t - ik_l x} \qquad (5)$$

where $\Delta\phi_{c0}$ is the wave amplitude at $x = 0$, β_l is the damping coefficient, and ω_l and k_l are the wave angular frequency and wave number, respectively. The

damping coefficient β_l and wave number k_l are measured through the lock-in technique. With the longitudinal waves dispersion equation, surface viscoelasticity is therefore obtained (*16*).

Modified Langmuir Trough. At low frequencies (0.001 Hz - 0.1 Hz) surface viscoelasticity is measured using the modified Langmuir trough technique. The measurement of surface viscoelasticity is especially important in the study of the relaxation of polymeric surfactants or proteins at an air/water interface, where the relaxation process of the polymers and proteins is expected to be slow. The apparatus we used in our laboratory is, in principle, similar to the instrument built by Giles and Lucassen (*17*). It consists of a precision machined Teflon trough mounted on an aluminum plate, two identical Teflon barrier and an electrical-balance for measurement of surface tension. These two symmetrical barriers are attached to two rail tables which are driven by two step DC motors. A computer is used to control the motions of these motors through a RS232 interface; this enables the barriers to compress or dilate the surface sinusoidally with a small amplitude $\Delta A / A$. The resulting surface tension change is simultaneously recorded while the surface area is subjected to small amplitude sinusoidal area variations. As stated in eq. (1), the surface dilational modulus ε at a particular frequency is characterized by its absolute value $|\varepsilon|$ and by a loss angle θ, which describes the phase difference between the surface tension variation and area variation. The elastic modulus $|\varepsilon|$ is simply obtained by the ratio of the amplitude of surface tension variation $|\Delta\sigma|$, as measured, and the amplitude of relative surface area variation as applied:

$$|\varepsilon| = \frac{|\Delta\sigma|}{|\Delta A| / A} \tag{6}$$

The value of the phase angle θ was calculated from the time lag between the occurrence of the maximum or minimum in the surface tension and of that in area. It also can be obtained by fitting the surface tension variation data to a sinusoidal expression and then comparing with the area variation data.

Recently another method involving the use of Fourier transformation has been developed (*18,19*). In this technique, surface viscoelasticity is obtained through the following Fourier transformation

$$\varepsilon(\omega) = F\{\Delta\sigma(t)\} / F\{\Delta \ln A(t)\} \tag{7}$$

Here, $\Delta\sigma(t)$ represents the resulting variation in interfacial tension due to a change in surface area $\Delta \ln A(t)$ and F is the Fourier transformation operator. It seems that this method is more experimentally convenient. In both aforementioned methods, a capillary wave, instead of a Wilhelmy plate, can be employed to
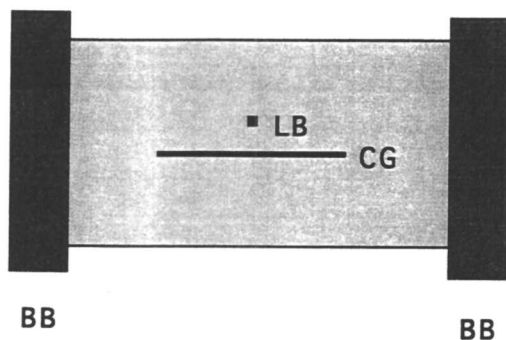
Figure 1a.   Experimental arrangement for the measurement of dilational elasticity at liquid/liquid interfaces. CG: Capillary wave generator; LB: Laser beam; BB: Thin stainless steel barrier.
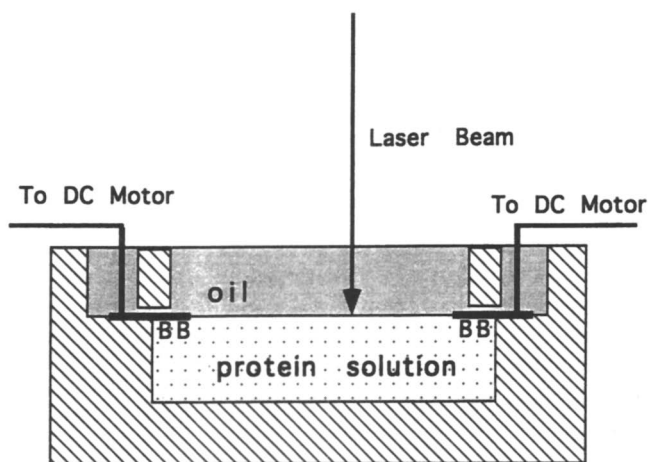
Figure 1b.   Side view of the Langmuir trough.

measure the surface tension response to a small surface area variation (*20*). The detection principle is the same as in the study of a longitudinal surface wave. The advantage of using capillary wave is that the detection is done without mechanically touching the surface.

Methods for measuring surface dilational elasticity at liquid/liquid interfaces

Longitudinal Waves. Because the two liquids above and below the liquid/liquid interface have a similar mass densities and viscosities, the capillary and longitudinal waves are almost completely de-coupled (*15,21*). Therefore, capillary waves can no longer be applied to study the dilational viscoelasticity at a liquid/liquid interface. However, capillary waves at liquid/liquid interfaces can be used to detect a propagating longitudinal wave in the same way as at an air/water interface (*15,22*). The detection principle is also based on the Kelvin equation for liquid/liquid interface

$$\sigma = (\rho + \rho') \frac{\omega_c^2}{k_c^3} \tag{8}$$

which relates the interfacial tension σ to liquid densities ρ and ρ', and the capillary wave number k_c at a given capillary wave frequency ω_c. The capillary wave is generated at the oil/aqueous solution interface by applying a high AC voltage to a metal blade which is located in the oil phase (note that the oil is non-conductive) and just above the oil/water interface. For an oil/water system, there are two phase interfaces: the air/oil interface and the oil/water interface. Both interfaces reflect the incident laser beam. The beam reflected from the air/oil interface is very close to that reflected from the oil/water interface. Thus, a small glass plate tilted at a small angle is placed at the air/oil interface to separate these two reflected beams. Only the laser beam reflected from the oil/water interface is directed to a position photodiode and subsequently measured through lock-in amplifier. The longitudinal waves are generated by oscillating a Pt wire at the oil/solution interface.

Modified Langmuir trough. A Langmuir trough allowing the measurement of interfacial viscoelasticity at low frequencies (less than 0.1 Hz) at a liquid/liquid interface has been constructed in our laboratory. Its principle is similar to the instrument that we built for the study of dilational properties at an air/water interface. In this instrument, two thin stainless steel sheets sitting at the oil/aqueous solution interface were used as two movable barriers for compressing or expanding the interface. The resulting interfacial change is measured through a propagating capillary wave. The overall arrangement of this set up is shown in Fig. 1. Figures 1a and 1b schematically show the top view and the side view of the trough, respectively. A thin blade about 8 cm long is placed about 2 mm above the
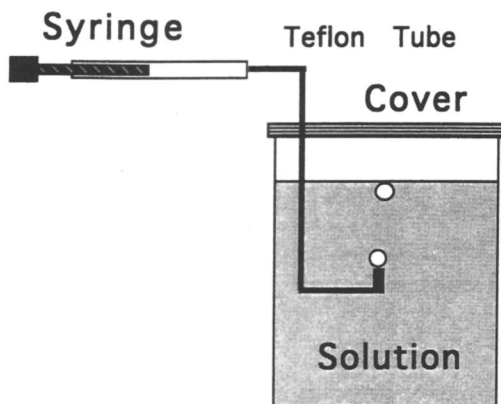
Figure 2.   Experimental setup for the measurement of life times of air bubbles.
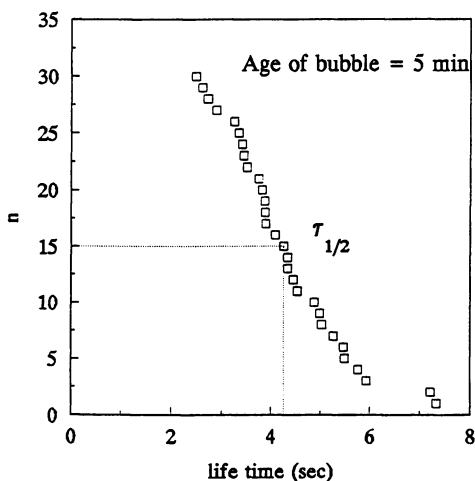
Figure 3.   Life time distribution curve of air bubbles at air/protein solution interface. The quantity n represents the number of bubbles that did not coalesce within time t. The air/solution interface is in equilibrium with the protein solution. The age of the bubbles is 5 minutes and the solution contains 1×10^{-2} wt% lysozyme and 0.1 M NaCl. The volume of bubbles is $2\mu l$. The pH of the solution is 6.8.

interface. A high AC voltage is than applied between the blade and the solution to generated a capillary wave propagating in the widthwise direction. A laser beam focused on the oil/aqueous solution interface can be moved in the widthwise direction by a linear translation stage in order to measure the capillary wave number k_c, and hence the interfacial tension by using the Kelvin equation, eq. (8). It should be noted that the laser beam is almost normal to both the air/oil and oil/aqueous solution interfaces. To deflect the unwanted reflected beam from he air/oil interface, a small glass plate, tilted at a small angle from the interface, is placed just above the air/oil interface, as Ting et al. (*22*) did in the study of longitudinal waves at oil/aqueous solution interface. The experiment begins by first placing the two barriers which are made of thin stainless steel sheet about 0.5 mm thick on the step of a Teflon trough as shown in Fig. 1b. Aqueous solution (which is the bottom liquid phase) is slowly poured into the trough until the solution just touches the barriers. Oil is then carefully introduced into the trough from the side to form an oil/aqueous interface with the barriers sitting right on the interface. Two thin stainless steel rods with diameter 2.5 mm were soldered with silver on the barriers. These two thin rods are mechanically attached to two step DC motors that controlled by a computer. As the rods move, they introduce some undesired disturbances. To circumvent this problem two Teflon bars are placed just above the barriers as shown in Fig. 1b. The two bars thus block the disturbances induced by the motion of the rods from the rest of the system. By manipulating the DC motors, the interfacial area of oil/aqueous solution interface is thus changed by a small fraction. The resulting interfacial tension change is measured by monitoring the capillary wave phase angle ϕ_c at a distance l away from the generator (see Fig. 1a). Through equation 3, the interfacial tension change $\Delta\sigma$ is therefore obtained.

Measurements of life-times of air bubbles at air/aqueous solution interface and oil droplets at the oil/aqueous solution interface

The apparatus shown in Fig. 2 was used to measure the life times of air bubbles at an air/aqueous solution interface and of oil droplets at a corn oil/aqueous solution interface . To determine the life time or coalescence times of air bubbles, air bubbles were generated at the tip of a Teflon tubing by injecting air through a Hamilton micrometer syringe. These bubbles are sufficiently small to detach from the tip of the tubing. They were allowed to "age" for a specified time duration, and were subsequently released by slightly tapping the tubing. The life-time of the bubble is taken to be the interval between its arrival and its eventual coalescence with the planar air/aqueous solution interface . For a given system (with different surface age and protein concentration), the life-times of air bubbles are not constant, but can be conveniently described represented by a distribution curve. Fig. 3 shows the distribution curve for the life-time of air bubbles coalescing with an air/ aqueous solution interface , where N represents the number of air bubbles having coalescence time longer than t. This curve is obtained for 5 minute aged
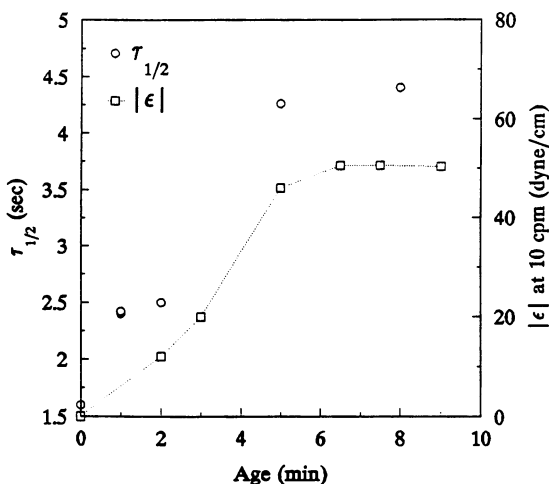
Figure 4.   Half-life time $\tau_{1/2}$ of air bubbles coalescing with an equilibrium air/solution interface is plotted against the age of the bubble. Also, surface elastic modulus $|\epsilon|$ measured at 10 cycles per minute is plotted as a function of interface age. The solution contains 1×10^{-2} wt% lysozyme and 0.1M NaCl. The pH of the solution is 6.8.
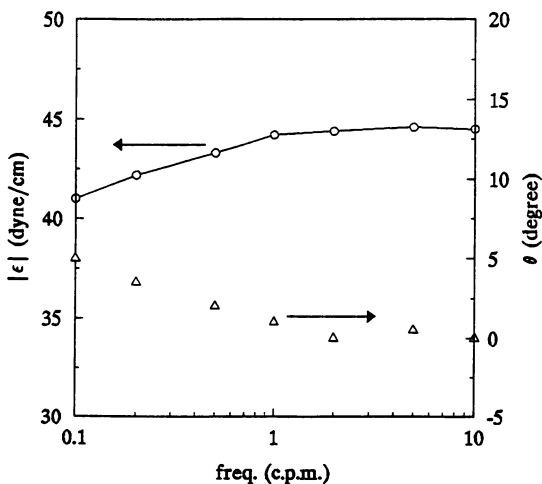
Figure 5.   Surface elastic modulus $|\epsilon|$ and loss angle θ are plotted as a function of surface deformation frequency. The air/aqueous solution interface is in equilibrium with the protein solution which contains 1×10^{-2} wt% lysozyme and 0.1M NaCl. The pH of the solution is 6.8.

bubbles with a volume of 2 μl coalescing with an equilibrated air/aqueous solution interface in a 1x10^{-2} wt% lysozyme solution. The overall life-times of bubbles is characterized by its half-life time $\tau_{1/2}$. In the study of the life-times of oil droplets at an corn oil/aqueous solution interface, oil was injected through a stainless steel tubing using a Hamilton micrometer syringe. Again an oil droplet with a specified volume was released by slightly tapping the tubing, and its life time at the planar oil/aqueous solution interface was measured. A similar distribution curve and its half-life time were then obtained.

Materials and Methods

Crystallized and lyophilized chicken-egg-white lysozyme and corn oil were purchased from Sigma Chemical Co. (St. Louis, MO) and they were used without further purification. Purified water from a Milli-Q ultrapure water system with a resistivity of 18.2 mΩ.cm was used in preparing the protein solutions. All measurements were performed at room temperatures (24±1°C). Dilational viscoelasticity of air/aqueous solution and corn oil/aqueous solution interfaces on which protein lysozyme adsorbed are measured using the modified Langmuir trough as described in the previous sections. Here, we primarily focused our attention on the effect of the age of the interface on the interfacial elasticity and stability of droplets. In the study of air/aqueous solution interface, we measured the surface elasticity of lysozyme solution as a function of the age of the interface, and the life-time of air bubbles with varying surface age. In the case of corn oil/aqueous solution interface, we examined the relationship between the interfacial elasticity and the life-time of fresh corn oil droplets coalescing with a planar corn oil/aqueous solution interface as a function of the age of the planar interface. The pH of the lysozyme solution is 6.8.

Results and discussion

Air/Aqueous Lysozyme Solution Interface. The time required for lysozyme solution to attain its equilibrium at the air/aqueous solution interface depends strongly on the protein bulk concentration. Fig. 4 shows the surface elasticity, measured at 10 cycles per minute (cpm), plotted as a function of time after a fresh interface is created by sweeping a Teflon barrier over the air/aqueous solution interface. It is seen that after about 6 minutes the surface elasticity becomes constant indicating that the surface is in equilibrium with the bulk. The measurement of dynamic surface tension shows a similar time dependence. After the surface has attained equilibrium, we also measured the surface viscoelasticity as a function of surface deformation frequency ω. The surface elastic modulus $|\varepsilon|$ and loss angle θ are plotted against frequency as shown in Fig. 5. It demonstrates that surface elastic modulus $|\varepsilon|$ increases, while the loss angle θ decreases, with increasing surface deformation frequency. When the frequency is greater than 1

cpm, the surface elastic modulus becomes constant and the loss angle is close to zero, implying that the surface behaves like an insoluble and purely elastic interface. The surface elasticity would remain constant even at higher frequencies as expected from the diffusion theory. This is also the reason that we only used the modified Langmuir trough to measure the surface elasticity of lysozyme solutions. To establish a correlation between the stability of foams with surface elasticity, we also investigated the life time of air bubbles coalescing with a lysozyme adsorbed air/aqueous solution interface. The experiments begin after the air/aqueous solution interface has attained its equilibrium. An air bubble is generated inside the solution and held for a specified time before releasing and allowing it to coalesce with the aged interface. An aged air/aqueous solution of 1×10^{-2} wt% lysozyme solution has an elasticity of 50 dyne/cm, while the elastic modulus of the interface of an air bubble in the solution depends on the age of the bubble. Fig. 3 shows the life-time distribution curve for 5-minute old air bubbles. The half-life time $\tau_{1/2}$ is then obtained form the distribution curve. Fig. 4 shows the half-life time $\tau_{1/2}$ of air bubbles coalescing with an aged air/aqueous solution interface as a function of the age of the air bubbles. Comparisons of surface elastic modulus $|\varepsilon|$ and half-life times $\tau_{1/2}$ with age of bubbles seem to suggest that there is a correlation between surface elasticity and bubble stability. Studies at other lysozyme concentrations also show similar observations.

Corn Oil/Aqueous Lysozyme Solution Interface. To study the interfacial elasticity of corn oil/aqueous solution interface, we employed our newly constructed Langmuir trough which was described in previous sections. In order to measure the interfacial tension, we scan the interface with the laser beam in the widthwise direction of the trough (see Fig. 1a) to measure the capillary wave number, and then calculate the interfacial tension through Kelvin's equation, eq. (8). The measured interfacial tension of corn oil/pure water interface is about 18 dyne/cm. The dilational interfacial elastic modulus is obtained by step compressing or dilating the interface and at the same time measuring the capillary wave phase angle change $\Delta\phi$ at a fixed distance l away from the wave generator. An example of such a measurement is shown in fig. 6 which plots the capillary wave phase angle as a function of time. At about $t = 0.5$ minutes, the interfacial area was dilated by 5.5% and then held constant. The capillary wave phase immediately increases following the dilation and then remains relatively constant for about 2 minutes before relaxing due to the adsorption of lysozyme. This kind of "induction" period has been observed in the adsorption of lysozyme at an air/water interface through surface radioactivity measurements (23). The phenomenological explanation for this adsorption behavior has been discussed in the literature (24). Nevertheless, the interfacial elasticity ε can be obtained by sing eq. (3) to calculate the interfacial tension change $\Delta\sigma$ and hence the elasticity. It should be noted that the elasticity obtained by this technique is the high frequency limit elasticity. The variation of elasticity with age of the interface is obtained by imposing a series of

square-pulse area disturbances and simultaneously measuring the capillary wave phase response.   A typical adsorption measurement for a corn oil/aqueous lysozyme solution (1×10^{-3} wt%) interface is displayed in Fig. 7.   The overall capillary wave phase ϕ decreases with time after the formation of the interface is due to the adsorption of lysozyme onto the interface.   The square-like changes in the phase angle are caused by the imposed square-pulses of area variation.   In our experiments the amplitude and duration of the pulses are small ($\Delta A/A$=0.055 and t_{pulse}=30 seconds) in order to minimize disturbances to the overall adsorption process.   From the overall time-dependent capillary wave phase, we are able to obtain the dynamic interfacial tension.   From the height of the phase angle response, we obtained the elastic modulus $|\varepsilon|$ as a function of time (i.e., the age of the interface).   The variation of the elastic modulus $|\varepsilon|$ with time (up to approximately 60 minutes) is shown in Fig. 8.   It initially increases with time (i.e., age of the oil/aqueous solution interface) very rapidly and then gradually slows down.   It should be mentioned that for $t \gg 60$ minutes, the surface becomes rigid and erratic capillary wave phase angles were obtained.   This seems to suggest that a chemical reaction involving protein may have occurred which renders the corn oil/aqueous solution interface rigid.

Because of the formation of this "rigid" interface, there is no clear indication as to when the interface reaches equilibrium.   Hence, we were not able to determine the equilibrium value for $|\varepsilon|$ for the lysozyme adsorbed interface. Therefore, we decided to study the coalescence of fresh corn oil droplets with an aged corn oil/lysozyme solution interface.   After the planar interface has attained a given age, typically fifteen corn oil droplets, each with a volume of 1 μl, were generated in the protein solution; these droplets were immediately released and allowed to coalesce with the planar interface.   The half-life time $\tau_{1/2}$ was then obtained as a function of the age of the planar interface.   These are displayed in Fig. 8.   Close examination of Fig. 8 indicates that there exists a correlation between the life-times of corn oil droplets and the age of the corn oil/aqueous lysozyme solution interface.

It is noticed that the values of the interfacial elastic modulus $|\varepsilon|$ at oil/aqueous solution interfaces are much less than those at air/aqueous solution interfaces, while the half-life times at oil/water interfaces are about an order of magnitude greater than those at air/water interfaces.   This comparison suggests that interfacial elastic modulus $|\varepsilon|$ is not the only controlling factor in determining the coalescence time of air bubbles and oil droplets, or stability of foams and emulsions; other physical properties such as interfacial shear rheological properties and bulk viscosity do contribute to their stability.

The techniques and approaches employed in this study and described in this chapter can be easily applied to the study of the interfacial rheological properties of oil/water systems involving flavor oils.   Such a study will provide information and insights to the stability of flavor oil emulsions.
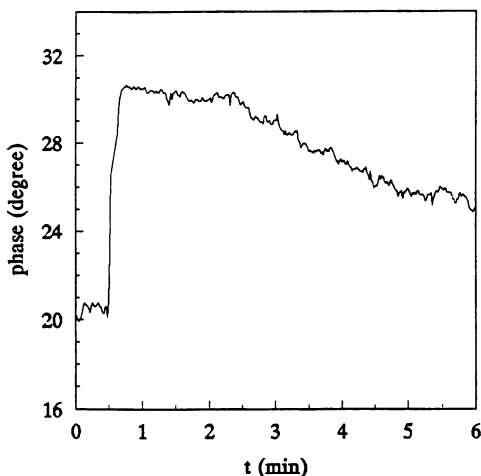
Figure 6.   Capillary wave phase response of a corn oil/lysozyme solution interface (surface age is three hours) when it is subjected to a step interfacial area dilation. The phase angle was measured at 1.6 cm away from the wave generator. Capillary wave frequency was 7 Hz. The upper liquid phase is corn oil while the lower liquid phase is 1×10^{-3} wt% lysozyme solution.
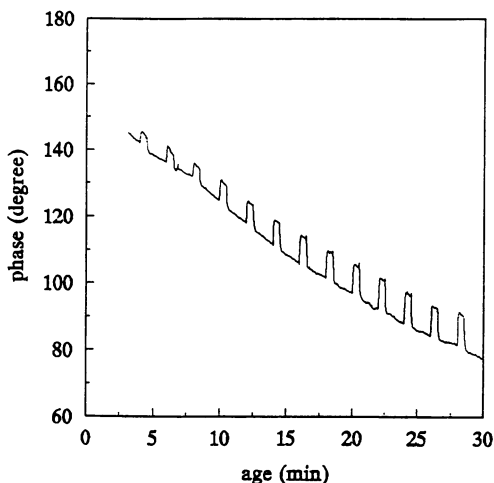
Figure 7.   Capillary wave phase, measured at a distance l=1.6 cm away from its generator, is plotted as a function of time after the formation of a fresh corn oil/lysozyme solution interface (2×10^{-2} wt%). Capillary wave frequency was 7 Hz. The measured square-like phase angle responses were caused by a series of imposed square-pulses of interfacial area variation.
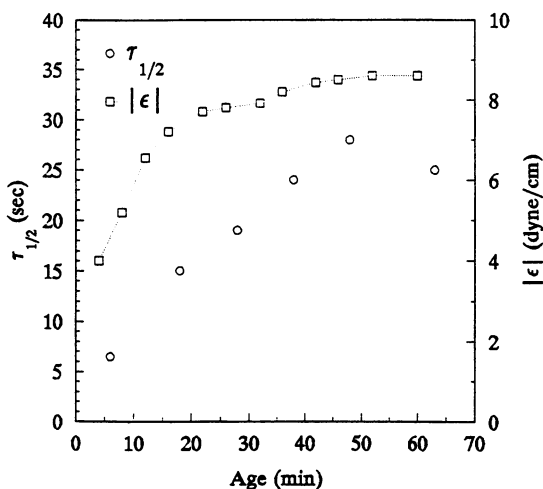
Figure 8.   The interfacial elastic modulus $|\varepsilon|$ and half-life time $\tau_{1/2}$ of corn oil droplets coalescing with a planar corn oil/lysozyme solution interface are plotted as a function of the age of the planar interface. The size of oil droplets was $1\,\mu l$, and the lysozyme concentration was 2×10^{-3} wt%.

Acknowledgment

Literature Cited:

(*1*)   Bee, R. D.; Richmond, P.; Mingins, J., *Food Colloids*, The Royal Society of Chemistry, London, 1989.
(*2*)   Larsson, K.; Friberg, S. E., *Food Emulsions*, 2nd ed., Marcel Dekker, NY, 1990.
(*3*)   El-Nokaly, M.; Cornell, D., *Microemulsions and Emulsions in Foods*, ACS Symp. Ser. 448, American Chemical Society, Washington DC ,1991.
(*4*)   Langevin, D.; Sonin, A. A., *Adv. Colloid Interface Sci.* **1994**, *51*, 1.
(*5*)   Velev, O. D.; Nikolov, A. D.; Denkov, N. D.; Doxastakis, G.; Kiosseoglu, V.; Stalidis, G., *Food Hydrocolloids* **1993**, *7*, 55.
(*6*)   Lucassen-Reynders, E. H., *Food Structure* **1993**, *12*, 1.
(*7*)   Dickinson, E.; Murray, B. S.; Stainsby, G., *J. Chem. Soc. Faraday Trans. I* **1988**, *84*, 871.

(8)   Cockbain, E. G.; McRoberts, T. S., *J. Colloid Sci.* **1953**, *8*, 440.

(9)   Lee, G. W. J.; Tadros, Th. F., *Colloids Surfaces* **1982**, *5*, 129.

(10) Jiang, Q.; Chiew, Y. C.; Valentini, J. E., *J. Colloid Inter. Sci.* **1993**, *155*, 8.

(11) Jiang, Q.; Chiew, Y. C.; Valentini, J. E., *Langmuir* **1992**, *8*, 2747.

(12) Lucassen, J., *Trans. Faraday Soc.* **1968**, *64*, 2230.

(13) Lucassen, J.; van den Temple, M., *J. Colloid Inter. Sci.* **1972**, *41*, 491.

(14) Miyano, K.; Abraham, B.; Ting, L.; Wasan, D., *J. Colloid Inter. Sci.* **1983**, *92*, 297.

(15) Lemaire, C.; Langevin, D., *Colloids Surfaces* **1992**, *65*, 101.

(16) Jiang, Q.; Chiew, Y. C.; Valentini, J. E., *J. Colloid Inter. Sci.* **1993**, *159*, 147.

(17) Lucassen, J.; Giles, D., *J. Chem. Soc. Faraday Trans. I* **1972**, *68*, 2129.

(18) Loglio, G.; Tesei, U.; Cini, R., *Colloids and Polymer Sci.* **1977**, *264*, 712.

(19) Loglio, G.; Tesei, U.; Cini, R., *J. Colloid Inter. Sci.* **1979**, *71*, 316.

(20) Jiang, Q.; Chiew, Y. C., *Colloids Surfaces*, in preparation.

(21) Lucassen-Reynders, E. H.; Lucassen, J., *Adv. Colloid Interface Sci.* **1969**, *2*, 347.

(22) Ting, L.; Wasan, D.; Miyano, K., *J. Colloid Inter. Sci.* **1985**, *107*, 345.

(23) Xu, S.; Damodaran, S., *Langmuir* **1994**, *10*, 472.

(24) Xu, S.; Damodaran, S., *Langmuir* **1992**, *8*, 2021.

Chapter 15

The Role of Specialty Food Starches in Flavor Emulsions

Paolo C. Trubiano

Food Products Division, National Starch and Chemical Company,
Finderne Avenue, Bridgewater, NJ 08807

Sodium starch octenyl succinates are unique specialty food starches
characterized by excellent emulsion stabilizing properties. The article
discusses the functionality and typical uses of these products in
concentrated flavor emulsions, clouds and the resulting soft drink
beverages. The principles of flavor emulsion stabilization and
functionality of the stabilizers are reviewed in systems containing
orange flavor, vegetable oil and blends with typical weighting agents.
The results show the unique advantages of the specialty starch
products over spray-dried gum arabic in terms of lower use level,
facilitated processing and improved emulsion properties.

Starch is an excellent raw material for the preparation of ingredients that are
formulated in many food products because it is plentiful, renewable and relatively low
in cost. A unique application of specialty food starches is in the preparation of oil-in-
water emulsions which are formulated into a variety of soft drink beverages. This
article reviews the properties of these starches and illustrates their uses and
advantages in typical flavor and cloud emulsions.

Properties and Uses of Food Starches

Some of the features of food starches are ability to provide a broad viscosity range,
resistance to high shear and high temperature, resistance to acid hydrolysis, enhanced
filming properties, appealing and palatable texture, excellent gelling properties, low
temperature stability and the ability to form stable oil-in-water emulsions and to
encapsulate (1). The wide range of functionality of starches (Table I) is at the base of
their use in a variety of foods products such as soups, sauces, breaded products,
fillings, confections, flavors and beverages, desserts, bakery items, frozen foods,
snacks and dressings (2). Most food starches do not have the ability to form stable oil-
in-water emulsions because the starch molecule has no lipophilic groups which favor

compatibility with water insoluble substances. As described in U. S. Patent issued to Caldwell and Wurzburg (3), emulsion properties can be introduced into the starch molecule by treating the starch with small amounts of cyclic dicarboxilic acid anhydrides, such as octenyl succinic anhydride. Sodium starch octenyl succinates are specialty starches that are characterized by excellent emulsion properties and are approved by the Food and Drug Administration for use in foods (4). In the specific area of food emulsions, such as beverage emulsions, dressings and non dairy creamers, these specialty starches have also replaced scarce and/or expensive products, such as spray-dried gum arabic, casein and gelatin.

Table I. Functions of Specialty Starches in Foods

Function	Food
Thickening	Gravies, soups, pie fillings
Adhesion	Breaded products, snacks
Binding	Formed meats, extruded foods
Clouding	Cream fillings, drinks
Dusting	Bread, gums
Flowing aid	Sugar, baking powder
Expansion	Extruded snacks and cereals
Texturizing	Smooth products, pulpy products
Emulsions	Beverages, vitamins, creamers
Encapsulation	Flavors, vitamins, fats
Fat enhancement	Beverages, dressings, bakery products
Form strengthening	Marshmallows, drinks
Anti-staling	Bakery products
Gelling	Gum drops, puddings
Glazing	Nuts, bakery products
Moisture retention	Breading, cakes
Moulding	Gum drops
Shaping	Meat products, pet foods
Stabilizing	Beverages, salad dressings

Uses of Specialty Food Starches in Beverage Emulsions

Beverage emulsions, which include flavor concentrates and clouds, are added in small quantities to water containing a sweetener to prepare a variety of soft drinks, many of which are carbonated. Typical beverages include orange, lemon, pineapple, colas and chilled juice drinks. The concentrated flavor emulsions impart flavor as well as some opacity or cloudiness to the finished drink. On the other hand, the concentrated cloud

emulsions are primarily used to give opacity to clear beverages or to enhance their juice-like appearance. In the first case the oil phase is the flavor (such as orange oil), in the second it is a flavorless ingredient, such as orange terpenes or a vegetable oil. Sometimes the flavor oil and the vegetable oil or terpenes are emulsified together. The aqueous phase of these emulsions is a solution of highly functional hydrocolloids, such as specialty food starch or gum arabic. The oil is dispersed into the water phase by processing the mixture at high shear or pressure. These hydrocolloid emulsion stabilizers differ radically from typical surfactants or emulsifiers which can give fairly good oil-in-water emulsions without much agitation, but these emulsions do not have the stability that is required in the beverage applications.

Table II illustrates the use of food starch in a typical orange oil emulsion concentrate. The main components in the formula are water, flavor and stabilizer. Typically, a level of equal parts of the oil blend and the starch-based emulsion stabilizer represents a good starting point in development work. If the emulsion is not used immediately some sodium benzoate, or other food grade preservative, is normally added to improve the storage stability. The pH is usually below 4 and is obtained through the addition of an acidulant, such as citric or phosphoric acid.

A typical procedure for the preparation of beverage emulsions consists in first dissolving the sodium benzoate in the water and then adding the citric acid and, if desired, the coloring substance. The food starch is added under moderate agitation and mixing is continued until the solution is free of lumps. Warm water or moderate heating of the mixture can be used to expedite the starch solubilization process. The flavor oil is added under good agitation to obtain a coarse emulsion. The mixture is then reduced to a fine oil-in-water emulsion by subjecting it to very high agitation, shear or pressure. A typical method used to prepare fine beverage emulsions is to pass the mixture twice through a 2-stage pressure homogenizer at 3000 pounds per square inch in the first stage and 500 pounds per square inch in the second stage. Concentrated flavor or cloud emulsions that are used in beverages meet very stringent requirements for extended shelf stability. These include a fine particle size, no tendency of the flavor oil to separate, cream or form a sediment on storage and long term stability of the cloud and of the flavor profile.

The final beverage is prepared by adding a small amount of the concentrated emulsion to a sugar solution normally containing more sodium benzoate for preservation and citric acid. Many beverages are carbonated, some are pasteurized. The flavor oil or cloud base typically makes up from 0.005% to over 0.3% of the final beverage. For a cola beverage a level of 0.005% or 50 PPM of the flavor is typical. On the other hand, the flavor oil level for a citrus beverage can vary from 0.01 to 0.02% (100 - 200 PPM). Finally, the vegetable oil level in a chilled juice drink can be as high as 0.3% because in such beverages the intense cloud is very desirable. A typical level of flavor oil blend in the orange drink prepared with the emulsion of Table II is about 180 ppm. A stable beverage is characterized by long term emulsion stability or absence of "ringing" which is the formation of an undesirable white ring around the neck of the bottle and is made up of coalesced emulsion particles that have risen to the top. Other requirements of the final beverage include a stable cloud and flavor profile and absence of sediment formation over a period of at least 6 months.

Even if dispersed as a very fine emulsion flavor oils, vegetable oils and terpenes will eventually separate or cream in the concentrated form or ring in the final beverage primarily because of the difference in the specific gravity of the oil phase and that of the water phase. Typical flavor oils have a specific gravity below 0.9 while that of water in the final drink can be 1.04 or higher, depending on the amount of sweetener present.

Table II. Use of Food Starch in an Orange Oil Emulsion Concentrate

Ingredients	%
Water	73.6
Flavor oil blend	12.0
Starch stabilizer	12.0
Citric acid	0.3
Sodium benzoate	0.1
Yellow #6	2.0

Procedure:
1. Dissolve the sodium benzoate in the water
2. Slowly add the citric acid
3. Add the coloring agent
4. Slowly add the food starch stabilizer under moderate agitation. Continue mixing until the starch is fully dissolved
5. Adjust the pH, if necessary.
6. Add the flavor oil while mixing under vigorous agitation.
7. Homogenize in a pressure homogenizer (or equivalent equipment) by passing the emulsion twice at 3500 psi.

Uses of Specialty Starches With Weighting Agents

The tendency of the oil phase to separate can be eliminated or, at least, substantially reduced, by increasing the specific gravity of the oils (5). This is achieved by blending the flavor with certain oil soluble substances which have a specific gravity higher than one. Two of these products are glycerol ester of abietic acid, a crystalline material with a specific gravity of 1.08 (6), and sucrose acetate isobutyrate (SAIB), a thick liquid with a specific gravity of 1.146 (7). These substances are often called weighting agents because they actually make the flavor oils or vegetable oils heavier by increasing their specific gravity. Since they also affect the optical properties of the oil phase and make the beverage cloudier, they are often referred to as clouding agents. Sometimes they are called stabilizers because they have a positive effect on the stability of the

flavor emulsions. However, simply increasing the specific gravity of the oil by means of the weighting agents does not fully prevent the dispersed oils from coalescing and separating in time. Futhermore, government regulations limit the use of weighting agents in the final beverage to a maximum level which does not always assure optimum stability. Also, when used at high levels, weighting agents can affect negatively the flavor of the final beverage and can also cause the formation of a sediment.

Functions of the Emulsion Stabilizer

Excellent stability of the beverage emulsion concentrates and the resulting beverages can be obtained by means of an effective emulsion stabilizers, such as specialty food starch or gum arabic. The function of the hydrocolloid in flavor or cloud emulsions is four fold (*8*). One is to decrease the surface tension of the water so that under high agitation or pressure the oil is more readily dispersed in the water phase in the form of very fine droplets. The second is to link the oil droplet to the water phase by means of the hydrophobic sites in the hydrocolloid molecule. The third is to provide a network of starch molecules in the water phase which physically slows down the coalescing and separation process by reducing the number of collisions among the oil droplets. And, since the specific gravity of the starch is 1.5, it is believed that the fourth function of the stabilizer is to increase the specific gravity of the oil phase by forming a film around the oil droplets thus bringing it closer to that of the continuous phase. Starch-based emulsion stabilizers are characterized by cold water solubility, excellent emulsion properties, good solution stability and excellent microbiological quality.

Figure 1 is a typical particle size profile of an orange flavor emulsion stabilized with specialty food starch and obtained with a laser beam particle size analyzer. The emulsion particles range in size from 0.1 to 1.0 micron with a mean of 0.351 and a median of 0.335 micron. 50% of the particles is below 0.335 micron and 100% is below one micron. Over a period of 2 years beverage emulsions stabilized with food starch will not separate or show a significant change in particle size. The excellent stability of the emulsion is also confirmed by the fact that the beverages made with the fresh and aged emulsions do not ring or show changes in opacity or cloudiness for a period of at least 6 months.

Sucrose Acetate Isobutyrate

Table III illustrates the functionality of specialty food starch and gum arabic in the preparation of orange flavor emulsions containing from 0 to 66% of sucrose acetate isobutyrate (SAIB) as the weighting agent. In all cases the level of the oil phase in the emulsion was maintained at 12% while the level of stabilizer was 15% for gum arabic and 12% for food starch. The emulsions were inspected for creaming and separation over a period of six months. The beverages made with the fresh emulsions were evaluated for opacity and ringing after two weeks. As the level of SAIB increased, the specific gravity of the oil blend increased from 0.840 for the straight orange oil to 1.042 for the mixture containing 66% of the weighting agent. It is obvious that the

Table III. Stabilization of Orange Oil Emulsions Containing Sucrose Acetate Isobutyrate (SAIB)

Stabilizer (level)	Oil blend		Concentrate		Beverage	
	% SAIB	Specific gravity	Particle size (Micron)	Creaming (6 months)	Opacity (% T)	Ringing
Food Starch (12%)	0	0.840	1.231	severe	45	excessive
	20	0.901	0.427	slight	26	moderate
	40	0.962	0.319	slight	37	slight
	50	0.993	0.347	very slight	38	very slight
	60	1.024	0.325	none	31	none
	66	1.042	0.359	none	31	none
Gum Arabic (15%)	0	0.840	1.284	severe	42	excessive
	20	0.901	0.785	slight	22	moderate
	40	0.962	0.462	slight	30	slight
	50	0.993	0.354	very slight	32	very slight
	60	1.024	0.446	none	34	none
	66	1.042	0.409	none	33	none

weighting agent does play an important role in the formation of a fine emulsion. This is particularly evident at the lower levels of SAIB in the blends where there is a fairly direct relationship between the amount of weighting agent and the particle size of the emulsion. The higher the level of SAIB, the finer and more stable the emulsion. After 6 months there was no creaming in the emulsions containing at leat 60% SAIB and only very slight creaming in those containing 50% weighting agent. The opacity of the final drink increases with increasing levels of weighting agent as shown by the drop in percent light transmission from 45% to 22%. The higher opacity of the beverages containing only 20% SAIB is due to the larger particle size of the corresponding emulsions when compared to those containing higher levels of the weighting agent. There is no ringing in the beverages containing at least 60% of SAIB in the oil phase and only very slight ringing in those beverages containing 50% weighting agent. These results suggest that it is not really necessary to increase the specific gravity of the oil blend to match exactly that of the aqueous phase in the finished beverage in order to obtain a stable beverage. 60% SAIB in the oil blend seems adequate even though the specific gravity of the oil blend is only 1.024. At this level of SAIB in the oil blend one would expect serious separation in the final beverage because of the still significant difference between the specific gravity of the oil phase and that of the water phase which is about 1.04. The improved stability is due to the functionality of the starch-based emulsion stabilizers. The same trend was observed with gum arabic with which stable beverages were also obtained at the same level of SAIB in the flavor blend. However, even though used at a higher level than the food starch, gum arabic gave slightly larger emulsion particles throughout the whole range of the weighting agent. SAIB is not yet approved in the United States but is used already in a number of countries, including Canada and Japan. In general, the same results were obtained when the food starch stabilizer was tested with oil blends containing various levels of glyceryl abietate, a weighting agent approved in the United States, at a level of 100 PPM in the beverage. Here, too, the specific gravity of the oil phase does not have to match exactly that of the aqueous phase. Our results indicate that, under normal storage conditions, 45% of glyceryl abietate in the orange oil blend having a specific gravity of 0.946 seems to be sufficient to obtain a stable beverage. Just as we have seen in the case of SAIB blends, glyceryl abietate, too, contributes substantially to the reduction of the particle size of the emulsion. However, as the level of weighting agent increased to 60% or higher we noticed a reversal in the trend and, therefore, an increase in the particle size of the emulsion.

Stability of Beverages Without Weighting Agents

There are many beverages, such as cola types, whose flavor emulsions do not contain a weighting agent. One reason is that the beverage has to be relatively clear. Therefore, in the absence of a weighting agent greater demands are placed on the stabilizer to improve the stability of the concentrated emulsion as well as the beverage. Figure 2 illustrates the effect of the weighting agent (35% glyceryl abietate) on the initial particle size of an orange oil emulsion and on the rate of change of particle size over a period of 3 weeks. In the presence of the glyceryl abietate the initial particle size of

Frequency, %   **Cumulative, %**
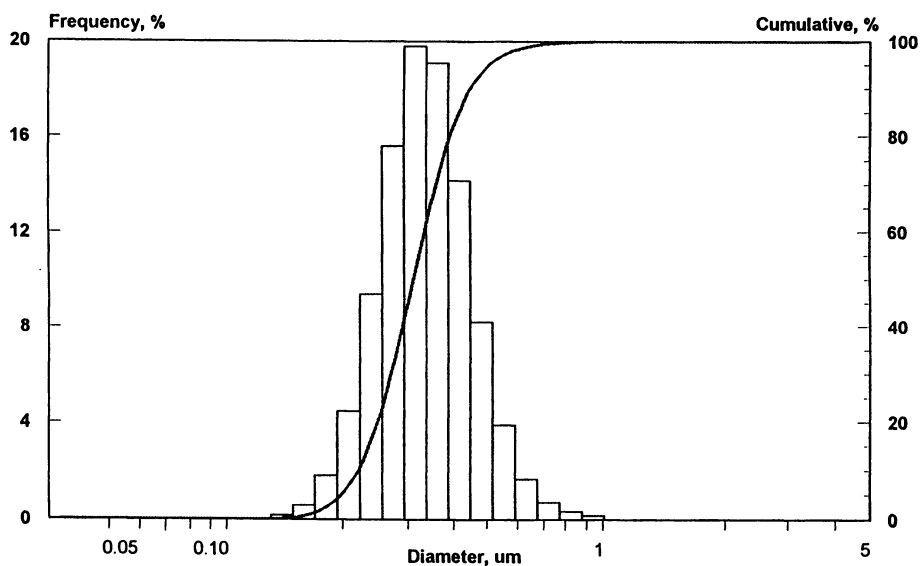
Mean (um)	Median (um)	Spec. Area (cm2/cm3)	Std. Dev.	Mode
0.351	0.335	185180	0.11	Volume

Figure 1. Particle size distribution of flavor emulsion stabilized with food starch.

Particle Size, microns

STRAIGHT ORANGE OIL

WEIGHTED ORANGE OIL

Time, weeks
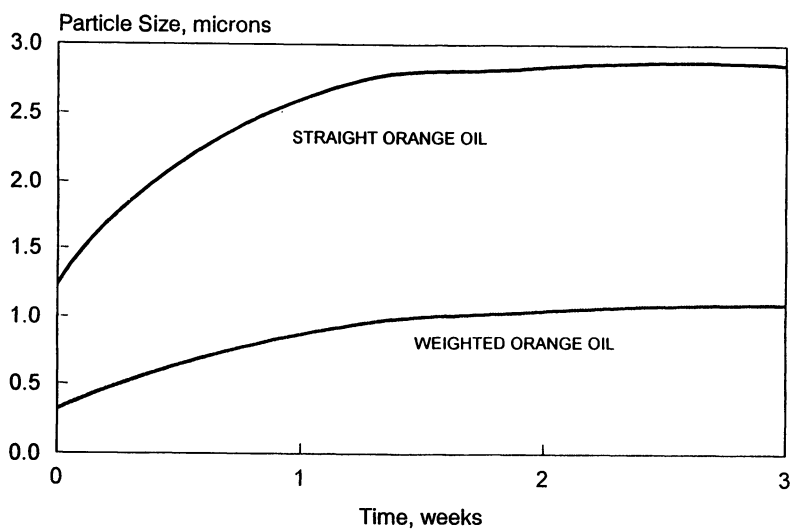
Figure 2. Effect of weighting agent on emulsion stability.

the fresh emulsion is much smaller (0.35 vs. 1.2 microns), just as we have seen above. Furthermore, in the presence of the weighting agent the particle size of the emulsion increases much more slowly and eventually levels off slightly above one micron. This is not the case with the straight orange oil whose particles are much larger to begin with and increase to 2.5 μ in three weeks. Naturally, a beverage made with the non-weighted emulsion of this example will show serious ringing while the emulsion itself will cream and/or separate seriously on storage.

Stokes' law (Equation 1) summarizes the principles we have discussed so far and gives some additional hints to further improve the stability of non-weighted emulsions and beverages.

$$v = \frac{2 \, g \, r^2 \, (\rho_1 - \rho_2)}{9 \, \eta_2} \qquad (1)$$

v = Rate of creaming or sedimentation
g = Acceleration of gravity
r = Droplet radius
ρ_1 = Density of oil phase
ρ_2 = Density of water
η_2 = Viscosity of water phase

The stability of the emulsions or the speed of separation (v) of the oil droplets is directly related to the difference in the specific gravity of the continuous phase (ρ_2) and that of the discontinuous phase (ρ_1). The smaller the difference, the slower the speed of separation and, therefore, the more stable the emulsion which is the basis for the use of the weighting agent. Also, the speed of separation decreases and the stability of the emulsion increases with decreasing radius (r) of the emulsion particles. This is the reason why the flavor industry aims at obtaining a particle size well below 1 micron. According to Stoke's law, the speed of separation also decreases and the stability of the emulsion improves as the viscosity (η) of the system increases. In some beverages, such as chilled juice drinks, this is typically achieved by adding a small amount of a thickener in the beverage which helps slow down the coalescing process of the larger emulsion particles. Obviously, there is a limit as to the level of thickener that one can add in the beverage without altering its organoleptic properties. Chilled juice drinks are characterized by a very opaque, full bodied juice-like appearance which is obtained by using a high level of emulsified oil in the final beverage, but these beverages generally do not contain a weighting agent. If they do, the permitted level is usually not high enough to raise significantly the specific gravity of the oil phase. Therefore, in the chilled juice drinks, there is often a very serious problem of creaming in the concentrated emulsion as well as ringing in the finished beverage.

Another approach to improve the stability of the beverage is to increase the level of the emulsion stabilizer which helps reduce the initial particle size of the emulsion and the ringing problem associated with unweighted beverages. To illustrate this in a typical chilled juice drink emulsion the level of food starch stabilizer was

increased from 0.5 to 4 times that of flavored vegetable oil. The formula consisted of 10 parts of vegetable oil containing the flavor, 10 parts of food starch stabilizer and 80 parts of water containing small amounts of sodium benzoate and citric acid. To maintain the viscosity of the emulsion constant water was added as needed before the homogenization step. The mixture was passed twice through the pressure homogenizer at 2500 pounds per square inch. The final beverage was prepared by adding small quantities of the concentrated emulsion to approximately one liter of syrup so as to give the same quantity of the oil blend in the chilled juice drink. Therefore, the basic composition of the beverage was 0.1% of flavored oil, 11.5% sugar, 0.2% citric acid, 0.05% sodium benzoate and varying levels of starch stabilizer. The results in Table IV show that the higher starch level improved the particle size of the unweighted emulsion from 0.730 micron at a starch/oil ratio of 0.5 to 0.551 micron at a ratio of 4. At the highest starch level the ringing in the beverage after one week was reduced from 2.5 mm to 1mm, 40% of the ringing observed with the standard one to one ratio.

Table IV. Effect of Food Starch Level on Stability of Chilled Juice Drink

Starch/Oil Ratio	Particle Size (micron)	Ringing, mm 3 weeks
0.5	0.730	3.0
1	0.674	2.5
2	0.664	2.0
4	0.551	1.0

Conclusions

A unique characteristic of sodium starch octenyl succinates is the ability to form and stabilize very fine oil-in water emulsions. The broad functionality of these specialty food starches accounts for their use in flavor and cloud emulsions that are formulated into a variety of soft beverages, such as citrus, colas and chilled juice drinks. These starch products offer unique advantages over conventional emulsion stabilizers, such as spray-dried gum arabic, in terms of domestic availability, cold water solubility, excellent emulsion properties, lower usage level and overall lower costs.

Literature Cited

1.   Light, J. M. *Cereal Foods World* **1990**, Nov. 35.
2.   National Starch & Chemical Co. *How to Choose, A Professional Guide to Food Starches;* 1994 Edition.
3.   Caldwell, C. G.; Wurzburg, O. B. U.S. Patent # 2,661,349; 1953.

4. Code of Federal Regulations, Title 21, Chapter 1, Part 172, Food Additives Permitted in Foods for Human Consumption, Section 172.892, Food Starch-Modified, U.S. Government Printing Office, Washington, D.C., 1981.

5. Preston, H. D. *Developments in Soft Drink Technology-1*; Green L. F., Ed. Applied Science Publishers Ltd.: London, 1978, pp. 87-93.

6. Hercules Chemical Specialties Inc., Ester Gum 8BG Synthetic Resin, Technical Information, 06/30/94.

7. Eastman Chemical Inc., Eastman SAIB-SG Bulletin, Publication ZM-90A, September 1993.

8. Tan, C. T. In *Food Emulsions*; Larson, K.; Friberg, S., Eds.; Marcel Dekker Publisher: N.Y., N.Y., 1990; pp. 445-477.

Chapter 16

Phospholipid Liposomes: Properties and Potential Use in Flavor Encapsulation

Norman Weiner

College of Pharmacy, University of Michigan, Ann Arbor, MI 48109

Phospholipid liposomes, defined as structures consisting of one or more concentric spheres of lipid bilayers separated by water compartments, show great potential for flavor encapsulation. Since liposomes can be custom-tailored to release their entrapped materials at predetermined rates, they offer unique opportunities to program complex flavor patterns in food products, even in the absence of the oily vehicles generally used to solubilize the flavor components. Since liposomes can now be prepared that are both stable and economical, their commercial application is now realizable.

Liposomes have shown great potential as a drug delivery system. An assortment of molecules have been incorporated in liposomes, which can then be used for a variety of purposes. Various amphiphathic molecules have been used to form the liposomes, and the method of preparation can be tailored to control their size and morphology. Molecules can either be encapsulated in the aqueous space or intercalated into the lipid bilayer; the exact location of the encapsulated material in the liposome will depend upon its physicochemical characteristics and the composition of the lipids. Whereas liposomes have been used extensively in pharmaceutical and cosmetic products, there is an emerging consensus that they show great potential for flavor encapsulation.

A liposome is defined as a structure consisting of one or more concentric spheres of lipid bilayers separated by water or aqueous buffer compartments (Fig. 1). These spherical structures can be prepared with diameters ranging from 80 nm to 100 μm. When wall materials are dispersed in an aqueous phase, hydration of the polar head groups of the lipid results in a heterogeneous mixture of structures, generally referred to as vesicles, most of which contain multiple lipid bilayers forming concentric spherical shells. These were the liposomes first described by Bangham (*1*) and are now referred to as multilamellar vesicles (MLV). Sonication of these lipid dispersions results in size reduction of these liposomes to vesicles containing only a single bilayer with diameters ranging from 25-50 nm. These structures are referred to as small

unilamellar vesicles (SUV). A number of laboratories have developed single bilayer liposomes which exhibit a size range of 100-500 nm in diameter and these vesicles are referred to as large unilamellar vesicles (LUV). The nomenclature describing liposomes can be confusing (see Table I) since liposomes have been classified as a function of the number of bilayers (e.g., MLV, SUV), or as a function of the method of preparation (e.g., REV, FPV, EIV) or as a function of size (e.g., LUV, SUV).

Table I. Examples of Nomenclature Used to Describe Liposomes

TYPE OF VESICLE	TERM USED	APPROX. SIZE (μm)
Small, Sonicated Unilamellar	SUV	0.025-0.05
Large, Vortexed Multilamellar	MLV	0.05-10
Large Unilamellar	LUV	0.1
Reverse Phase Evaporation	REV	0.5
French Press	FPV	0.05
Ether Injection	EIV	0.02

The lipids most commonly used to prepare phospholipid- based liposomes are shown in Figure 2.

Glycerol containing phospholipids are by far the most commonly used component of liposome formulations. The general chemical structure of these types of lipids is exemplified by phosphatidic acid. The "backbone" of the molecule resides in the glycerol moiety. At position number 3 of the glycerol molecule the hydroxyl is esterified to phosphoric acid (hence the name glycerolphospholipids). The hydroxyls at positions 1 and 2 are usually esterified with long chain fatty acids giving rise to the lipidic nature of these molecules. One of the remaining oxygens of phosphoric acids may be further esterified to a wide range of organic alcohols including glycerol, choline, ethanolamine, serine and inositol. The phosphate moiety of phosphatidic acid carries a double negative charge only at high pH. The pK values for the two oxygens are 3 and about 7. At physiologically relevant pH values this molecule presents more than one net negative charge, but not quite 2. The most abundant glycerol phosphatides in plants and animals are phosphatidylcholine (PC), also called lecithin, and phosphatidylethanolamine (PE), sometimes referred to as cephalin. These two phosphatides constitute the major structural component of most biological membranes. In phosphatidylserine (PS), the phosphoric acid moiety of phosphatidic acid (PA) is esterified to the hydroxyl group of the amino acid L-serine, and in phosphatidylinositol (PI) to one of the hydroxyls of the cyclic sugar alcohol inositol. In the case of phosphatidylglycerol (PG), the alcohol that is esterified to the phosphate moiety is glycerol. Table II shows the fatty acid composition of two common

MULTILAMELLAR VESICLE — **UNILAMELLAR VESICLE** — **LIPID BILAYER**
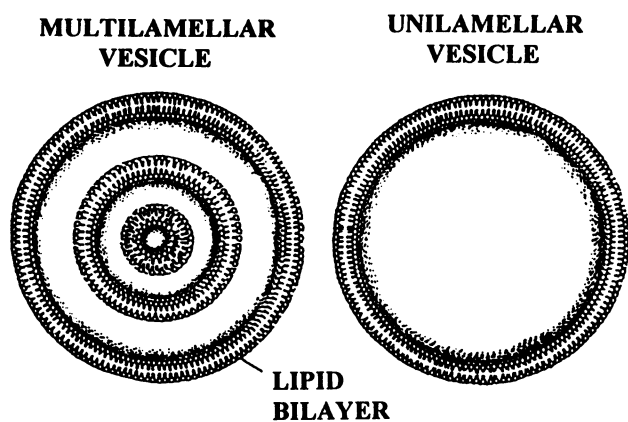
Fig. 1. Diagramatic representation of multilamellar and unilamellar vesciles. Source: Ostro, M.J. (1987) Scientific American, 102–11.
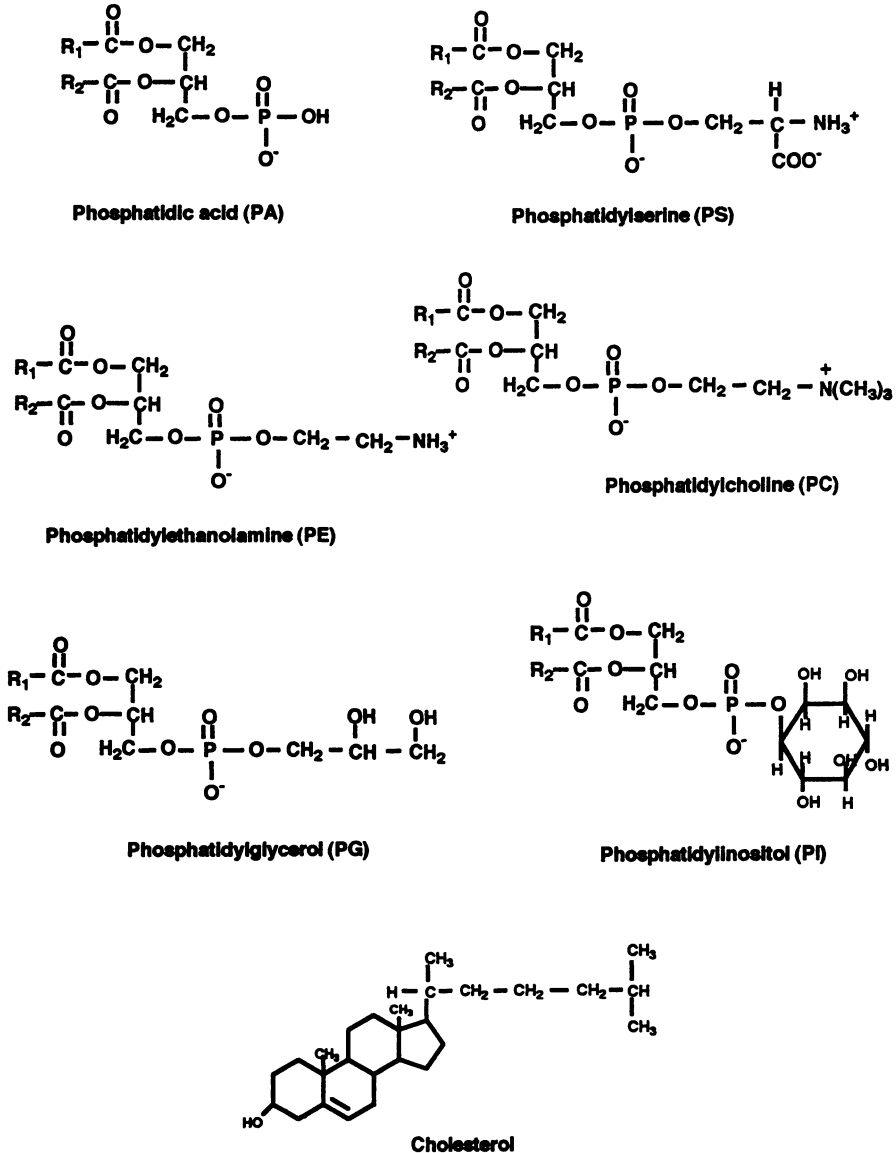
Fig. 2. Chemical structures of lipids commonly used to prepare liposomes.

phosphatidylcholines, one extracted from egg yolk and the other from soy bean oil. Notice the difference in the degree of unsaturation between egg and soy PC. Soy PC contains a greater proportion of unsaturated bonds and is thus more susceptible to peroxidation.

Table II. Fatty Acid Composition of Two Common Phosphatidylcholines, One Extracted from Egg Yolk and the Other from Soy Bean Oil

Fatty Acid Composition		Egg PC	Soy PC
16:0	Palmitic	32	12
16:1	Palmitoleic	1.5	<0.2
18:0	Stearic	16	2.3
18:1	Oleic	26	10
18:2	Linoleic	13	68
18:3	Linolenic	<0.3	5
20:4	Arachidonic	4.8	<0.1
22:6	Docosahexaenoic	4.0	<0.1

Factors Affecting Entrapment. The amount and location of a material within a liposome is dependent on a number of factors. Its location within a liposome is based on the partition coefficient of the drug between aqueous compartments and lipid bilayers, and the maximum amount of material that can be entrapped within a liposome is dependent on its total solubility in each phase. The total amount of liposomal lipid used and the internal volume of the liposome will affect the total amount of non-polar and polar material, respectively, that can be loaded into a liposome. The method of preparation can also affect drug location and overall trapping efficiency.

Incorporation of charged lipids into bilayers increases the volume of the aqueous compartments by separating adjacent bilayers due to charge repulsion resulting in increases in trapped volume. It should be pointed out that for hydrophobic materials, entrapment efficiency usually approaches 100% almost irrespective of liposomal type and composition.

Size and Size Distribution. The average size and size distribution of liposomes are important parameters with respect to physical properties and characteristics of the liposomes and their entrapped substances. There are a number of methods used to determine this parameter, but the most commonly used methods are:

a. Light Scattering. There are a variety of techniques available to size liposomes based on light scattering. The popularity of this method depends on its ease of operation and the speed by which one can obtain data. The newer instruments are based on dynamic laser light scattering.

b. Light Microscopy. This method can be used to examine the gross size distribution of large vesicle preparations such as MLV. The inclusion of a fluorescent probe in the bilayer permits examination of liposomes under a fluorescent microscope and is a very convenient method to obtain an estimate of at least the upper end of the size distribution.

c. Negative Stain Electron Microscopy. This method, utilizing either molybdate or phosphotungstate as a stain is the method of choice for size distribution analysis of any size below 5 μm. It should be used to validate light scattering data that will ultimately be used for quality assurance. For accurate statistical evaluation (±5%), one should count at least 400 particles and not rely on a single specimen for counting.

d. Freeze Fracture Electron Microscopy. This method is especially useful for observing the morphological structure of liposomes. Since the fracture plane passes through vesicles that are randomly positioned in the frozen section, resulting in nonmidplane fractures, the observed profile diameter depends on the distance of the vesicle center from the plane of the fracture. Mathematical methods have been devised to correct for this effect.

For all of the microscopy procedures used, one should always be on the lookout for aggregated particles or flocs.

Phase Behavior of Liposomes. An important feature of membrane lipids is the existence of a temperature-dependent reversible phase transition, where the hydrocarbon chains of the phospholipid undergo a transformation from an ordered (gel) state to a more disordered fluid (liquid crystalline) state. These changes have been documented by freeze-fracture electron microscopy but are most easily demonstrated by differential scanning calorimetry (DSC). The physical state of the bilayer profoundly affects the permeability, leakage rates and overall stability of the liposomes. The phase transition temperature (T_m) is a function of the phospholipid content of the bilayer.

By proper admixture of bilayer forming materials, one may design liposomes to "melt" at any reasonable temperature. This strategy can be used to deliver complex flavors at desired increments of time. The phase transition temperature can be altered by controlled hydrogenation of phospholipid mixtures or by adding sterols such as cholesterol.

Liposome Preparation Methods

Multilamellar Vesicles (MLV). Multilamellar vesicles are by far the most widely studied type of liposome and, as pointed out by Alec Bangham in 1974, exceptionally simple to make. In general a mixture of lipids is deposited as a thin film on the bottom of a round-bottom flask by rotary evaporation under reduced pressure. MLV form spontaneously when an excess volume of aqueous buffer is added to the dry lipid.

The time allowed for hydration and conditions of agitation are critical in determining the amount of the aqueous buffer entrapped within the internal

compartments of the MLV. For example, a similar lipid concentration can encapsulate 50% more of the aqueous buffer per mole of lipid when hydrated for 20 hours with gentle shaking, compared to a hydration period of 2 hours with vigorous shaking, despite the fact that the two preparations exhibit a roughly similar particle size distribution. If hydration time is reduced to a few minutes with vortexing, a suspension will exhibit a still lower capture volume and a smaller mean diameter. Thus the hydration time, method of suspension of the lipids and the thickness of the film can result in markedly different preparations of MLV, in spite of identical lipid concentrations and compositions, and volume of the suspending aqueous phase. The presence of negatively charged lipids such PS, PA, PI or PG will tend to increase the interlamellar distance between successive bilayers in the MLV structure and thus lead to a greater overall entrapped volume. Generally about 10-20 mole percent of a charged species is used although it is possible to produce MLV from a purely charged lipid such as PS. The presence of charged lipids also reduces the likelihood of aggregation following the formation of MLV.

Small Unilamellar Vesicles (SUV). The classical methods of dispersing phospholipids in water to form optically clear suspensions involve various mechanical means and began with the sonication method reported in the mid 60's (2-4). These types of SUV dispersions have been rigorously characterized and shown to consist of rather uniform closed bilayer vesicles of about 25-50 nm diameter. Solvent injection methods have also been devised to produce SUV. These typically involve the slow injection of a lipid solution in either ethanol or ether into warm water containing a drug or other marker to be entrapped. There is no apparent advantage to the use of SUV for flavor entrapment

Large Unilamellar Vesicles (LUV). Large unilamellar vesicles provide a number of important advantages as compared to MLV including high encapsulation of water soluble compounds, economy of lipid and a greater probability of reproducible flavor release rates. However, LUV are perhaps the most difficult type of liposome to produce. "Large" in the context of liposomes usually means any structure larger than 100 nm; thus large unilamellar vesicles refers to vesicles bounded by a single bilayer membrane that are above 100 nm in diameter. The primary methods used to produce LUV are a sophisticated reverse emulsification technique and sequential extrusion of MLV through small pore size polycarbonate membranes under high pressure. With the reverse phase evaporation technique, LUV are prepared by forming a water-in-oil emulsion of phospholipids and buffer in excess organic phase followed by removal of the organic phase under reduced pressure. The two phases are usually emulsified by sonication but other mechanical means have also been used. Removal of the organic solvent under vacuum causes the phospholipid-coated droplets of water to coalesce and eventually form a viscous gel. Removal of the final traces of solvent results in the collapse of the gel into a smooth suspension of LUV. The method which was pioneered by Szoka and Papahadjopoulos in 1978 (5) has been used extensively for applications which require high encapsulation of water soluble molecules. Entrapment efficiencies up to 65% can be obtained with this method. The extrusion method is also widely used.

Hope, et al (*6*) among others have shown that as MLV are repeatedly extruded through very small pore diameter polycarbonate membranes (0.8-1.0 micron) under high pressure (up to 250 psi) their average diameter becomes progressively smaller reaching a minimum of 60-80 nm after about 5-10 passes. Moreover, as the average size is reduced, the vesicles become more and more single layered. MLV prepared from pure PG convert to 60-70 nm single layer vesicles following about 10 passes through a 1.0 micron capillary pore membrane. The mechanism at work during such high pressure extrusion appears to be much like peeling an onion.

Methods for Controlling Size and Size Distribution of Liposomes

In those cases where a fairly small particle size is desirable, homogenization has proven to be the most useful approach. In much the same way as milk is homogenized, the average particle size and polydispersity of vesicle dispersions can be reduced by passage through a high pressure homogenizer. One such devise marketed by the Biological Development Corporation under the trade name Microfluidizer* has been shown by Mayhew and his colleagues (*7*) to generate vesicles in the 50-200 nm size range. Such homogenizers are amenable to scale up, and throughput rates are high. As with other high pressure devices, however, heat regulation can sometimes present problems, and the shear forces developed within the reaction chamber can lead to partial degradation of the lipids. Another technique that has gained widespread acceptance for the production of liposomes of defined size and narrow size distribution, introduced by Olson et al. (*8*) in 1979, involves the extrusion of a heterogeneous population of fairly large liposomes through polycarbonate membranes under moderate pressures (100-250 psi). Such membranes have uniform straight-through capillary pores of defined size and polycarbonate does not bind liposomes containing charged species. This simple technique can reduce a heterogeneous population of MLV or REV to a more homogeneous suspension of vesicles exhibiting a mean particle size which approaches that of the pores through which they were extruded. MLV with a mean diameter of 260 nm can be obtained following a single extrusion through 200 nm pore size polycarbonate membranes; 75% of the encapsulated volume resides in vesicles between 170 and 370 nm (as measured by negative stain electron microscopy). Upon additional extrusions through the same pore size membrane the average size is reduced further finally approaching about 190 nm with greater than 85% of the particles in the 170-210 nm range.

Stability of Liposomes

Chemically, phospholipids are susceptible to hydrolysis. Additionally, phospholipids containing unsaturated fatty acids can undergo oxidative reactions. Much of the data on liposomes that have appeared in the literature can be considered suspect due to the use of phospholipids containing significant amounts of oxidation and hydrolysis products. These reaction products can cause dramatic changes in the permeability properties of liposomes. Preparative procedures (e.g., sonication) or storage conditions (e.g., exposure to different pH values) can affect the decomposition rate of the liposomal lipids Most of the phospholipid liposomal dispersions used contain unsaturated acyl chains as part of the molecular structure. These chains are vulnerable to oxidative

degradation (lipid peroxidation). The oxidation reactions can occur during preparation, storage or actual use. Oxidative deterioration of lipids is a complex process involving free radical generation and results in the formation of cyclic peroxides and hydroperoxides.

Most of the procedures used to measure lipid peroxidation are nonspecific and are either based on the disappearance of unsaturated fatty acids (determined by lipid extraction techniques followed by GLC analysis) or the appearance of conjugated dienes. The latter technique is now widely used since oxidation is accompanied by increased UV absorption in the 230-260 nm range. If unsaturated phospholipids are used to prepare liposomes, and no special precautions are used to minimize oxidation, the reaction will occur readily. Oxidation of the phospholipids may be minimized by a number of ways:

1. Minimum use of unsaturated phospholipids (if appropriate).
2. Use of argon or nitrogen to minimize exposure to O_2.
3. Use of light resistant containers.
4. Removal of heavy metals (EDTA).
5. Use of antioxidants such as α-tocopherol or BHT.

The most important degradation product resulting from lecithin hydrolysis is lyso-lecithin (lyso-PC), which results from hydrolysis of the ester bond at the C_2 position of the glycerol moiety. Many workers choose the formation of lyso-PC as a standard measure for the chemical stability of phospholipids since the presence of lyso-PC in lipid bilayers greatly enhances the permeability of liposomes. It is therefore extremely important that the formation of lyso-PC be kept to a minimum during storage. Lyso-PC is usually analyzed by phospholipid extraction followed by separation of PC and lyso-PC by TLC. The spots are then usually scraped and assayed for total phosphorous content. Although factors such as sonication could affect the degree of lyso-PC formation, probably the single most important method of minimizing this problem is by the proper sourcing of the phospholipids to be used. They should be essentially free of any lyso-PC to start with and, of course, be free of any lipases.

Literature Cited

1.   Bangham, A. D. *Methods Membr. Biol.* **1974**, *1*, 1-68.
2.   Saunders, L. *J. Pharm. Pharmacol.* **1962**, *14*, 567-572.
3.   Hamilton, R.L.; Guo, L. In *Liposome Technology*; CRC Press: Boca Raton, FL, 1984,Vol. 3.
4.   Barenholz, Y.; Amselem, S.; Litman, B.J.; Goll, J.; Thompson, T.E.; Carson, F.D. *Biochem.* **1977**, *16*, 2806-2810.
5.   Szoka, F. ; Papahadjopoulos, D. *Biochem.* **1978**, *75*, 4194-4198.
6.   Hope, M.J.; Bally, M.B.; Webb, G.; Cullis, P. *Biochim. Biophys. Acta* **1985**, *812*, 55-65.
7.   Mayhew, E.; Nikolopoulos, G.T.; King, J.J.; Siciliano, A.A. *Pharm. Manufac.* **1985**, *2*, 18-22.
8.   Olson, F.; Hunt, C.A.; Szoka, F.; Vail, W.J.; Papahadjopoulos, D. *Biochim. Biophys. Acta* **1979**, *557*, 9-23.

Chapter 17

Nonphospholipid Liposomes: Properties and Potential Use in Flavor Encapsulation

Rajiv Mathur and Phil Capasso

IGI, Inc., Wheat Road and Lincoln Avenue, Buena, NJ 08310

In recent years considerable effort has been directed toward the development of lipid bilayer vesicle delivery systems employing lipid amphiphiles other than phospholipids. Amphiphiles have been shown to form lipid vesicles of different types and stabilities.

Our efforts have focused on the production of non-phospholipid paucilamellar vesicles that we called "Novasomes". These vesicles are 0.1-1.0 microns in diameter, with 2-5 bilayer shells surrounding an unstructured space that can be occupied by hydrophilic or hydrophobic materials. The vesicles can be produced in amounts ranging from milliliter continuous flow batches at costs equivalent to those of making simple emulsions.

The uses of Novasome vesicles are extensive and range from cosmetics and pharmaceuticals, to foods. In all such applications, non-phoshpolipid Novasomes offer the advantages of high stability, low cost, and availability in large amounts. Novasome vesicles can be used for many functions in foods and beverages because of their ability to protect, transport, and deliver flavor oils, nutrients or other active ingredients.

Early work on lipid bilayer vesicles, as well as most current studies have dealt with structures made from phospholipids. Since 1973, however, numerous experiments have shown that a lipid bilayer can be formed by molecules other than phospholipids. These molecules include fatty acids, dialkyldimethylammonium amphiphiles, dialkyl amphiphiles with ionic or zwitterionic head groups, polyglycerol alkyl ethers and polyethoxylated analogues, two-tailed sucrose fatty acid esters, and appropriate mixtures of single-tailed cationic and anionic surfactants (*1-6*).

In 1987 scientists of Micro Vesicular Systems, Inc. (MVS) invented a new type of lipid microcapsule with unusual stability and transport properties called

Novasome lipid vesicle, hereafter named "Novasomes vesicles". These lipid microspheres are highly versatile and have been used in the encapsulation, transport, controlled release, and other manipulations of a wide array of molecules with applications for flavor and food, agriculture (7-8) and aquaculture, coating and paints (9), cosmetics and other personal care products, environmental cleanup and protection, pest control, animal and human biologicals and pharmaceuticals (10-11), in large amounts using MVS' patented, scalable continuous flow systems (12-13).

This review focuses on Novasome vesicles, uniquely structured, paucilamellar vesicles that can be formed from single-tailed non-phospholipid amphiphiles. They possess an aqueous or non aqueous core surrounded by one or several lipid bilayer shells, each composed of amphiphilic molecules, alone or in combination with a steroid (14-16).

The manufacture of non-phospholipid liposomes, as here described, relies on the conversion of micellar solutions of membrane-mimetic amphiphiles to liposomal structures by manipulation of environmental variables (e.g., temperature, hydration) in an appropriate temporal sequence.

As the concentration of a membrane-mimetic amphiphile in water increases, a sudden transition in the properties of the system occurs, representing the conversion of a molecular solution to a micellar solution. The transition concentration is known as the critical micelle concentration. The critical micelle concentration of the membrane-mimetic amphiphiles that we employ lie well below $10^{-6}M$.

Micellar solutions consist of amphiphile molecules in small clusters (50-200 molecules) dispersed in water. The shapes of micellar clusters depends on the amphiphile type (e.g., head group, apolar chain) and the solution conditions (e.g., concentration, electrolytes, temperature). Micelle shape is determined by the surface area of the amphiphile molecules, the nature of the hydrophobic/hydrophilic interface and the curvature of that interface. Micelles form in various phases. Hexagonal phases consist of long, normal or reversed, rod-shape structures with hexagonally packed arrays, and spherical micelles have been classified into two types of cubic packaging: body-or face-centered.

The concentration of free amphiphile [A] is related to the proportion of amphiphile in micellar aggregates, $[A_n]$ by a constant, K, which equals:

$$[A_n]/[A]^n = K \qquad (1)$$

When the concentration of free amphiphile [A] becomes equal to $K^{-1/n}$, equivalent to the critical micelle concentration, the formation of micelles begins and, as the value of [A] continues to increase above $K^{-1/n}$, the concentration, $[A_n]$, of micellar aggregates rises rapidly. An increase in total amphiphile concentration above the critical micelle concentration thus implies an increase in the size and/or number of micelles, not the concentration of free amphiphile.

The methods to be discussed for the manufacture of non-phospholipid liposomes involves the formation of micellar aggregates of membrane-mimetic amphiphiles and the controlled coalescence of these aggregates into membrane-bound vesicles (*20*). The membranes of such vesicles are stabilized by a number of interactions, including the hydrophobic effect driving apolar moieties out of water, van der Waals attractions between ordered amphiphile residues, and hydrogen-bonding of amphiphile head groups to the water at the hydrophilic surfaces of each bilayer.

Major Constituents of Novasomes

The non-phospholipid liposomes made by Micro Vesicular Systems, Inc. are engineered for particular applications. Appropriate Novasomes are assembled using a series of membrane "modules", each module imparting desired characteristics to the Novasome vesicles. The modular approach provides great breadth and flexibility to the membrane design (Figure 1). It also allows combination of numerous amphiphiles with each other, or with phospholipids to yield membrane hybrids with novel properties (*21-24*).

Major Structure Modules. Table I lists some of the major structural membrane amphiphiles currently used in this non-phospholipid liposome vesicle designing for flavor and food application. In any given liposome type these molecules account for more than 50% of the membrane lipid.

The fatty alcohols (Table I, #I) form bilayer vesicles only in association with a modulating module (Table II) and an ionogenic module.

Table I. Principal Wall-forming Material

Classification	Hydrocarbon Chain	Bond	Head Group
1. Fatty alcohol	C_{12}-C_{20} (0-1 unsat.)		-OH
2. Fatty acid	C_{12}-C_{20} (0-1 unsat.)		-COOH
3. Glycerol fatty acid monoester	C_{12}-C_{20} (0-1 unsat.)	-CO-O	-$CH_2CHOHCH_2OH$
4. Glycerol fatty acid diester	C_{12}-C_{18} (0-1 unsat.) C_{12}-C_{18} (0-1 unsat.)	-CO-O -CO-O	-CH-CHO -CH_2
5. Propylene Glycol fatty acid monoester	C_{12}-C_{20} (0-1 unsat.)	-CO-O	-OCH_2 CHOH CH_3

Amphiphiles   Modulators   Ionogens   Spacers

A Novasome™ vesicle membrane bilayer
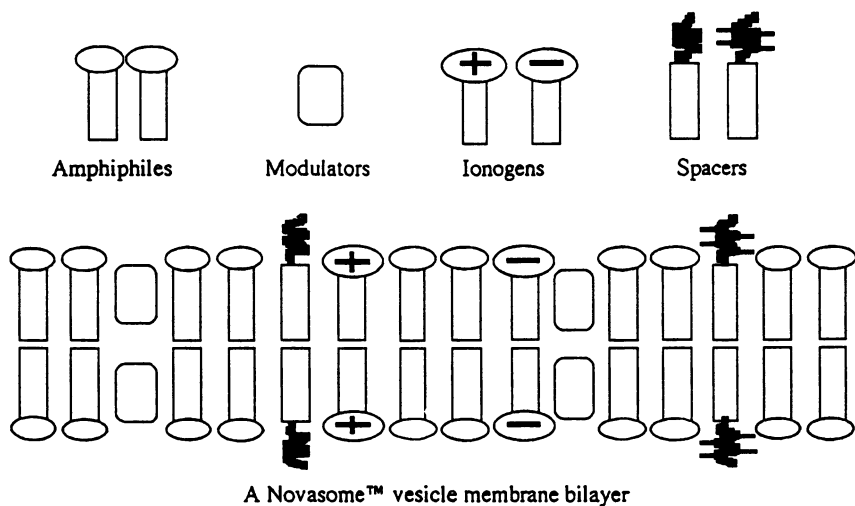
Figure 1.   Schematic representation of membrane modules of the Novasome bilayer.

The fatty acids (Table I, #2) serve as structural modules for acid pH-sensitive non-phospholipid liposomes. They form stable bilayers only when they are partly ionized (at bulk pH levels between 6 and 8, corresponding to membrane pH levels near 4-6) and in association with a nonionic amphiphile, such as fatty alcohol, and a modulator module (Table I). Full ionization of the carboxyl groups causes disruption of the bilayer, as does full protonation.

Fatty acid monoesters and diesters (Table I, #3,4,5) form satisfactory lipid bilayer vesicles when appropriately combined with a modulator, spacer modules and an ionogenic module.

Table II. Membrane Modulators

Classification	Apolar Residue	Head Group
1. Cholesterol	Δ 5 Cholestene 3-β	-OH
2. Phytosterol (β)	Δ 5 Stigmastene 3-β	-OH

Modulator Modules.   The modular approach used in the design of non-phospholipid liposomes relies on the use of sterol modulator molecules (Table II). Sterols can intercalate amphiphile hydrocarbon chains in bilayers, and thereby allow the intermixing of different acyl chains without phase segregation and broaden the range of temperature within which the crystalline- liquid-crystalline transition occurs.

It appears that sterol interacts strongly with the polar termini of the chain, leaving them less free to change conformation than the more disordered long chain segments.

Ionogenic Modules. The major ionogenic membrane amphiphiles currently used in our non-phospholipid liposomes which have GRAS status are fatty acids. They can be used in conjunction with any of the nonionic modules listed in Table I in preparations ranging from 0.05 to 10 moles percent.

Spacer Modules.   Spacer modules are employed to widen the interlamellar space, reducing the number of lamellae, and to make the external bilayer less accessible than in the case with compact head groups. Polyoxyethylene derivatives of sorbitan fatty acid esters, fatty alcohols and fatty acids allow the placement atop the outermost bilayer surface of bulky residues acting as steric barriers to regulate interaction of the vesicle surface with, for example, viruses and phagocytitic cells.
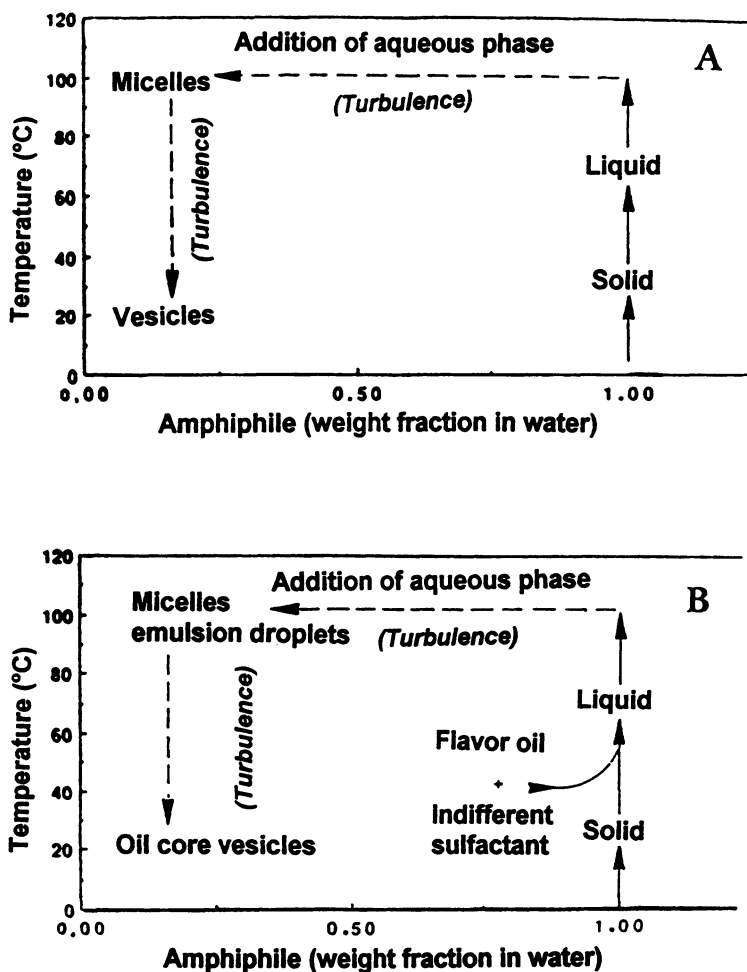
Figure 2. Schematic representation of novasome vesicle formation. (A) Incorporation of aqueous medium only; (B) encapsulation of water and water immiscible fluid (oil, indifferent surfactant, etc.)

Chain Matching.   Provided there are no steric or other interferences between head groups, the most stable membranes are produced by optimal matching of the chain length of the membrane modules. However, the action of sterols allows assembly of membranes from modules of varying chain length, thereby providing some control over permeability.

Preparation of Novasome Vesicles

The manufacture of Novasome utilizes a unique process specifically designed for the formation of vesicles under rigorous conditions, in any amounts (from a few microliters to very large volumes), and at a cost equivalent to that of making simple emulsions. In laboratory experiments, two syringes, one containing the lipid and the other the aqueous phase, connected with a double hubbed needle are used. In the industrial process, vesicles are formed in a specially designed apparatus at volume flow rates of 6 L/min and above.

Vesicles with a Predominantly Aqueous Core.   The   generation   of   such vesicles is based on the known phase behavior of single-chain lipid amphiphiles at temperatures below 85°C. The membrane-forming amphiphile (plus modulating molecules such as sterol, fatty anions) is heated to give a liquid. This liquid is then injected at high velocity (10 to 50 m/s) through small channels (1 to 3 mm diameter) or needle (0.9 to 2.05 mm diameter) with turbulent mixing into excess aqueous phase and immediately cooled. The injection step causes the lipid to be disrupted into minute droplets that are quickly converted into micelles. Subsequent cooling under conditions of continued turbulence causes the micelles to fuse into paucilamellar vesicles within milliseconds (Figure 2A, Table III).

This vesicle formation is facilitated and vesicle size distribution narrowed by inclusion of small amounts of nonamphiphilic, nonpolar, water-immiscible fluids in the lipid phase. Possibly microdroplets of these fluids segregate from amphiphile during micelle formation and subsequently act as nuclei around which micelles coalesce to form vesicles (Figure 2B). By use of this approach the loading of vesicles with water-soluble cargo can approximate theoretically 90% of the internal volume for vesicles 0.5 μm in diameter, with two peripheral membranes.

Vesicles with a Predominantly Water-immiscible Core (Flavor Oil).   The preceding technique can be adapted for loading the novasome vesicle core with a wide variety of water-immiscible materials (including a broad range of flavor oils and nutrients) and solutions of substances in water-immiscible materials.

Hot Loading. In this system, the water-immiscible, apolar substance is incorporated - together with a small amount of "indifferent surfactants" (surfactants that do not form bilayers) into the liquid lipid used to make novasome membranes. During injection of the liquid lipid into the aqueous phase, the water-

immiscible substance forms microdroplets (diameter <0.1 μm) stabilized by the in-different surfactant, around which the micelles of membrane-forming surfactants coalesce.

Table III. Particle Size Changes during Novasome Vesicle Formation

Time (min)	Size + SD (nm)
Estimated micellar diameter	6
A. Slow cooling	
1	130 ± 14
5	218 ± 23
21	362 ± 58
50	488 ± 270
B. Rapid Cooling	
1	436 ± 160

Note: (A) Lipid heated to 85°C, injected into excess 0.15 M NaCl with turbulent mixing, passed through a 0.22-μm filter, diluted with 0.15 M NaCl at 85°C, and placed in a coulter N4SD submicron Particle Analyzer at 23.5°C. Over 85% of particles were located in the single peak. (B) As A, except that filtered sample was immediately cooled to 23.5°C.

By use of this approach, the loading of Novasome vesicles with water-immiscible material can be selected to range from trace amounts to 90% of solids. (percent solid = mass of oil/mass of oil + wall lipid). The theoretical value for a 0.5-μm vesicle with two peripheral membranes is near 90%. Mixtures can be employed to adapt the melting temperature of the lipid core to specific needs. By selection of appropriate proportions of indifferent surfactant, and wall-forming amphiphile, control over the Novasome wall thickness and vesicles diameter is achieved. When the loading with the water-immiscible material is moderate, an important capacity for carrying hydrophilic substances can be retained (Figure 3), allowing the vesicle to act as a multifunctional carrier.

Loading of Preformed Vesicles.   In this second system, the vesicles are mixed under low-shear conditions with the water-immiscible cargo in the presence of indifferent surfactant (22). In the process, microdroplets of the apolar material enter the central vesicle space within seconds at an ambient temperature. With triglycerides, mineral oils, and some flavor oils, loading near 90% solids can be attained.

This second process is particularly useful for the loading of fragile materials (e.g., flavor or fragrance oils) and substances (such as terpenes) that interfere with micelle formation or fusion at high temperatures (*25-26*).

Membrane Structure of Novasome Vesicles.   The membranes that limit phospholipid vesicles have been characterized (more than 1000 publications) as bimolecular layers with externally disposed hydrophilic components, nearly always in crystalline array, and internally disposed paraffin chains either crystalline (below the T_c) or liquid (above the T_c).

Although less work has been done on the components of novasome vesicles than on those of phospholipid vesicles, basic information is available on some of these molecules. These studies suggest that in the presence of excess water, nonionic amphiphiles can exist in crystalline, liquid-crystalline, gel, and various micellar arrays (*27-30*).

Concerning novasome vesicle membranes composed of single-tailed amphiphiles, some important features have been defined by electron microscopy, X-ray diffraction, Raman spectroscopy, and other methods that we summarize hereafter.

Negative-staining micrographs of novasomes vesicles, composed of single-tailed amphilphiles, show that such vesicles are bound by two or more membranes, each with the "railroad track" or "unit membrane" image characteristic of lipid bilayers, and each about 6 nm thick. The cores of the most commonly used novasome are typically 0.1 to 0.5 μm in diameter (Figure 4). Freeze-fracture electron microscopy confirms results obtained with negative staining.

Commercialization of Novasomes in the Food Industry

Definition of Novasomes for Food Uses.   The Novasome is basically a water dispersible, submicroscopic entrapment system that can be programmed to release its water or oil soluble cargo in a predetermined fashion.

The extremely small size of the micro vesicles (range 0.3 - 1.2 microns) also allows them to act as ball bearings in some applications, thereby producing a fat mimetic effect.

Novasomes can also be trapped inside conventional spray dried particles without losing their integrity, for use in dry mix products.

Uses. Novasomes can be used for many functions in foods and beverages. Novasomes for food use are specially produced to conform to FDA or FEMA GRAS status. Some of the uses are as follows:

- As a delivery system for flavorings, nutraceuticals or other active ingredients to the food product.
- As a method to isolate ingredients that may cause unwanted interactions in the food product.
- As a method for preserving the efficacy of particular ingredients throughout the shelf life of the food product.
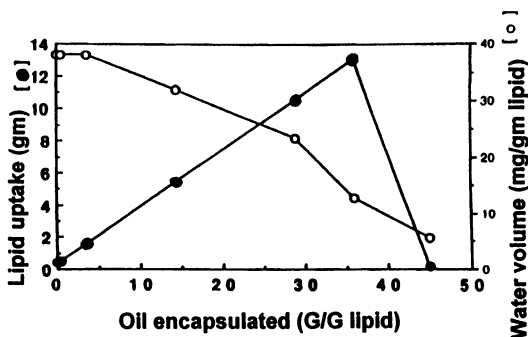
Figure 3. Oil and water uptake by C_{16} novasome vesicles. A fixed quantity of vesicle lipid was combined with increasing amounts of oil; any free oil removed by centrifugation before measuring lipid uptake. The water uptake was measured according to calcein encapsulation.
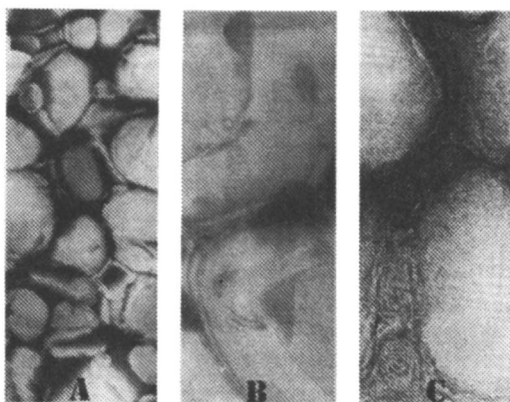
Figure 4. Electron micrograph of novasome vesicles observed by negative staining (A) Field of homogeneous vesicles; (B) abutting vesicles showing a sharply resolved peripheral membrane; (C) novasome vesicles prepared in the presence of a lipid excess. Note the myelinic structures between the vesicles. Magnification (A) X 40,000; [B and C] X 200,000.

- As a method to extend the shelf life of the food product.
- As a fat mimetic to enhance the "fatty mouthfeel" of certain food products.
- To impart novel flavor effects such as long lasting flavor or sequential flavor to a food or beverage.
- To add flow ability to food products.
- To add moisture to food products.
- To distribute ingredients evenly throughout food products.

Applications. Novasomes have been successfully applied for various reasons to the following foods and beverages:
- bakery products
- dressings, sauces and gravies
- beverages
- confectionery products
- tablet products
- microwavable products
- dairy products

Example: Vanilla Flavor Novasomes

	Percent
Bilayer Forming Lipids	
1. Membrane wall lipids	10
2. Membrane condensation lipids	4
3. Membrane charged lipids	1
Core Forming Lipids and Flavor	
4. Secondary surfactant	1
5. Oil soluble vanilla flavor	20
Aqueous components	
6. Salts	0.1
7. Sugars	1.0
8. Polymer thickeners	1.0
9. Preservatives	0.20
10. DI water	

Acknowledgments

Literature Cited

1.   Tanford, C. *The Hydrophobic Effect*, Wiley: New York, 1980.
2.   Murakand, Y.; Nakano, A.; Fukuya, K. *J. Amer. Chem. Soc.* **1980**, *102*, 4253.

3.   Murakami, Y.; Nakano, A.; Fkeda, H. *J. Org. Chem.* **1982**, *47*, 2137.
4.   Ishigami, Y.; Machida, H. *J. Amer. Oil Chem. Soc.* **1989**, *66*, 599.
5.   Schenk, P.; Ausbom, M.; Bendas, F.; Nuhn, P.; Amdt, D.; Meyer, H. W. *J. Microencapsulation* **1989**, *6*, 95.
6.   Kaler, E. W.; Murthy, K.; Rodriguez, B. E.; Zasadzinski, J. A. *Science*, **1989**, *245*, 1371.
7.   Tabibi, E.; Sakura, J. D.; Mathur, R.; Wallach, D. F. H.; Schulteis, D. T.; Ostrom, J. K. In *Pesticide Formulations and Application Systems*, Vol. 12, ASTM STP 1146, Devisetty, B. N.; Chasin, D. G.; Berger, P. D., Eds.; Amer. Soc. Testing & Materials, Philadelphia, p.155, 1991.
8.   Wallach, D. F. H. U.S. Patent 5,019,392, 1991.
9.   Wallach, D. F. H.; Mathur, R.; Chang, A. C.; Tabibi, E. U.S. Patent 5,164,191, 1992.
10.   Wallach, D. F. H. U.S. Patent 5,019,392, 1991.
11.   Vandergriff, K.; Wallach, D. F. H.; Winslow, R. K. *Art. Cells Immob. Tech.*, in press.
12.   Wallach, D. F. H.; Yiournas, C. U.S. Patent 4,895,452, 1990.
13.   Wallach, D. F. H.; Yiournas, C. U.S. Patent 5,013,497, 1990.
14.   Wallach, D. F. H. U.S. Patent 4,911,928, 1990.
15.   Wallach, D. F. H. U.S. Patent 4,197,951, 1990.
16.   Wallach, D. F. H. U.S. Patent 5,032,457, 1991.
17.   Wallach, D. F. H. U.S. Patent 4,855,090, 1989.
18.   Wallach, D. F. H. U.S. Patent 5,104,736, 1992.
19.   Wallach, D. F. H. U.S. Patent 5,147,723, 1992.
20.   Tabibi, E.; Wallach, D. F. H. INTERPHEX-USA, Proc. of 1991 Tech. Prog. 61, 1991.
21.   Wallach, D. F. H. U.S. Patent 5,032,457, 1992.
22.   Wallach, D. F. H.; Mathur, R. U.S. Patent 5,160,669, 1992.
23.   Wallach, D. F. H.; Mathur, R. M.; Reziniak, G. J. M.; Trenchant, J. F. *J. Cosmet. Chem.* **1992**, *43*, 113.
24.   Wallach, D. F. H.; Philippot, J. In *Liposome Technology*, 2nd Ed., Gregoriadis, G., Ed., CRC Press: Boca Raton, FL, p. 141, 1992.
25.   Mathur, R.; Wallach, D.F.H. U.S. Patent 5,260,065, 1993.
26.   Mathur, R. U.S. Patent 5,405,615, 1995.
27.   Mitchell, J.; Tiddy, G. J. T.; Waring, L.; Bostock, T.; McDonald, M. P. *J. Chem. Soc. Faraday Trans.*, *1* **1983**, *79*, 975.
28.   Adam, C. D.; Duffant, J. A.; Lowry, M. R.; Tiddy, G. J. *J. Chem. Soc. Faraday Trans.*, *1* **1984**, *80*, 789.
29.   Randall, K.; Tiddy, G. J. T. *J. Chem. Sac. Fraraday Trans.*, *1* **1984**, *80*, 3339.
30.   Carvell, M.; Hall, D. Y.; Lyle, 1. G.; Tiddy, G. J. T. *Faraday Dis. Chem. Soc.* **1986**, *81*, 223.

RECEIVED July 29, 1995

Chapter 18

Use of Cyclodextrins for Flavors

Z. Helena Qi and Allan R. Hedges

American Maize-Products Company, 1100 Indianapolis Boulevard, Hammond, IN 46320

Among enzyme modified starch derivatives, cyclodextrins possess a unique cyclic structure with the ability to entrap various guest molecules. The chemical and physical characteristics, such as solubility, stability, and volatility, of the included compounds may be favorably modified as a result of complexation with cyclodextrins. Cyclodextrins have been found advantageous in various flavor applications. The major beneficial effects of cyclodextrins as well as the basic concepts related to the molecular inclusion are illustrated through examples. Complexation techniques are also discussed.

Liquid flavor concentrates have been used in the food industry for several decades. Many components of flavor concentrates exhibit considerable sensitivity to air, light or heat. Moreover, they are oils or liquids, which are difficult to work with in some applications. To overcome these disadvantages, numerous materials have been tested for use as flavor encapsulating agents. Thus, powdered or encapsulated flavors produced can be used by food manufacturers in goods such as beverages, puddings, cake mixes and other desserts in which shelf-life and flavor stability are important.

However, each of these encapsulating agents has one or more limitations. For instance, gum arabic, a traditional material of choice, provides excellent emulsification and good retention of volatiles but exhibits poor protection against oxidation (1). Partially hydrolyzed starches (i.e.), maltodextrins and glucose syrup solids) give very good protection results but yield poor retention of volatiles (2). Therefore, the search continues for superior flavor carriers that exhibit multiple desirable functionalities.

Among the most recent and sophisticated flavor encapsulating processes, cyclodextrin complexation has emerged as a unique way of flavor entrapment: molecular encapsulation. This paper is intended to provide a brief overview of the structural and physicochemical properties of cyclodextrins, cyclodextrin-flavor

complexation techniques, as well as the advantages of utilizing cyclodextrins for flavor applications.

Cyclodextrins

Molecular Structure. Cyclodextrins are a series of cyclic oligosaccharides produced by the action of cyclodextrin glucosyltransferase (CGTase) upon starch. They are composed of D-glucose residues connected through alpha 1-4 linkages. The most common members of the family are α-, β- and γ-cyclodextrins, made up of six, seven and eight glucose units, respectively. As a result of the C1 (chair) conformation of each D-glucose residue and the lack of free rotation about the glycosidic bonds which connect the glucose units, a cyclodextrin has the shape of a hollow truncated cone. All hydroxyl groups (C2-OH, C3-OH, and C6-OH) are directed toward the outside of the cyclodextrin cone while two rings of the non-exchangeable hydrogen atoms (H-3, and H-5) and the glycosidic oxygens are located on the interior of the cavity. This distinct structural feature bestows upon cyclodextrins a combination of a hydrophilic external surface and a hydrophobic inner cavity, which leads to the intriguing characteristic of forming inclusion complexes with various molecules (guests). Table I lists some dimensional parameters of cyclodextrin molecules (*3*).

Table I. Important molecular parameters of α-, β- and γ-cyclodextrins (CDs)

	α-CD	β-CD	γ-CD
glucose residues	6	7	8
molecular weight	973	1135	1297
cavity diameter (Å)	4.7-5.3	6-6.6	7.5-8.3
cavity height (Å)	7.9	7.9	7.9
cavity volume (mL/mol)	174	262	472

The varying dimensions of different cavities allow each cyclodextrin to exhibit an optimal binding with the included molecule of appropriate size or geometry. Therefore, selectivities of cyclodextrins for different guest compounds are observed.

Chemical and Physical Properties. Cyclodextrins are non-reducing. Periodate oxidation of cyclodextrins opens the glucopyranose ring but no formaldehyde or formic acid is formed, consistent with the fact that they do not contain free end groups. Although cyclodextrins are more resistant to acid hydrolysis than starch, strong acids such as hydrochloric or sulfuric acid hydrolyze cyclodextrins. The rate of acid

hydrolysis increases as a function of both increased acid concentration and temperature. In the presence of weak acids, such as most of organic acids, hydrolysis of cyclodextrins is minimal or does not occur. Cyclodextrins are stable toward alkalis, even at elevated temperatures. The stability of cyclodextrins in alkaline solution is similar to that of cellulose. Cyclodextrins are rather heat stable. Thermal analysis shows that melting of crystals and the thermal decomposition of cyclodextrins occur simultaneously at near 300°C.

The aqueous solubilities differ quite significantly among three cyclodextrins. Solubilities of all three cyclodextrins increase as temperature increases (Table II). Solubilities of complexes, on the other hand, can be either greater or less than those of the uncomplexed components depending both on the guest and the cyclodextrin.

Table II. Aqueous solubilities (g/100 mL) of cyclodextrins (CDs) at various temperatures (4,5)

temperature (°C)	α-CD	β-CD	γ-CD
20	9.0	1.64	18.5
25	12.7	1.88	25.6
30	16.5	2.28	32.0
35	20.4	2.83	39.0
40	24.2	3.49	46.0
45	28.5	4.40	58.5
50	34.7	5.26	
60		7.49	
70		12.03	
75		14.80	
80		19.66	

Cyclodextrins are non-hygroscopic, although their crystals contain water molecules. The contents of water (wt%) in the crystals of α-, β-, and γ-cyclodextrins are 10.2%, 13.2%-14.5%, and 8.1%-17.7%, respectively (3). But even when a cyclodextrin carries the maximum amount of water it remains a free-flowing powder, dry to the feel. This is a desirable property for cyclodextrins to be used as flavor carriers. Water retention of foods may thus be improved by cyclodextrins (6,7).

Metabolism and Toxicology. Beta-cyclodextrin is the most commonly encountered and most thoroughly studied among cyclodextrins, owing to its large-scale commercial availability and relatively much lower price. When ingested, only an insignificant

portion of β-cyclodextrin is absorbed from the intestinal tract (8). The bulk of orally administered β-cyclodextrin passes through the digestive system to the colon to be partially hydrolyzed by the colonic flora (9). Once the macrocyclic ring is opened the cyclodextrin is further metabolized and absorbed as other starch hydrolysates.

Metabolism of α-cyclodextrin is slower than that of β-cyclodextrin. Alpha-cyclodextrin is not only resistant to salivary and pancreatic amylases (10), it is believed to pass through the colon without being hydrolyzed even by the colonic enzymes (11). On the contrary, γ-cyclodextrin is rather susceptible to hydrolysis by amylases. As a result, it is metabolized and absorbed like the starch.

A series of toxicological studies have been performed on cyclodextrins, particularly on β-cyclodextrin. No LD_{50} values have been determined for the oral toxicity of β-cyclodextrin because the administered high doses result in no mortality of the animals. No toxic effects have been found in 90-day and one-year studies in rats or dogs, or in multigeneration studies in rats. Upon intravenous injection β-cyclodextrin forms crystals in the kidneys, causing renal damage (12).

Various other toxicological tests including dermal irritation, ocular irritation, inhalation, mutagenicity, Ames test, chromosomal aberration, and teratology have shown no adverse effects of β-cyclodextrin. While GRAS petitions for use of β-cyclodextrin are still pending at the Food and Drug Administration in the United States, it is already approved as an food additive in countries including West Germany, France, Japan, China, Hungary, Netherlands, Luxembourg, Belgium and Spain.

Cyclodextrin Derivatives. Natural cyclodextrins can be modified chemically or enzymatically in order to obtain a variety of derivatives with altered properties, such as increased or decreased solubility or different complexation characteristics.
Chemically modified derivatives of cyclodextrins have been the subject of numerous investigations and publications. Interested readers may refer to the comprehensive reviews by Croft and Bartsh (13), Wenz (14), and the references provided by Szejtli (3). Briefly, modifications of cyclodextrins can be made through chemical reactions by:
-substitution of one or more hydroxyl groups
-replacement of one or more hydrogen atoms of the hydroxyls
-oxidation on the C6 position or on C2-C3 bond
-polymerization by crosslinking, or cyclodextrin rings being strung on a polymer chain.
One of the cyclodextrin derivatives that is of particular importance in applications for flavor and food is insoluble polymer. These polymers are manufactured by covalently crosslinking five or more cyclodextrin monomers using appropriate di- or poly-functional reagents. Though not soluble in any solvents, the water swelling polymers are capable of forming inclusion complexes with a variety of molecules in aqueous solution. The complexed or adsorbed compounds can be subsequently removed from the polymer for recovery, and the polymer regenerated for repeated use.

Another cyclodextrin derivative of commercial and practical importance is hydroxypropyl cyclodextrin. The monomeric cyclodextrin ring is substituted, to varying degrees, with 2-hydroxypropyl side chain on the hydroxyl oxygen atoms.

Hydroxypropyl derivatives have much increased aqueous solubilities compared with unmodified cyclodextrins. For instance, while the solubility of β-cyclodextrin is less than 2% at room temperature, its hydroxypropylated derivatives with a degree of substitution of 3 or higher can be readily soluble to 60%. The hydroxypropyl cyclodextrins can complex and solubilize many guest compounds of poor water solubilities, including some flavor components, to make them much more soluble than the complex made with unmodified cyclodextrins.

Complexation of Cyclodextrin with Flavors

Inclusion Complexation by Cyclodextrins. One of the most intriguing characteristics of cyclodextrins is their ability to include various guest compounds into their cavities to form an inclusion complex without involving covalent bonding. This property was first discovered by Schardinger early in 1911 (*15*). The terminology of inclusion complex ('Einschlussverbindungen') was introduced in 1951 by Schlenk (*16*), and it is now most frequently used in the literature although other names, such as adduct, clathrate, cryptate, molecular compound, etc. are sometimes used as well.

The binding of a guest molecule with the cavity of a cyclodextrin involves several forces, including dipole-dipole, hydrophobic, van der Waals and hydrogen bonding interactions. The success of forming a cyclodextrin-guest complex and the binding strength of the complex are closely related to the properties of the guest molecule.

One of the basic requirements for complex formation is the geometric compatibility of the guest with the cavity of the cyclodextrin. As shown in Table I, α-, β- and γ-cyclodextrins have cavities of increasing diameters, which may hold guest molecules of different sizes. For example, while cyclohexane and biphenyl can form inclusion complexes with all three cyclodextrins, naphthalene is too bulky for α-cyclodextrin, and anthracene fits only into γ-cyclodextrin. On the other hand, propionic acid is compatible with α-cyclodextrin, but it has a rather loose fitting in the larger cavities of β- and γ-cyclodextrins. Nevertheless, complex formation does not always require inclusion of the entire guest molecule into a cyclodextrin cavity. Very often, a cyclodextrin can complex with compounds that are significantly larger than its cavity by only including part of the guest molecule, such as a hydrophobic side chain or a functional group. Some guests will complex with more than one cyclodextrin.

Other factors affecting the formation of an inclusion complex include hydrophobicity (or polarity) of the guest, the presence of water, solution pH and temperature. Generally 1:1 (cyclodextrin:guest) complex is formed although other molar compositions have also been observed in some cases.

Preparation of Cyclodextrin-Flavor Complexes. Many flavor components have molecular sizes and properties suitable to be complexed by cyclodextrins. In most cases, production of these complexes is a rather straightforward process. Usually, it simply involves a thorough mixing of the cyclodextrin with the guest compound to

allow molecular contact, followed by subsequent drying of the formed complex, with or without an isolation step. In some applications complexes are used without drying. If the guest component is known, the ratio of the guest to the cyclodextrin in the complex can be estimated according to the molecular dimension and the cavity size. Therefore, the appropriate weight ratio of cyclodextrin to guest is derived, which very often is 1:1 in molar ratio. However, since most flavorings are multi-component mixtures, a good starting point is to target a 10% (w/w) guest load in the complex and make further adjustments according to the results and requirements.

Virtually any type of mixing device can be used to prepare cyclodextrin-flavor complexes. Selection of methods or equipment should depend on the properties of the guest, the scale of production, as well as the cost effectiveness. The major difference among the methods developed thus far is the amount of water present in the initial complexation reaction mixture. Complexation can be done with the cyclodextrin in the form of a solution, slurry or paste, depending upon the amount of water used.

For an initial laboratory evaluation, the co-precipitation method is most convenient and suitable. The example of the β-cyclodextrin/lemon oil complex formation is used here to illustrate the procedures of the co-precipitation approach. A 15% (w/v) solution is made by first mixing 120 grams of β-cyclodextrin in 800 mL of water and then heating the mixture to about 75°C. To this solution, 30 grams of natural lemon oil was added in one portion with vigorous stirring. The flask was covered to prevent the evaporation of the oil, and the heat was turned off after adding the lemon oil. The mixture was allowed to cool to room temperature while stirring continued. The precipitated complex was collected by filtration and dried at 100°C for 6 hours, yielding 145 g of dry product. For analysis, a small sample (20-50 mg) was partitioned in an equal volume of water and dichloromethane. The organic layer was analyzed using gas chromatography against a series of lemon oil standards which were treated with the same partition process as the sample of the complex. The load of lemon oil was 20.36% (w/w). The chromatograms (Figure 1) show that the composition of the natural lemon oil essentially remains unchanged after complexation with β-cyclodextrin. It should be noted that heating needs to be reduced or eliminated if a guest compound is thermally unstable.

For large-scale production a slurry or paste method is more preferable since there will be less water to remove following the complexation reaction. Virtually any mixing device which can handle the high viscosity of the materials, such as a kneader or extruder, can be used. Appropriate mixing time has to be determined through testing. Drying of complexes can be done using conventional means. Tests for the optimized time and temperature should be carried out to prevent the loss of highly volatile guest compounds.

Release of the Complexed Flavorings. In aqueous solutions there is a dynamic equilibrium between the free and complexed states of the guest and cyclodextrin. The guest molecule can get in and out of the cavity of the cyclodextrin rapidly. When a dry complex is used, the first step in release is the dissolution, followed by the partial dissociation, of the complex. If some of the dissociated guest compounds are

consumed or removed, the complexation equilibrium will shift steadily toward the direction of decomplexation, leading to further release of the included guests. In flavor applications, multiple factors will affect the release of the complexed flavors. For instance, water in the saliva will dilute the complex, allowing more of the complex to dissolve and release the guest. Some components in the food may complex with the cyclodextrin or associate with the released flavors so that the dissociated guest is unable to recomplex with the cyclodextrin. As a result of these factors, the guest can be rapidly released from the complex to elicit the desired flavor response.

Application of Cyclodextrins as Food Additives.

As food additives, cyclodextrins may be used to achieve several different types of effects. The major advantages of cyclodextrins are illustrated as follows.

Stabilization.   Many flavor components have labile chemical moieties that are sensitive to light, heat or air (oxygen). Cyclodextrin complexation can provide protection against these destabilizing factors. When a guest is complexed it occupies the limited space of the cavity of cyclodextrin. Therefore, it is isolated and thus out of contact with the hazardous environment. As a result of this stabilization, increased shelf-life, reduced loss of active ingredients owing to degradation or evaporation are generally observed.

Benzaldehyde is a component of many flavors and it has recently been found to have antitumor activity (*17*). However, it is an oily liquid with sparing solubility in water. Its instability to air and light presents considerable problems in its food and pharmaceutical applications. In order to overcome these difficulties the complexes of benzaldehyde with all three cyclodextrins have been prepared. In one study (*18*), the autoxidation rates of free benzaldehyde and its inclusion complex with α-cyclodextrin in neutral solution were determined at 70°C. The half-life of the complex was 3.6 times that of the free guest. Detailed structural investigations have revealed interesting insight of the benzaldehyde/α-cyclodextrin (1:1) complex. The x-ray data shows that in the solid state the phenyl ring end of benzaldehyde is inserted into the center of the α-cyclodextrin cavity (*19*). But in aqueous solution strong experimental evidence indicates that the aldehyde end is now included inside the cavity (*18*). In another experiment, the oxidation of benzaldehyde and its complex with β-cyclodextrin was measured in pure oxygen atmosphere using a Warburg apparatus (*20*). During a period of time when observations were made, while the complexed benzaldehyde remained virtually intact, the free guest was rapidly oxidized to yield the inactive benzoic acid.

Volatility is another reason that flavors lose strength over time. For example, menthol readily sublimes. On the lid of a bottle in which menthol is kept, one can typically observe crystals that are formed from the evaporated menthol vapor. However, when menthol is complexed with cyclodextrins, the odorless powder exhibits high stability. A sample of menthol/β-cyclodextrin has been kept in our laboratory for nearly nine years with virtually no loss of menthol from the complex. But when the complex is tasted, a strong menthol flavor releases immediately. Data
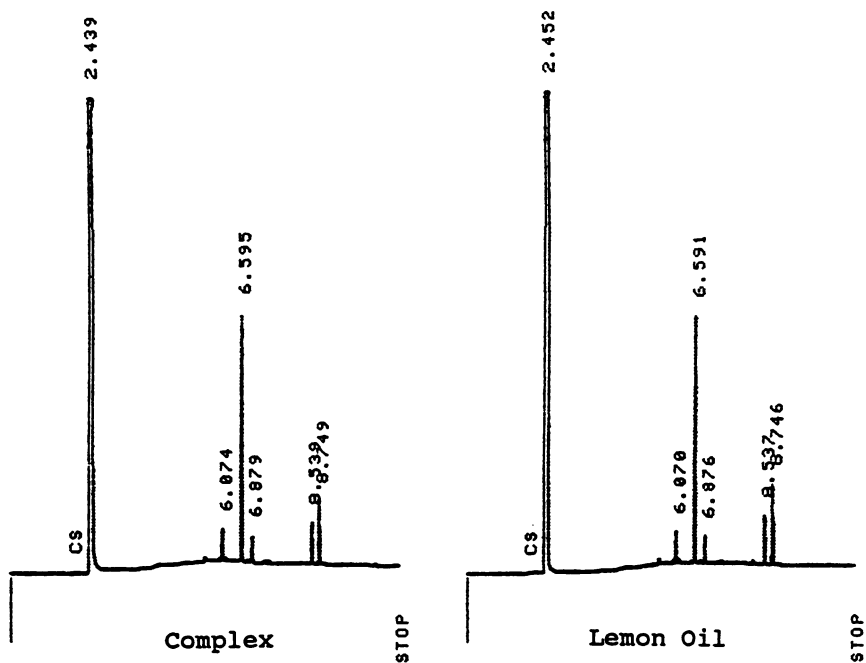
Figure 1. GC chromatograms of free lemon oil and its complex with β-cyclodextrin.
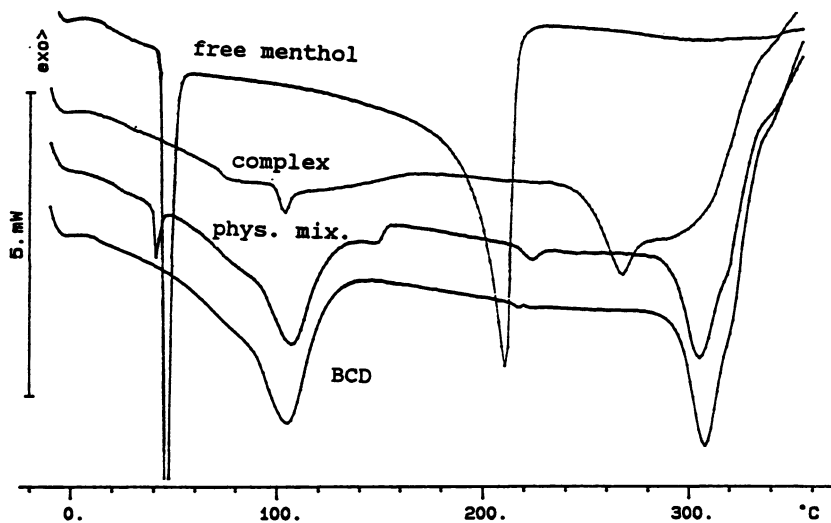
Figure 2. Differential scanning calorimetry (DSC) curves (from top to bottom) of: free menthol, its 1:1 inclusion complex with β-cyclodextrin, its 1:1 physical mixture with β-cyclodextrin and free β-cyclodextrin.

from differential scanning calorimetry (Figure 2) clearly shows that inclusion complexation reduces the volatility of menthol by increasing both its melting and boiling temperatures. The melting isotherm of menthol is observed near 42°C only for the free menthol and the physical mixture, but not for the inclusion complex. Because menthol molecules are surrounded by cyclodextrins in the inclusion complex, no crystals of menthol can be formed, thus leading to the disappearance of the melting isotherm. At about 100°C, water evaporates from the cyclodextrin. As temperature further increases, uncomplexed menthol is evaporated around its boiling point of 212°C, while the menthol in the complexed form boils at a much higher temperature.

Solubilization. The water solubility of guests can be modified by complexation with cyclodextrins. Due to the interaction of the hydroxyl groups with water, cyclodextrins themselves have sufficient hydrophilicity to be soluble in water. When a highly water insoluble compound is included inside the cavity of cyclodextrin, the hydrophobic moiety is surrounded by the cyclodextrin. As a result, remarkable solubility increase may be achieved. There are many such examples in the pharmaceutical area in which the solubilities of sparingly water soluble drugs have been enhanced drastically by natural cyclodextrins or some of their hydrophilic derivatives (*21,22*). The same principle holds for flavors as well.

Hesperidin is a bitter-tasting component of certain citrus fruits. Its poor solubility sometimes leads to formation of a precipitate in canned citrus products. Konno et al (*23*) discovered that the precipitation could be prevented by addition of 0.005%-1% β-cyclodextrin. Sweetening agents chalcone and dihydrochalcone easily precipitate from soft-drinks, especially on cooling. Similarly, the precipitate disappeared when β-cyclodextrin was added to the drink (*24*).

Taste Modification. Taste of foods may be improved with cyclodextrins by masking off-flavors and unpleasant odors through complex formation. The fish odor in processed foods can be penetrating and undesirable. By addition of cyclodextrins to canned fish and shellfish before sterilization, Osada and Kikuchi discovered that the fish odor was reduced (*25*). When the cans were opened and the contents analyzed, data showed that concentrations of the free odor-causing compounds were actually lower in the cyclodextrin-containing cans. For example, the content of hydrogen sulfide was 137.7 μg% in the control, but only 3.3 μg% when cyclodextrin was added. The concentrations of the volatile basic nitrogen were 4.6 mg% and 3.7 mg% in the absence and presence of cyclodextrin, respectively. Milk casein hydrolysate has an astringent taste. However, the taste can be eliminated by the addition of β-cyclodextrin (*26*). Use of the cyclodextrin thus provides a way of utilizing this source of readily digestible protein.

Other Beneficial Effects. Flavor concentrates, either in the form of oleoresins or essential oils, are difficult to handle as oily liquids. Furthermore, their compositions or concentrations often vary from different sources and preparation processes. This presents problems for food manufacturers in making standardized food products.

Complexation with cyclodextrins converts liquid flavorings to the non-hygroscopic, powdered flavor, thus providing a clean, standardized form of flavor ingredient. Moreover, the powderization of flavors can facilitate mixing, storage, as well as transport. Many materials, such as sugar, salt, gum arabic, cellulose ethers, or starch derivatives, have been used to encapsulate flavor concentrates. But as data in Table III demonstrate molecular inclusion by cyclodextrins holds the flavor more strongly than other carriers which function mainly based on the surface-adsorption mechanism. In this experiment all samples of carrier/anise oil were kept at 100°C for 6 hours. The retained oil in each sample was determined with GC and UV analyses. Results are reported as percentage of the oil initially mixed with the carrier. Lo-DEX 5 and 15 are maltodextrin products, and Frodex 42 is a product of corn syrup solid manufactured by American Maize-Products Company.

Table III. Retention of anise oil by different carriers

flavor carrier	anise oil retained (%)
β-cyclodextrin	91.5
Lo-DEX 5	54.4
Lo-DEX 15	35.1
Frodex 42	10.7
sucrose	6.5

Use of flavor-cyclodextrin complexes instead of the free flavor can result in considerable reduction of the ingredient needed. This may come from increased solubility, decreased volatility, reduced loss due to degradation, or a combination of these effects. In one experiment, cookies were baked in our laboratory using β-cyclodextrin/lemon oil complex or with uncomplexed lemon oil. Only 75% equivalent lemon oil was present in the recipe using the complex. However, stronger aroma and flavor intensity than the control were recognized unanimously by the panelists in the cookies made with the β-cyclodextrin/lemon oil. In another chewing gum study, we discovered that only half of the amount of flavor oil supplied in a β-cyclodextrin complex was needed to achieve the same initial intensity of flavor as the free oil. Use of cyclodextrin-flavor complexes in chewing gum has also been found to provide longer lasting and more intensive taste (27). Emulsion stability and water retention can be improved in many cases by use of cyclodextrins. For example, addition of cyclodextrins to emulsified foods (6) or cheese (7) increased the water retention and the shelf life.

Application of Cyclodextrins as Process Aids.

Besides being utilized as food additives, cyclodextrins and some of their derivatives have also been widely employed as process aids. In this type of application, a cyclodextrin is initially introduced into a food system to selectively complex certain components. The cyclodextrin, along with the included guest, is then separated from the food product by centrifugation or filtration.

One application of such separation is to extract or enrich desirable flavor components. For instance, β-cyclodextrin has been used to extract onion and garlic oils from their natural sources. An aqueous suspension of the vegetable homogenate was first made. After removal of the vegetable mass through filtration, β-cyclodextrin was added to the filtrate to form a complex, which was then separated. The solid complex can be dried for subsequent application as a powdered onion or garlic flavor, or it can be dissociated in heated water to release the complexed oil for collection. The free β-cyclodextrin, now dissolved in aqueous layer, can be recycled for the continued oil extraction. It was interesting to discover that the onion and garlic oils extracted with cyclodextrin had flavors identical to that of the fresh vegetables, unlike the oils obtained using conventional distillation processes. Menert reported a similar study in which caraway seed and laurel oils were isolated from raw material in up to 80% yield by complexation with β-cyclodextrin (*28*). Solid β-cyclodextrin/oil complexes thus obtained have oil content and odor quality similar to those obtained by a solution-solution extraction method.

Alternatively, unwanted components can be removed from a flavor preparation using cyclodextrins. In this type of application, insoluble cyclodextrin polymers are especially useful. These crosslinked cyclodextrin polymers can be conveniently packed in a column and used as affinity chromatography. Polymers containing natural or modified α-, β-, and γ-cyclodextrins have been prepared, and they have shown selective affinities toward different components. For instance, some citrus juices have excessive bitterness that adversely affects the flavor of products made from these juices. The undesirable flavor is mainly attributable to the bitter components such as naringin, limonin, and momilin. Shaw at al. (*29,30*) have tested a variety of methods for a commercial process that removes bitter components without adding anything to the juice. They found polymers made from β-cyclodextrin to be very effective for debittering citrus juices. In comparison, the polymers appeared to have about 10 times the capacity of the cyclodextrin monomer in forming inclusion complexes with these bitter components (*30*).

Conclusion.

Cyclodextrin complexation represents one of the most advanced flavor encapsulating technologies. Molecular inclusion by the cavity of cyclodextrins provides protection against the damaging factors of the environment for flavor constituents. The major advantages of cyclodextrin application in the flavor and food industry include:

1)   protection of active ingredients from degradation by heat, light and oxidation,

2)   prevention or reduction of loss of flavor through sublimation and   volatilation,

3)   solubilization of less water-soluble flavor components,

4)   modification of taste profile by masking or removing off-flavors and unpleasant odors,

5)   conversion of liquid flavor concentrates to dry powder for easy dosing, mixing, packaging and handling,

6)   selective separation of components either for the purpose of isolation or removal.

As briefly illustrated, cyclodextrins can be used both as food additives and process aids. Current level of application is still in its beginning stage. In some cases, unmodified cyclodextrins have exhibited certain limitations. As research continues together with the commercial availability of natural and modified cyclodextrin products, cyclodextrins will inevitably find more widespread use in the flavor and food industries.

Literature Cited:

1.   Marion, J. P. *Int. of flavors and dye stuffs into formulated food products*, Congress Nice, 1987.

2.   Anandaraman, S.; Reineccius, G. A. Food Technol. **1986**, *40*, 89.

3.   Szejetli, J. *Cyclodextrin Technology*, Kluwer Academic Publishers: Dordrecht, Boston, London, 1988.

4.   Wiedenhof, N.; Lammers, J. N. J. J. *Carbohydr. Res.* **1968**, *7*, 1.

5.   Jozwiakoski, M. J.; Connors, K. A. *Carbohydr. Res.* **1985**, *143*, 51.

6.   Kanegafuchi Chem. Ind. K. K. *Jpn. Kokai* JP 78,072,839, 1978.

7.   Ota, T.; Takeda, F. *Jpn. Kokai* JP 81,75,060, 1981.

8.   Olivier, P.; Verwaerde, F., and Hedges, A. *J. Am. Coll. Toxicol.* **1991**, 10, 407.

9.   Gergely, V.; Sebestyen, G.; Geyen, G.; Virag, S. in *Proceedings of the 1st International Symposium on Cyclodextrins*, Szejtli, J. (ed), Academic Kiado: Budapest, Hungary, 1982, 109.

10.   Marshall, J. J.; Miwa, I. *Biochem. Biophys. Acta* **1981**, *66*, 142.

11.   Suzuki, M.; Sato, A. *J. Nutr. Sci. Vitaminol.* **1985**, *31*, 209.

12.   Frank, D. W; Gray, J. E., Weaver, R. N. *Am. J. Pathol.* **1976**, *83*, 367.

13.   Croft, A. P.; Bartsch, R. A. *Tetrahedron*, **1983**, *39*, 1417.

14.   Wenz, G. *Angew. Chem. Int. Ed. Engl.* **1994**, *33*, 803.

15.   Schardinger, F. *Zentralbl. Bakteriol. Abt. II*, 1911, 29.

16.   Schlenk, W. Jr. *Fortschr. Chem. Forsch.* **1951**, *2*, 92.

17.   Sakaguchi, R.; Hayase, E. *Agric. Biol. Chem.* **1979**, *43*, 1775.

18.   Chang, C-J.; Choi, H. S.; Wei, Y. C.; Mak, V.; Knevel, A. M.; Madden, K. M.; Carlson, G. P.; Grant, D. M.; Diaz, L.; Morin, F. G. *Biotechnology of Amylodextrin Oligosaccharides*, ACS Symposium Series 458, Friedman, R. B. (ed), American Chemical Society, Washington, D. C. 1991.

19.   Harata, K.; Uekama, F. E.; Saenger, W. *J. Am. Chem. Soc.* **1977**, *99*, 1735.

20.   Szejtli, J.; Szente, L.; Bánky-Elöd, E. *Acta Chim. Acad. Sci. Hung.* **1979**, *101*, 27.

21.   Loftsson, T.; Brewster, M. E.; Derendorf, H.; Bodor, N. *Pharm. Ztg. Wiss.* **1991**, *1*, 5.

22.   Loftsson, T.; Bodor, N. *Acta Pharm.* **1989**, *1*, 185.

23.   Konno, A.; Miyawaki, M.; Misaki, M.; Yasumatsu, K. *Agric. Biol. Chem.* **1982**, *46*, 2203.

24.   Hashimoto, S.; Katayama, A. *Jpn. Kokai*, JP 75,35,349, 1975.

25.   Osaka, H.; Kikuchi, Y. *Jpn. Kokai*, JP 88,49,037, 1988.

26.   Suzuki, Y. *Jpn. Kokai*, JP 75,69,100,1975.

27.   Marmo, D.; Rocco, F. L. *US. Pat.* 4,001,438, 1977.

28.   Menert, A. A. *Tallinna Tehnikaulik. Toim.* **1990**, *715*, 58.

29.   Shaw, P. E.; Wilson, C. W., III. *J. Food Sci.* **1983**, *48*, 646.

30.   Shaw, P. E.; Buslig, B. S. *J. Agric. Food Chem.* **1986**, *34*, 837.

Chapter 19

The Role of Specialty Food Starches in Flavor Encapsulation

Paolo C. Trubiano

Food Products Division, National Starch and Chemical Company, Finderne Avenue, Bridgewater, NJ 08807

Sodium starch octenyl succinates are special food starches that are characterized by good filming properties and the ability to form very fine, stable emulsions, two key factors for very effective encapsulation of flavor oils by spray-drying. The results show the superior performance of these starch products over other encapsulating agents or carriers, such as powdered gum arabic and maltodextrins. Parameters used to evaluate these unique encapsulating agents include emulsion particle size and stability, level of orange oil that is actually retained in the spray-dried powders, exposed surface oil, stability of the flavor toward evaporation, oxidation resistance of the encapsulated powders and spray-drying rates.

The natural film forming properties of starch make it an excellent raw material for the preparation of encapsulating agents whose function is to coat an active substance, to bind it or to trap it within a matrix. Starch films can be tough, hard, flexible and elastic. They can have good mechanical properties, are virtually impermeable to oxygen and offer a broad range of water solubilities. These properties of starch have made possible the development of highly functional encapsulating agents designed to meet the stringent requirements of the flavor industry.

Filming Properties of Starch

Table I shows typical tensile strength and elongation values obtained with free film cast out of aqueous solutions of three types of corn starches (*1*): waxy corn starch which is made up of 100% amylopectin, the branched chain molecule; regular corn starch which contains 27% amylose, the straight chain molecule, and 73% amylopectin and high amylose corn starch which is made up of 72% amylose and 28% amylopectin. The other starches derived from potato, tapioca and wheat contain 20%, 17% and 25% amylose respectively, the rest is amylopectin. While the

elongation or extensibility of native starch films does not vary greatly from source to source, the tensile strength varies considerably and this depends, to a large extent, on the amount of the straight molecules in the starch. Thus the tensile strength of starch films ranges from 4800 pounds per square inch for waxy corn starch to almost 7000 pounds per square inch for high amylose corn starch. Regular corn, tapioca, wheat and potato starch have an amylose content between 17 and 25% and are fairly comparable in filming characteristics. The mechanical properties of starch films, such as elongation, flexibility and impact resistance, can be improved using small amounts of plasticizers, such as glycerol (2). Naturally, the plasticizer level must be determined very carefully because while it improves the flexibility of the starch film it will also reduce its tensile strength and overall toughness.

Table I. Filming Properties of Starch

Starch	Tensile Strength (psi)	% Elongation
Corn starch	6340	2.5
Waxy corn	4800	1.7
Tapioca	6050	3.4
Potato	6080	3.1
Wheat	6370	2.9
High amylose corn	6916	2.5

The molecular weight of the starch-based encapsulating agent also has an effect on the characteristics of the film. In general, the lower the molecular weight or viscosity of the starch, the more brittle the film is. Below a certain degree of polymerization the molecular weight of the starch is too low and the toughness and strength of the resulting film can become insignificant for encapsulation purposes (3). Another characteristic that makes starch a viable raw material for encapsulation is its excellent oxygen barrier properties (4).

Emulsion Properties of Specialty Food Starches

Filming properties are not always the only requirements of an effective encapsulating agent. Very often the film former must also be capable of forming fine oil-in-water emulsions. This is particularly the case when water insoluble substances, such as flavor oils, are encapsulated by means of spray-drying where the efficacy of the encapsulating agent is closely related to how fine the emulsion is before drying. However, conventional food starches do not give fine stable emulsions because the molecule has no hydrophobic groups and has, therefore, no affinity for flavor oils.

The preparation of excellent starch-based emulsion stabilizers is described in a patent granted to Caldwell and Wurzburg (5) in which starch is modified with small amounts of cyclic dicarboxylic acid anhydrides, such as octenyl succinic anhydride. Sodium starch octenyl succinates are specialty food stanches (6) that combine excellent emulsion properties and filming characteristics, two key factors for the efficient encapsulation of flavors.

Encapsulation by Spray-Drying

The emulsions made with food starches can be dried by a number of processes. While the most popular, versatile and economical seems to be spray-drying, other methods are also used very effectively to carry out encapsulation with starch products. These include spray-cooling, fluid bed collection, spraying the emulsion into a dehydrating liquid, air suspension coating, depositing the emulsion on cold drums, extrusion and drum-drying. Some of these methods are sometimes preferred over spray-drying because they meet specific needs such as larger and denser particles, improved mechanical stability, controlled solubility and improved oxidation resistance. In general, regardless of the encapsulation process used, when the encapsulated powders prepared with specialty starches are added to water they readily reconstitute into the original emulsion and release the active ingredient immediately. This is so because the molecular weight and molecular shape of the base starch used are chosen to give films which are soluble in cold water.

Products that can be encapsulated with starch-based encapsulating agents include a wide range of flavors as well as vitamins, fats, oils and fragrances. The spray-dried flavors are generally formulated with other ingredients in a variety of food products. These include instant beverages, bakery dry mixes, dessert mixes, non-dairy creamers, vitamin formulations and tablets. In addition to the specialty food starches, other products that are also used to prepare spray-dried powders include gum arabic, gelatin, casein, dextrins and maltodextrins. A typical formula and procedure used in our laboratory to encapsulate flavors by spray-drying are found in Table II. The resulting spray-dried powder contains about 20% of orange oil. The first step of the procedure is to disperse the starch-based encapsulating agent in water under good agitation. Some of these products are completely cold water soluble, others will give best results if the water suspension is heated to ~70°C. If the starch suspension is heated and the flavor to be encapsulated is very volatile it is best to cool the solution before adding the oil and preparing a pre-emulsion under moderate agitation. The mixture is then homogenized with a 2-stage pressure homogenizer at 2500-3500 pounds per square inch or with a suitable high shear mixer to obtain a fine emulsion with an average particle size of at least one micron. The emulsion is then spray-dried at typical temperatures, such as 200°C inlet and 90° C outlet. All the results reported here were obtained with powders spray-dried in an Anhydro laboratory spray-dryer equipped with a centrifugal spray head. The emulsions were prepared using a Greerco benchtop homogenizer characterized by a fixed clearance between the turbine and the stator, both immersed in the liquid mixture. During homogenization unrefined material is continuously drawn from the bottom of the container and forced to pass through restricted openings.

Table II. Spray-dried Orange Flavor

Ingredients	Parts by weight
Food starch	80
Orange oil	20
Water	130

Procedure:
1. Disperse the starch in water under good agitation.
2. Heat the suspension to 70°C under moderate agitation.
3. Cool the solution to the desired temperature.
4. Slowly add the flavor oil under moderate agitation to form a pre-emulsion.
5. Emulsify until a particle size of one micron or less is obtained.
6. Spray dry the emulsion at 200°C/90°C (inlet/outlet) temperature.

Spray-dried flavors are free-flowing, relatively low in bulk density and consist of fairly spherical particles ranging in size from about 10 to about 100 microns. A scanning electron microphotograph of a typical spray-dried orange oil encapsulated in a starch matrix magnified 600 times is found in Fig. 1. Very often the particles show craters which are due to the collapse and shrinking of emulsion droplet in the final stages of drying. On close examination the surface of the spray-dried particles appears porous and having many cracks which explain why poor oxidation stability is often a problem with some spray-dried flavors. Fig. 2 is a cross section of a particle of spray-dried orange oil magnified 1,800 times. Typically, the spray-dried particle is made up of a hollow center and a thick wall matrix in which are imbedded the flavor oil droplets. The diameter of the droplets is related to the fineness of the original emulsion. Normally the smaller and more uniform the droplets within the matrix, the more efficient the encapsulation. When the spray-dried powder is added to water the starch matrix dissolves completely and the original flavor emulsion is reconstituted.

Key Parameters in Spray-Drying Encapsulation

Regardless of the process that one intends to use, the choice of the best encapsulating agent depends on the right balance of several variables, some of which relate to the encapsulating agent itself, some to processing and some to the properties desired in the encapsulated product. Reference to the importance of the filming properties of the encapsulating agent and its ability to form a fine emulsion was made already. Other key variables in flavor encapsulation are the viscosity of the encapsulating agent which affects spray pattern and drying rates, the amount of active material desired in the final product, the flavor losses during drying, the acceptable level of active
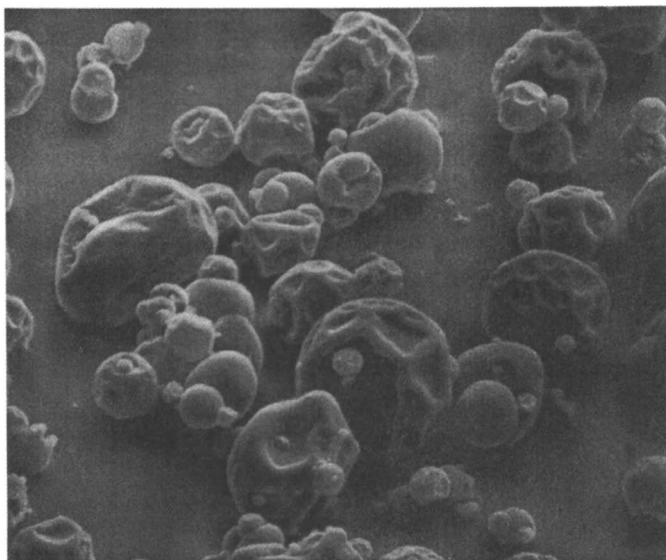
Figure 1. SEM micrograph (600x magnification) of spray-dried orange oil.
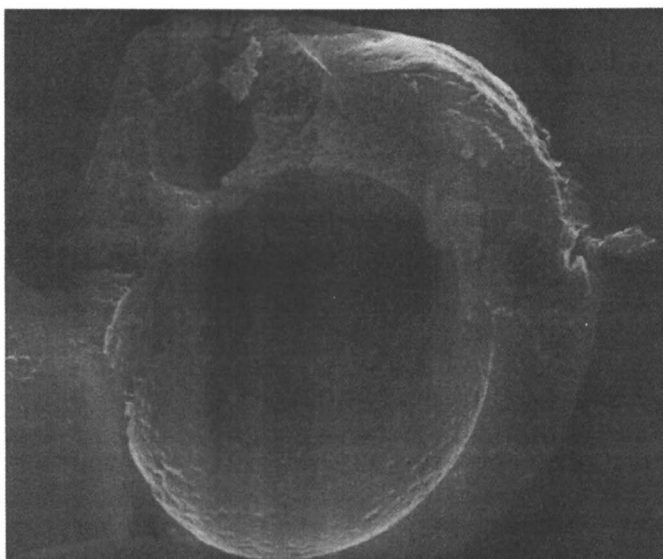
Figure 2. SEM micrograph (cross section, 1800x magnification) of spray-dried orange oil particle.

material on the surface of the powder, the stability toward oxidation and the rate of flavor release.

The amount of single fold orange oil in the spray-dried powders discussed in this paper was determined via a standard steam distillation procedure. For oils that cannot be easily steam distilled the starch encapsulating agent can be broken down enzymatically or with acid and the active ingredient can then be extracted with a suitable solvent. The amount of active ingredient on the surface of the spray-dried powder was determined by washing the powder with petroleum ether and evaporating the solvent. The surface oil was calculated by subtracting the oil content of the washed powder from the oil content of the unwashed powder. The oxidation resistance of the encapsulating agent was determined by ageing the spray-dried powders in a closed container for two weeks at 50°C, steam distilling the flavor oil and determining the amount of oxidized limonene (ex: carvone) in the extracted oil by gas chromatography. The higher the percent of carvone, the poorer the oxidation resistance of the encapsulated powder. In general, results obtained with orange oil can be used to predict the performance of the encapsulating agent with other oxygen sensitive substances such as lemon oil, vitamin A and fats.

The viscosity of the encapsulating agent is a very important variable in spray-drying encapsulation. Since the higher solids of the emulsion give faster drying rates, the molecular weight of the food starch should be as low as possible. However, the molecular weight of the encapsulating agent cannot be too low because the filming properties of the product would be lost. Commercially effective starch-based encapsulating agents represent a balance between emulsion properties, film properties and spray-drying rates.

Encapsulated Orange Oil Powders

The results in Table III were obtained with spray-dried powders of orange oil encapsulated with food starch and other encapsulating agents, such as powdered gum arabic from two sources, a maltodextrin with a dextrose equivalent of 10 and a special corn starch dextrin. All the emulsions contained 20% flavor oil on a dry basis with the exception of the emulsion made with maltodextrin which contained only 10% oil. Best results were obtained with the starch-based encapsulating agent which gave a 96.4% retention of the orange oil that had been added to the emulsion before spray-drying and only 3.8% of that oil was found on the surface of the powder. The level of orange oil recovered in the powder after ageing at 50°C for two weeks was 91.2% which is also the highest recovery of all the encapsulating agents tested. The two samples of powdered gum arabic gave relatively good fresh retentions of 94.9 and 93.4% and corresponding surface oil of 6.5 and 6.3%. After ageing the spray dried powders for two weeks at 50°C the level of orange oil in the powders was 89.1 and 88.3% respectively. Because the maltodextrin does not have good emulsion properties we limited the level of flavor oil in the emulsion to 10% instead of 20% that was used with the other encapsulating agents. Nevertheless, this product showed the greatest loss of oil upon spray-drying with a fresh retention of only 76.8% while 7.5% of the retained oil was on the surface of the spray-dried powder. The aged

retention for the maltodextrin sample was only 70.4%. The special corn dextrin gave a fairly good fresh retention of 89.8% but lost a considerable level of oil on ageing, giving an aged retention of 82.1%. Surprisingly, the dextrin showed a low level of surface oil of 2.4%. As we shall see later, good flavor oil retention is, to a large extent, closely related to a small particle size of the emulsion.

Table III. Flavor Retention of Typical Encapsulating Agents

Encapsulating agents	Oil retention Fresh	Oil retention Aged	% of oil on surface	% Carvone
Special food starch	96.4	91.2	3.8	0.626
Gum arabic I	94.9	89.1	6.5	1.080
Gum arabic II	93.4	88.3	6.3	0.633
Maltodextrin (10 D.E.)	76.8	70.4	7.5	1.280
Special dextrin	89.8	82.1	2.4	0.932

In terms of oxidation resistance the powder containing the food starch showed the lowest level of carvone in the oil extracted from the powders aged for two weeks at 50°C. Only 0.6% of the limonene became oxidized to carvone on ageing. One of the two gum arabic products performed about the same as food starch with 0.63% carvone in the aged spray-dried powder while the second product was much poorer showing 1.08% oxidized limonene. The high level of carvone in the spray-dried powder containing maltodextrin showed that this carrier is not very effective in protecting the oil from oxidation, most likely because about 7.5% of the oil was exposed on the surface of the powder. The corn dextrin protected the oil against oxidation better than the maltodextrin but was much poorer than the food starch and better than one of the two products of gum arabic.

The results in Table IV were obtained with another set of experiments based on the same formula and procedure outlined in Table II. These data show that there is a fairly direct relationship between the particle size of the emulsion before spray-drying and the amount of oil retained in the spray-dried powder. In general, the finer the emulsion, the better the flavor retention. The fresh emulsion made with the special food starch had the smallest particle size (0.789 micron) and the resulting spray-dried powder retained 96.0% of the flavor oil that was in the original emulsion. The two samples of gum arabic, which gave slightly larger particle size (0.903 and 0.989 micron) gave slightly lower retentions than the food starch (95.3% and 95.6% respectively). Before spray-drying, the maltodextrin emulsion had an average particle size of about 3 microns (constantly mixed to prevent oil separation) and the oil retention of the spray-dried powder was only 72.5%. In this set, the corn dextrin, whose emulsion particle size was 1.297 microns, gave a retention of 86.9%.

Table IV. Effect of Particle Size of Emulsion on Flavor Retention and Clouding Ability

Encapsulating agents	Mean particle size, micron		Flavor retention	Clouding % T @ 0.1%
	Fresh	Overnight		
Special food starch	0.789	1.220	96.0	16.0
Gum arabic I	0.903	1.326	95.3	19.0
Gum arabic II	0.989	1.784	95.6	19.0
Maltodextrin (10% Flavor)	2.934 (mixed)	separated	72.5	34.0 (0.2%)
Special dextrin	1.297	1.707	86.9	24.0

There are other reasons why a fine particle size of the flavor emulsion is very desirable in the encapsulation of flavor oils by spray-drying. For example, the cloudy appearance of reconstituted dry mixes, such as drinks and coffee creamers, is largely due to the emulsified oil. For a reconstituted orange beverage, the finer the emulsion the more opaque and juice-like the drink appears, which is desirable. These results illustrates the direct relationship between the particle size of the emulsion before spray-drying and the opacity of the water containing 0.1% of the spray-dried powder. The lower the percent light transmittance, the better the opacity of the reconstituted product. The best opacifying effect was obtained with the food starch emulsion which also had the smallest particle size. Because of poor emulsion the opacity obtained with the maltodextrin encapsulated flavor was the poorest even though the powder was reconstituted in water at twice the level of the other powders since the original emulsion contained only half of the flavor oil.

In spray-drying encapsulation it is also very desirable to prepare a fine emulsion especially if it is going to be held in the mixing tank for a long time before drying because the tendency of the emulsion to coalesce and break with time increases with increasing particle size. To illustrate this we held samples of the fresh emulsions described above overnight for 16 hours under moderate agitation and then measured the particle size. All the emulsions increased in particle size with time, but the emulsion made with maltodextrin actually separated because it had the largest particle size. It is always best to spray-dry the fresh emulsion right away because a coarser emulsion will result in higher losses of flavor oil during the drying process and more of the oil will be on the surface of the spray-dried powder. Therefore, selecting the encapsulating agent that gives a very fine and stable emulsion is an assurance of best encapsulation efficiency particularly under unexpected adverse plant conditions.

The level of flavor oil that can be encapsulated in the spray-dried powder depends primarily on the emulsion and filming properties of the encapsulating agent. In this set of experiments (Table V) we compared a starch-based encapsulating agent

that has been especially designed for high flavor loads in the spray-dried powder to two commercial grades of powdered gum arabic, maltodextrin and corn dextrin in their ability to retain higher levels of flavor oil. The level of orange oil varied from 10% to 30%. The results show that relatively higher retentions throughout the whole range are obtained only with specialty food starch. At 10 and 20% oil level this starch had only negligible losses of flavor oil during spray-drying while at 30% oil level the retention was still very good (94%). Both samples of gum arabic gave lower flavor retention than the food starch and lost a substantial amount of the flavor oil above 25% level. The maltodextrin gave very poor retention at all levels while the dextrin showed reasonably good performance only at low levels of flavor oil.

Table V. Effect of Flavor Level on Retention

Encapsulating agents	% Retention			
	10%	20%	25%	30%
Special food starch	99.0	99.0	98.5	94.0
Gum Arabic I	94.9	94.2	94.1	82.5
Gum Arabic II	93.5	93.4	90.9	85.3
Maltodextrin	76.8	42.0	—	—
Corn dextrin	92.7	89.8	83.5	—

Starch-based encapsulating agents have been designed to give low viscosity when dispersed at high solids. This is important because higher solids mean that the emulsion can be dried at higher and more economical rates since less water has to be evaporated. In these experiments the level of orange oil in the emulsion was, again, 20% and that of the encapsulating agent was 80%. The encapsulating agents tested were the specialty food starch, powdered gum arabic and 10 DE maltodextrin (Table VI). Where necessary, the viscosity of the emulsion before spray-drying was adjusted with water to 100 cps which gave best atomization of the emulsion in the laboratory spray-dryer. Gum arabic was initially dispersed in water at 28% solids. After adding the flavor oil and adjusting the viscosity, the total solids (gum and flavor) of the emulsion were 32.7%. To generate data on the relative increase in spray-drying rates, for reference it was assumed the drying rates obtained with gum arabic at those solids to be equal to 100. The increase in drying rates that could be realized with the other encapsulating agents was then calculated on the basis of the lower amount of water to be evaporated from the higher solids emulsions made with them. The lower viscosity of the special food starch permitted a suspension in water at 38% solids and a total spray-drying solids of 43.4%. This made possible a 58% increase in drying rates over gum arabic. Maltodextrins, and similar products, can be used even at higher solids than special food starches designed for encapsulation but they do not

give good emulsions and result in considerable loss of flavor oil during spray-drying. These experiments show, once again, that the food starch encapsulating agent gives excellent flavor retention while permitting very good spray-drying rates.

Table VI. Effect of Solids on Spray Drying Rates

Encapsulating agents	Enc. agent % Solid	Total Spray-drying Solid, %	% Increase in drying rates	Flavor Retention %
Special food starch	38	43.4	58	98.0
Gum Arabic	28	32.7	—	97.0
Maltodextrin (10 D.E.)	45	50.5	110	<75

Conclusions

The unique functionality of starch-based encapsulating agents in spray-dried flavors is related to their ability to form very fine, stable emulsions and to their filming properties. Sodium starch octenyl succinates offer a number of advantages over other encapsulating agents, such as gum arabic and maltodextrins. These include reduced processing costs, higher levels of active ingredient in the spray-dried powders, less flavor exposed on the surface of the powders, better stability toward evaporation and oxidation, rapid flavor release characteristics and excellent opacifying properties.

Literature Cited

1. Trubiano, P. C., Unpublished data, 1974
2. Wolf, I. A.; Davis, H. A.; Cluskey, J. E.; Gundrum, L. J.; Rist, C. E. *Ind. Eng. Chem.* **1951**, *43*, 915-919.
3. Lloyd, N. E.; Kirst, L. C. *Cereal Chem.* **1963**, *40*, 154-161.
4. Mark, A. M.; Roth, W. B.; Mehltretter, C. L.; Rist C. E. Oxygen Permeability of Amylomaize Starch Films, *Food Technol.* **1965**, *21 (1)*, 72-74
5. Caldwell, C. G.; Wurzburg, O. B. U.S. Patent # 2,661,349. 1953.
6. Code of Federal Regulations, Title 21, Chapter 1, Part 172. Food Additives Permitted in Foods for Human Consumption, Section 172.892, Food Starch Modified, U. S. Printing Office, Washington, D.C., 1981.

Author Index

Affiliation Index

Subject Index

Author Index

Affiliation Index

Subject Index

A

Activation energies
  flavor compounds, 38–39
  Maillard reaction kinetics in propylene
    glycol based model systems during
    microwave heating, 46f,47
  pyrazine formation, 50

Adsorption
  applications, 14
  carriers, 14
  procedure, 14
Air–aqueous lysozyme solution
  interface, surface dilational
  rheological properties,
  192f–194